LOI Identification Nº 19

FAIR- PAC:

APPA	[x]
NUSTAR	[ ]
QCD	[ ]

Date: 15.12.2005

Technical Proposal for the Design, Construction, Commissioning and Operation of

FLAIR

Abstract:

FLAIR, the Facility for Low-energy Antiproton and Ion Research, makes use of the beams of antiprotons and highly-charged ions from NESR to further decelerate and cool them in two storage rings (LSR and USR) and a universal trap facility HITRAP. Antiprotons will be provided in both slow and fast extraction down to the keV-range with intensities that are about two orders of magnitude larger than currently available and phase space densities that are unprecedented, enabling many new experiments. The facility will be also used with highly charged ions, leading to a strong overlap with the SPARC collaboration.

Spokesperson

Eberhard Widmann eberhard.widmann@oeaw.ac.at (+43 1) 4277 29701

Members of the *FLAIR* Collaboration

AUSTRIA
M. Cargnelli, H. Fuhrmann, P. Kienle, H. Marton, E. Widmann, H. Zmeskal
Stefan Meyer Institute for Subatomic Physics, Austrian Academy of Sciences, Vienna
J. Burgdoerfer, C. Lemell, S. Yoshida
Institute for Theoretical Physics, Vienna University of Technology

CANADA
E. A. Hessels
Department of Physics and Astronomy, York University, Toronto, Canada
M.C. Fujiwara
TRIUMF, Vancouver, Canada

DENMARK
S. P. Møller
Institute for Storage Ring Facilities, Aarhus University
H. Knudsen, U. I. Uggerhøj
Department for Physics and Astronomy, Aarhus University

FRANCE
É.-O. Le Bigot, S. Boucard, P. Indelicato
Laboratoire Kastler-Brossel, École Normale Supérieure et Université P. et M. Curie, Paris

GERMANY
T. Beier, H. Beyer, M. Block, F. Bosch, S. Borneis, A. Bräuning-Demian, B. Franzke, S. Hagmann, F. Herfurth, A. Kellerbauer, H.-J. Kluge, C. Kozhuharov, T. Kühl, D. Liesen, R.Mann, P. Mokler, F. Nolden , H. Orth, W. Quint, M. Steck, T. Stöhlker, M. Tomaselli
GSI Darmstadt
G. Plunien, G. Soff[1]
Institut für Theoretische Physik, Technische Universität Dresden
U. Ratzinger, A. Schempp
Institut für Angewandte Physik, Universität Frankfurt
R. Dörner
Institut für Kernphysik, Universität Frankfurt
A. Müller
Institut für Kernphysik, Universität Giessen
M. Grieser, R. von Hahn, T. Ichioka, U. Jentschura, R. Moshammer, J. Ullrich, C.P. Welsch, A. Wolf
MPI für Kernphysik (MPI-K), Heidelberg
A. Gillitzer, D. Gotta, D. Grzonka, K. Kilian, W. Oelert, J. Ritman
Forschungszentrum Jülich
K. Blaum, I. Bloch, S. George, S. Stahl, M. Vogel, J. Walz, C. Weber, G. Werth
Institut für Physik, Universität Mainz
W. Nörtershäuser
Institut für Kernchemie, Universität Mainz

[1] Deceased

A. Saenz
Institut für Physik, Humboldt-Universität zu Berlin

HUNGARY
D. Barna, D. Horvath
KFKI Research Institute for Particle and Nuclear Physics, Budapest
B. Juhász, B. Horváth, E. Takács, K. Tőkési
Institute of Nuclear Research of the Hungarian Academy of Sciences (ATOMKI), Debrecen
E. Takacs
Department of Experimental Physics, University of Debrecen

INDIA
A. Ray
Variable Energy Cyclotron Center, Kolkata

ITALY
M. Corradini, M Leali, E. Lodi Rizzini, L. Venturelli, N. Zurlo
Dipartimento di Chimica e Fisica per l'Ingegneria e per i Materiali-
Universita' di Brescia & INFN-Gruppo Collegato di Brescia
G. M. Tino
Dipartimento di Fisica, Laboratorio LENS, INFN, Universita' degli Studi di Firenze
G. Testera
Istituto Nazionale di Fisica Nucleare, Genova

JAPAN
Y. Kanai, N. Kuroda, A. Mohri, Y. Nagata, H. Saito, M. Shibata, M. Wada
Atomic Physics Laboratory, RIKEN, Wako
Y. Yamazaki
Institute of Physics, University of Tokyo, and Atomic Physics Laboratory, RIKEN, Wako
A. Dax, R.S. Hayano, M. Hori, T. Ishikawa
Department of Physics, University of Tokyo
K.-I. Komaki, H. A. Torii
Institute of Physics, University of Tokyo

NETHERLANDS
K.S.E. Eikema, W. Hogervorst, W. Ubachs
Laser Centre Vrije Universiteit, Faculty of Science, Amsterdam
L.D. Noordam
FOM Institute for Atomic and Molecular Physics, Amsterdam

POLAND
J. Jastrzebski, A. Trzcinska
Heavy Ion Laboratory, Warsaw University
S. Wycech
Soltan Institute for Nuclear Studies, Warsaw
K. Pachucki
Institute of Theoretical Physics, Warsaw University

RUSSIA
I. Meshkov, I. Seleznev, A. Smirnov, A. Sidorin, E. Syresin, G. Trubnikov, S. Yakovenko, Yu. Korotaev, A. Kobets
JINR Dubna
V.V. Balashov
Institute of Nuclear Physics, Moscow State University
S. G. Karshenboim
D.I. Mendeleev Institute for Metrology (VNIIM), St. Petersburg
L. N. Labzowsky, V. M. Shabaev
Department of Physics, St. Petersburg State University
A.V. Nefiodov
St. Petersburg Nuclear Physics Institute
L.A. Bureyeva
Institute of Spectroscopy of the RAS, Troitsk
S. Minaev
Institute for Experimental and Theoretical Physics, Moskva

SWEDEN
G. Andler, L. Bagge, H. Danared, M. Engström, A. Källberg, L. Liljeby, P. Löfgren, A. Paál, K.-G. Rensfelt, A. Simonsson, Ö. Skeppstedt
Manne Siegbahn Laboratory (MSL), Stockholm
R. Schuch, E. Lindroth
Department of Atomic Physics, Stockholm University

UNITED KINGDOM
R. McCullough
Queens University, Belfast, Ireland
M. Charlton, N. Madsen
Department of Physics, University of Wales Swansea

USA
G. Gabrielse
Department of Physics, Harvard University, Cambridge, Massachusetts
M.H. Holzscheiter, C. Maggiore
Pbar Labs, LLC Santa Fe, New Mexiko
B. Bassalleck
University of New Mexico, Albuquerque, New Mexico
Hans A. Schuessler
Department of Physics, Texas A&M University, College Station, Texas
Alan Kostelecky
Indiana University, Bloomington, Indiana
P. Kingsberry
Massachusetts Institute of Technology, Duke University, North Carolina

Members of the steering committee are underlined

Spokesperson:	Eberhard Widmann	eberhard.widmann@oeaw.ac.at	(+43 1) 4277 29701
Deputy:	Wolfgang Quint	w.quint@gsi.de	(+49) 6159-71-2141
	Jochen Walz	Jochen.Walz@uni-mainz.de	(+49) 6131-39-25976
Contact @ GSI:	Wolfgang Quint	w.quint@gsi.de	(+49) 6159-71-2141
Editor:	Carsten P. Welsch	carsten.welsch@mpi-hd.mpg.de	(+41) 79-261 17 34

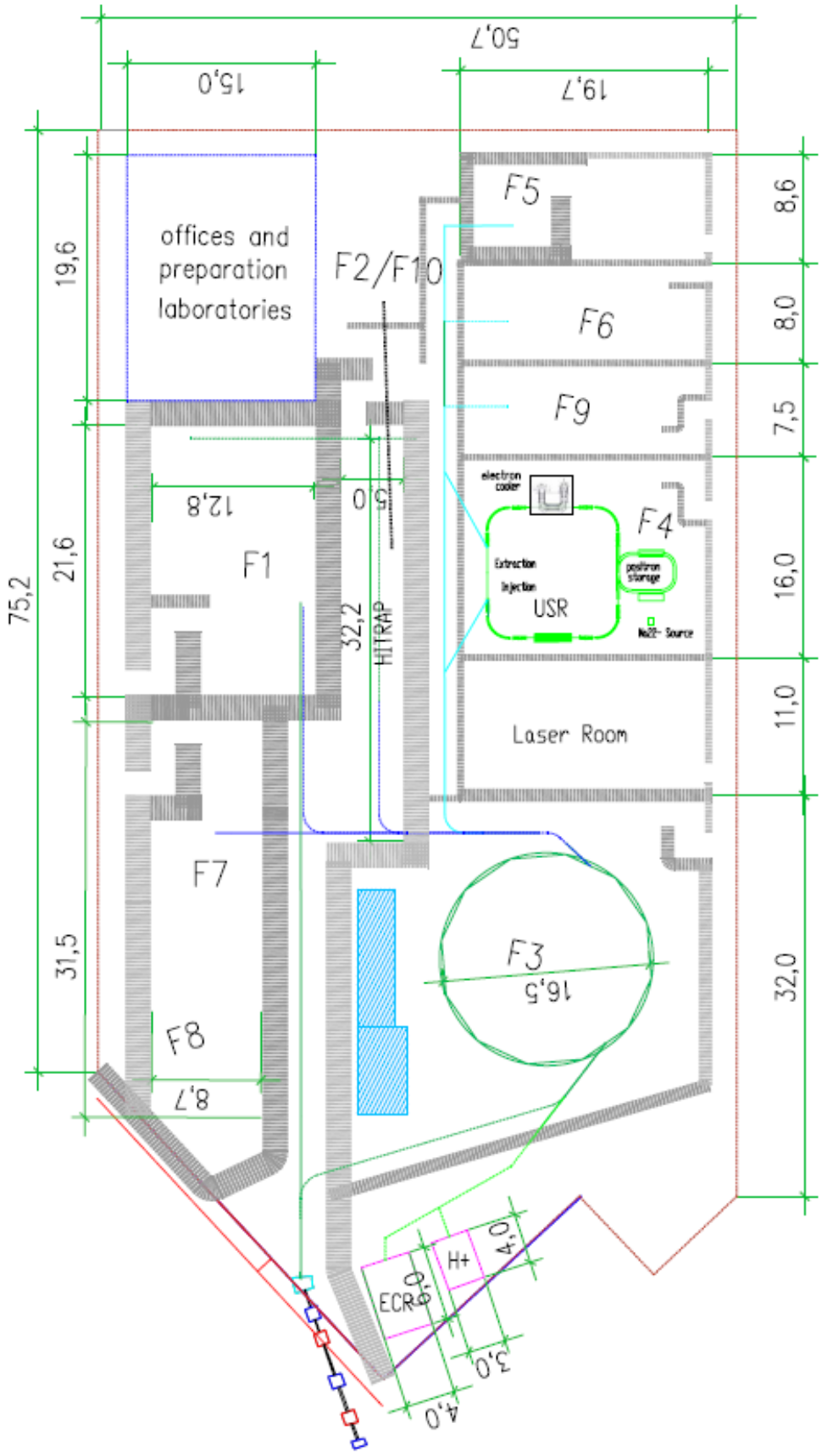

Fig. 1: Preliminary overview of the FLAIR facility.

Table 1: Experimental areas in the FLAIR building
(HCI = highly charged ions, RIB = radioactive ion beams)

Nr.	Area name	Beam parameters	Experiment	Area Responsible
1.	F1	HCI, E_{ion} < 130 MeV/u from NESR and LSR	Interaction of low-energy HCI with composite and solid targets	A. Bräuning-Demian *GSI Darmstadt*
2.	F2	HCI, E_{ion} = 4 MeV/u $\bar{p}$, E = 4 MeV from NESR and LSR	HITRAP	W. Quint *GSI Darmstadt*
3.	F3	HCI, E < 15 MeV/u $\bar{p}$, E = 30 MeV from NESR	Low-energy Storage Ring (LSR)	H. Danared *MSL, Stockholm*
4.	F4	$\bar{p}$, E < 300 keV from LSR	Ultra-low Energy Storage Ring (USR)	Carsten Welsch, Manfred Grieser *MPI, Heidelberg*
5.	F5	$\bar{p}$, E < 20 keV from USR	Antihydrogen-Experiment	J. Walz *MPQ Garching*
6.	F6	$\bar{p}$, E < 20 keV to rest from USR and HITRAP	Antihydrogen-Experiment	E. Widmann *SMI, Vienna*
7.	F7	$\bar{p}$, 300 keV < E < 30 MeV from LSR	Nuclear and particle physics with antiprotons	D. Grzonka *FZ Jülich*
8.	F8	$\bar{p}$, 30 MeV < E < 300 MeV from NESR	$\bar{p}$ interaction with biological probes	M. Holzscheiter, *Pbar Labs, USA*
9.	F9	$\bar{p}$, E < 20 keV from USR / HITRAP and RIBs from SFRS	Cusp trap for $\bar{H}$ production, $\bar{p}$ atom formation, $\bar{p}$ radioactive nuclei	M. Wada, Y. Yamazaki *Tokyo University*
10	F10	HCI and $\bar{p}$ in the keV energy range from HITRAP	Heavy-ion experiments, ion surface interaction, collision dynamics, $\bar{p}$ atom X-ray spectroscopy	W. Quint *GSI Darmstadt*

Table of Contents

A Introduction and Overview

The Future FAIR facility will produce the highest flux of antiprotons in the world. Within the planned complex of storage rings, it is possible to decelerate antiprotons to about 30 MeV kinetic energy, opening up the possibility to also create low-energy antiprotons. A letter of intent [1] has been presented to the APPA-PAC in January 2004 for FLAIR, a Facility for Low-energy Antiproton and Ion Research, and gotten the green light to produce the current document, the technical proposal for FLAIR.

Low-energy antiproton physics is currently being done at the Antiproton Decelerator (AD) of CERN, Geneva. Due to the low intensity ~ 10^5 $\bar{p}$/s and the availability of only pulsed extraction, the physics program is limited to the spectroscopy of antiprotonic atoms and antihydrogen formed in charged particle traps or by stopping antiprotons in low-density gas targets. Furthermore, the output energy of the AD (5 MeV kinetic energy) is still significantly higher than the < 100 keV energy best suited for these experiments.

A next-generation low-energy antiproton facility must overcome these limitations by providing cooled beams at higher intensities and a factor 10 or more lower energy. In addition it should have the possibility of slow (i. e. continuous) extraction, which will allow nuclear/particle physics type experiments requiring coincidence measurements to be performed. Here, we describe a facility consisting of two storage rings, a magnetic (LSR) and an electrostatic (USR) one, and a universal trap facility (HITRAP). These components of the facility can provide stored as well as fast and slow extracted cooled beams at energies between 30 MeV and 300 keV (LSR), between 300 keV and 20 keV (USR), and cooled particles at rest or at ultra-low eV energies (HITRAP). This will allow a large variety of new experiments to be performed, as described in section B4 and the FLAIR LOI [1]. Among the unique experiments only possible at such a facility are nuclear physics studies using antiprotons as a hadronic probe to investigate the structure of nuclei, including radioactive isotopes produced at the future facility, and many atomic-collision type experiments with internal targets in both storage rings with effective intensities as large as 10^{10} $\bar{p}$/s. An important synergetic aspect is that the whole structure will also be used to study highly charged ions, including storing, cooling (LSR, USR) and trapping them in Penning traps like HITRAP and investigating them in the new Low-energy HCI cave. The trap facility HITRAP and the new Low-energy HCI cave were already part of the atomic physics program of FAIR as described in the Conceptual Design Report [2] and were included into the LOI of the SPARC collaboration [3]. This proposal concentrates on physics with slow antiprotons, keeping in mind that the proposed facility is as well suited for experiments with stable or radioactive highly charged ions. The physics with highly charged ions will be presented in the technical proposal of the SPARC collaboration.

The planned LSR is a typical storage ring, and it is proposed to modify and transfer the CRYRING storage ring of the Manne Siegbahn Laboratory (MSL), Stockholm, to FLAIR. CRYRING is supposed to stop operation for physics within a few years, and its usage as well as the expertise provided by the staff of MSL is invaluable for FLAIR. The USR needs to be newly constructed. Electrostatic storage rings are already in operation in several places in the world (Denmark and Japan), and more are being planned for use in molecular physics. The MPI-K in Heidelberg presently designs such a next generation low-energy ring for molecules and highly-charged ions and will, in parallel, take over the responsibility for the development of key technologies needed for the USR.

The subprojects described in section B consist of “facilities” like the FLAIR building itself, LSR, USR, HITRAP, and the low-energy HCI cave, as well as the experiments that were proposed in the

FLAIR letter of intent. As the facilities are used for both antiprotons and highly charged ions, their description is also included into the technical proposal of the SPARC collaboration. For the experiments we restrict ourselves here to those using antiprotons, although some method will be also applied to HCI and are also listed in the SPARC TP.

Section B1.10 lists some experiments which were either not yet approved by the APPA PAC, or where the technically feasibility is not yet demonstrated. These are to be considered as options, which can be realized if approved by the PAC or after the technical questions will be solved. One of the topics, the experiment with antiprotonic radioactive nuclei (Exo+par, section B1.10.2), is also part of the NUSTAR proposal. This experiment requires a beam line for bringing short-lived unstable nuclei from the low-energy branch of the SuperFRS to FLAIR. The study of the feasibility of such a beam line was requested by the APPA PAC and is described in section C1.4. In the meantime, the AGATA experiment of NUSTAR has expressed interest to use low-energy continuous beam of HCI for in-beam spectroscopy. As shown in section C1.4, it is possible to design the beamline connecting FLAIR and SuperFRS in a way, that it can be used (in opposite directions) for both types of beam. The cost and final feasibility of this beam line depends strongly on the relative location of the FLAIR and SFRS buildings, which at the moment is uncertain because the overall planning of the FAIR civil construction is not yet finalized.

After the submission of the Technical Proposal to the APPA PAC in early 2005, a few new developments have happened which are reflected in this modified version of the original TP. On the one hand, a change in the overall layout of FAIR has allowed relaxing the previously strong constraint on the width of the FLAIR hall, making it easier to work on a design optimized for the needs of the experiments. New calculations of the radiation levels in the high-energy zones have verified the necessity of concrete wall thicknesses of 2-2.5 metres. A shift of the FLAIR hall with respect to the NESR has led to a design where the LSR and the low-energy antiproton areas are now located in the eastern part of the hall. This also affects the optional extraction of highly-charged ions towards the Superfragmentseperator easier as there is no more 180 degree bend needed. The beam line for this and for Exo+pbar is not any more shown in the layout of Fig. 1, but due to the low energies it can be added at a later stage without big effort. This reflects the situation that Exo+pbar was rejected by the PAC, but it was recommended to try to keep the option open for the future.

Last but not least a new experimental idea has emerged just short time ago: the possibility to produce deeply bound kaonic nuclear systems containing two antikaons (see sec. B1.11). This idea, which has not yet been discussed by a PAC, would require space for a large 4π detector, which is available in the combined F7/F8 areas. The emerging of such a new idea shows that the field of physics with low-energy antiprotons and ions is vivid and that more ideas are likely to appear until the start of operation of FLAIR. Therefore the design has to be kept as flexible as possible, allowing for changes of the layout even after construction of the building by e.g. making as many of the walls as possible out of concrete blocks rather than rigid structures.

B Systems / Facilities

1.1 The FLAIR Hall

The experiments which use decelerated and cooled Highly Charged Ions and Antiprotons with rigidities below 4 Tm (E_{ion} < 130 MeV/u and E_{pbar}< 700 MeV) extracted (slow and fast) from the NESR will be accommodated in the FLAIR building, placed in the neighbourhood of the NESR.

This building is designed as a complex which includes the experimental areas requested by the experiments presented in the LoIs submitted by the FLAIR and SPARC collaborations, the hall for the Low-Energy Storage Ring (LSR) an the additional areas needed for the off-line mounting and testing of the setups, control and data acquisition rooms, laser labs, power supplies storage rooms, a small workshop and social rooms. The floor space needed only for the proposed experimental setups, both for $\bar{p}$'s and HCI, of about 3200 m^2, is divided between

- the low-energy antiproton experimental areas (41%) : the halls F4 to F9
- the low energy highly charged ions experimental areas (14%): F1 and F2
- the Low-Energy Storage Ring (LSR) (21%): F3

The difference of about 24% of the building area is needed for the beam lines, shielding and access ways. In Table 1 the sharing of the experimental area between different experiments, as proposed today, is presented.

F1 to F9 areas will be placed on the ground floor. Due to the trap design (see subsection 1.4), part of the experiments using decelerated and stored ions at HITRAP will be placed on the top of the F2 cave and request an area F10 of about 140 m^2. Another part will be performed in area F1.

A preliminary layout of the FLAIR building (only the ground floor) is presented in Fig. 1. This layout is based on estimations of the beam transport from the NESR - parallel and through the LSR- towards the experimental areas and partly considers the beam parameters requested at different experimental places. The subsequent deceleration of the antiprotons requested by different experiments (especially for trapping) implies a certain relative location of the LSR, USR, HITRAP and the experiments. This puts some constraints on the building layout (minimum width of about 50 m, minimum length of about 75 m). The final layout depends also on the FLAIR location within the general FAIR layout and will be established after more detailed beam transport simulations and in consent with the civil construction planner.

The main FLAIR building is planned to be a light construction with a clearance of 10 m. Inside, the different experimental areas will be separated by concrete walls of different thicknesses, as imposed by the radiation safety rules (for details see Section C). Although the clearance of the different experimental areas will differ, depending on the geometry of the accommodated setup and the ceiling thickness, it is planned to partly use the second floor, where it is possible, as storage, mounting and/or data acquisition rooms.

Additionally, an area of 700 m^2, distributed over two storeys is requested for off-line mounting and testing, laser labs, control rooms, social rooms (see section C1.6).

1.2 The Low Energy Storage Ring (LSR)

1.2.1 Introduction

CRYRING is an accelerator facility at the Manne Siegbahn Laboratory (MSL) at Stockholm University. Its main components are a 52-m-circumference synchrotron and storage ring with electron cooling, an RFQ, an EBIS ion source, an ECR ion source and ion-source platform for singly charged ions. CRYRING has been in operation since 1992 for experiments mainly in atomic and molecular physics, but also in accelerator physics and applied physics. In 2002, the Swedish Research Council decided to discontinue the funding of the facility, and it was agreed with Stockholm University in 2003 that funding level should reach zero by the end of 2006.

Since the CRYRING synchrotron has an energy range from approximately 300 keV (for protons) and up to the lowest energies that can be reached with the NESR ring at FAIR, and since it has already been operating with acceleration and deceleration and has the required beam cooling, vacuum, etc., it has been suggested that CRYRING be moved to FAIR for use as the LSR ring of FLAIR, decelerating antiprotons and highly charged ions behind the NESR. The LSR/CRYRING installation would, in addition to the synchrotron, include a dedicated low-energy injector for commissioning of the FLAIR facility and its experiments, as well as for training of operators, continuous development of the facility and experiments with ions of other species than those provided from the NESR.

The Manne Siegbahn Laboratory proposes to move CRYRING, including the low-energy injector, to FAIR as a complete system. This includes that MSL takes part in the planning of the FAIR infrastructure related to LSR/CRYRING, designs the modifications that are necessary for the new role of the ring, implements and commissions these modifications at MSL as far as it is possible, and disassembles the ring with all its sub-systems and ships it to FAIR at the time when the FLAIR building is ready to receive it. Up until that time, the ring is kept in operation, albeit at a rather small scale, at MSL, and it is maintained such that it is a fully functional machine that is moved to FAIR. MSL could also take part in the reassembly and re-commissioning of the ring at FAIR.

In the following, we will describe those properties of CRYRING that are most relevant to its proposed new role, the modifications that will have to be made to it and the requirements on the FAIR infrastructure that are needed for a re-installation of CRYRING at FAIR and FLAIR.

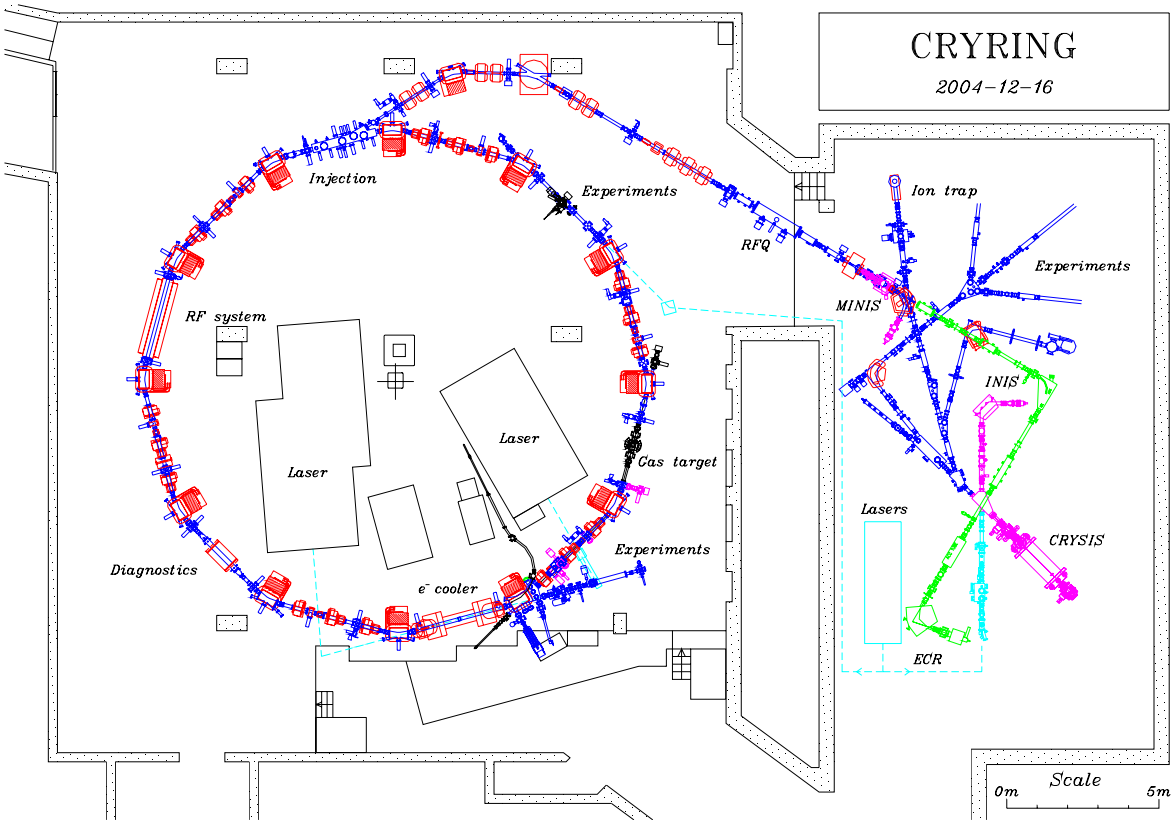

Fig. 2: Present layout of the CRYRING facility at the Manne Siegbahn Laboratory

1.2.2 Low-Energy Injector

a) Singly Charged Ions

The dedicated low-energy injector for LSR/CRYRING will provide protons and H^- for commissioning of the antiproton part of the FLAIR facility. Ion sources for protons and H– will be mounted on a high-voltage platform similar to the present MINIS platform at MSL. For protons and H^-, the platform voltage needs to be 10 kV, and the particles will then be accelerated by the present CRYRING RFQ from 10 keV/u to 300 keV/u, the latter being the present injection energy in CRYRING when ions are accelerated in the RFQ.

The RFQ is designed for ions with mass-to-charge ratios, m/q, between –4 and 4, but ions outside that range can be transported through the RFQ without acceleration, and they are then injected into the ring at the energy defined by the ion-source platform voltage. The platform voltage is at present usually 40 kV. With or without acceleration in the RFQ, ions with m/q between 1 and 208 and between –1 and –130 have been injected into CRYRING.

b) Highly Charged Ions

The injector will also have an ECR (electron cyclotron resonance) ion source for commissioning of the atomic-physics part of FLAIR, and possibly also for experiments using highly charged ions. The CRYRING facility at MSL is operating with an ECR ion source on a 300-kV platform, injecting

through the RFQ. Whether such an arrangement will be used at FLAIR is still a subject of investigation (c.f. Milestones). Other alternatives are a smaller platform and/or a new RFQ.

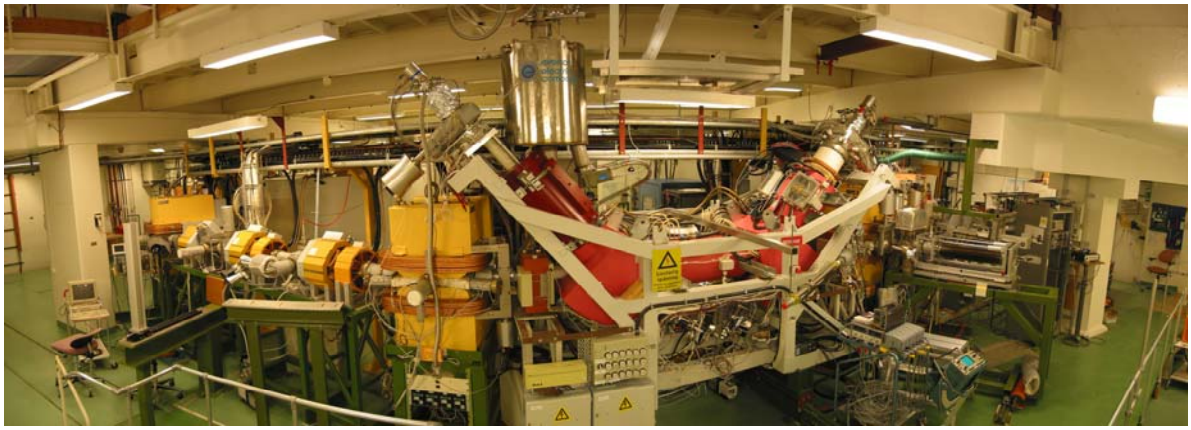

Fig. 3 Fish-eye view of the CRYRING synchrotron and its electron cooler

1.2.3 Synchrotron

a) Introduction

It is proposed that the CRYRING synchrotron is moved to FLAIR with essentially all its present components, including magnets, vacuum system, rf system for acceleration/deceleration, electron cooler, diagnostics, power supplies, etc. The only major modifications to be done is to replace the injection system with a new one that allows injection of 30 MeV antiprotons from NESR, or ions of the same rigidity, and to add an extraction beamline. In addition, a number of old power supplies should be changed to new ones of more modern design.

CRYRING has a maximum magnetic rigidity of 1.44 Tm, corresponding to 96 MeV (anti)protons. The minimum rigidity is 0.052 Tm, corresponding to 130 keV (anti)protons, but operation becomes increasingly difficult below 0.08 Tm or 300 keV (anti)protons due to remanence and hysteresis effects in the ring magnets. Transfer of antiprotons and ions from the NESR to LSR/CRYRING is foreseen to take place at the rigidity of 30 MeV antiprotons, i.e. 0.80 Tm. The beam from the NESR is cooled at the NESR extraction energy, so it can be decelerated immediately after injection into LSR/CRYRING to an intermediate energy of around 4 MeV/u. At that energy the beam will be electron-cooled for one or a few seconds, then decelerated to the extraction energy of 300 keV/u, where it will be electron-cooled again before actually being extracted. Alternatively, the deceleration cycle can be interrupted at a higher energy for experiments that need beam above 300 keV/u. As an example, extraction to HITRAP would take place at 4 MeV/u immediately after electron cooling at that energy. The optimum sequence for deceleration and cooling will be investigated at MSL. This can be done by accelerating protons to 30 MeV, manipulating the phase-space in order to approximate a beam injected from NESR, and then decelerating again and cooling.

b) Subsystems

Magnets: The synchrotron has 12 dipole magnets, 18 quadrupole magnets, 12 sextupole magnets and 12 correction dipoles. These will be moved to FLAIR, together with their power supplies, essentially without modifications. A particular feature of CRYRING is its two ramping modes: In the fast ramping mode, the magnet current can ramp from 10% to 90% of full value, or vice versa, in 150 ms, and in the slow mode the ramping time is 1 s or longer. The fast ramping requires a higher rf voltage and is therefore not the standard mode of operation at present, although it has been used for a small number of experiments where the lifetime of the ionic state being studied has been very short.

Injection: The present injection system in CRYRING is designed for 300 keV/u, and it must thus be completely redesigned. This design has only begun, and at present a system combining fast injection of a short antiproton bunch at 30 MeV/u (or ions of the same rigidity) and multiturn injection of low-energy ions from the dedicated injector is being considered. The injection channel has a magnetic septum followed by two short pairs of electrostatic deflectors. The electrostatic deflectors are active only for low-energy injection and compensate the thickness of the magnetic septum. The injection straight section also has four pairs of electrostatic deflectors that produce the closed-orbit deformation needed for the multiturn injection. There is also a magnetic kicker in a ceramic vacuum chamber at a suitable betatron phase advance for the high-energy injection.

Extraction: CRYRING was designed with extraction in mind, and one of the straight sections that are at present used for experiments will be rebuilt to house the extraction channel with a septum magnet. Both slow, resonant extraction and fast kicker extraction will be available at all beam energies. The slow extraction will use a third-order resonance, and the sextupoles needed to drive that resonance are already part of the machine. For slow extraction an additional electrostatic septum on another straight section will be needed, and for the fast extraction a kicker magnet with a ceramic vacuum chamber must be installed. The new injection and extraction should, as far as possible, use standardized hardware (septum magnets, kickers, etc.) being developed at GSI for other machines in the FAIR complex.

Radio frequency: The acceleration/deceleration in CRYRING uses a non-resonant driven drift tube rather than a more common resonant cavity. The drift tube, 2.7 m long, is connected to a power amplifier providing up to 7.5 kV peak-to-peak on the drift tube, or an effective acceleration/deceleration voltage of 2.5 kV, between 40 kHz and 2.5 MHz. For slow ramping, only about 1 kV on the drift tube is needed. The present installation uses several old power supplies that will be replaced by new ones before the move to FLAIR. The exact extent of the modifications will depend on the need for fast ramping at FLAIR.

Electron cooling: The use of electron cooling is necessary to keep the beam emittance small during deceleration. No modifications of the present cooler are foreseen, and it is planned that the superconducting gun solenoid is kept. The superconducting solenoid, allowing larger electron-beam expansion and lower electron temperature, is not needed for cooling of antiprotons. It is, however, of considerable interest to the SPARC community, thus motivating the extra cost of handling liquid helium.

Vacuum: Pumping in CRYRING relies mainly on NEG (non-evapourable getter) pumps, with ion pumps for gases that are not pumped by the NEG. There are also turbo-molecular pumps giving extra pumping speed for heavy rest-gas components. The entire vacuum system is bakeable to 300 degrees. The true average pressure in the ring (mainly H_2) is approximately 1×10^{-11} torr,

corresponding to less than 7.5×10^{-12} torr nitrogen-equivalent pressure. This pressure is fully sufficient for antiprotons at all energies, but it will limit the lifetime of heavy, highly charged ions to, in some cases, less than 100 ms at the lowest energies.

Diagnostics: CRYRING is equipped with sensitive diagnostics of different kinds: In the injection line, and to some extent also in the ring, destructive diagnostics such as fluorescent screens, strip detectors and Faraday cups are used. In the ring there are in addition DC and AC beam transformers for absolute current measurements, electrostatic pickups for measuring the beam position and also Q values with the help of horizontal and vertical kickers, residual-gas beam profile monitors and a Schottky detector for longitudinal and transverse Schottky signals. These will all be included in the move to FLAIR. With the exception of instrumentation for closed-orbit measurements that needs improvement, the diagnostics is fully up-to-date and adequate for the new role of CRYRING.

Power supplies: The ring and the injector have a large number of power supplies. The large supplies for the ring dipoles, quadrupoles and the electron-cooler magnets together with switchgear and transformers will probably have to be disassembled, moved and reassembled by Imtech Vonk, a company related to the manufacturer Holec. Many of the smaller supplies can be moved as they are, but some are old and must be replaced by new ones. In particular this applies to supplies for magnets in the injection line and some supplies used for the acceleration system. If funding can be obtained well in advance, these can be installed and commissioned at MSL before the ring is transferred to FLAIR.

1.2.4 Control System

CRYRING at present has its own pc-based control system which was taken into operation in 2003. The software of the control system was developed at Aarhus University, originally for use at the ASTRID storage ring, and is fully modern. The hardware is based on older standards such as G64 and CAMAC, with some more recent additions based on newer standards. While it will be perfectly possible to continue running LSR/CRYRING with this system, there ought to be a substantial advantage in integrating not only the LSR/CRYRING controls and diagnostics, but also the control of all beamlines in the FLAIR hall into the general FAIR control system. No reliable cost estimate is available at the moment for the integration of LSR/CRYRING into the FAIR control system.

1.2.5 Beam Transfer from NESR

We at present assume that a cooled beam in NESR with an emittance of 1 π mm·mrad or better is transferred to LSR/CRYRING in a single bunch, and that the rigidity of the transferred beam is that of 30 MeV antiprotons. As an alternative, in order to reduce the incoherent tune shift in LSR/CRYRING, the NESR beam could be bunched at a higher harmonic, and the smaller bunches could be transferred and decelerated in successive machine cycles of LSR/CRYRING. The space-charge limit is discussed further in the following paragraph. Details of the transfer must be coordinated with the NESR team.

1.2.6 Intensity Limits

In CRYRING, the space-charge limit for a coasting beam of protons at 300 keV is $N = 5\times10^{8}$, assuming $\Delta Q = -0.1$ and $\varepsilon = 1\ \pi$ mm mrad. The electron cooling at 300 keV is probably not strong enough to reach down to 1 π mm mrad with 5×10^{8} particles, but in a recent quick test it was shown that 1×10^{8} protons could be stored at 300 keV with an emittance of approximately 1 π mm mrad. This is thus, at a minimum, what LSR/CRYRING should be able to deliver once every NESR cycle

of 20 s, losses during extraction not counted. Since the space-charge limit is proportional to energy (non-relativistically) while equilibrium emittances in our case shrink with energy, one can expect that the number of antiprotons per unit time and emittance increases at least linearly with energy.

Some improvement could be obtained if the NESR beam is bunched at the 4th harmonic before extraction, and the four bunches are transfered to LSR/CRYRING and decelerated in four consecutive machine cycles. Each cycle taking about 5 s, LSR/CRYRING could thus be able to deliver four batches of 1×10^8 antiprotons, minus extraction losses, within approximately 1 π mm mrad emittance every 40 s.

For highly charged ions, the space-charge limit scales with A/Z^2. The rates for intrabeam scattering and electron cooling also change, such that one can expect that the equilibrium emittance, at the space-charge limit, does not depend strongly on the ion species for a given particle velocity. Again, the emittance shrinks with increasing energy. From this scaling, we can find, for example, that 1×10^8 antiprotons at 300 keV corresponds to 4×10^7 U^{92+} at 4 MeV/u.

1.2.7 Building, Facilities

The hall for LSR/CRYRING should preferably be big enough to have 3 m free space between the ring (which has a diameter of 16.5 m) and the walls. Additional space is needed for the injectors. The power supplies, except main magnet power supplies, need a floor space of approximately 40 m^2 plus some space inside the ring. Also the 40 m^2 area could be inside the ring, although this would make access more difficult. Another alternative would be on a second floor above the ring. At MSL, the main magnet power supplies at present occupy a hall of dimensions 10×18 m^2, which could perhaps be reduced to 9×15 m^2 with the entrance at an optimal location. The height of this hall is 4 m (with a computer floor at 0.9 m and 3.1 m above that). In addition, switchgear occupy 3.6×11 m^2 and transformers 4×7 m^2, although these need not be located in the FLAIR building if one accepts the cost for longer cables.

The heaviest parts of CRYRING are the dipole magnets with a weight of 4.5 tons each and a footprint of approximately 1 m^2. Total weight is estimated at 100 tons.

Beam height of CRYRING is at present 1.5 m, but it is suggested that this be increased to 2.0 m at FLAIR.

Required crane hook height is approximately 5.5 m and required ceiling height is approximately 6.0 m with 2.0 m beam height.

Power supplies consume, at maximum load, 1 MW active power and 3.5 MVA reactive power. Input voltages are 10 kV, 400 V and 230 V at 50 Hz.

A water-cooling capacity corresponding to the active power is required at 7 bar and 4 bar overpressure. Also, a cooling system with 3.5 bar and 10°C is used at present.

According to a rough estimate, 25 kW is released into the air.

Compressed air in the vicinity of LSR/CRYRING is required.

The superconducting electron-cooler magnet consumes approximately 50 l of liquid helium per week.

1.2.8 Alignment and Commissioning

The initial alignment of CRYRING used a Distometer together with calibrated invar wires for distance measurements, a level instrument, a theodolite and a number of specially made mechanical devices like targets for the optical instruments and devices for attaching the Distometer and its invar wires to the magnets and a central pylon. All these are still available at MSL. Although the original alignment was made using the magnet gaps as references, there are also fiducials on the top of the magnets, allowing the alignment to be checked after the gaps have been filled with vacuum chambers. Alignment issues will put restrictions on the positioning of columns for roof support inside the ring. The realignment at FLAIR can use much of the existing equipment but should be done in collaboration with GSI.

Commissioning of LSR/CRYRING, as well as other equipment in the FLAIR building, can be made using the dedicated low-energy injector. This means that commissioning of the ring with protons, H^- or highly charged ions can start as soon as assembly and alignment has been completed, provided that the relevant infrastructure in terms of electrical power, cooling water, etc. is available in the FLAIR building. Also the control system for the ring, which preferably is integrated into the general FAIR control system (see above), must be available. Beamlines, the USR ring and parts of experiments can be commissioned with the same ions as soon as they, together with controls and diagnostics, are ready to accept the beam from LSR/CRYRING.

1.3 The Ultra-low Energy Storage Ring (USR)

1.3.1 General remarks

The ultra-low energy storage ring (USR) shall provide antiprotons in the energy range between 20 keV and 300 keV for both in-ring experiments and effective injection into traps. The machine is of central importance for essentially all experiments exploring antimatter–matter interactions, for in-ring experiments at an internal gas jet target, as well as for all experiments employing traps as they can be efficiently filled using the decelerated and cooled antiproton beam.
In this energy range – especially if one thinks about realizing a real multi-purpose facility with not only antiprotons but also various highly-charged stable and radioactive ions to be stored and investigated – electrostatic storage rings have clear advantages compared to their magnetic counterparts. In case one envisions to even approach the eV range, which is highly desirable for some very interesting experiments with the antiprotons (formation of a slow antihydrogen beam for hyperfine structure measurements and precision spectroscopy, formation of antiprotonic atoms in collisions with atoms, etc.) electrostatic machines are the only possible choice.
Aiming to be a true multiuser facility, the ring should provide an antiproton beam that can be used by various in-ring and external experiments "at the same time", i.e. from bunch to bunch, the different experiments may be served at different energies of the antiprotons, different intensities and beam characteristics (bunched, slowly extracted quasi-dc operation).
High luminosity, low emittance and low momentum spread are some of the main characteristics of the electron-cooled antiproton beam that shall be achieved and that the various experiments may take advantage of. Some experience is available on the international scene although many of the key challenges like ultra-short pulses and electron cooling at lowest energies have never been realized so far. However, electrostatic storage rings in Denmark [4] and Japan [5] could already prove the benefits from the mass independence of the electrostatic rigidity in these machines for a variety of research areas. Various geometrical shapes can be realized [6], where the size of the machine is mainly determined by the size of the electron cooler and the experimental sections.
For the USR to fulfill its key role in the FLAIR project, the development of novel and challenging methods and technologies is required: Combination of the electrostatic storage mode with a deceleration of the antiprotons from 300 keV to 20 keV (as needed for in-ring experiments as well as for efficient injection into traps), electron cooling at all energies for the phase-space optimization of the stored beam, RF bunching for in-ring experiments with the reaction microscope and for the deceleration process, as well as incorporation of an internal gas jet and an in-ring reaction microscope for collision experiments. A cryogenic storage ring (CSR) planned at MPI-K [7] shall prove the technical feasibility of the machine and serve as a test stand for most practical challenges.

Presently, there are two options under discussion, which will be presented at the end of this section. First, the USR could be used for a much broader physics program if the storage of highly charged stable and radioactive ions would be included. Nuclear properties of isotopes far-off stability could be investigated with unprecedented precision by laser spectroscopy of the hyperfine transition in one- or few-electron systems or by dielectronic resonances since uncertainties due to many-electron contributions are avoided. Collisions of highly charged ions with atoms involve few to many-electron transfer reactions proceeding within the collision time between a few femtoseconds down to a few attoseconds, thus being ideal prototype reactions to explore ultra-fast, correlated electron dynamics. Such a program would require vacuum conditions better than 10^{-13} mbar in order to achieve adequate beam life times and thus, the USR would have to be operated at a few degrees Kelvin.

A second option could be a merged positron beam for in-flight creation of antihydrogen. Even though technical requirements would be similar to the original design, modifications in the machine layout are necessary to guarantee easy access to the neutral beam.

1.3.2 Ring Layout

The symmetric, four sided machine consists of 90° cylinder deflectors and quadrupole doublets that are used for transverse modulation of the beam. As can be seen in Fig. 4, the experimental sections and the integrated electron cooler mainly determine the overall size of roughly 6m x 6m of the storage ring.

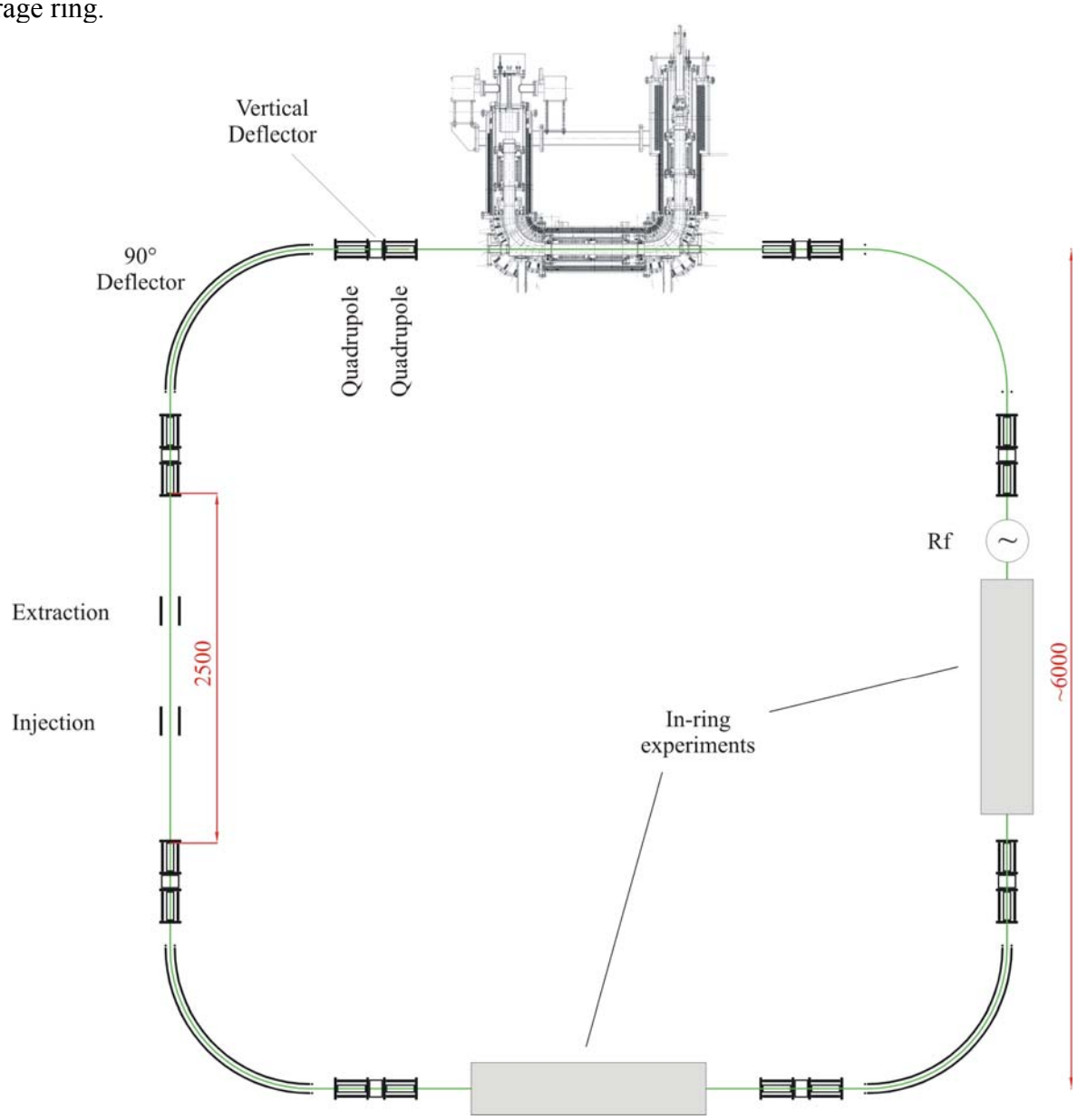

Fig. 4: Overview of the USR

Single turn injection of the beam will be realized by a pulsed deflector. Both slow and fast extraction will be available over the complete energy range. In contrast to existing or planned fixed energy electrostatic machines [4], [5], [8], [9] an rf operated drift tube with voltages < 100 V is used in combination with an electron cooler to obtain a longitudinal small bunches for in-ring experiments.

Depending on the experimental needs, the machine can be set to different modes. Four working points and the surrounding stable regions are shown in the following stability diagram, Fig. 5.

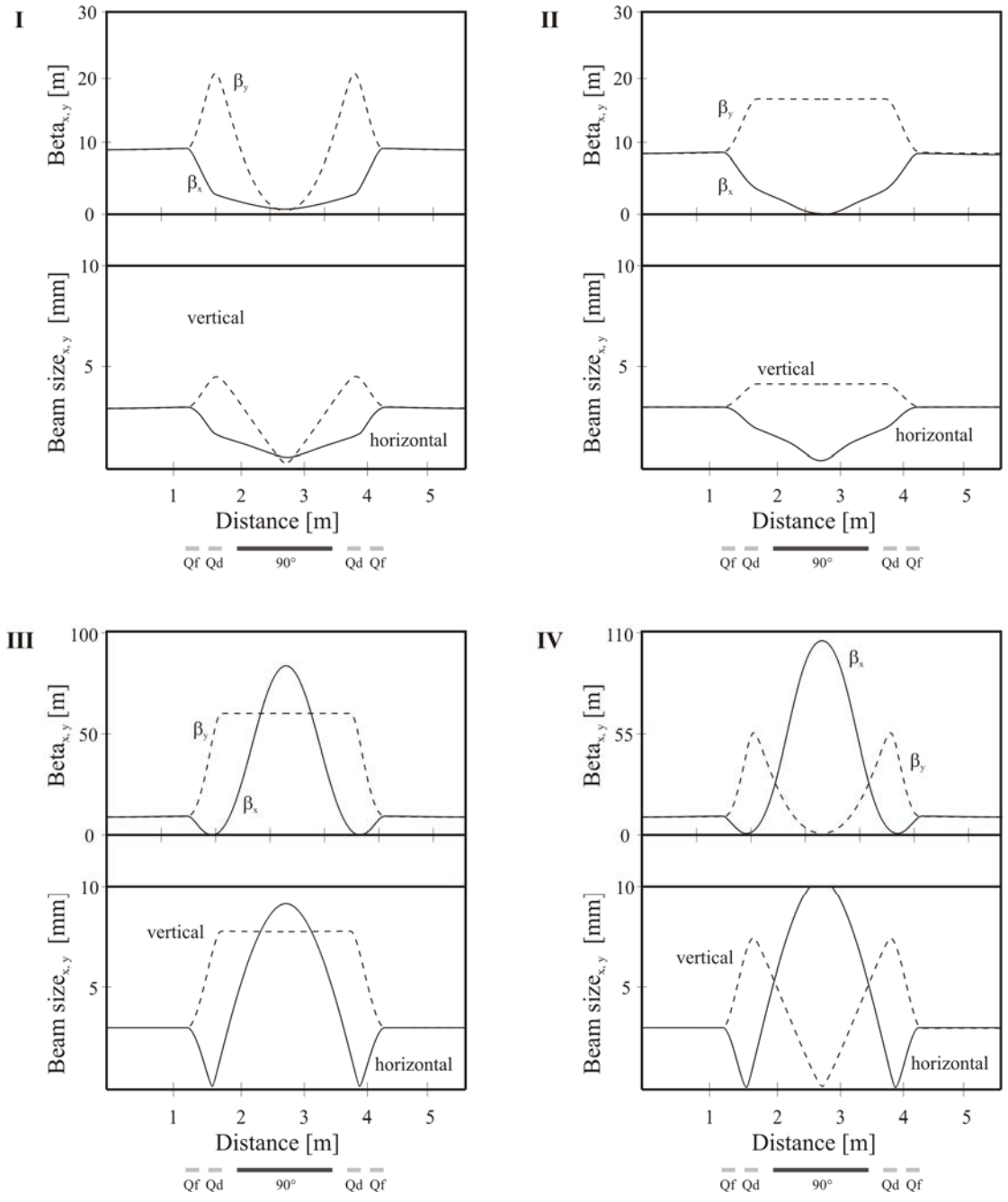

Fig. 5: Lattice functions and sizes in a quarter ring section at working points I – IV. Detailed description in the text

All calculations were made for an antiproton beam with an emittance of $\varepsilon = 1 \cdot mm \cdot mrad$ and an initial momentum spread of $\Delta p/p = 1 \cdot 10^{-3}$. The necessary quadrupole strengths at working point I are $k_x = 7.6\ m^{-2}$ and $k_y = -10.4\ m^{-2}$, with chromaticities $\xi_x = -3.8$ and $\xi_y = -13.7$, respectively, where $\xi_i = \Delta Q_i / (\Delta p / p)$ and $k_i = q \cdot U_i / (E_{Kin} \cdot r_{ap}^2)$.

At point II, the corresponding quadrupole strengths are k_x=*4.9* m^{-2} and k_y=*-3.9* m^{-2}, with respective chromaticities ξ_x=*-3.0* and ξ_y=*-1.5*. A beam waist present at working point I and, thus, higher space charge forces occur. This waist is not obtained at point II where the vertical size is always larger inside the 90° deflector.

Stable conditions exist also at working points III and IV, where k_x=*19.5* m^{-2} and k_y=*-9.3* m^{-2}, with chromaticities ξ_x=*-14.1* and ξ_y=*-24.6* for the former and k_x=*20.2* m^{-2} and k_y=*-14.9* m^{-2}, with chromaticities ξ_x=*-12.7* and ξ_y=*-51.8* for the latter. Regardless of the high chromaticities, these points are less suitable for beam storing since the horizontal beam size reaches its maximum inside the cylinder deflector, where the mechanical aperture is smallest. The calculated tune values are shown in Fig. 6 together with resonances up to third order.

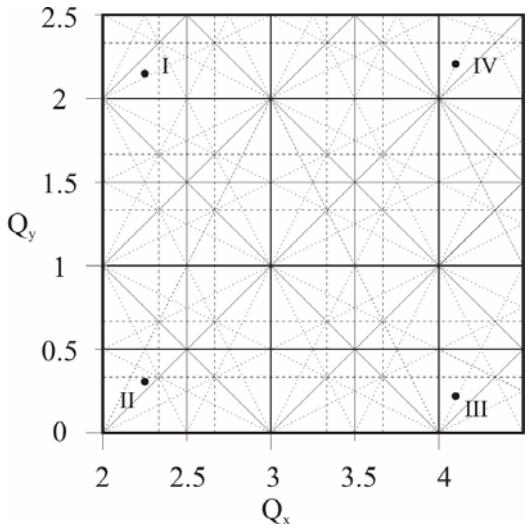

Fig. 6: Tune values in horizontal (Q_x) and vertical (Q_y) directions at working points I – IV

As an illustration, the motion of the beam through one complete quarter ring section at working point I is shown in Fig. 8. Corresponding to an emittance of 1 mm·mrad, the initial coordinates in both transverse dimensions were assumed to be 3 mm and 0.33 mrad (1). After a short drift to the first quadrupole (2), the beam gets focused in horizontal phase space, while it gets defocused in vertical phase space (3, 4). The second quadrupole turns the ellipses again (5, 6) and leads to a focusing in both planes. At the symmetry point in the middle of the 90° deflector both phase space ellipses are upright (7).

Since the all optical elements are mirrored along the center of the cylinder deflector, the phase space representation of the beam motion is also mirrored and follows the same sequence as before (8-13). Fig. 7 illustrates the positions at which the ellipses are drawn.

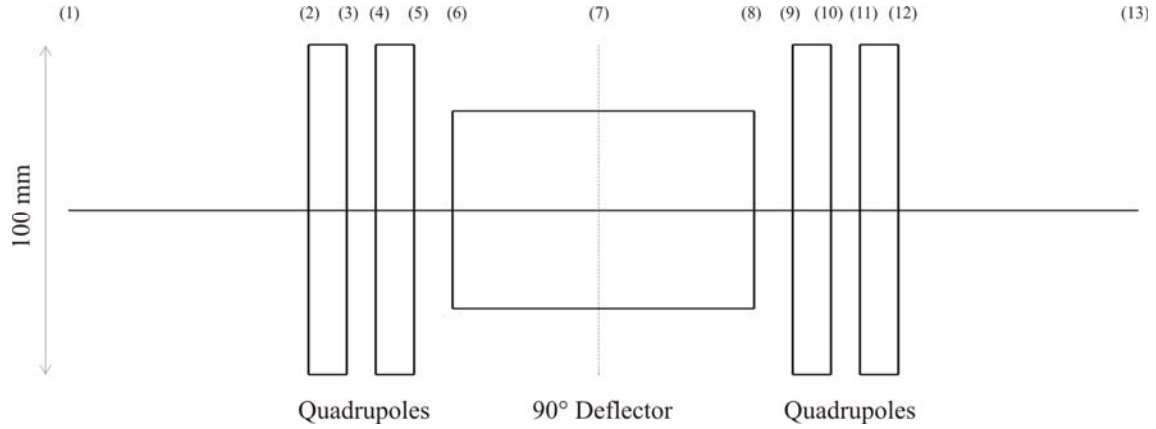

Fig. 7: Side view of one quarter ring section. The positions at which the phase space ellipses are drawn are numbered.

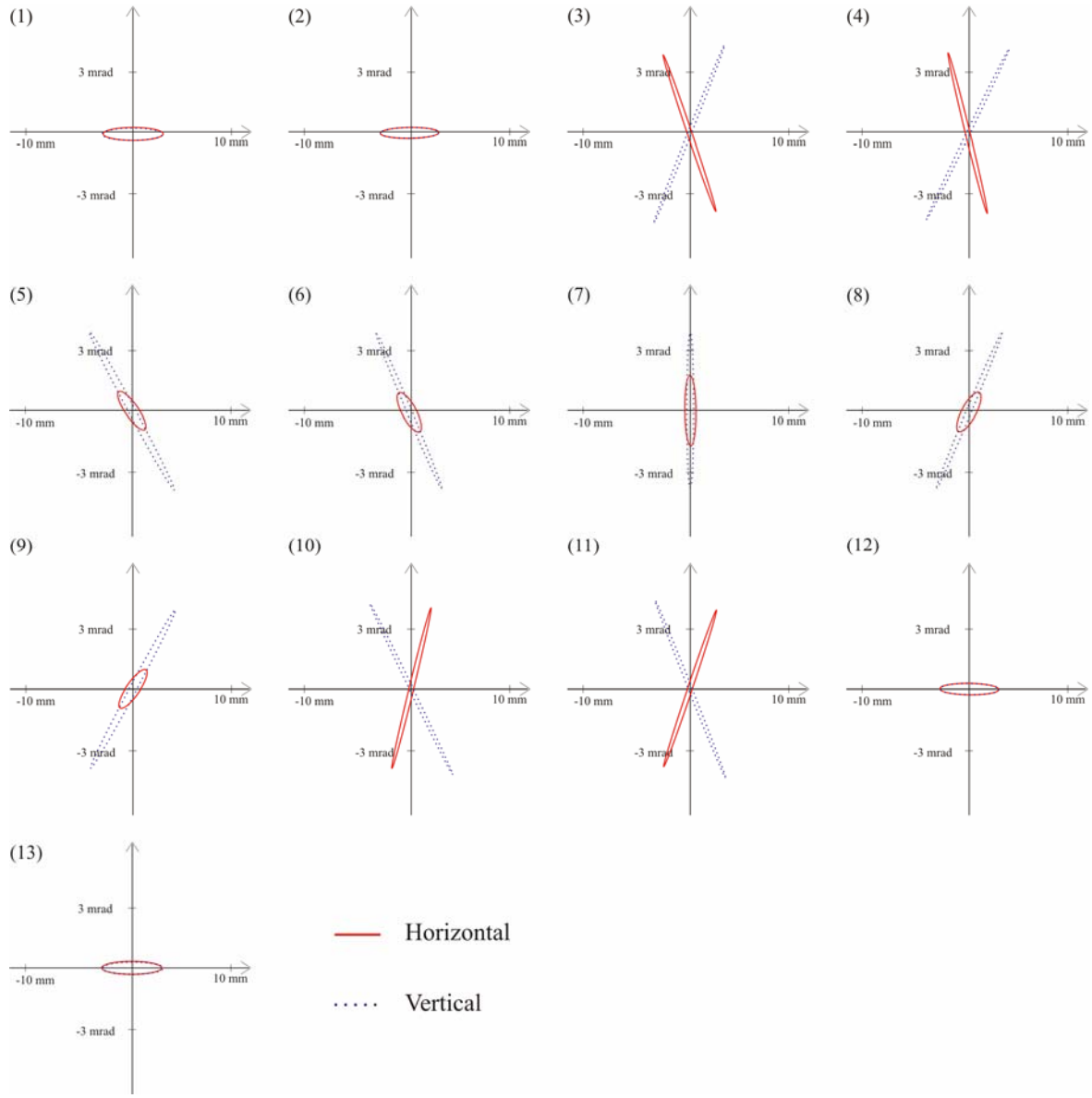

Fig. 8: Beam ellipses in transverse phase space through one quarter ring section

1.3.3 Optical Elements

Exclusively electrostatic elements are used throughout the USR. Besides the already mentioned mass-independence of the electrostatic rigidity, this has the clear advantage to allow stable storing of ions at energies as low as a few 10 keV. The lattice was kept as simple as possible in order to guarantee easy operation and reduce costs. All voltages were kept below 30 kV.

a) 90° Cylinder Deflector

The entire bending in the storage ring is achieved using 90° cylinder deflectors as shown in Fig. 9. These consist of two metal electrodes with a central bending radius of 1 m. They measure 160 mm in height and are placed at a distance of 60 mm. Grounded shields at the entrance and exit of each bend reduce the extension of the fringe fields to small region of 20 mm. The necessary field to bend 300 keV antiprotons leads to voltages of +/- 19 kV on the electrodes.

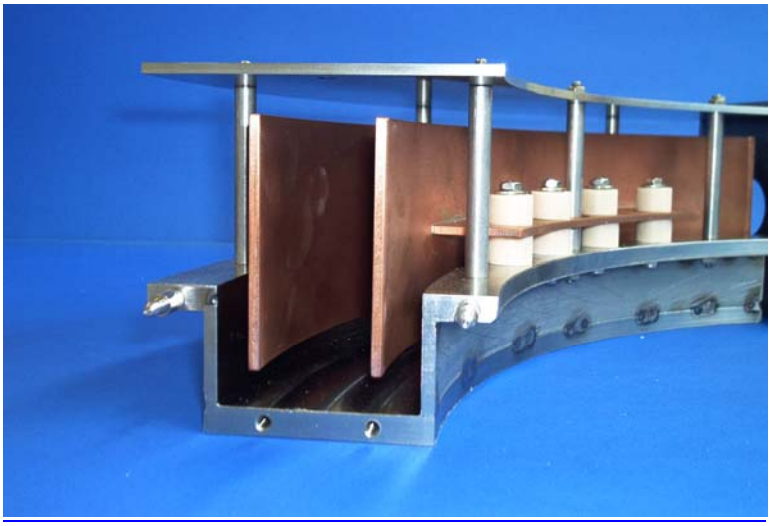

Fig. 9: Electrostatic cylinder deflector [8]

In an electrostatic cylinder deflector there is always an unavoidable coupling between transverse and longitudinal phase space. In order to find out how large these defocusing effects are, tracking simulations were done with COSY infinity [10].

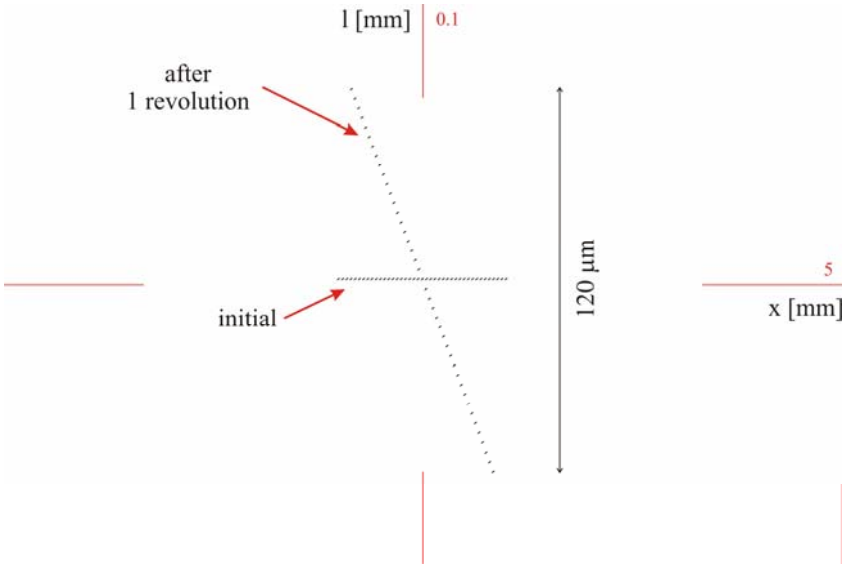

Fig. 10: Minimum longitudinal dispersion in the USR after one revolution in the machine

The minimum extension in the longitudinal direction can be found if one assumes an initially perfect beam with zero length, Fig. 10. Therefore, 40 particles where placed inside an initial beam radius of 1 mm. After one revolution, the length of the bunch is +/- 60µm, which corresponds to a time structure of 75 ps at 300 keV and 300 ps at 20 keV beam energy. With the integrated rf buncher and longitudinal and transversal cooling it should be possible to counteract this effect. However, intra beam scattering also leads to longitudinal defocusing of the beam and is particularly strong at these low energies. Since theoretical models can hardly predict the amount of additional dispersion caused by the ion-ion interaction at these low energies, systematic measurements will be carried out at the TSR in Heidelberg.

b) Quadrupole Doublets

The transverse modulation of the beam is controlled by electrostatic quadrupole doublets. In existing electrostatic storage rings, closed orbit correction is accomplished with additional steerers placed closed to the corner sections of the machine. In a very compact machine like the USR, this space is not available. For that reason and for a clear decoupling of the quadrupole lenses [11], a vertical steerer was introduced between each two quadrupoles as shown in Fig. 11.

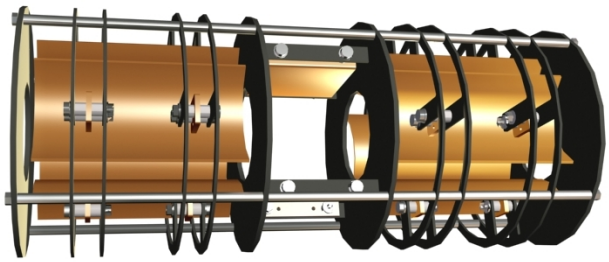

Fig. 11: Electrostatic quadrupole doublet with integrated steerer

The distance between the two quadrupoles was extended to 150 mm, which completely decouples the fields of the elements. In case the beam is disturbed by e.g. field errors, small voltages can be applied on the vertical steerer to counteract beam shifts. The horizontal steering is achieved by the

parallel plate deflectors used for injection and extraction. On both elements small voltages can be added, if necessary.

The electric and mechanic parameters of the machine and its components are summarized in Table 2.

Table 2: Summary of design parameters

General Parameters	
Energy range	20 keV – 300 keV
Circumference	22.28 m
Base pressure	< 5.10-11 mbar
90° Deflectors	
Height	160 mm
Radii	970 mm and 1030 mm
Shield Distance	15 mm
Voltage |U|	< 20 kV
Quadrupoles	
Length	200 mm
Distance between lenses	150 mm
Aperture Radius	50 mm
Shield Distance	10 mm
Voltage	+/- 10 kV
Steerer Length	100 mm
Steerer Plate Distance	120 mm
Antiproton Rates	
space charge limit (20keV)	$1 \cdot 10^{7}$
Effective rate (20 keV)	$1 \cdot 10^{12}$ 1/s
Extracted rate (20 keV)	$5 \cdot 10^{5}$ 1/s

1.3.4 Vacuum System, Lifetimes

The lifetime of antiprotons in the energy range between 20 keV and 300 keV depends on single and multiple scattering. From measurements in existing machines [12], [13] and direct scaling, lifetimes in the order of minutes at E=300 keV can be extrapolated at a residual gas pressure below $5 \cdot 10^{-11}$ mbar. Standard stainless steel along with XHV technology could be used in this case.

An integrated electron cooler counteracts the effects due to small angle scattering and limits the loss mechanisms to single scattering, Fig. 12.

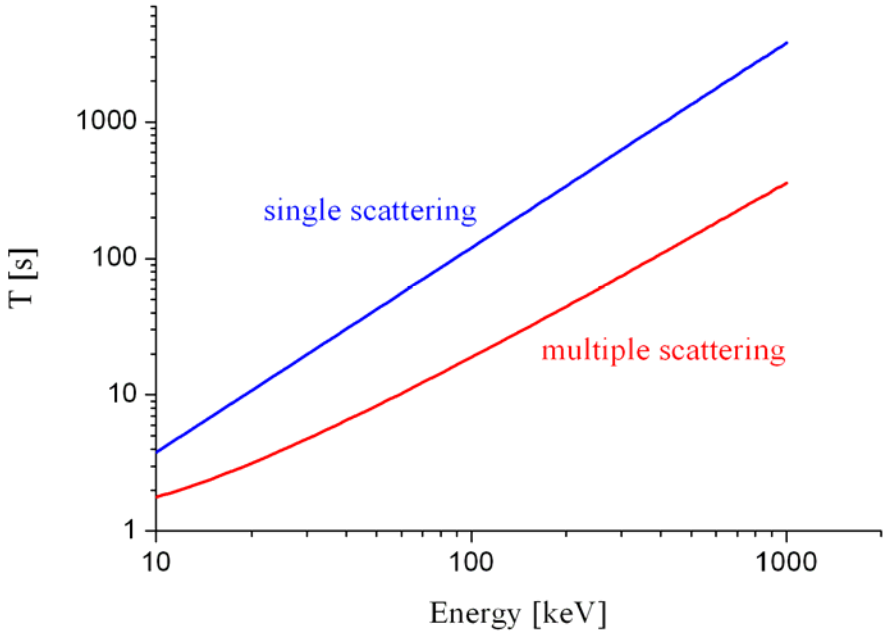

Fig. 12: Lifetime of antiprotons as function of energy at a base pressure of $5 \cdot 10^{-11}$ mbar, own estimations

1.3.5 Electron Cooling

Electron cooling reduces the diameter and the divergence of the stored ion beam and, in connection with rf bunching of the stored beam, can produce short ion pulses as necessary for measurements with the in-beam reaction microscope. At the USR, an electron beam moving at the same average velocity as the ion beam will be merged with the circulating beam over a length foreseen to be 0.8 m, representing 3.6% of the storage ring circumference.

In contrast to electron cooling in the magnetic storage rings operating at higher beam velocities, the electrical power transported by the electron beam will be extremely low (ranging from ~1 W at the highest electron energy down to <1mW at 5 eV); moreover, only a low magnetic guiding field (<10 mT) is required. The principal parameters for electron cooling of (anti)protons as well as of highly charged ions (for two sample cases) are listed in Table 3. The electron energy for cooling of the antiproton beams in the envisaged USR energy range is above 10 eV. Reasonable cooling times result with an electron beam from a small (2 mm diameter) thermocathode magnetically expanded to 10 mm diameter (field-strength ratio of 25). The cooling performance seems sufficient to suppress multiple scattering (cf. Fig. 9) down to ~20 keV antiproton energy, while this will become difficult at even lower energies. The cooling performance can be improved by using a GaAs photocathode [14], [15] which should yield “cold beam” cooling times shorter by about a factor of 30. Before a detailed layout of the electron cooler can be designed, several further questions should be considered, among them: (a) the detailed competition of electron cooling and multiple scattering; (b) the cooling power needed with an internal target; (c) the expected values of the longitudinal electron temperature and its influence of the cooling performance, in particular at small beam velocities; (d) the cooling performance required for highly charged ions. On this basis it will also be decided whether the electron cooler should be equipped by a photocathode or a thermal cathode.

Table 3: Estimated parameters for electron cooling at the USR.

Ion mass [amu]	Ion charge [e]	Ion energy [keV]	Electron energy [eV]	Electron current [mA]	Electron density [10^6 cm^{-3}]	Cooling time *cold beam* kT = 4.2 meV [s]	Cooling time *cold beam* kT = 0.44 meV [s]
1	1	300	165	4.2	44	0.06	0.002
1	1	20	11	0.072	2.9	0.9	0.03
100	50	300	1.6	0.0042	0.44	0.12	0.004
238	92	300	0.7	0.0011	0.18	0.42	0.014

The cooling times "cold beam" are calculated from the thermal equilibration time of a two-component plasma for an electron temperature kT of 4.2 meV (cathode temperature $kT_c = 105\ meV$) and 0.44 meV ($kT_c = 11\ meV$) with an adiabatic expansion by a factor of 25, setting the Coulomb logarithm to 3.3 and neglecting the ion velocity spread. Scaling of cooling times with ion mass A and charge q as A/q^2. Listed are 1/e cooling times for the transverse ion beam divergence or the ion beam size (4 times the temperature equilibration times) assuming that the electron beam fills 3.6% of the storage ring circumference; the electron current is given for the space-charge limit at a perveance of 2 $\mu A V^{-3/2}$; the ion beam diameter is assumed to be 10 mm.

In the limit of small beam energies (in particular below 20 keV for antiprotons, and at correspondingly higher energies for the heavy ions, see Table 2, the realization of efficient electron cooling, employing electron energies of only a few eV (or maybe even fractions of an eV) is a new challenge. It is currently taken up in the cryogenic storage ring (CSR) project at the MPI-K and the experience gained in this project will be available to the USR. In particular, cryogenic GaAs photocathodes have already been shown to provide much lower initial electron temperature at the electron source (~10 meV instead of 100 meV for thermoemission cathodes) as demonstrated by the operation of a cold electron beam target from GaAs photocathodes at the TSR (MPI-K).

The cooling times given in Table 3 were estimated neglecting the ion beam velocity spread. At the antiproton beam emittance of 1 mm·mrad and the momentum spread of 10^{-3} assumed above, the ion beam velocity spread is comparable to that of the electrons in the case of the photocathode, and smaller by about a factor of 3 for the thermocathode. In the photocathode case, the cooling times for a "hot" antiproton beam may increase by a factor of ~3 as compared to the listed values. In all cases, the electron beam diameter of 10 mm would completely cover the size of the "hot" ion beam. Estimates for the cooling time of a "hot" antiproton beam at 20 keV would thus be ~0.1 s with a photocathode and ~1 s with a thermocathode.

It should be noted that the scaling of electron cooling times from previous experimental results to the low-energy conditions of interest here is not straightforward, as many details of the theoretical description are not fully understood. Systematic measurements of electron cooling times with protons at low energies started recently at the TSR. Fig. 13 shows the measured transverse cooling times of 480 keV protons averaged over 20 injections. The magnetic rigidity in the storage ring was 0.1 Tm and thus only one third of the lowest rigidity ever used in the TSR before. The measured cooling time of $\tau = 1\ s$ fits nicely into the estimated values. More measurements will be done in the near future.

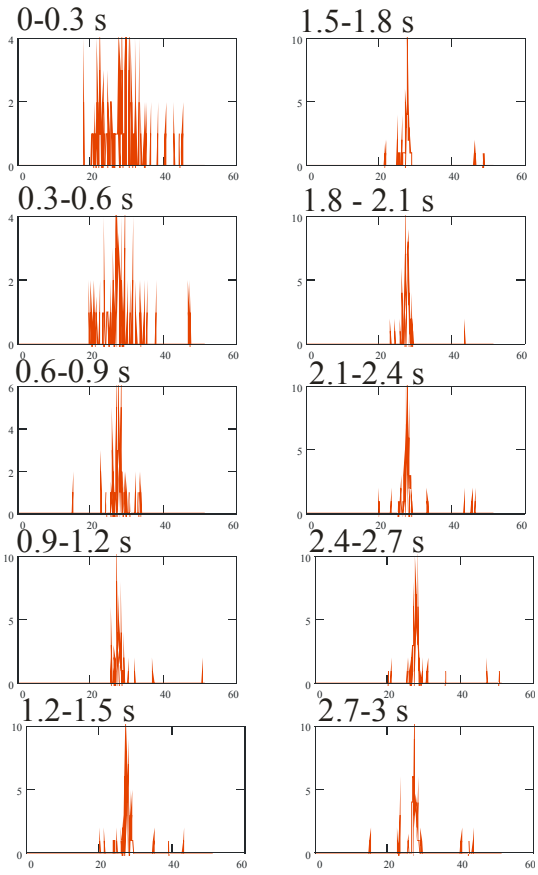

Fig. 13: Measured horizontal cooling time of a 480 keV proton beam in the TSR

1.3.6 Options

As pointed out before, other attractive options could make the USR an even more flexible machine. However, depending on the final decision on the physics program, different demands on the vacuum and/or ring layout arise. In the following two sections, the possibilities to store highly charged ions in the USR and to realize in-flight creation of anti hydrogen with a merged positron beam are discussed.

a) Highly Charged Ions

The option to store radioactive highly-charged ions is particularly attractive at the future facility, where a large variety of such ions are produced and stored in the NESR. It offers unique research possibilities that - especially in the ultra-low energy regime - can not be realized elsewhere.

The layout of the optical elements could be identical to the one presented in chapter 1.3.2. Changes in the charge states can be detected with highest resolution. Fig. 14 shows the horizontal separation of different beams with charge state differences $|\Delta q/q|$ = 1%…3%.

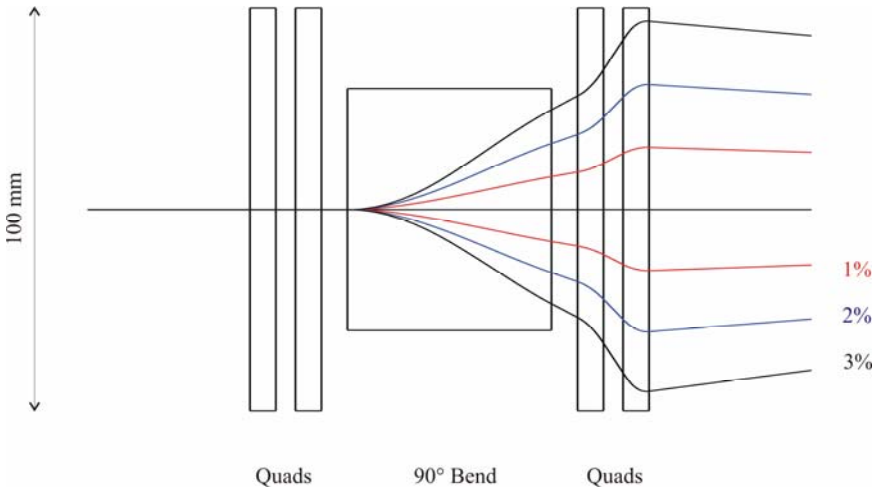

Fig. 14: Separation of different charge states after the first bend of the USR

However, the demands on the vacuum system are substantially higher in the case of highly charged stable or radioactive ions. As can be seen in Fig. 15, the lifetime of U^{91+} at the USR maximum energy is only 20 ms at a base pressure of $5 \cdot 10^{-11}$ mbar. To achieve reasonable lifetimes, the vacuum needs to be improved to the order of 10^{-14} mbar or better, which is on the limit of present technology.

A cryogenic ring comparable to the approved CSR at MPI-K, dedicated to study e.g. molecules in their rotational ground states [16], will be necessary, doubling the cost of the machine.

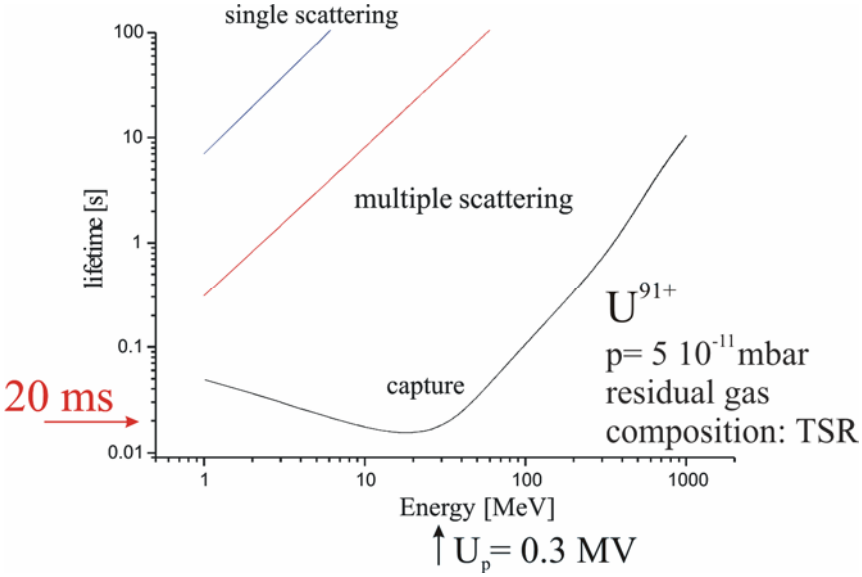

Fig. 15: Lifetime of U^{91+} as function of energy at a base pressure of $5 \cdot 10^{-11}$ mbar

The design goals for different ring specifications are summarized in the following Table 4.

Table 4: Design goals to be reached for different USR specifications

Feature	**Antiprotons**	**Highly Charged Ions**
Ring temperature	300 K	< 10 K – 300 K
Base pressure	$1 \cdot 10^{-11}$ mbar	$1 \cdot 10^{-14}$ mbar
Beam energy	20-300 keV	20-300 keV
Bunch time-structure	1 ns	1 ns
Electron cooler	x	x
Transverse jet target	x	x
Reaction microscope	ion and electron imaging	ion and electron imaging
Laser merged beam	x	x
Ion sources	LSR	LSR
Charge change detectors	2	2
Schottky detectors	3	3
Neutral beam imaging	x	x

b) Merged Positron Beam

One can cover a number of additional research areas by combining the USR with a special positron cooler storage ring (PCSR) for storage and electron cooling of positrons analogous to the LEPTA ring [17]. This combined facility can be used for the following topics:

- Storage and cooling of positrons
- Positron cooling of antiprotons at ultra low energy
- Generation of antihydrogen in-flight
- Generation of ortho-Positronium in-flight

The antihydrogen generation is realized in one of the straight sections of the USR where the antiproton and positron beams are overlapped and have equal velocities. The energy of the circulating positron beam is chosen on one hand from requirements on the positron beam life-time due to scattering on residual gas atoms. On the other hand, the positron energy has to be large enough to allow beam superposition and separation during electron cooling of the positrons. The optimum circulating beam energy lies between 2 – 3 keV. To achieve the equality of the positron and antiproton velocities some potential is applied to an electrostatic screen, which surrounds both beams and is isolated from the ground in the recombination section. In the following, antihydrogen generation at 100 keV antiproton energy is being discussed. Correspondingly, the positron energy in the recombination section is about 50 eV. Deceleration of the positrons in the recombination section leads to an increase of the positron density and at positron numbers of a few times 10^8 the positron beam can provide the same cooling rate as a conventional electron cooling system.

The positron injector for the PCSR can be similar to the positron part of ATHENA facility [18]. There, positrons are produced by an active Na^{22} β^+ isotope, moderated in a solid moderator and stored in a Penning-type trap for about 100 sec. After completion of the storage process, the positron bunch is extracted from the trap, electrostatically accelerated to an energy of 2 - 3 keV and finally injected into the ring. Single turn injection is performed with either a fast electric or magnetic kicker. With difference to the LEPTA storage ring, septum coils for the positron injection are not necessary.
The PCSR will be a small ring with a solenoidal focusing system (focusing in longitudinal magnetic field) and an electron cooling system for circulating positrons. It consists of four straight and four bending sections, Fig. 14. The total ring circumference is immersed into a longitudinal magnetic field, which is produced by straight and toroidal solenoids surrounded by a common magnetic shielding. The vacuum chamber is placed inside the solenoids, which have an external diameter of 10 cm including the magnetic shielding.

The first of the straight solenoids is common for both rings – USR and PCSR. It is used for positron cooling of the antiproton beam and for antihydrogen generation [19]. For single turn injection of the positron bunch into the PCSR one can use a magnetic or electric kicker.
The long term stability of the circulating positron beam is provided by an additional helical coil, which forms a quadrupole magnetic field, similar to the one in a “stellarator”. The straight section of the PCSR opposite to the electron cooling section for antiprotons is used for electron cooling of positrons. Superposition and separation of the cooling electron and circulating positron beams in the vertical plane are realized by a centrifugal drift of the electrons in toroidal solenoids. The particle dynamics in such a machine has been studied in detail [20]. The ring parameters are summarized in Table 5.

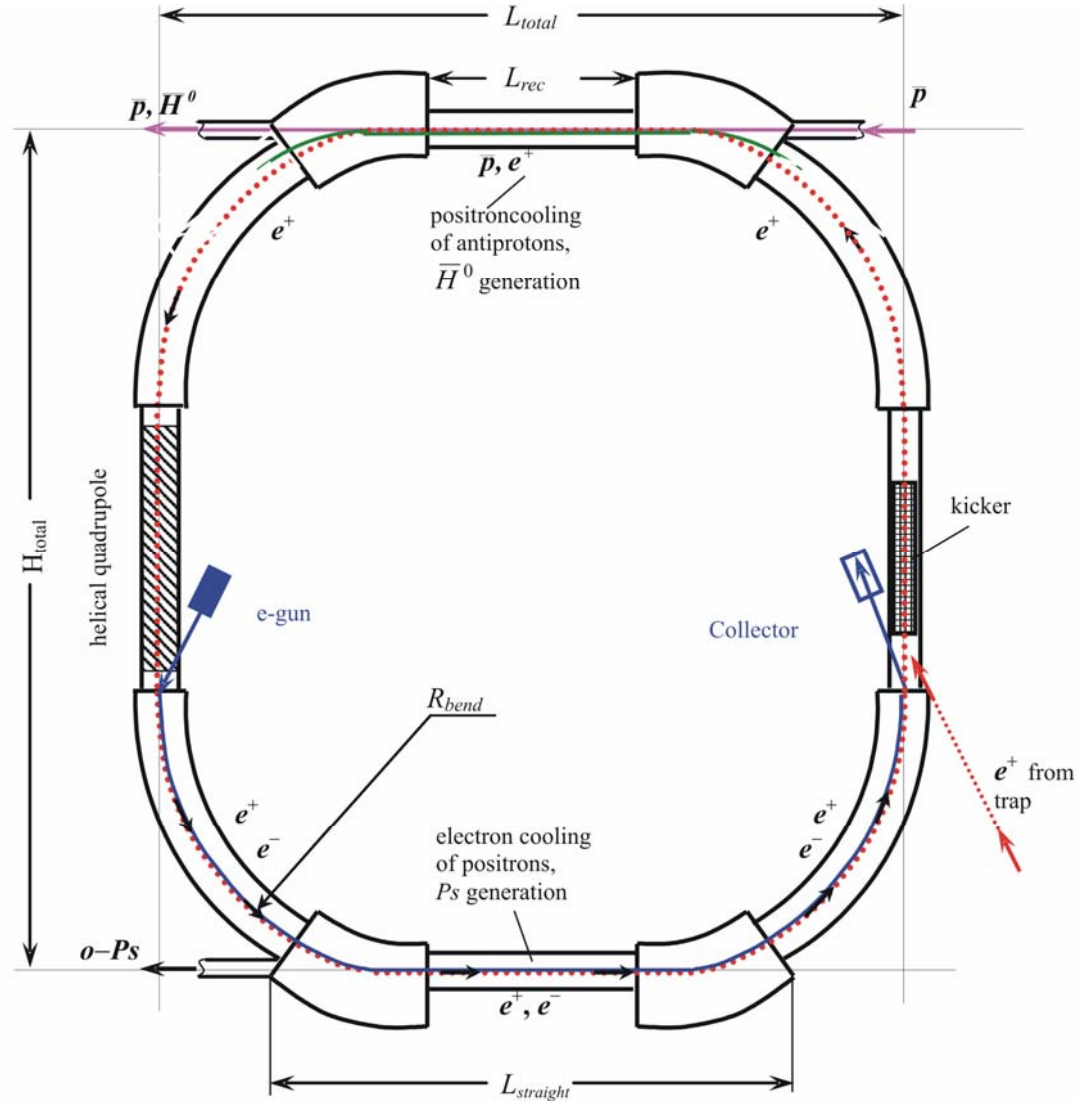

Fig. 16: Schematic layout of the PCSR

L_{rec} Length of the section for recombination and electron cooling of the antiprotons stored in the USR; it is defined by the necessary cooling time and may not be shorter than 1m.
$L_{straight}$ Length of the section for electron cooling of the positrons and two toroids, ~ 2 m.
R_{bend} Toroidal solenoid radii, ~ 1m.

Table 5: General parameters of the PCSR

Parameter	**Value**
Circumference	10 m – 11 m
L_{cool}	~ 1 m
L_{total} (Fig. 16)	~ 3 m
Lstraigh	~ 2 m
Positron energy	2 keV – 2.7 keV
Revolution period	~ 500 ns-600 ns
Longitudinal magnetic field	50 G
Minimum solenoid diameter	10 cm

Positron Larmor radius	~ 3 cm
Major radius of the toroidal solenoids	1 m
Bending magnetic field	1 G – 2 G
Gradient of the helical quadrupole field	1 G/cm – 2 G/cm
Positron beam radius	0.5 cm
Number of positrons	$1 \cdot 10^{8} – 1 \cdot 10^{9}$
Recombination section length	1 m
Positron energy in the recombination section	50 eV
Positron density in the recombination section	$6 \cdot 10^{5}$ cm^{-3} – $6 \cdot 10^{6}$ cm^{-3}
Recombination rate per 1 antiproton	$1 \cdot 10^{-7}$ s^{-1} – $1 \cdot 10^{-6}$ s^{-1}
Residual gas pressure	$1 \cdot 10^{-11}$ Torr
Positron beam life time	100 s

Electron cooling system	
Cooling section length	1 m
Beam current	0.1 A
Beam radius	1 cm
Electron temperature	0.1 meV

These parameters show that the overall size of the USR will also have to increase in case the positron ring is integrated.

1.4 HITRAP

The ion trap facility HITRAP – see also the Conceptual Design Report (CDR) 2001 - will employ deceleration of heavy highly-charged ions and antiprotons from 4 MeV/u down to cryogenic temperatures. The HITRAP facility will be installed and operated at the ESR storage ring at the present GSI facility, and then moved to the future project, where it is an integral part of the FLAIR facility. HITRAP is a GSI-midterm project and is supported within the Helmholtz-Gemeinschaft by 'additional funding'. Technical and financial details are presented in the HITRAP Technical Design Report, see http://www.gsi.de/documents/DOC-2003-Dec-69-2.pdf.

Ions up to uranium U^{92+} at 4 MeV/u will be provided by the NESR through a direct beamline between the NESR and the HITRAP facility. Antiprotons at 4 MeV will be provided to HITRAP by the LSR (see Fig. 17). The deceleration in the HITRAP facility is performed by a single Interdigital-H (IH) structure operated at 108.408 MHz, which reduces the energy down to 500 keV/u, followed by a Radio-Frequency-Quadrupole (RFQ) structure operated at the same frequency for further deceleration to 6 keV/u. In order to increase the efficiency, two buncher cavities (first harmonic/second harmonic) will be placed before the IH structure, and another one between the IH and the RFQ structure. Existing 200-kW RF-tube amplifiers can supply both decelerator structures. This considerably reduces the costs for the set-up. After the RFQ structure, the ions and antiprotons will be trapped and cooled down to cryogenic temperatures by means of electron and resistive cooling in the HITRAP cooler trap.

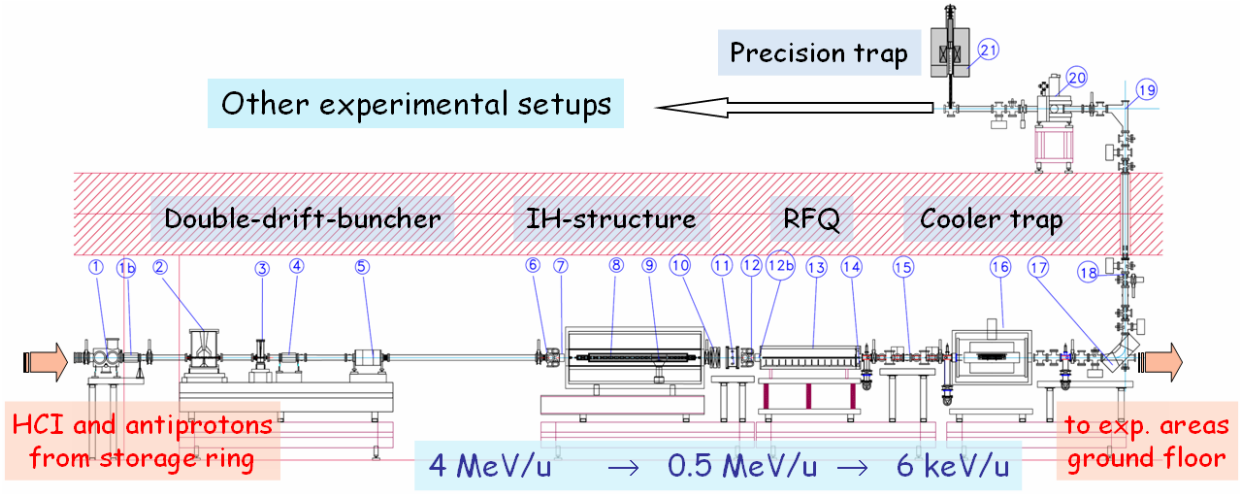

Fig. 17: Outline of HITRAP facility at FLAIR (longitudinal cut along the beamline).

Table 6: HITRAP facility: list of subcomponents.

1	Diagnostics box
2	double-drift buncher
3	1st pair of x/y steerers before the IH cavity
4	Quadrupole triplet before the IH cavity
5	Diagnostics box
6	2nd pair of x/y steerers before the IH cavity
7	IH cavity, first decelerator stage
8	Quadrupole triplet inside the IH cavity
9	Quadrupole triplet in the inner-tank section
10	1st pair of x/y steerers in the inner-tank section
11	3-gap re-buncher before the RFQ cavity

12 Diagnostics box in the inter-tank section
13 2nd pair of steerers in the inter-tank section
14 RFQ cavity, second decelerator structure
15 Diagnostics box after the RFQ cavity
16 1st solenoid magnet of the LEBT section
17 1st pair of steerers in the LEBT section
18 Fast shutter
19 2nd pair of steerers in the LEBT section
20 2nd solenoid magnet in the LEBT section
21 90° bender for extraction from the trap to experiments
22 Diagnostics box ahead of the cooler trap
23 UHV valve to separate the trap from the beamline
24 Ball valve to close the trap in the 4 K region
25 Cooler Trap

The decelerator and the trap can be equally well used for heavy ions and antiprotons to bring them down to sub-thermal energies as all components have been carefully designed to be operable in a q/A range of > 1/3. From the cooler trap, the particles will be extracted and delivered to heavy-ion and antiproton physics experiments. Extraction is possible both in DC mode and bunched mode at a time-averaged rate of 10^4 ions/sec and 10^6 antiprotons/sec. Beam transfer takes place in transfer lines at ultra-high vacuum. Typical extraction voltages will be around 15 kV.

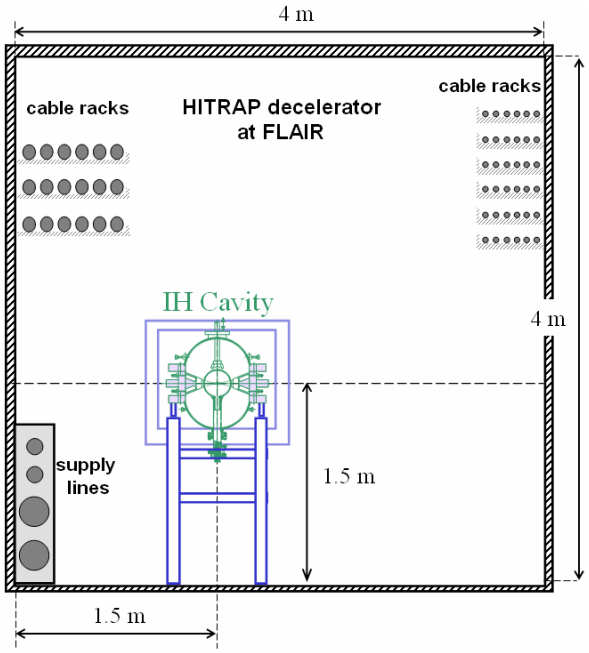

Fig. 18: HITRAP decelerator at FLAIR: Transversal cut across the location of the IH cavity, view to the north (in direction of the beam).

Bunchers, IH, RFQ, and cooler trap will be located in the HITRAP cave next to the Low-Energy HCI Cave. Including sections for drifting after re-bunching and for differential pumping between the RF cavities and the UHV of the ESR on one side and the traps on the other, the total length of the decelerator section before the cooler trap is planned to be not longer than 16 m. The height of the HITRAP cave will be 4 m, see Fig. 18. The experiments behind the cooler trap will be located i) in the low-energy experimental areas (F5, F6, and F9) and ii) on a platform on top of the HITRAP cave (F10) in the FLAIR building. The necessary supplies and the control rooms for the HITRAP facility will also be put on the platform on the second level.

The experience gained at the present GSI facility will allow for a successful operation of HITRAP without too many transition losses. Essential is the compatibility of HITRAP with the future facility in all major components (decelerator, traps, beamlines). After successful operation at the ESR and the final shut-down of this storage ring, the HITRAP components will be dismounted and mounted again at the FLAIR facility. Further work for development will not be required, except adjusting controls, beam diagnostic tools etc. to the then new standard for FAIR, which at present does not yet exist. It is expected that these relatively minor modifications will allow for a successful start of the experimental work almost immediately after start of operation of the NESR and thus contribute to the scientific output of the new facility right from the beginning.

A
Simulations of the beam transport from the storage ring to the HITRAP decelerator:

For the matching of the beam coming from the storage ring to the entrance of the IH tank, a quadrupole triplet located half way between the buncher and the tank and two pairs of steerers are planned. The steerer positions are close to the buncher and at the entrance of the IH. In addition, two profile grids should be used, one in the pumping section and the other one near the steerers close to the IH.

Basis for the ion-optical calculation was the beam coming from the ESR at the existing GSI facility. The first two dipole magnets and the first quadrupole doublet as currently installed in the re-injection line directly after the ESR are considered in these calculations. For the matching conditions, the acceptance of the IH (2.2 and 2.3 π mm mrad) was used although the emittance of the ESR is expected to be smaller by a factor of at least two. Fig. 19 shows the phase-space ellipses at the entrance to the IH. With the proposed position of the triplet, the beam size in the buncher region can be kept reasonably small, and so are the required magnetic-field gradients. Shifting the triplet towards the IH, the beam in the buncher could be made even smaller, but the necessary field gradients would increase. For the present solution, three lenses of 100 mm length and 40 mm aperture diameter are planned. For safety margins, this aperture is about a factor of two larger than the expected beam size. The magnetic-field gradients are 15 T/m at maximum. Fig. 20 shows the beam envelopes, starting at the exit from the ESR.

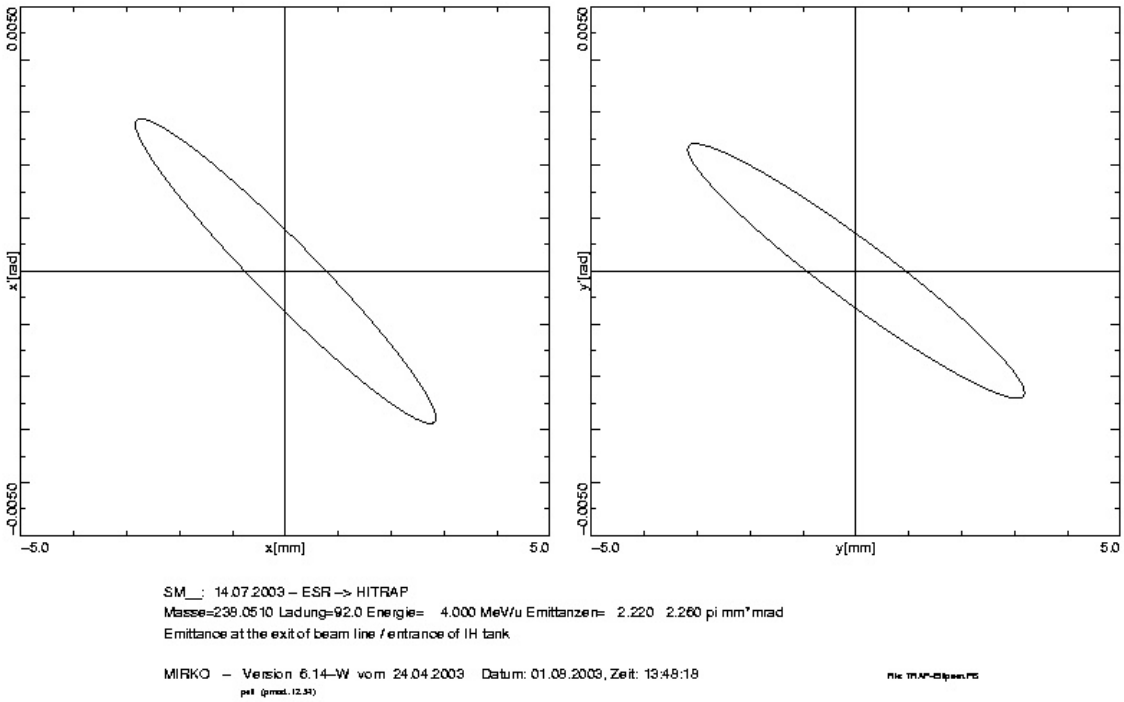

Fig. 19: Transversal phase-space ellipses of the beam at the entrance of the IH tank. Normalized emittances are $\varepsilon_{x,\,n} = \varepsilon_{y,\,n} = 0.21\ \pi$ mm mrad.

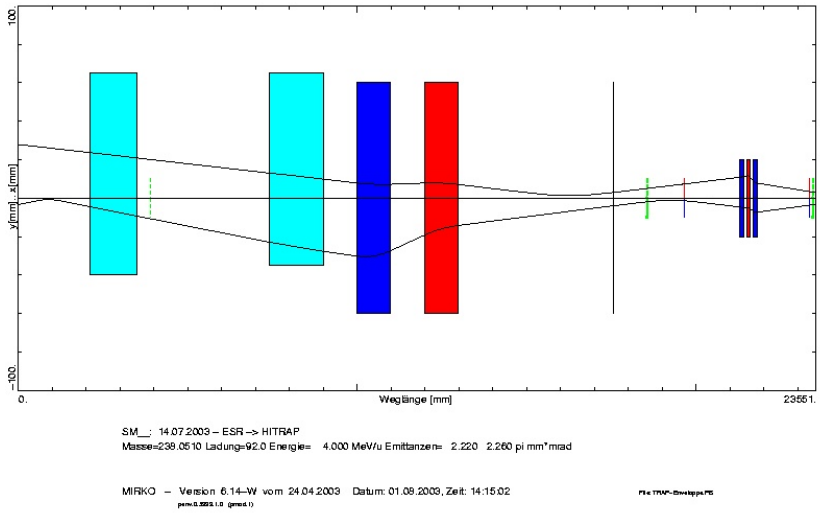

Fig. 20: Beam envelopes between ESR (left) and IH-tank (right). The cyan-coloured boxes to the left are the existing dipole magnets after the ESR, blue and red boxes are horizontally defocusing and focusing quadrupoles, respectively. Green dotted lines indicate beam diagnosis elements, and blue and red lines vertical and horizontal steerers. Above the axis the horizontal beam at half size and below it the vertical beam at half size is shown.

For steering, two pairs of steerers dedicated for the low magnetic rigidity should be used. The required field strength corresponds to less than 3 mrad horizontal deflection and 8 mrad vertical deflection assuming that the uncorrected beam just fits into the aperture.

Simulations of the Low Energy Beam Transport from the HITRAP decelerator to the cooler trap:
After the final deceleration in the RFQ, the ions and antiprotons have to be injected into the cooler trap for further reduction in energy. The cooler trap has to be at an extremely good vacuum and also the beamline ahead of it, which is also used to feed the experiments, should be kept at UHV. Therefore, a differential-pumping stage is planned directly after the RFQ structure. The ion-optical calculations along this line are described here. It will be shown that the required fields can be generated by solenoid magnets existing at GSI. Suitable power supplies also exist and therefore no additional costs for beam transport have to be considered here. In addition, a study is included which shows that a beam with the properties at the end of the differential pumping section can be injected into the cooler trap with its strong solenoidal magnetic field (B = 6 Tesla).

Ion optics in the differential pumping section after the RFQ

The low-energy beam transport system (LEBT) performs the imaging of the transversal beam parameters at the RFQ exit onto the required focus at the ion-trap entrance. The RFQ-output emittance is nearly symmetric in its horizontal and vertical planes. This allows the use of solenoid magnets and dedicated power supplies, which are available at GSI from the former EPOS and ORANGE experiments. Therefore equipping the LEBT beamline with ion optical elements will not contribute to the cost of the HITRAP project.

The transversal envelope of the proposed layout of the LEBT is shown in Fig. 21. Between the two solenoids, there is space of more than two meters for a differential pumping section, beam diagnostics, and two steerer magnets, each acting in horizontal and vertical direction. Downstream behind the second solenoid, space is foreseen for the installation of a 90°-bending unit, to transport the cooled ions and antiprotons from the ion trap further to the experiments.
For the design ion $^{238}U^{92+}$ with beam energy of 6 keV/u, the calculated magnetic inductions of the two solenoids are B = 0.35 and 0.17 Tesla, respectively. The fields required for antiprotons are lower due to their smaller A/q ratio. The apertures are 60 and 80 mm.
The expected beam-energy spread of $\Delta T/T = \pm 7\%$ causes a beam halo, which is partly considered by normalized emittance values of $\varepsilon_{x,y}$, norm = 0.55 π·mm·mrad which are 50% above the calculated RFQ-output emittance numbers of 0.37 π·mm·mrad. Finally, a beam focus of a radius r = 6 mm at a fixed position inside the ion trap is performed. Fig. 22 shows the transversal RFQ-output emittance with the assumed high divergence (diagonal ellipses) and the phase space ellipses at the desired focus within the ion trap (horizontal ellipses).

The presented calculation shows the possibility of matching the beam out of the RFQ into the cooler trap with the required boundary conditions imposed by the field of the trap. The exclusive use of existing equipment for guiding the ion beam along the LEBT section is a particularly welcome side effect in keeping the costs of the HITRAP set-up within reasonable limits.

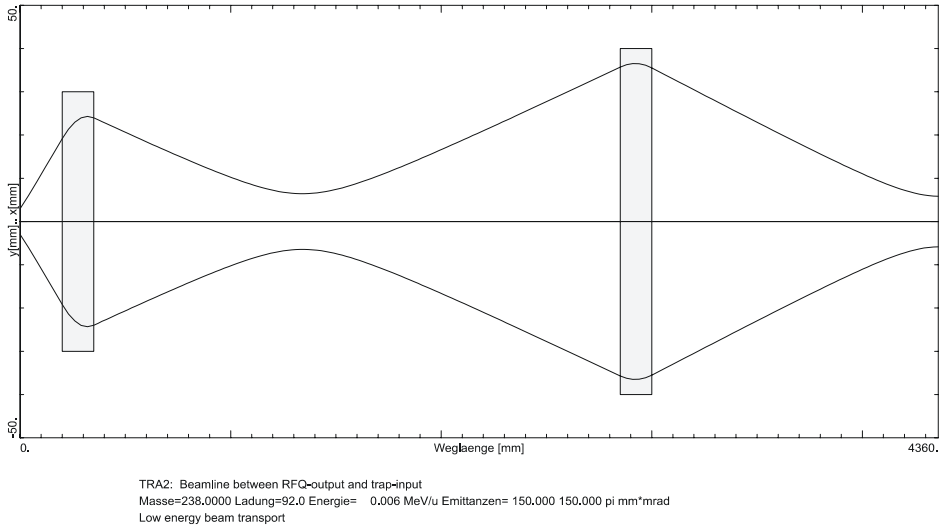

Fig. 21: Envelope along the LEBT section from the exit from the RFQ (left) to the entrance into the cooler trap (right). The normalized emittances are $\varepsilon_{x,\,n} = \varepsilon_{y,\,n} = 0.55\ \pi$·mm·mrad.

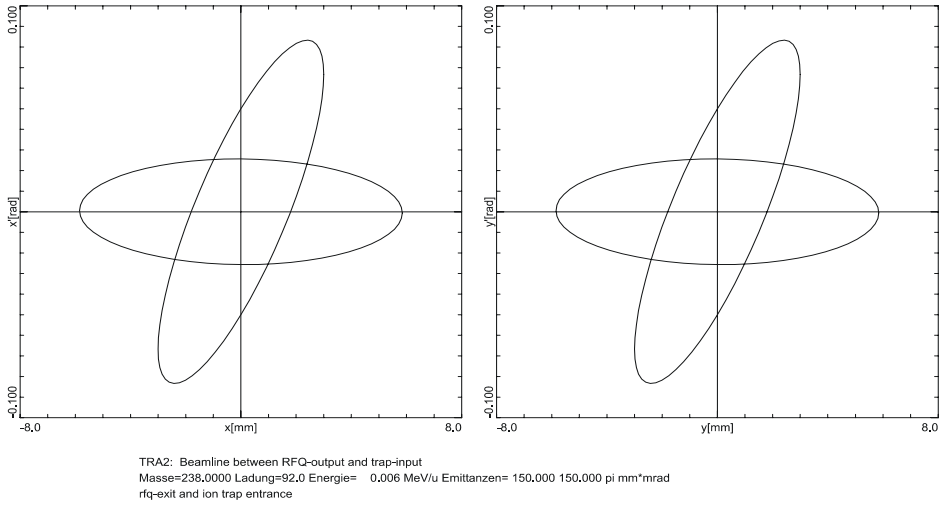

Fig. 22: Transverse phase-space ellipses at the exit from the RFQ (diagonal) and at the entrance into the cooler trap (horizontal). The normalized emittances are $\varepsilon_{x,\,n} = \varepsilon_{y,\,n} = 0.55\ \pi$·mm·mrad.

Injection of highly charged ions and antiprotons into the cooler trap: a feasibility study
In the HITRAP project highly charged ions and antiprotons are decelerated by a RFQ decelerator and then injected into the cooler Penning trap. This ion-optical study investigates the injection of a beam of highly charged ions into the strong magnetic field of the cooler trap and can be applied to the case of antiprotons by simple scaling rules. The simulations are based on beam data shown in Table 7 and the magnetic field plot as displayed in Fig. 23 which is similar to that provided by an iron-shielded superconducting magnet system at ASACUSA, CERN.

Table 7: Properties of the U^{92+} ion beam as used in the simulation 2m ahead of the trap centre.

Ion mass	Charge state	Total energy	Total energy Spread	Bunch length	Emittance (at initial energy of 1428 keV)
238	92	1428 keV (6 keV/u)	$\pm$ 100 keV $\Delta E/E = \pm 4$ %	1 μs	100 π mm mrad (norm.: 0.37 π mm mrad)

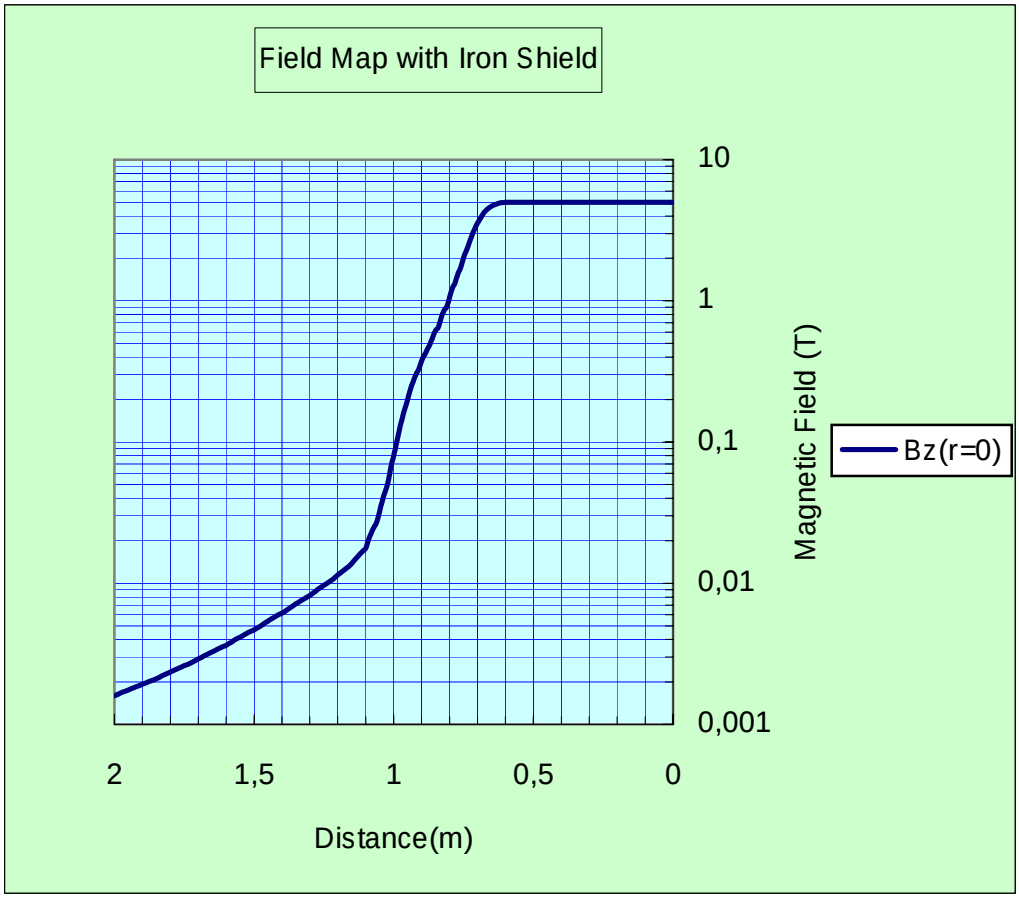

Fig. 23: Magnetic field strength on the axis of the solenoid of the cooler trap. The distance given is the distance from the centre of the cooler trap.

Simulation goal

The basic idea of the simulations is to focus the injected ions and antiprotons into the strong magnetic field in such a way that their trajectories follow the magnetic field lines as closely as possible. This way, the reflection of the injected ions at the steep magnetic gradient ('magnetic-mirror effect') is completely avoided. The goal of the simulations is to find the optimum injection parameters, in particular (i) the size rfoc of the focus and (ii) the position zfoc of the focus on the field axis. With optimum injection parameters the radial-energy pickup, i.e. the conversion of axial energy into radial energy, is minimized. In this case, the time structure of the ion bunch is very little affected.

Simulation Procedure and Results

The simulations were carried out with SIMION 3D 7.0. The magnetic potential required by SIMION was calculated from the magnetic field data (Fig. 23). For the injection into the magnetic field, the ion trajectories are calculated from the starting position at z_0=2500 mm, with the field centre at z=0. In the simulation, the magnetic field is taken into account only over a distance of 2000 mm from the field centre. Beyond z=2000 mm, the magnetic field strength is negligibly small. The ions and antiprotons are focused to a point z_{foc} such that without magnetic field and for the given emittance a beam with radius r_{foc} would be obtained at the focus. The virtual focus parameters z_{foc} and r_{foc} are used to characterize the beam injection. The energy and time distributions of the ion bunch are taken into account in a Monte-Carlo type variation of the initial conditions for different particle trajectories. The particles are injected into the magnetic field and allowed to pass through it. Their radial energy and time-of-arrival distributions are ‘measured’ in the trap centre.

According to Fig. 23, the magnetic-field gradient reaches its maximum at a distance of about 1100 mm from the field centre. Basically, it can be expected that the best injection conditions are achieved if the virtual focus z_{foc} is close to that point and between this point and the field centre. The optimum value of the focus size r_{foc} is less obvious. The task of finding the global minimum for the radial energy pickup ΔE_r as a function of the focus position z_{foc} and the focus size r_{foc} is solved in the following iterative optimization procedure:

- A virtual focus position z_{foc} is chosen, and the radial energy pickup ΔE_r is determined for different focus sizes r_{foc}.
- The focus size r_{foc} is fixed to the value which gives the lowest radial energy pickup, and the focus position z_{foc} is varied. With the new focus position, step I is repeated.

In the beginning of the optimization procedure, a number of beams with different focus sizes rfoc and with a fixed focus position at z_{foc}=1100 mm are simulated. The focus size with the lowest radial energy pickup is r_{foc}=6 mm (see Fig. 24). For this focus size the focus position z_{foc} is now varied with results shown in Fig. 25. The best focus position is z_{foc}=800 mm. For this position the radius is varied once more (Fig. 26) and a better radius of r_{foc}=4 mm is found. A final iteration of z_{foc} verifies that an overall minimum has been found (Fig. 27).

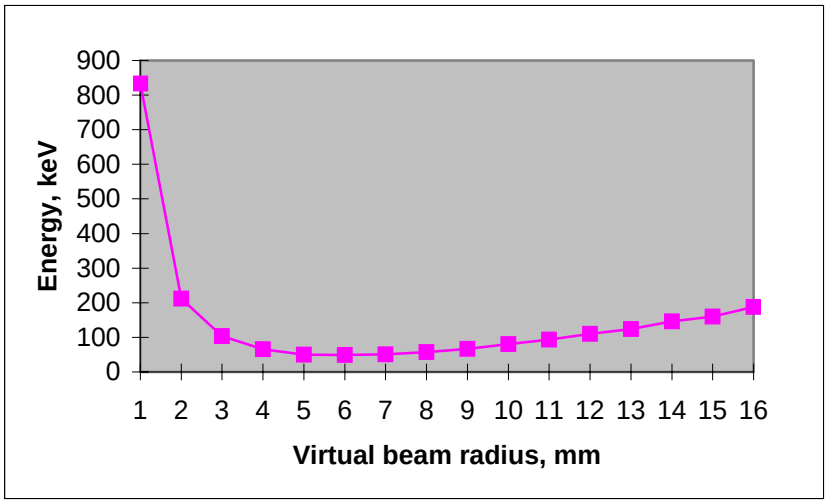

Fig. 24: Iteration step 1: Radial energy as a function of the radius r_{foc} of the virtual beam focus for z_{foc} = 1100 mm.

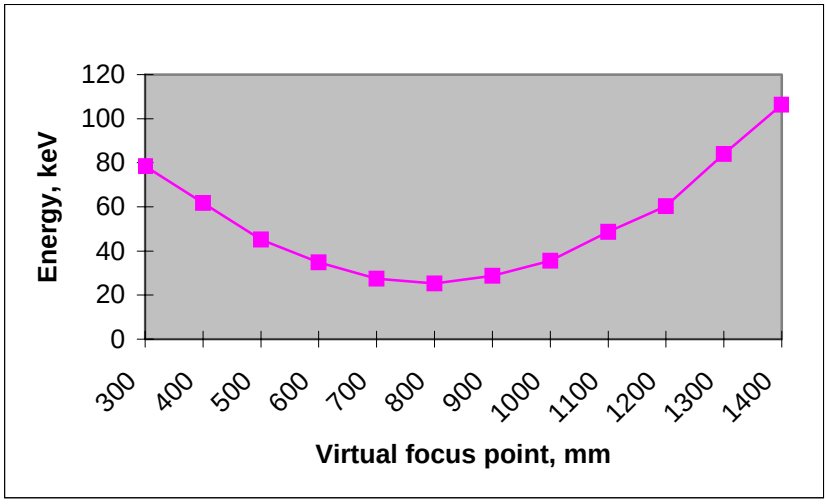

Fig. 25: Iteration step 2: Radial energy as a function of the position of the virtual focus z_{foc} for r_{foc} = 6 mm.

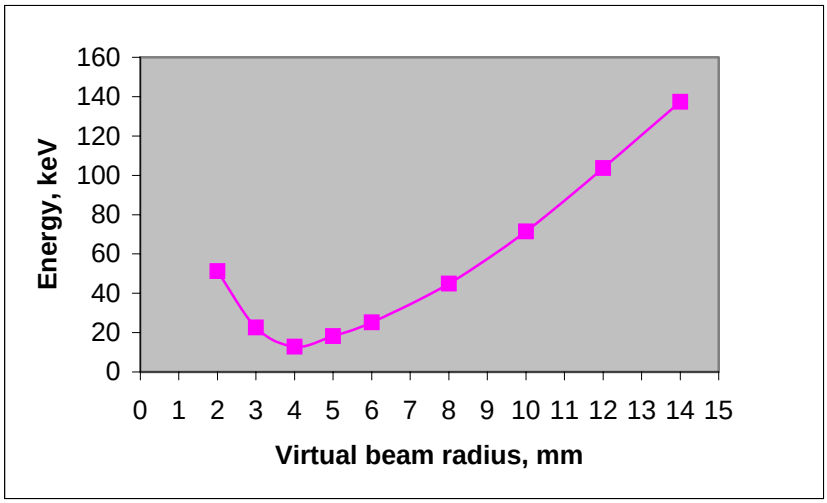

Fig. 26: Iteration step 3: Radial energy as a function of the radius r' of the virtual beam focus for z' = 800 mm.

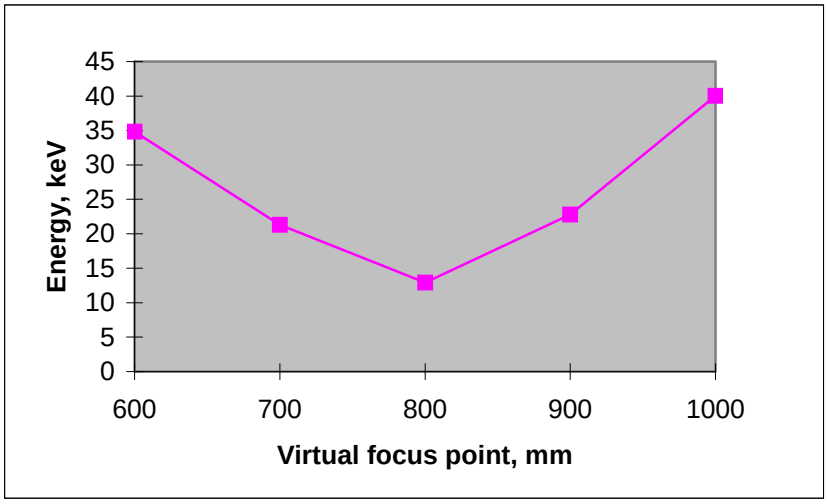

Fig. 27: Iteration step 4: Radial energy as a function of the position of the virtual focus z_{foc} for r_{foc}= 4 mm.

Fig. 28 shows ion trajectories calculated with SIMION for the best case found in the iteration process described above. The maximum radial energy pickup for this optimised beam injection and the corresponding loss of axial energy is about 13 keV (total energy). This is small compared to the +/- 100 keV spread of the injected beam.

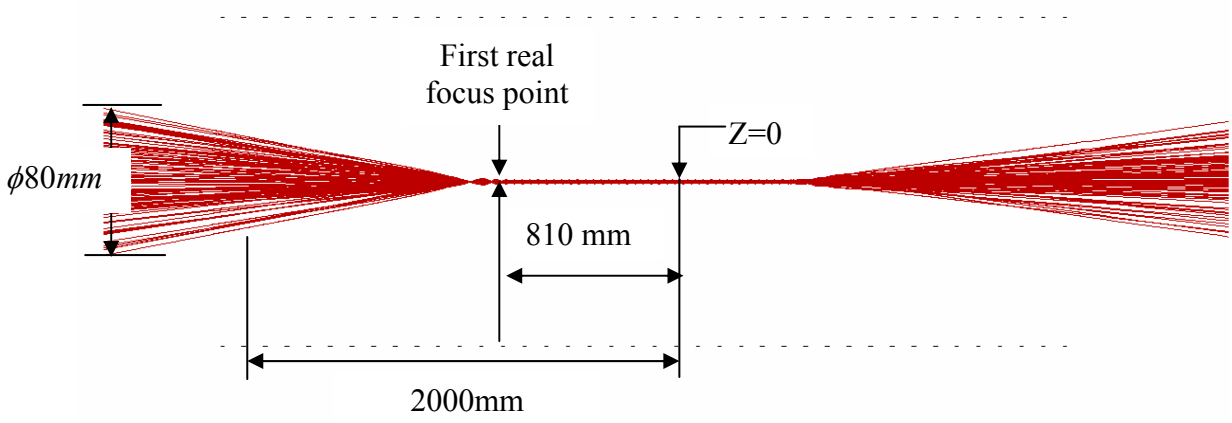

Fig. 28: Injection of ions into the magnetic field of the cooler trap. Beam trajectories for a focus size of r_{foc}= 4 mm and a focus position of z_{foc}=800 mm. The beam diameter at the focal point is about 0.03 mm.

The initial ion bunch length of 1 µs at the exit of the RFQ decelerator is increased to about 1.2 µs at the entrance of the cooler trap due to the energy spread of the ion bunch. The cooler trap will be operated at a high voltage of about +8 kV in order to retard the incoming bunches of ions and antiprotons. The resulting spatial length of the retarded ion and antiproton bunches in the cooler trap is then about 0.8 m. A cooler trap length of only half the ion bunch length is required for capturing the ions and antiprotons because the incoming particles are reflected at the end of the cooler trap. Therefore, the total particle bunch can be captured in the 0.5 m long cooler trap.
The question of the optimum retardation voltage has been investigated as well. Taking the initial energy and time spread, it is easy to calculate the pulse length in the field centre for different retardation voltages. For the case studied here, it is assumed that the initial bunch length is 1 µs and that the retardation takes place 1 m from the field centre. Fig. 29 shows the calculated spatial bunch length as a function of the beam energy after retardation. A broad minimum can be observed. Therefore, the value for the retardation voltage of the cooler trap is not a critical parameter.

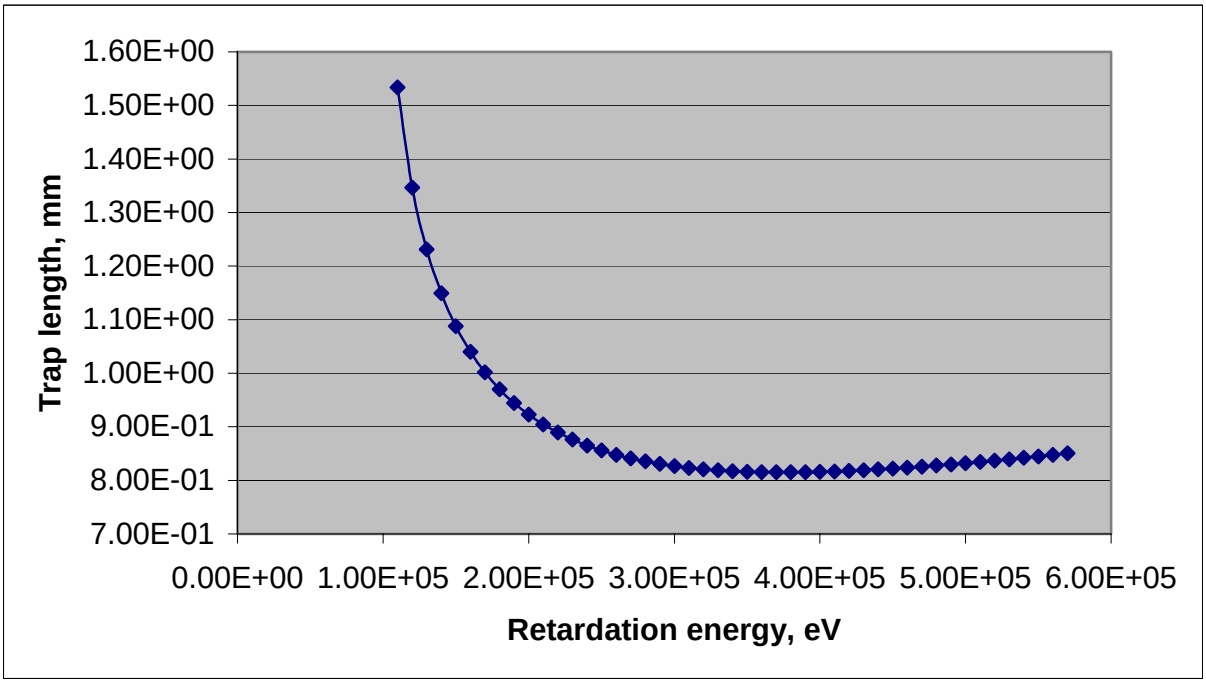

Fig. 29: Spatial length of ion pulse at field centre as a function of the energy of the retarded beam.

Conclusions

- A beam with properties as specified in Table 17 can be injected without losses into a field as depicted in Figure 6-3.
- Good injection parameters are: focus size r_{foc}=4 mm and focus position z_{foc}=800 mm. With these parameters, the radial energy pickup is about 13 keV which is much smaller than the initial energy spread of the beam.
- Without changing the initial beam energy or further retardation, a pulse length of about 1.2 m is observed. The length is practically fully determined by the initial beam energy and time spread. If the beam is retarded inside the magnetic field, the pulse length can be reduced to about 0.8 m fitting well to the length of the cooler trap of 0.5 m (a trap length of only half the ion bunch length is required, because the ions are reflected at the end of the cooler trap). In total, the proposed solution is well suited for the final injection of the beam into the cooler trap after deceleration in the IH and RFQ structures seams.

Summary of the beam transport calculations
The results of the beam transport calculations are summarized in the Table 8 and Table 9.

Table 8: Beam energies, velocities, magnetic rigidities and particle numbers for $^{238}U^{92+}$.

HITRAP Section	Energy [MeV/u]	β	B ·ρ [Tm]	Trans-misson	tot. Trans.	No. of particles	Notes
ESR	5.0	0.1032	0.834			1×10^6	measured
	4.0	0.0924	0.746			(6×10^5) estimated	ejection energy
	3.0	0.0800	0.645			2×10^5	measured
Entrance of double-drift tube buncher	4.0	0.0924	0.746	100 %	100 %	6×10^5	
Entrance IH	4.0	0.0924	0.746	95 %	95 %	5.7×10^5	loss by bunching
Exit IH / Entr. RFQ	0.5	0.0328	0.263	70 %	67 %	4.0×10^5	
Exit RFQ	0.006	0.0036	0.029	85 %	57 %	3.4×10^5	
LEBT, up to entrance of trap	0.006	0.0036	0.029	95 %	54 %	3.2×10^5	

Table 9: Emittances along the HITRAP decelerator

HITRAP Section	Energy [MeV/u]	ΔT	$\varepsilon_{x,n}$ (=$\varepsilon_{y,n}$) [π mm mrad]	ε_x (=ε_y) [π mm mrad]	Δφ	Notes
ESR	5.0	dp/p = 2.4×10^{-4}	0.093	0.9		measured
	3.0	dp/p = 1×10^{-4}	0.06	0.7		measured
Entrance IH	4.0	ΔT/T = 1.3×10^{-2}	0.2	2.2		[1])
Entrance RFQ	0.5	ΔT/T = 2×10^{-2}	0.24	7.3	± 9°	
Exit RFQ	0.006	ΔT/T = 8.3×10^{-2}	0.37	100		

[1]) A safety margin of a factor of 2 is considered in the calculation of the emittances.

Radiation Hardness (of detectors, of electronics, of electrical components nearby)
Due to the relatively low beam energy of 4 MeV/u or smaller, radiation hardness of electronics and of electrical components nearby is not an issue in the HITRAP cave at FLAIR.

Design and
Construction (sections c. and d. combined)

General lay-out of the IH-type decelerator
Beams of highly charged heavy ions with a charge-to-mass ratio up to 1/3, covering $^{238}U^{92+}$ ions, and beams of antiprotons will be decelerated in the Interdigital-H drift-tube linac (IH-DTL) from 4 MeV/u down to 0.5 MeV/u. The main features of the beams delivered by the storage rings, after deceleration down to 4 MeV/u and cooling, are a small transverse emittance, a low energy spread and negligible space charge effects. The intermediate decelerating array has been designed as simple as possible with a minimum of necessary units. It includes the main IH tank with one internal quadrupole-triplet lens, a four-gap bunching cavity in front of the tank, a three-gap re-buncher behind the IH tank and two external triplet lenses which match the beam to the IH and RFQ sections, respectively. The last lens at the IH tank exit provides both a convergent beam for RFQ input and a short drift section for possible beam diagnostics (Fig. 30).
Effective RF voltages of 54 kV and 60 kV, respectively, have to be applied to the gaps at the first and second bunching cavity. The distances between the gap centres in these cavities are 124.6 mm and 45.2 mm, respectively. The distance between the centres of the first and the last gap of the IH structure is 2468.4 mm. Two decelerating sections separated by an internal lens contain 15 gaps and 10 gaps within lengths between gap centres of 1542.4 mm and 587.6 mm, respectively. The expected effective voltage distribution along the main IH tank is shown by Fig. 31.

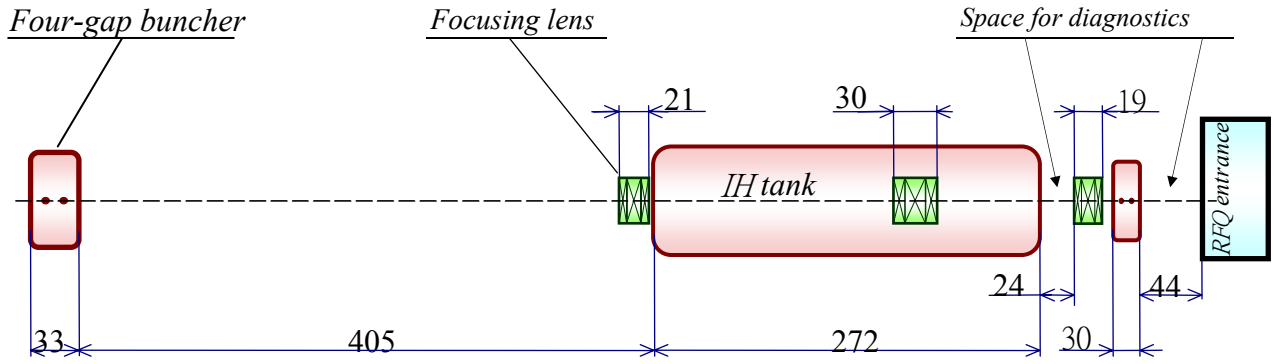

Fig. 30: Intermediate decelerating array based on the IH-DTL structure. Scale in cm. At the right there are the second buncher and the entrance to the RFQ. The first quadrupole triplet ('Focusing lens') at the entrance to the IH tank is located further to the left (beam up) in the final design.

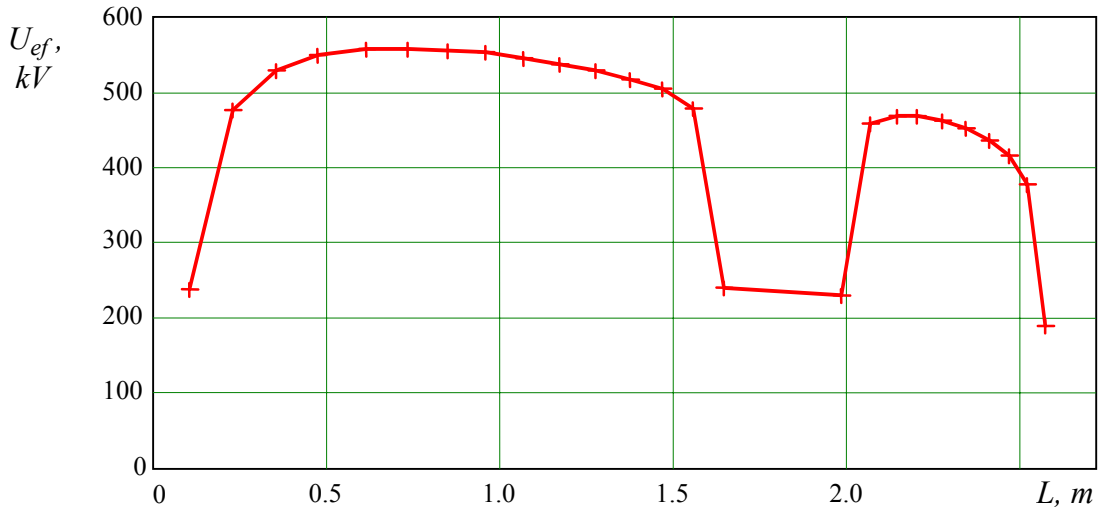

Fig. 31: Effective voltage distribution along the main IH tank. The gap in the middle corresponds to the location of the inner-tank quadrupole triplet.

According to estimations, an RF power of about 180 kW is necessary to drive the IH cavity. Although this value fits to the output power of the existing RF generators (200 kW), great care has to be taken to reduce the RF power losses as much as possible.

The parameters of the focusing triplet lenses are given in Table 10. The small aperture and modest magnetic gradient of the first and second lenses make their design quite comfortable. The numbers for the first triplet can be reduced if it is placed further beam-up. In that case, existing quadrupoles might be employed. The third lens needs twice the aperture in order to provide a relatively long drift towards the RFQ section. Nevertheless, the magnetic induction at the pole tips does not exceed the value of 0.8 T, which is close to the limit for the existing production technology, involving Vacoflux (a cobalt alloy). An additional magnetic field analysis will be performed at the final design stage.

Table 10: Parameters of the focusing magnetic quadrupole lenses.

Triplet No	Effective pole length (mm)	Magnetic gradient (T/m)	Aperture radius (mm)	Eff. longitud. distance between poles (mm)
1	40	45.0	8.0	25
	80	44.0		
	40	45.0		
2	70	53.3	8.0	20
	120	52.0		
	70	53.3		
3	40	53.1	15.0	20
	72	52.0		
	40	53.1		

Beam dynamics

Beam dynamics simulations have been done with the LORASR code, developed and suited especially for IH structures. The simulations were performed for q/A=1/3 ions at zero beam current and can also be applied to the case of antiprotons by simple scaling rules. Fig. 32 shows the 98%-beam-transverse envelopes for a normalized transverse beam emittance of 0.2 π mm mrad.

Within the decelerating sections, the beam is very close to axial symmetry. This provides minimum transverse size and maximum transmission. The beam radius in the drift-tube sections does not exceed 2 mm besides the very few gaps at tank injection. Designed aperture radii of 6 mm at the first section (before the internal quadrupole triplet) and 5 mm at the second section (after the triplet) provide enough safety for such a beam taking into account possible misalignments and even a larger emittance as will be discussed below.

Being decelerated down to 0.5 MeV/u, the beam has to be matched to the RFQ section where a convergent beam with a radius of less than 2 mm is required. Also, free space along the axis is necessary for diagnostics and steering. In order to avoid any second lens between the IH- and RFQ-sections, the output triplet is installed at a distance of 240 mm behind the IH tank, allowing the beam to expand up to 8 mm in radius. Then it is focused again to the RFQ entrance so that the independently driven re-buncher and a diagnostic box can be installed in front of the RFQ section.

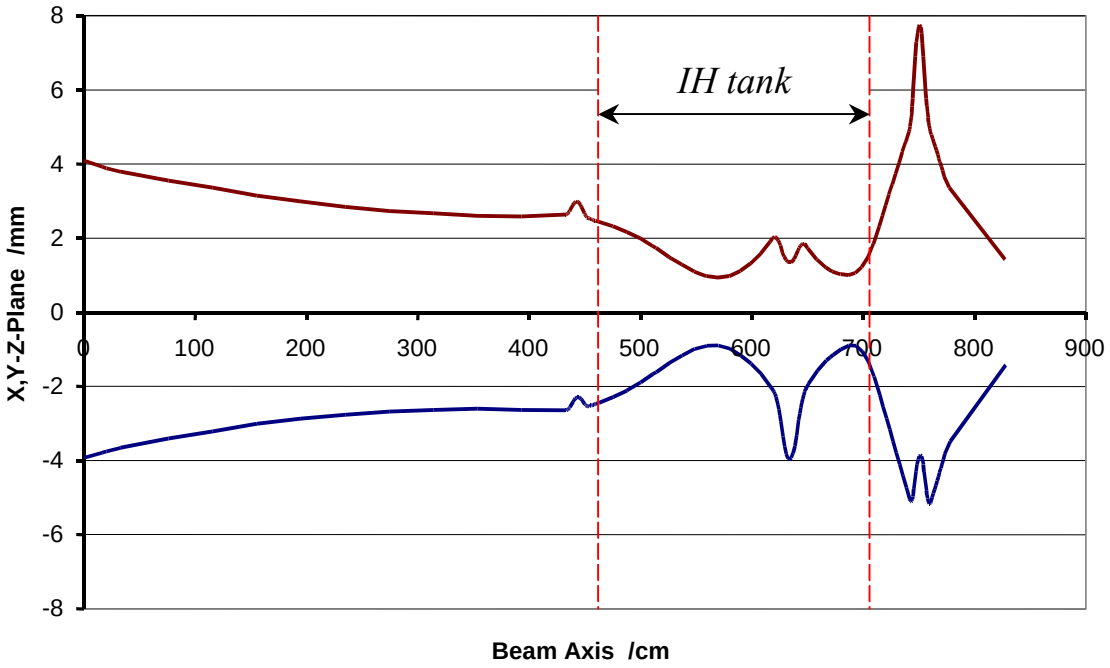

Fig. 32: Transverse 98%-beam envelopes along the IH deceleration array. Red: X, Blue: Y. The location of the IH cavity is indicated. The Z-axis is the beam axis.

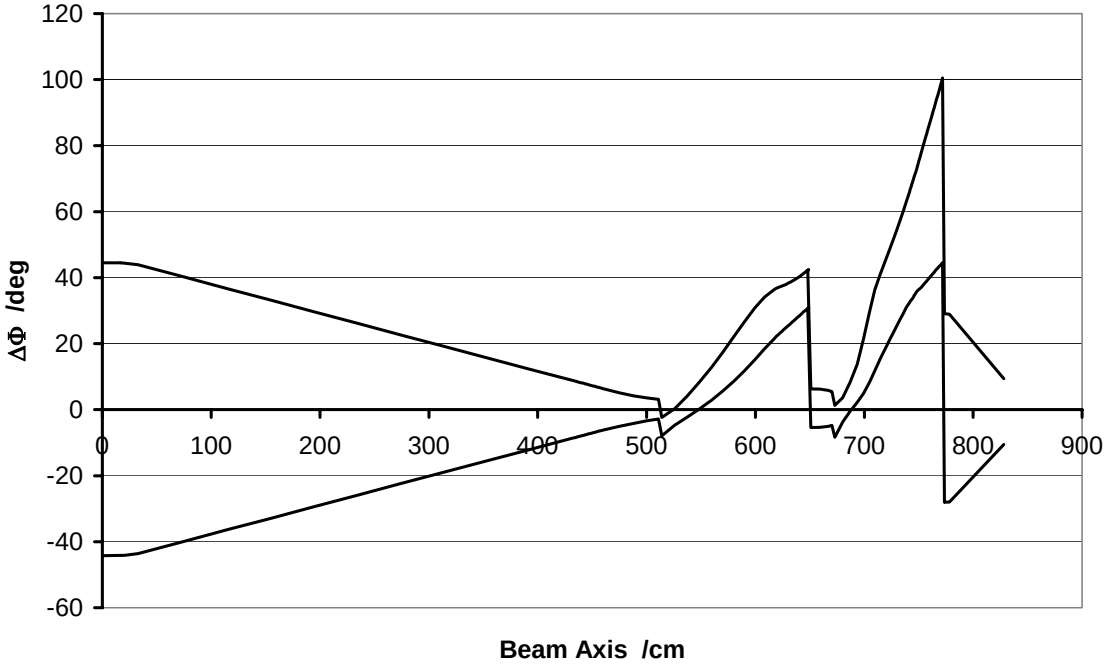

Fig. 33: Longitudinal 98% -bunch envelope along the IH deceleration array. The deviation from the reference axis is given for beginning and end of the bunch. The phase width at a given position is the difference between both curves.

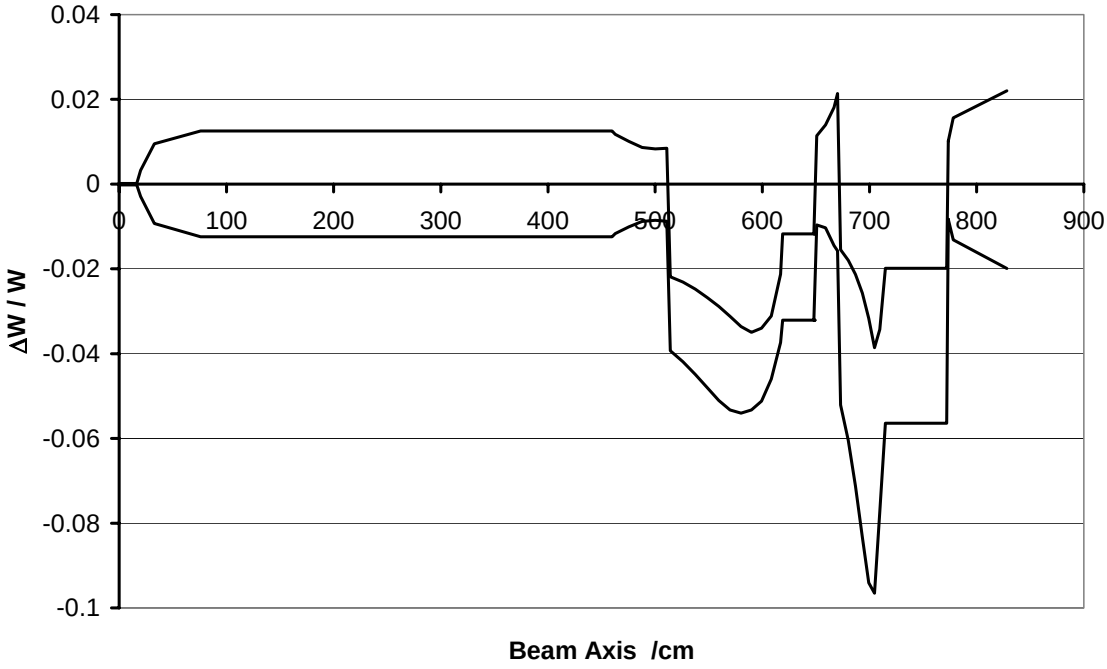

Fig. 34: Bunch-energy spread along the IH deceleration array. The deviation from the reference axis is given. The lines denote the particles with highest and lowest energy, respectively. The energy width at a given position is the difference between both curves.

Fig. 33 shows the longitudinal 98%-bunch envelope. The beam energy spread along the decelerating array is shown by Fig. 34. The phase and energy widths are given by the difference between both lines while the absolute deviations $\Delta\phi$ and ΔW correspond to the virtual parameters used for the design of the drift-tube array.

The double-drift buncher cavities in front of the decelerator are operated at a frequency of 108.408 MHz and 216.816 MHz, respectively. After this buncher, a short drift range of 4 m length has been chosen in order to relax the stability requirements for the bunching RF voltage amplitude and the RF phase. Since the bunch is too much convergent in the longitudinal direction after 4 m drift, the IH tank starts with four de-bunching gaps. After the exit from the IH tank, the bunch expands up to nearly ± 30° while drifting to the second re-bunching cavity, which then provides the required phase length of around ± 10° at the RFQ entrance.
The first buncher accepts 100° out of 360° injected by the ESR into the end bucket, corresponding to 28% of the particles from the ESR. A second, second-harmonic bunching cavity focuses up to 75 % of the particles into the IH structure.
The flexibility of the proposed system has to be underlined: The parameters of the output beam can be easily varied by the pre-bunching voltage and by the output lens gradient. Additionally, the beam energy may be tuned in some limits by the pre-buncher RF-phase variation.
Fig. 35 shows the projections of the beam emittance at the entrance to the first buncher and at the exit from the section under discussion here, i.e., the entrance to the RFQ structure. The beam is axially symmetric both at the input and at the output of the section. The configuration of the output projections satisfies the RFQ requirements in terms of emittance.

Beam input to the first buncher

ε_x=0.19 π mm mrad ε_y=0.19 π mm mrad ε_z=0.96 π keV/u ns

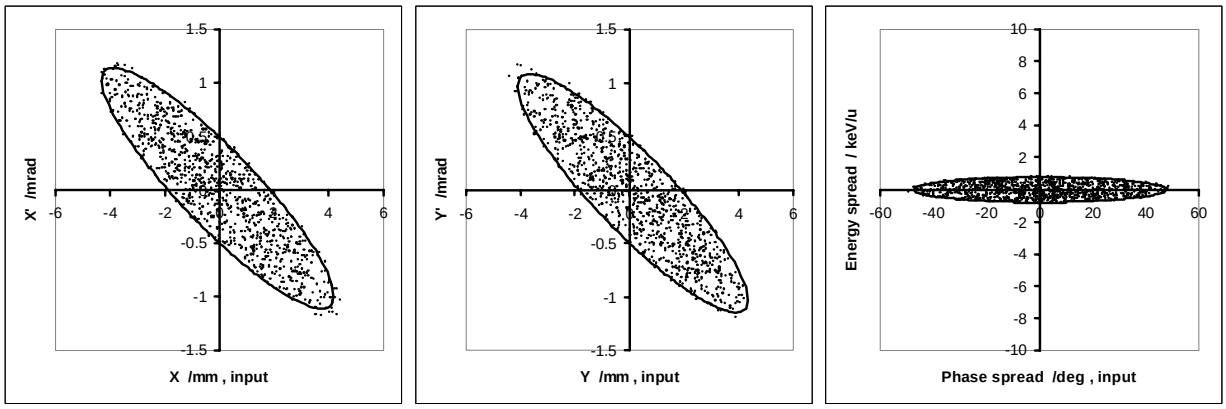

Beam output after the IH = Beam input to the RFQ

ε_x=0.24 π mm mrad ε_y=0.24 π mm mrad ε_z=4.22 π keV/u ns

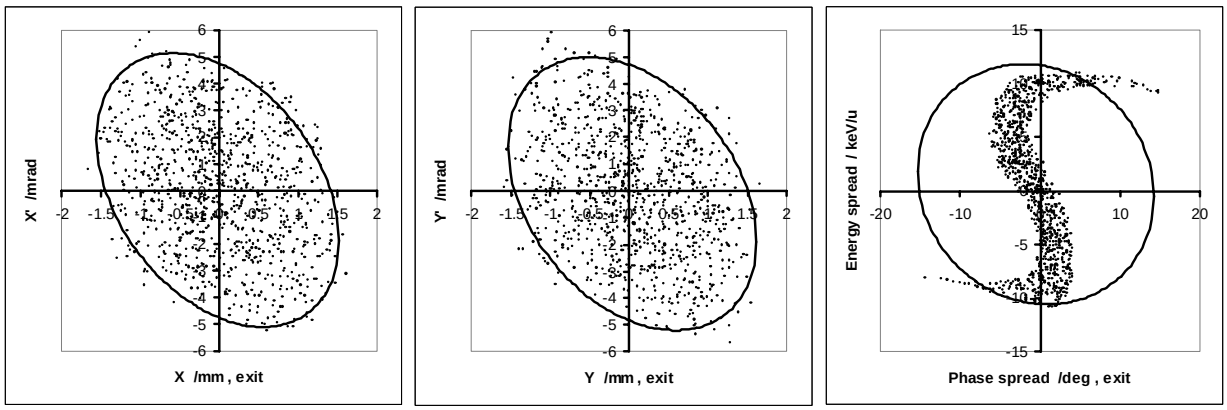

Fig. 35: Projections of the beam emittance at the input to the first buncher and at the entrance to the RFQ structure. All given emittance values are normalized emittances.

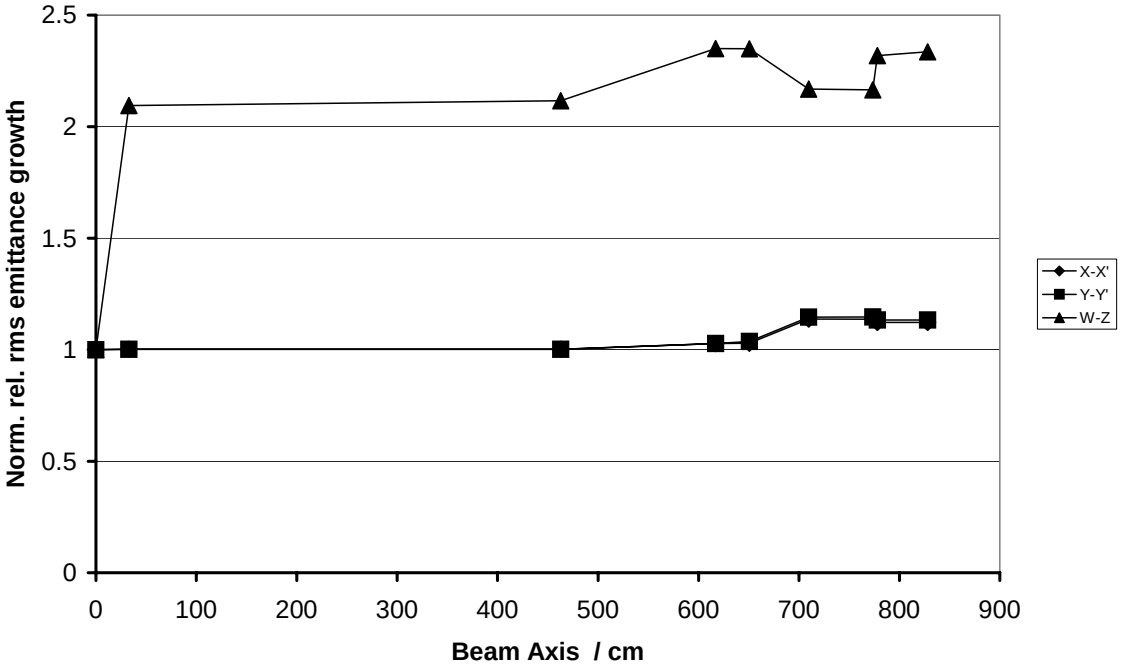

Fig. 36: Normalized rms emittance growth along the decelerating structure. The values for X-X' and Y-Y' almost coincide at any given point.
W-Z denotes the growth in energy spread along the structure.

In Fig. 36, the normalized rms-transverse-emittance growths during the deceleration are displayed. The normalized transverse rms-emittance growth is only 15%, while the increase in longitudinal rms-emittance is about a factor of 2.3. In practice, the final longitudinal emittance does not depend on the initial energy spread, but is determined by the non-linearity of the RF decelerating field, mainly at the first buncher. A remarkable improvement of the longitudinal beam emittance for the given input-bunch length can be achieved only by a second buncher before the IH structure.

Structure ability for larger emittance and beam displacement
It is clear that a structure, designed for small beam emittance and with small aperture, may be sensitive to the input-emittance increase and beam displacements, especially when including the long drift range from the storage ring to the IH-DTL. Fig. 37 shows the transverse beam envelopes for two values of the normalized transverse emittance, 0.2 π mm mrad and 0.45 π mm mrad, respectively. For the increased emittance, the envelopes for both x and y become larger by a factor of 1.5. Nevertheless, this is still quite safe within a drift-tube aperture of 5-6 mm radius. In the last lens, with an aperture radius as large as 15 mm, the beam with the increased emittance can be accepted and focused into the RFQ at $x,y < 2$ mm.

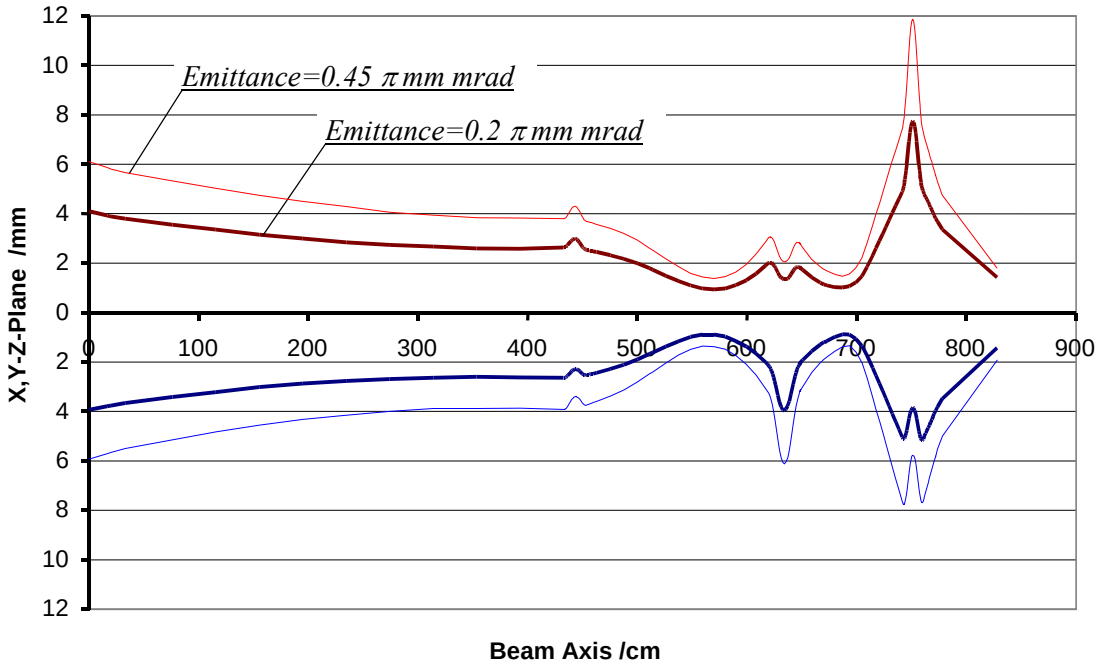

Fig. 37: Transverse 98%-beam envelopes for two different values of normalized transverse emittance. The larger of the two emittances (0.45 π mm mrad) shows the acceptance of the IH structure. The design value for the normalized transversal emittance is 0.2 π mm mrad which already includes a safety margin of a factor of 2 compared to the output value from the ESR.

In order to investigate effects of an off-axis beam, Fig. 38 and Fig. 39 show the transverse envelopes of the beam displaced by 1.5 mm in x and y directions, respectively, at the location of the first buncher. Such a displacement does not lead to particle losses in the IH structure. Efficient beam transport is still safe within the aperture. In front of the RFQ entrance, corrections can take place by steering.

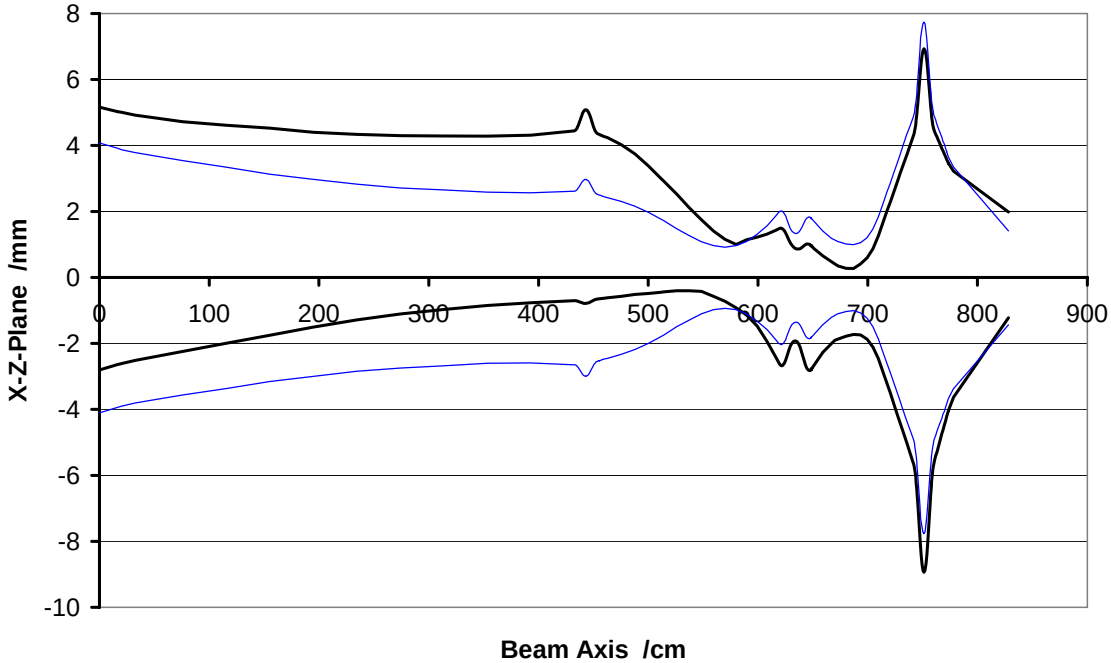

Fig. 38: Transverse 98%-beam envelope for a beam displaced by 1.5 mm in positive x direction. The blue curve indicates the envelope of the on-axis beam.

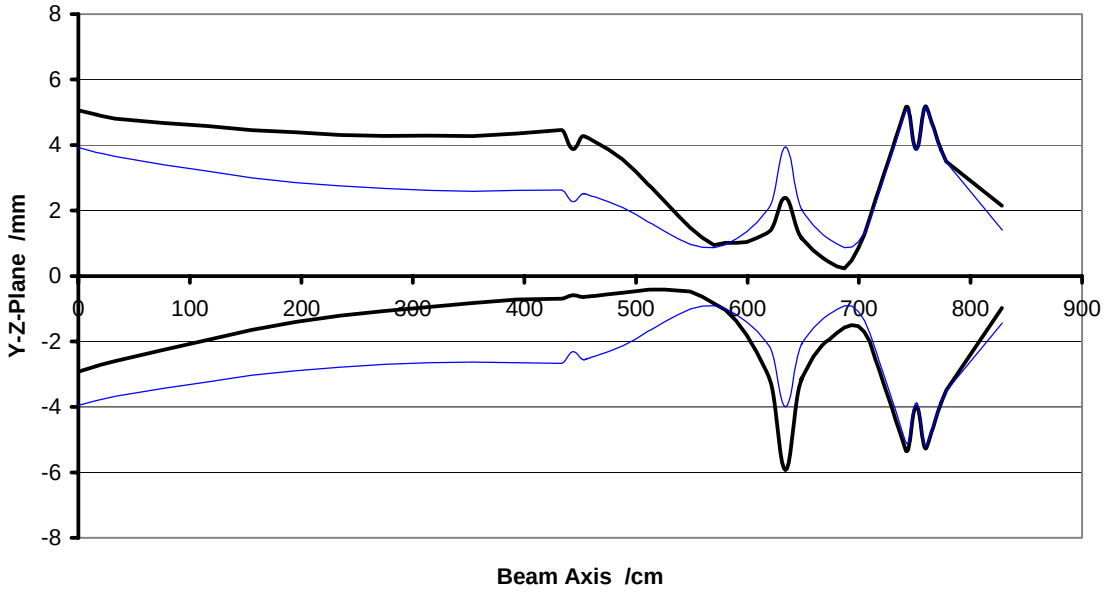

Fig. 39: Transverse 98%-beam envelope for a beam displaced by 1.5 mm in y direction. The blue curve indicates the envelope of the on-axis beam

Summary of the simulation

An IH-DTL cavity efficiently decelerates the ions with charge-to-mass ratio of 1/3 from 4 MeV/u to 0.5 MeV/u and matches the beam to the RFQ entrance. The total length and power consumption are much lower than compared to the case of an RFQ-only decelerator. On the other hand, an IH-DTL solution without any RFQ structure would need considerably more design efforts and would imply the bunching at a lower RF frequency (36 MHz) with the consequence of longer drift ranges at the high-energy side of the beamline. The suggested IH – RFQ combination provides an optimal solution with respect to cost minimization at an adequate performance. The relatively short 4 m drift range does not require extremely high stability of the bunching RF voltage and phase. The main parameters of the IH tank are given in Table 11. Great care has to be taken to keep the RF power consumption within the limit of 200 kW, determined by existing RF amplifiers.

Table 11: Parameters of decelerating IH-DTL tank and the bunchers

Simulated charge-to-mass ratio	q/A	1/3
Operating frequency	MHz	108.408
Tank length	m	2.72
Input / output energy	MeV/u	4.0 / 0.5
Aperture diameter	mm	12 – 10
Number of the internal triplet lenses		1
Number of accelerating gaps		25
Normalized transverse emittance (ellipse area)	π mm mrad	0.2
Transverse rms emittance growth	%	20
Normalized longitudinal emittance (ellipse area)	π keV/u ns	0.96 (input) – 4.2 (output)
Total effective RF voltage	MV	11.35
Average accelerating rate	MV/m	4.2
Maximum electric field on axis	MV/m	12
Estimated RF power consumption	kW	180
Total effective RF voltage at the first buncher	kV	216

Drift length	m	4
Total effective RF voltage at the second buncher	kV	120

Four-gap buncher before beforethe IH structure

The proposed buncher cavity is a quarter-wave coaxial line with two different inner diameters at the inductive and the capacitive side of the resonator. The number of accelerating gaps is four. The drift tube geometry is the same as that for any IH cavity. The original beam-transport simulation above was carried out using a two-gap buncher ahead of the IH. The four-gap cavity presented here has the same effects as a two-gap cavity if the total voltage in both gaps is the same. The simulation therefore is still according to the specified components. The reason to finally choose a four-gap buncher is a smaller need for RF power of only 2 kW. In the case of a two-gap buncher, about 5 kW would have been required, with the need for a considerably more expensive power supply. The 2-kW solution allows for the use of UNILAC spare parts in case of power-supply failure.

Three of such cavities are already in use at the UNILAC High-Charge-State Ion Injector HLI (see Fig. 40). Therefore, designing and operating this kind of cavity is well-known at GSI. During operation, these cavities have shown a high efficiency at room temperature for different energies.

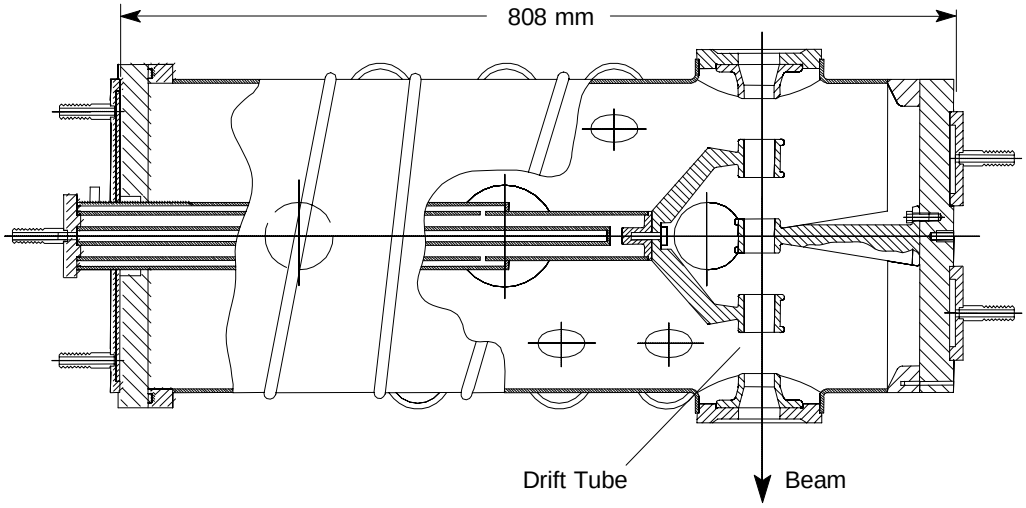

Fig. 40: Longitudinal cut of the four-gap buncher at the High Charge State injector at GSI.

The technical parameters of the 4-gap buncher are specified in Table 12.

Table 12: Parameters of the 4-gap buncher cavity

Resonance frequency	108.408 MHz
Beam energy	4 MeV/u
Length	675 mm
Outer diameter	511 mm
Inner diameter	110 mm / 57 mm
Estimated Q value	9500
Effective shunt impedance	80 MΩ / m
Effective voltage	216 kV
RF power	≤ 2 kW

IH-cavity engineering: Mechanical design

The IH cavity consists of three major parts:

- one central rectangular frame which carries the small drift-tube bodies
- two semi-spherical shells above and below the rectangular part which form an enclosed structure together with the rectangular part.

These three separate parts allow for easier machining, copper plating, handling, and mounting. The lower semi-spherical shell is connected to the support frame. The drift tube containing the quadrupole triplet is directly connected to the support frame by a stem. The stem passes through the lower shell via bellows. This drift tube therefore is completely independent from the tank.

Each piece of the tank cavity is to be manufactured by external companies. For a tank of the specified size, the choice of the shell material, mild steel or stainless steel, will hardly change the cost of manufacturing. All inner surfaces are not machined and ground, in order to prepare for the copper plating process. The mounting surfaces on the centre frame have to be machined very precisely because no transverse adjustments are foreseen to align the small inner drift tubes. However, it will be possible to adjust drift tubes longitudinally. Stem and drift-tube bodies are made from stainless steel and are copper plated. The copper plating will be carried out at GSI where the required specific knowledge is present.

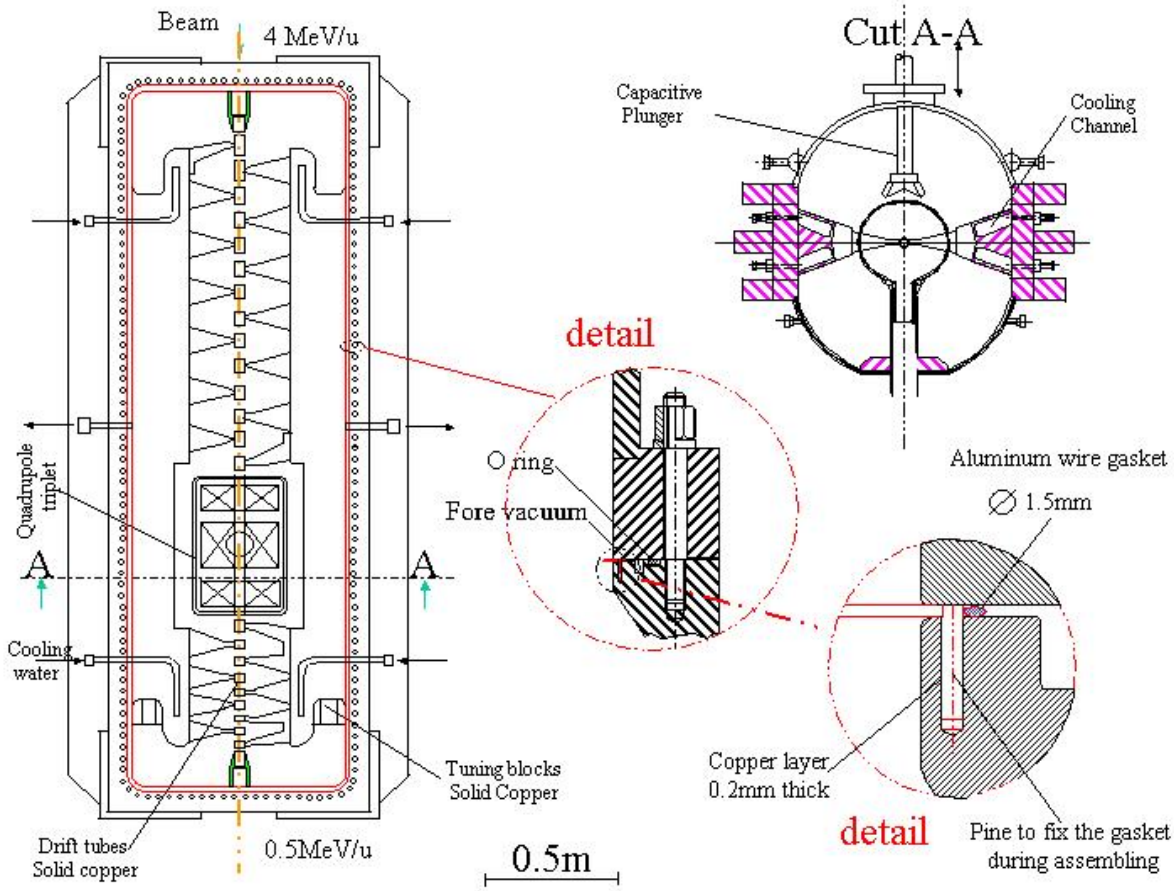

Fig. 41: Longitudinal and transversal cut through the IH cavity.

IH-cavity engineering: Alignment

The standard tolerance for mechanical misalignment at the GSI accelerator complex does not exceed 0.2 mm. This is well in the acceptable range. Deviations of the beam from the axis can easily be corrected by the steerers.

The alignment of the cavity will be done in the same way as for the HLI injector at GSI: Three screws under the lower shell assure alignment. Off-axis targets which are directly connected to the tank could be used to measure alignment (Fig. 42). This method will also be employed at the GSI future facility where HITRAP is going to be located.

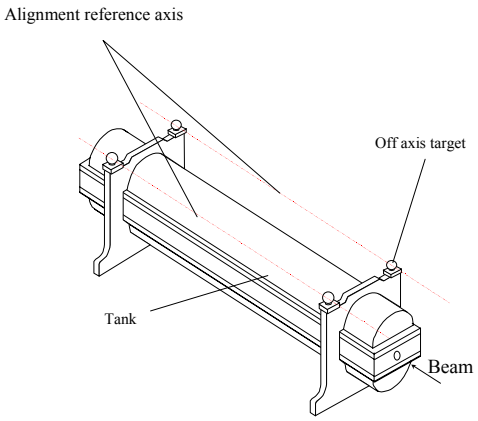

Fig. 42: Alignment of the IH cavity by external axes.

IH-cavity engineering: Vacuum
In order to obtain good vacuum, the complete tank will be aluminium sealed as shown in Fig. 41, detail. To obtain a good vacuum tightness and good RF contact, this 1.5 mm of aluminium has to be compressed to half of its diameter. About 130 screws are necessary to assure this compression. The cavity will be equipped with a turbo pump and three ion pumps.

Re-buncher between the IH structure and the RFQ structure
The re-buncher between the IH structure and the RFQ has to provide a longitudinal focus at the RFQ entrance at 500keV/u. An existing spiral-loaded cavity will be employed, which has been in use at the UNILAC.

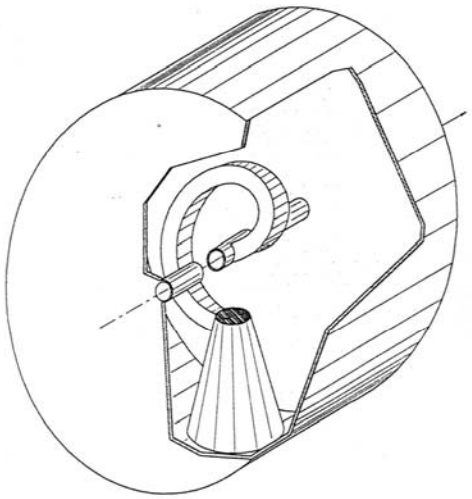

Fig. 43: Sketch of a spiral resonator.

Spirals are λ/2-transmission-line resonators and can be treated as coaxial resonators in which the inner conductor has been wound up to reduce its size (Fig. 43). This makes the frequency of the resonator independent of the outer cavity and allows for modifications and tuning in a wide range. These resonators are generally used as post-accelerator structures and as beam-matching devices.
In the decelerator, the resonator works at a fixed value of energy/nucleon. In order to reduce the power consumption, a three-gap electrode structure with a total length of 5 βλ/2 will be employed, which fits into the present re-buncher cavity.

Table 13: Parameters of the 3-gap re-buncher

Length / Diameter	300 /500 mm
Length per cell (βλ)	9 cm
No. of cells	3
Frequency	108.408 MHz
Cavity voltage Ueff	120 kV
Rp-value	9 MΩ
RF power	1.8 kW

Requirements for space and cooling water
The diameter of the IH tank is about 0.8 m. It forms the widest part of the decelerator. Cooling water is required for the quadrupole lenses and the IH tank. Due to the very low duty cycle (~ 0.15%), the cooling of the IH cavity is not a critical task. The energy to be dissipated in the tank is very low, only 300 J/s. The energy to be dissipated in the pulsed inner quadrupole triplet is comparable. The water flow to assure a constant temperature of 28° C (±1° C) should be approximately 4.5 litres per minute in the tank and the triplet. The cavity has to be cooled by 'black water', a very high quality water (<16µS/cm), if the tank is made from mild steel with its good heat conductivity. In this case, two different water-cooling systems are required, to avoid corrosion of the parts made from stainless steel, copper and plastic. Nevertheless, the low cooling requirement in total allows for manufacturing the tank in stainless steel and so using only one cooling system for the complete cavity. The cost estimates already consider the manufacturing of the tank cavity from stainless steel. The thin drift tubes are not cooled directly but just via the contact surface by heat conduction which will be sufficient at the low duty cycles of the HITRAP set-up.

Radio-Frequency Quadrupole decelerator structure (RFQ)

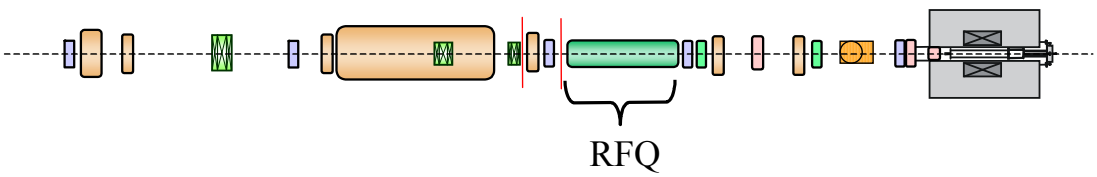

The RFQ is the second stage of the decelerators. It can decelerate and focus the beam from the first IH-decelerator stage to low energies. It is planned to inject the beams of highly charged ions and antiprotons from the IH-decelerator at 500 keV/u into the RFQ and decelerate down to 6 keV/u within this structure. The RFQ is designed to keep the radial-emittance growth small, (i.e., the normalized emittance approximately constant). In addition, it will yield a high transmission rate.

The RFQ is designed to be a 4-rod RFQ operating at 108.408 MHz at modest peak fields and low power consumption (Table 14). It is modelled along the lines of the GSI-HLI RFQ, which serves as injector for moderate charge states ($q/A > 1/9$) and accelerates heavy ions from 2.5 keV/u to 300 keV/u. The HITRAP decelerator is designed for high charge states of $q/A > 1/3$ (including antiprotons), which eases the rf-power problems and allows for a compact short structure.

Table 14: Parameters of the RFQ decelerator. Values for two different spreads of the input energy are given. For the longitudinal output emittance, the values for 80 % and 100 % of the particles are indicated separately.

Input phase width / energy spread	$\pm 9^o$ / $\pm$ 10 keV/u	$\pm 9^o$ / $\pm$ 5 keV
Injection energy / output energy	500 keV/u / 6 keV/u	
Charge-to-mass ratio q/A	> 1/3	
Operation frequency	108.408 MHz	
Electrode voltage	70 kV	
Modulation	2.44	
Phase range	–18° – –70°	
RFQ length	1.9 m	
Aperture	4 mm radius	
Input emittance (normalized)	0.24 π mm mrad	
Output energy spread	$\pm$ 0.5 keV/u (8.3 %)	$\pm$ 0.38 keV/u (6.3%)
Longitudinal input emittance	23 nsec .keV/u	11.5 nsec keV/u
Longitudinal output emittance (80 %)	10 nsec keV/u	5.6 nsec keV/u
Longitudinal output emittance (100 %)	23 nsec keV/u	9.0 nsec keV/u
Radial output emittance (normalized)	0.37 π mm mrad	0.25 π mm mrad
Transmission	93%	100%
Power consumption	80 kW	

The crucial RFQ-design parameters are the longitudinal emittance, the energy spread, and the phase width of the beam. A value of an energy spread of $\Delta T/T=1\%$ at the RFQ-high-energy input translates to 66% at the low energy end.
A design scheme has been developed which reduces the output-energy spread to approximately $\pm$ 6%. With an input-phase width of $\Delta\phi < 20^o$ and asynchronous deceleration, the beam pulse can be kept compact with reduced phase oscillations. The required output emittance restricts the possible input phase width and energy spread. A $\Delta T/T$ of 2% is the upper useful limit. For the radial emittance, a value of 0.24 π mm mrad has been used for input.

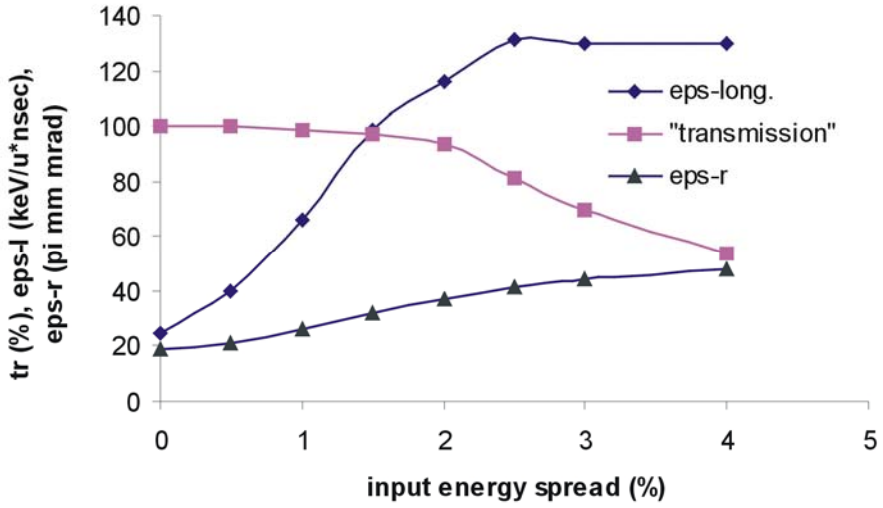

Fig. 44: Influence of the spread of the input energy on transmission (in %), $\varepsilon_{longitudinal}$, and $\varepsilon_{transversal}$.

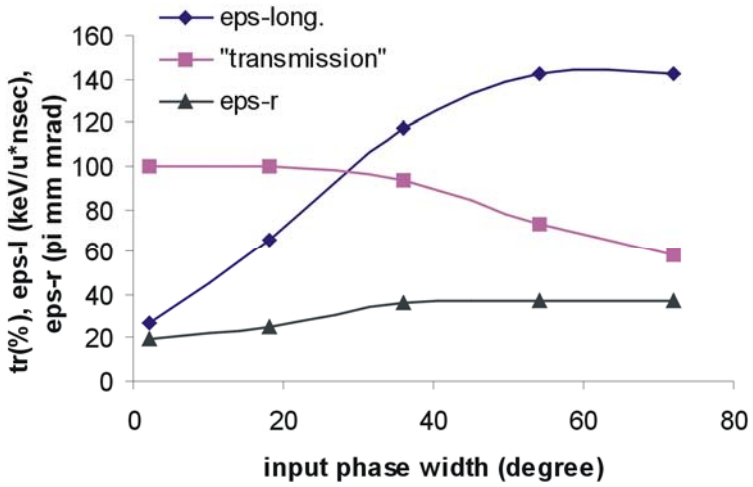

Fig. 45: Influence of the spread of the input-phase width on transmission (in %), $\varepsilon_{longitudinal}$, and $\varepsilon_{transversal}$.

The design is a compromise between acceptance, output emittance, transmission, length, and power consumption. Small input-beam emittance is favourable for output beam quality. Fig. 44 and Fig. 45 illustrate the strong influence of the input parameters bunch phase, width, and energy spread.

Fig. 46 and Fig. 47 show beam parameters for input and output of the decelerator RFQ.

From Fig. 47, a beam symmetrical in X and Y can be concluded at the output of the RFQ structure. This allows for the use of solenoid magnets as ion-optical components in the section between RFQ and cooler trap.

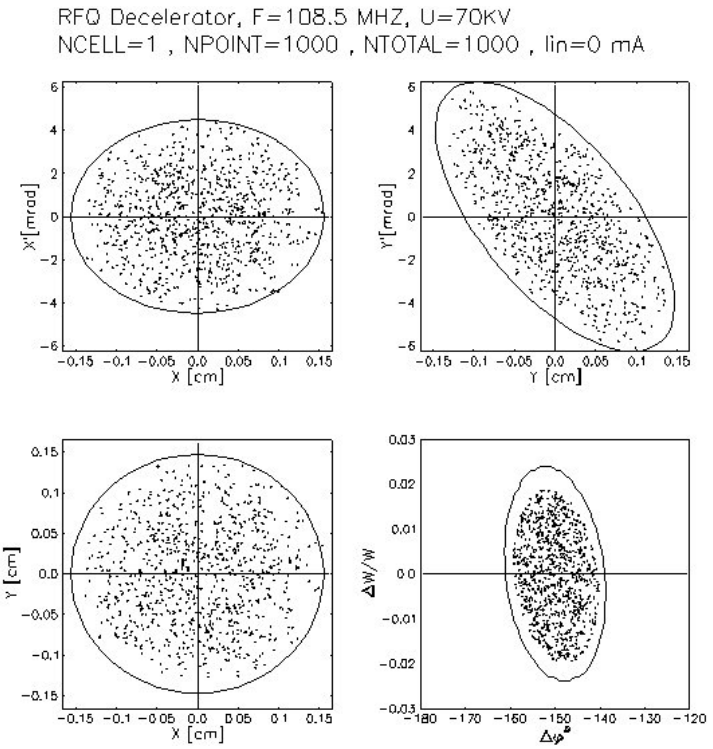

Fig. 46: Input-beam parameters for the transport calculations through the RFQ.
$\Delta T/T = \pm 2$ % is assumed.

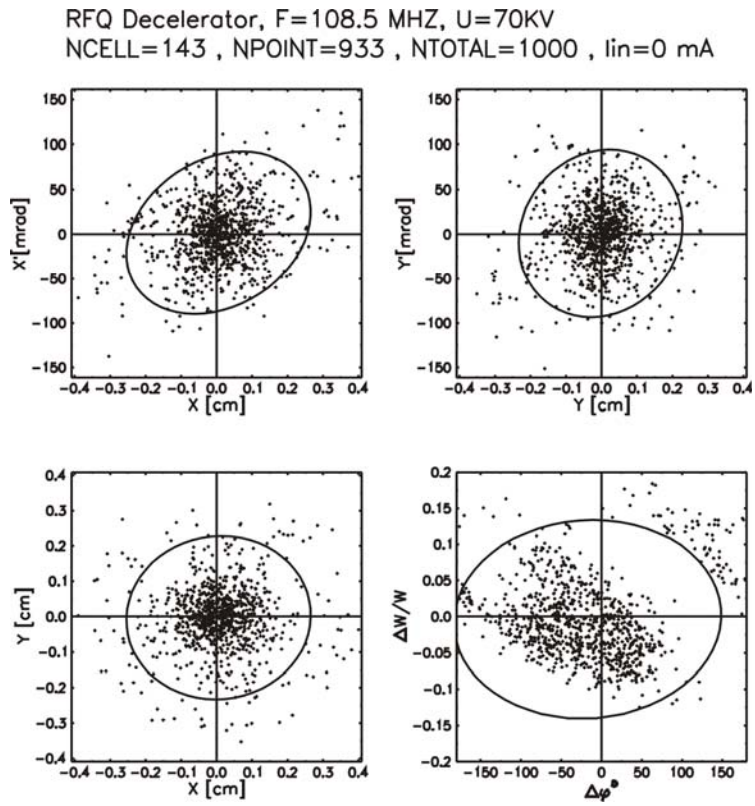

Fig. 47: Output from the RFQ for the input from
Fig. 46.

The decelerator-RFQ is planned to be 1.9 m long with an inner cavity diameter of 35 cm (Fig. 48). The cavity will be equipped with a turbo pump and two ion pumps. Power requirements and costs can be extrapolated from the experience with the HLI-RFQ and similar projects. Maximum support

is anticipated from the University of Frankfurt (IAP) for the design, assembly, tuning and installation of the RFQ decelerator.

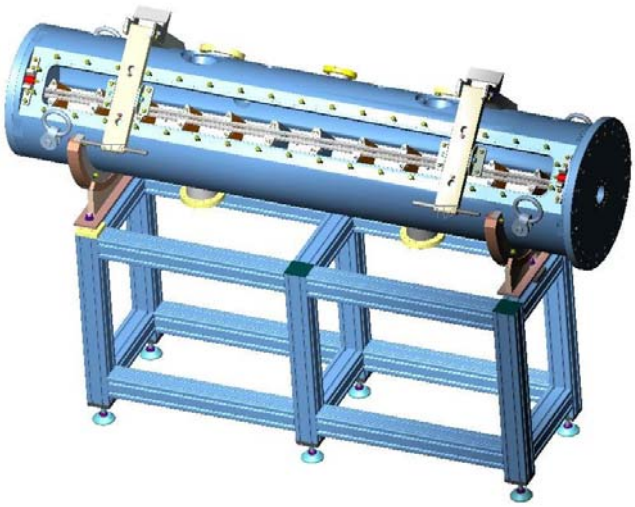

Fig. 48: Schematic drawing of the planned decelerator-RFQ. The inner diameter of the structure is 35 cm, the length 1.9 m.

Cooler Trap for heavy ions and antiprotons, and connection to experiments

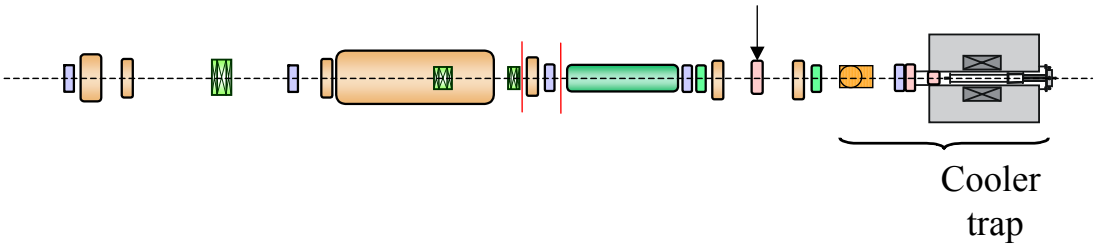

The cooler trap is designed to perform in-flight capture of a single bunch of ions or antiprotons, and to store them for subsequent cooling. As cooling principle, sympathetic cooling by trapped electrons has been chosen. The electrons are produced and captured inside the trap prior to ion bunch capture. Synchrotron radiation due to the electrons' motion in the magnetic field of the Penning trap cools them to the ambient temperature of 4 K with a cooling-time constant of about 100 ms. The captured ions or antiprotons are then sympathetically cooled due to Coulomb interaction with the electrons. Upon cooling and radial centring, the cold ion or antiproton bunch is ejected from the trap with a high brilliance and is available for all subsequent experiments. The cooler trap is pre-evacuated to below 10-8 mbar when first taken into use. During normal operation, the vacuum is ensured by the cryogenic surrounding to be better than 10-14 mbar, allowing for loss-free storage during the typical cycle time. To protect this vacuum from gas flow along the beamline, a fast commercial valve will be installed before the cooler trap and outside the magnetic field of the superconducting magnet, which produces the magnetic trapping field B. This valve will be opened only for loading of the cooler trap with a single particle bunch, i.e., it will have the same duty cycle as the cooler trap itself. Additionally, a diffusion barrier inside the 4 K region in close proximity to the trap will be installed to further reduce gas inlet to the trapping region.

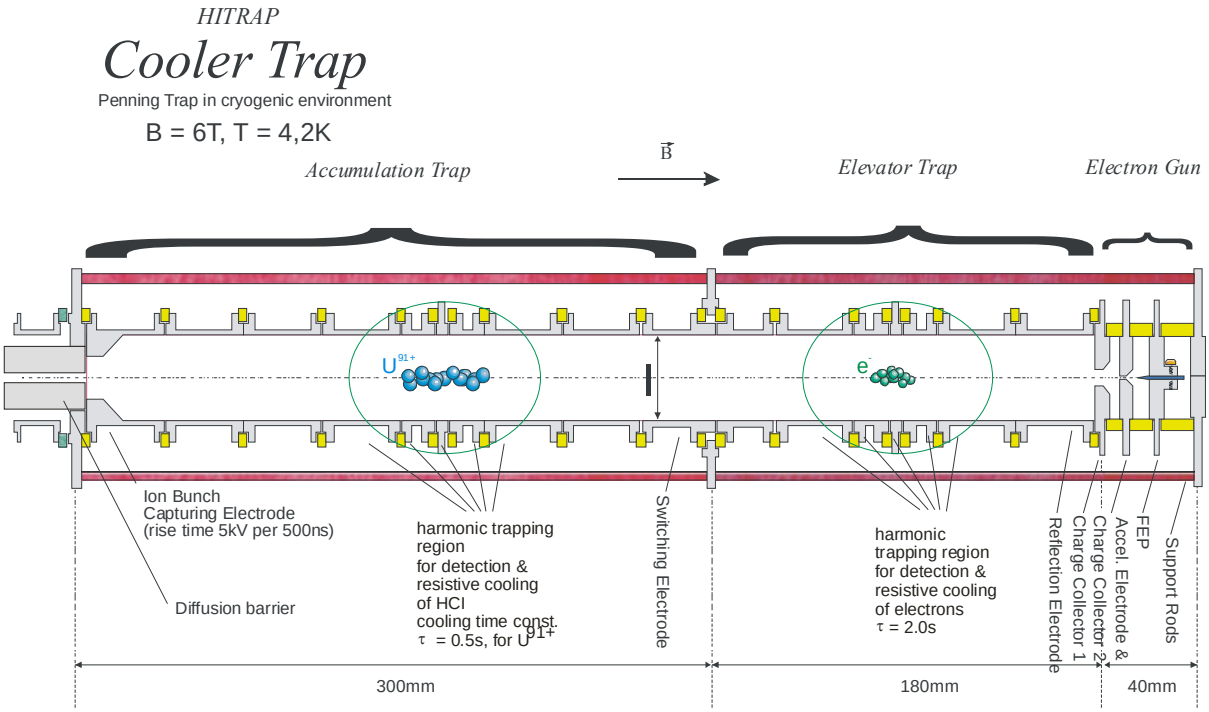

Fig. 49: Detailed sketch of the cooler trap.

The cooler trap consists of a horizontal stack of 21 cylindrical electrodes and is divided into three sections:

- an electron gun, based on a field-emission point (FEP) and designed to deliver 100 nA electron current at a low energy spread of about 0.1 eV,
- an 'elevator trap', used to collect and to transfer cold (ΔE = 0.1 eV) bunches of electrons (10^6 e- per bunch) into the accumulation trap, and
- the 'accumulation trap', which fulfils the main tasks to store electrons, let them cool down to 4 K environment temperature by synchrotron radiation, merge them together with captured ions or antiprotons in a 'nested trap' configuration and proceed with resistive cooling in order to perform the final cooling of the HCI or antiprotons to 4 K.

Fig. 49 shows the set-up of the cooler trap. Electrodes are manufactured from OFHC copper to avoid ferromagnetic impurities and magnetic field distortions. The electrodes are separated by sapphire elements for electric insulation. The stack of electrodes is mechanically stabilized by three rods spanning from the top of the electron gun to the bottom of the accumulation trap. The inner diameter (40 mm) is chosen to significantly exceed the expected diameter of the ion bunch and to avoid ion loss due to contact with the electrodes. It is not chosen larger than 40 mm since resistive cooling by attached tank circuits will become less effective with increasing electrode diameter.

Electron loading cycle

Before cooling the highly charged ions or antiprotons with cold electrons, the latter have to be created and loaded into the trap. Therefore, an electron loading cycle is proposed which consists of the following steps.

- collect electrons (1.5 µs): the current of the electron gun is switched on, the elevator trap is completely filled by a current of 100 nA within 1.5 µs with about 106 electrons in a flat (0.5 Volts) 'bath-tub' potential.
- *elevate (200 µs)*: these electrons, having an energy width of roughly 0.1 eV (mainly due to the FEP) are elevated to the bottom voltage of the accumulation trap, elevation time is roughly 200 µs, which is quasi-adiabatic (giving little heating effect).

- *merge (200 µs)*: the electrons are merged together in the trapping potential of the accumulation trap (having about 100 eV trap depth) by sweeping each electron bunch (~106 e-) into the accumulation trap. This process is also (more or less) adiabatic, since axial oscillation (bouncing between in the trap) happens within typically < 1.5 µs, whereas the merging process is performed by more than two order of magnitude more slowly within ~200 µs.

The heating effect (energy increase) during the merging process (according to Liouville's theorem) can be roughly estimated as the electron number in the elevator trap, divided by the electron number in accumulation trap, times energy spread in elevator trap. It therefore can be expected to result in a total increase of several eV after 2000 loading cycles, corresponding to 2×10^{10} loaded electrons after 1s. Due to fast collisional energy exchange on the millisecond time scale and radiative damping (with a cooling time constant of about 100 ms in a 6 T magnetic field) both axial and cyclotron energy of these 10^{10} electrons can be assumed to have the environmental temperature of 4 K (i.e. a thermal energy of less than 10^{-3} eV) within 5 s.

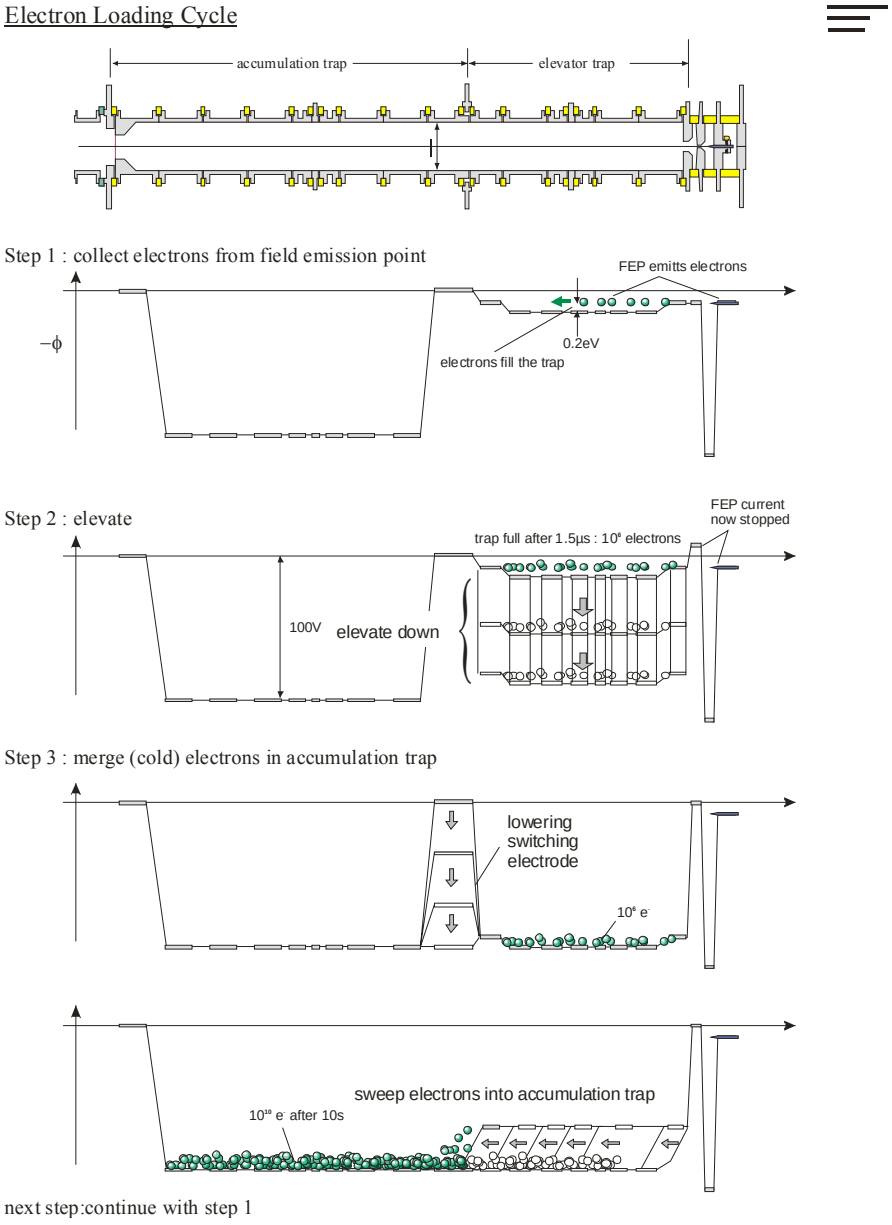

Fig. 50: Electron-loading cycle in the cooler trap

Ion and antiproton loading cycle

The decelerated ion (antiproton) bunches still consume a big phase-space volume. At an energy spread of several keV per charge they are supposed to enter the trap within about 2 µs. A capturing electrode which has to be switched by 5 kV at the trap entrance ensures the capture of a major part of the article bunch. Subsequently they undergo collisions in the interaction sections with cooling electrons, resulting in a residual energy spread of roughly 10 eV. Appropriate choice of the trap potentials ensures spatial separation and thus avoids recombination (of HCI). A following step merges the ions or antiprotons together into a harmonic trap region where final resistive cooling by means of a superconducting tank circuit is performed, resulting in an extremely low energy spread in the meV region. The parameters of the harmonic trapping region are:

- trap depth 20V × q
- axial frequency fz = 200 kHz
- resistive cooling time constant τ = 500 ms.

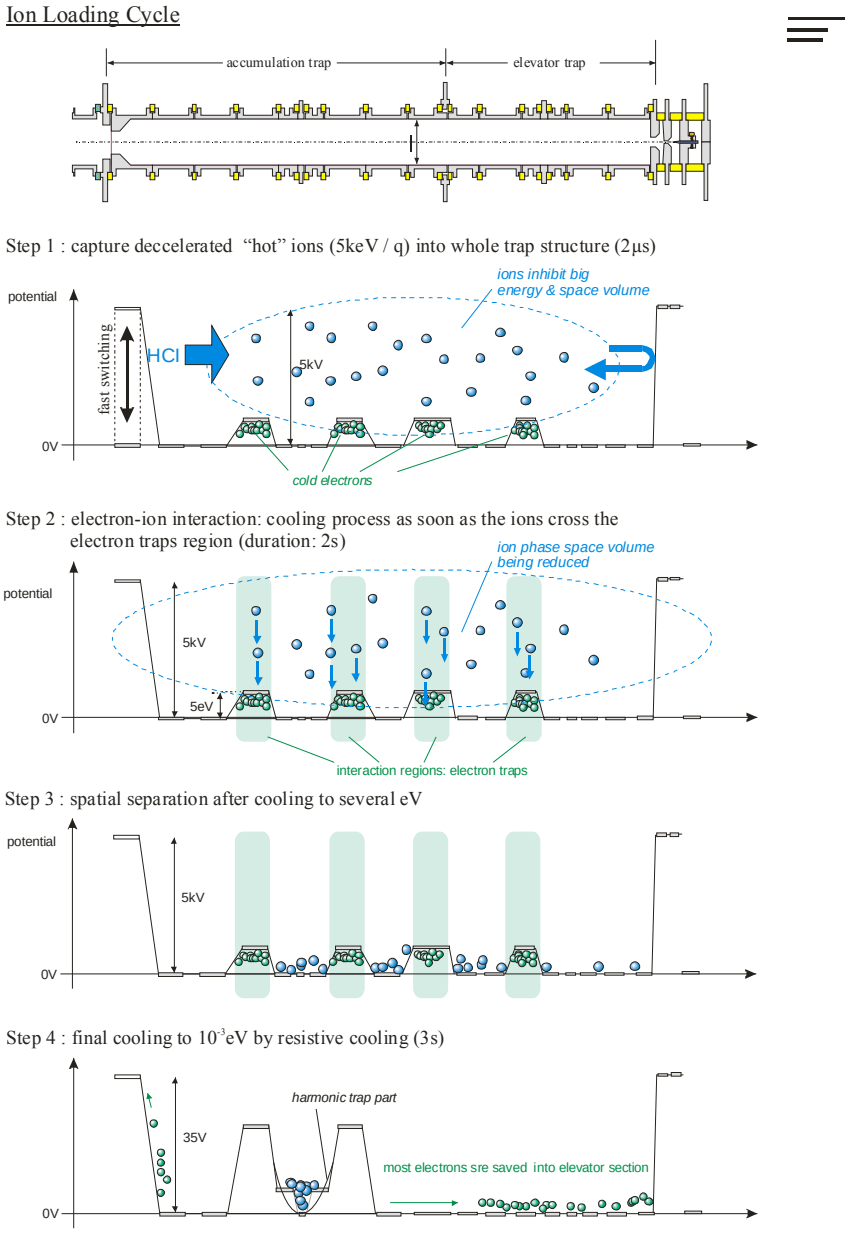

Fig. 51: Ion-loading cycle in the cooler trap

Diagnostics inside the Cooler Trap

The cooler trap is designed to allow for diagnostics of all relevant processes. For a quick particle-number determination, a destructive method will be implemented. It incorporates three charge-collector plates on which positively and negatively charged particles can be swept. In conjunction with a cryogenic charge amplifier, they can be detected with a high sensitivity and a big particle-number range of more than five orders of magnitude. Due to unipolar signal processing this is applicable for electrons, antiprotons, and for positively charged ions.
For the resistive cooling, radio frequency LC-circuits will be implemented which will operate at the cryogenic environment of 4 K. These allow also for the non-destructive bolometric and FT-ICR detection. Based on proven experimental results of the GSI-Mainz g-factor experiment, these methods exhibit an even higher particle sensitivity in the order of less than five highly charged ions or ten electrons and allow also for monitoring energetic and spatial distribution of the particle clouds in a non-destructive way, i.e. keeping the particles at rest inside the trap.
In order to observe the resistive cooling process and bolometric/FT-ICR-detection, the cryogenic tank circuits and subsequent cryogenic amplifiers will operate at frequencies of 200 kHz, 29 MHz, and 90 MHz, corresponding to the axial ion or antiproton motion (200 kHz), ion cyclotron motion (29 MHz), and antiproton cyclotron motion (90 MHz). The axial motion of stored electrons can deliberately also be tuned to 29 or 90 MHz in order to have a two-way use of one of the circuits. GaAs-based amplifiers are foreseen for the cryogenic environment to provide low-noise amplification, the 200 kHz circuit will be implemented as a Type-II superconducting coil, made of niobium-titanium.

Cryogenic Surrounding and Superconducting Magnet
The cooler trap is positioned horizontally in the homogeneous field region of a com-mercial superconducting magnet that provides a field strength of 6 T. It is in close thermal contact to a closed-cycle cryocooler at 4 K temperature. Shielding of the cryogenic region is provided by a surrounding thermal shield at 60 K and further passive shielding. The closed-cycle cryocooler does not require any filling of liquid helium or nitrogen. Both the cooler trap and the diagnostic electronics are in thermal contact with the 4 K region cooled by the cryocooler. The height of the setup in total is approximately 2 m, the diameter of the superconducting magnet is about 1.25m.

Infrastructural Requirements
The cooler-trap magnet is superconducting and operated in persistent mode, i.e. it requires no external power during normal operation. Power consumption of the trap is small, since only DC voltages are being pulsed at low frequencies and power dissipation is low. Spatial requirements are according to the set-up drawings (Fig. 17). The diameter of the cooler trap set-up (including cooling system and magnet) will not exceed 1.5 m, which allows for placement along the beamline. Integration into the whole HITRAP system has to take into account the filling requirements (accessibility of the magnet with dewars). Ferromagnetic materials in the direct surrounding to the magnet need to be avoided to the extent given by the map of the stray field of the magnet.

Extraction of heavy ions and antiprotons to experiments
In the trap, the ions or antiprotons are cooled to cryogenic temperatures (about 4 K). The cold particles will be extracted and guided to experimental set-ups outside the cooler trap without increase of temperature. The ions or antiprotons are ejected into the beamline ahead of the trap and then upward through the ceiling on top of which the ion and antiproton experiments will be located. An extraction voltage of up to 15 kV will be used to extract the particles from the trap at cryogenic temperatures. Extraction can take place in any mode from emptying the trap by one pulse of a few microseconds up to a DC-like beam. From the experience gained at ISOLTRAP, no problems are to be expected. Both the extraction voltage and the extraction mode will be adjusted to the need of the running experiment by the experimentalists themselves. In general, the construction and setting-up

of the components to transfer the beam of cold ions or antiprotons with extremely small emittance from the cooler trap to the individual experiments will largely be task of the experimental teams.

Acceptance Tests
HITRAP: Diagnostics in the beamline from the storage rings NESR and LSR to HITRAP must be tested after fast extraction at an energy of 4 MeV/u. The stability of the extracted beam is affected both by the elements in the storage rings (NESR for HCI, LSR for antiprotons) and by the components in the extraction line. The reproducibility of the parameters and the pointing stability of the extracted beam will be examined by suitable diagnostics.
Calibration: The detectors at the HITRAP facility will be calibrated by...

Requests for test beams
An H^- -beam at 4 MeV/u from LSR is required to test the HITRAP facility for the operation with antiprotons.
A beam of light HCI, e.g. Ne^{8+}, at 4 MeV/u from LSR or NESR is required to test the HITRAP facility for the operation with highly charged ions.

Trigger, DACQ, Controls, On-line/Off-line Computing
The operation of the HITRAP decelerator is planned as follows:
A 5 – 10 Hz pulser is employed to keep the RF transmitters at operation temperature. The pulser is synchronized with the 50 Hz mains.
About one second before an extraction from the NESR or LSR, the standard-system time ('Pulszentrale') sends an 'inhibit' signal to this pulser. The extraction and the operation of the decelerators get the 'sync' from the 'Pulszentrale'.
Describe: Trigger to trap, and trigger from trap to experiments

Safety

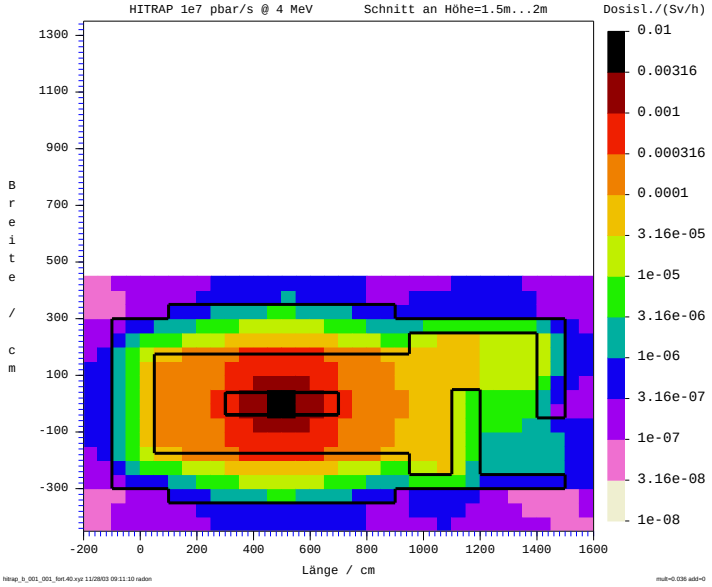

Fig. 52: Simulation of the radiation level in the HITRAP cave, assuming a worst-case scenario of a 4MeV-antiproton beam with an average intensity of 10^7 antiprotons/sec hitting a detector at the HITRAP decelerator. The spatial grid of the simulation has a resolution of 0.5 m.

Safety systems

Organisation and Responsibilities, Planning

The HITRAP project is an approved mid-term project at GSI, carried out by the Atomic Physics Group. After the approval, a number of external collaborators interested in the design of the HITRAP facility and experiments to be performed there formed an EU-RTD network coordinated by H.-J. Kluge from the Atomic Physics at GSI, in order to ensure ongoing collaboration in particular for experimental setups for the new facility. In parallel, teams from the Institute of Physics from the University of Mainz, led by G. Werth, the Institute for Applied Physics at the University of Frankfurt (groups of U. Ratzinger and A. Schempp), and the Michigan State University (group of G. Bollen, East Lansing, Michigan) work on the technical realization of the decelerator itself. H.-J. Kluge coordinates this realization stage together with T. Beier, C. Kozhuharov and W. Quint. From the GSI-accelerator department, W. Barth and L. Dahl coordinate the related activities. Agreements about contributions and deliverables from the different participants in particular for the experiments are fixed by the EU contract HPRI-CT-2001-50036 'HITRAP'. As far as the realization of the decelerator itself is concerned, obligations were only orally fixed so far. The deceleration within the ESR is part of the responsibility of the ESR operating team (M. Steck). Ion-optical calculations up to the IH structure are also performed by GSI. U. Ratzinger (Univ. Frankfurt, IAP) is responsible for the IH decelerator structure and A. Schempp (Univ. Frankfurt) has designed and will build the RFQ decelerator structure. The adjacent beamline into the cooler trap is being organized by GSI. The Cooler Trap itself lies within the responsibility of the group of G. Werth at Mainz. This responsibility is already fixed by the EU contract HITRAP (see above). Experiments behind the cooler trap have to be supplied by beamlines, which fall in the responsibility of the HITRAP collaboration.

The operation of the decelerator is planned to be carried out together with the ESR operation. The experimental operation will start only from the injection of particles into the cooler trap. Only this second part of the set-up will be controlled locally. The present TDR provides a suitable and cost-effective design for the complete decelerator structure, starting form the ESR and comprising all elements up to the beamline towards the experiments behind the Cooler Trap. The experiments themselves are tasks of the external collaborators (both in design and costs).

Support by EU: Experiments on heavy ions to be performed at HITRAP are prepared within the EU-RTD Network HITRAP (HPRI-CT-2001-50036), consisting of teams from GSI, GANIL Caen, KVI Groningen MPI-K Heidelberg, UJ Kraków, Imperial College London, Universität Mainz, MSI Stockholm, Technische Universität Wien, and are partly based on techniques developed within the EU Research Network EUROTRAPS (TMR Network CT-97-0144) and the EU RTD Network EXOTRAPS (ERBFMGE-CT-98-0099).

1.5 The Low Energy Experimental Area for HCI

An experimental area dedicated to the investigation of Highly Charged Ions (HCI) interactions with composite targets (molecules, clusters, nanostructures and solid target) in the energy range below 130 MeV/u is proposed to be built. It will take advantage of the high intensity cooled, decelerated ion beams extracted from the NESR. This experimental area will be placed in the FLAIR-building (Facility for Antiproton and Ion Research) adjacent to NESR. The heart of the experimental setup is a magnetic spectrometer for projectile charge separation with a momentum resolution below 5%. As focal plane detector for the projectile ions detection, a fast and radiation hard, two-dimensional position sensitive detector, based on CVD-Diamond is proposed. Additional detectors for the target fragments, electrons and x-rays detection are requested for the target region. The target itself will consist of solid foils or microstructures in form of diffusing jets (clusters), nanostructures and crystals. New advantages are opened by the possibility to use lower energy ion beams decelerated, cooled and extracted from the Low-energy Storage Ring (LSR) which is integral part of the FLAIR complex. Taking this into account, medium HCI of few MeV/u, will be available for tests and commissioning in this area.

The low-energy experimental area is dedicated to 'off-ring' experiments with decelerated and cooled highly charged ions extracted from NESR. Due to the ultra high vacuum requirements of the NESR and the geometrical configuration, with 'in-ring' experiments it is not possible to measure more then one or two different projectile charge states. For studying HCI-solid interactions, projectile- HCI-photon charge selective coincident measurements are the source for extremely valuable experimental information about the collision dynamics.

The proposed setup will be equipped with a magnetic charge separator for HCI, extracted, primarily from the NESR- with a maximum rigidity of 4.5 Tm. The design parameters of the NESR foreseen the possibility to store and cool all ions, up to bare Uranium with a rigidity of up to 13 Tm and A/q = 2.7. Deceleration down to 3 MeV/u in NESR is designed and regarded as specification for the hardware components. A slow extraction at betatron resonance or by charge changing processes will allow long extraction times, with the upper limit set by the required ion flux on the target and the intensity of the stored beam. For beams of HCI with energies in the region of few MeV/u the slow extraction time limit will be given by the life time of the beam. Fast beam extraction will be also available. Details about the available NESR beam parameters are presented in the Table 15.

Table 15: NESR beam parameter for the low-energy HCI beam available at the low-energy experimental area at FLAIR

Ions	all ions up to uranium
Energy	3 MeV/U to 130 Mev/u $B\rho_{max}$ = 4.5 Tm
Intensity	$< 10^8$ U^{92+} in NESR
Emittance (in NESR)	1 x 1 π mm mrad after cooling
Time structure	fast extraction slow extraction
Momentum spread	1x 10^{-4}

The Low Energy Storage Ring (LSR) which is proposed to be installed at FLAIR facility, and used as antiproton decelerator from 30 MeV down to 300 keV, can also decelerate / accelerate and cool highly charged ions below the NESR energy limit of 3 MeV/u. Having the possibility of fast and

slow extraction, the ion beam from the LSR will be an additional, very useful experimental tool which will increase the efficiency of this experimental area (for details see the CRYRING / LSR Subproject in this Technical report – Sec. 1.2).

Simulations

1) The Magnetic Spectrometer.

Charge identification of the projectile ions after the interaction with the target is absolutely necessary for the study of HCI- collisions with composite targets.

Particle-photon or particle-particle-photon coincident measurements will gain in precision through the projectile charge identification (background suppression).

For relativistic HCI charge separation is usually done by deflection in magnetic field: selected projectiles in a single charge state, interact with the target and the different resulting charge states separated in a dipole magnet will be detected in a position sensitive detector placed at the focal point of the spectrometer. Before entering the dipole, the beam is refocused by a pair of quadrupoles placed behind the target. In atomic physics experiments at relativistic energy is usually not necessary to precisely determine the projectile energy after the interaction with the target. But for experiments performed with solid state targets at projectile energies below 20 MeV/u, where the energy loss in target is large compared to the incoming energy and, in special cases, without charge state modification (channeling, [21]) the energy determination of the outgoing projectile ions is needed.

The spectrometer should fulfil the following requirements:

- magnetic rigidity 4.5 Tm
- large dispersion ~ 10 mm for U
- a momentum resolution of about 1%
- possibility to transport up to 20 different charge states to be imagined at the focal point by a 2-D position sensitive detector.

For the final design refined calculations of particle tracks in magnetic field are required. These will be performed for the design report. The GICO program will be used for this task. In parallel, ion-optical simulations for the beam transport through the whole system will be performed using MIRKO program. For the final decision the expertise of the group around the GSI Fragment Separator will be used. The final solution must decide not only about the configuration but also about the magnet type: normal or superconductor (Milestone).

2) Focal Plane Detector for Heavy Ions

The present status and the experience accumulated in the atomic physics group at GSI in HCI detection, point clearly towards a two dimensional position sensitive detector for the spectrometer focal plane.

This detector is a very important part of the experimental setup and it should mainly fulfil the following tasks:

- clear separation of different projectile charge states and in some cases the energy, to.
- beam monitoring: to check the beam focussing and to unambiguously determine the beam intensity. For the intensities available with the slow extracted HCI beams- expected maximum 10^8 Ions/spill stretched over 50 to 100 s - intensity determination via conventional integration methods (Faraday cup) can not be performed. This must be done using event-by-event counting. The accuracy of this measurement is very important for cross section measurements relaying on charge state separation.
- high sensitivity all over the energy range
- ion detection in the lower energy range requires a windowless, high vacuum compatible detector.

- in some exceptional cases, for measurements with ions at the high energy end (100 MeV/u and higher) it is useful to place the detector in air, outside the vacuum chamber.
- fast timing for coincident measurement.
- simplicity and reliability in use

Starting from all these requirements, following design parameters can be derived:

- *Two dimensional position read-out* with a resolution in both directions around 0.5 mm or better. This high position resolution is useful for the compact beams extracted from the storage ring and its final value is strongly coupled to the dispersion of the dipole magnet and the focussing properties of the system. 2-D read out proved to be extremely useful not only for beam monitoring but also for data analysis.
- *Fast response*: an intrinsic time resolution around 1 ns or better is needed for coincident measurements
- *Radiation hardness*: For most of the experiments almost the whole beam intensity is seen by the detector. Especially for the heavier ions at lower energy, the energy deposition in material is tremendous (ex. U^{92+} at 10 MeV/u losses all his energy of 2.38 GeV in 56 μm Diamond, $\rho = 3.5$ g/cm3) and the induced material defects are considerable.
- *High counting rate*: taking into account the beam intensity design value for Uranium a singe-particle count rate capability of up to 10^6 ions s^{-1} mm^{-2} is required.
- *Efficiency*: 100% detection efficiency over the whole energy range.
- *Large area*: It is extremely useful to be able to simultaneously measure more charge states. Considering a separation power for the dipole magnet of ~10 mm for U^{92+} / U^{91+} and a minimum number of 6 charge states, a minimum area of 80 x 40 mm^2 must be considered.

Taking all these into account, none of the today largely used detectors for relativistic highly charged ions such as semiconductors, gas based detectors and scintillators will properly perform. A completely new choice is offered today by diamond. This insulator is considered as the most important alternative to the use of semiconductors. The operating principle is the same as for semiconductors. Its main features are:

- Mean energy to produce a pair is ~ 13 eV (compared to 2. 96 eV for Ge and 3.62 eV for Si)
- Collection length is up to 250 μm for policrystaline material.
- Fast collection time supported by the high break-down field of up to 6 V/μm; this together with the collection length give an intrinsic time resolution below 100 ps
- Excellent radiation hardness
- Versatility for different configurations
- Affordable price: depending on the quality (layer thickness, polishing, homogeneity) the price is between 200 Euro/cm^2 to 1000 Euro/cm^2 and for large layers the price goes linear with the area.

The CVD technology (Chemical Vapour Deposition) used to produce the synthetic diamond allows today the production of good quality diamond layers of 10x10 cm2 at the lowest price.
Starting from this material, we propose to build a new generation of position sensitive detectors not only for the use in conjunction with the spectrometer, but even for beam diagnosis as beam profiler and position monitor.

Fortunately GSI is a front runner in the Diamond based detector development [22], [23]. In the atomic physics group a one-dimensional position sensitive, 60x40 mm^2 diamond detector [24], [25] is already available (see Fig. 53). Used in some experiments it revealed extremely good performances (fast response, 100% detection efficiency for 70 MeV/u few electron Bi ions, high counting rate). Despite this, the present design has few drawbacks which make it unsuitable as

focal plane detector for the future spectrometer, namely the low granularity (1.9 mm pitch) and the fact that is was designed to be used mainly for high energy beams extracted in air, i.e. the detector is not vacuum compatible.

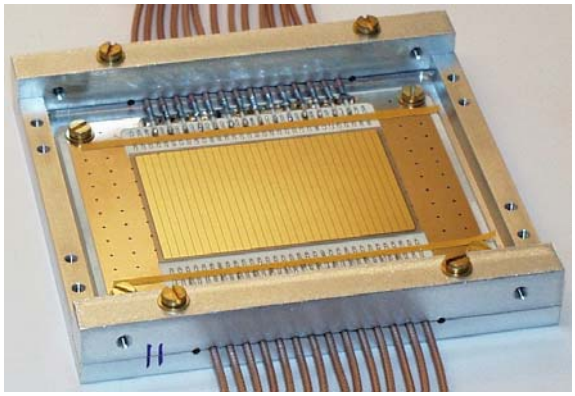

Fig. 53: One Dimensional position sensitive CVD-Diamond detector
presently used by the atomic physics group at GSI

Starting from these considerations a new prototype will be designed and built to clarify few points which are not yet decided:

- Which is the appropriate structure of the 2-D detector: strips or pads?
- What kind of read out will be used: single channel or delay line read-out
- Front-end electronics: The present detector is read out via a special developed broad band, low-noise charge integrating preamplifier. The signals are then feed into a level discriminator and scalers. The preamplifiers are connected to each individual strip and are stand alone external units. For a detector with 200 to 350 individually read out channels a new preamplifier concept must be developed. The proposed solution foresees to use specially designed integrated electronic chips (e.g. ASICs) mounted directly on the detector or as close as possible to it. This are much smaller compared to the actual preamplifiers and therefore the handling of the detector will simplify. Due to the large difference in the amount of charge created by the ions with the highest and the lowest energy into the diamond, the new preamplifiers must have variable amplification.
- The read out will tremendously simplify if it will possible to use the delay line technique. This possibility must be careful investigated because it is closely connected to the intrinsic diamond properties. This method is foreseen to be used for low energy beams which will be stopped into the diamond.

The prototype will be a 20 x 20 mm area detector with a granularity below 1 mm. With this detector the different read out solutions will be investigated (R&D Milestone).

Radiation hardness

The large amount of energy deposited by highly charged ions at intermediate energies poses serious constraints for the choice of the appropriate detector type. One can think about two scenarios: a cheap detector which can be replaced without high costs after few experiments or to choose a radiation hard material with good detection properties and trade the cost for the radiation hardness. The first choice is the one we have already at GSI. The present focal plane detector is based on an 80 mm diameter MCP chevron stack. Our experience shows that such a detector looses the detection efficiency after 'seeing' approx. 10^4 U^{91+} / microchannel at 20 MeV/u. In average, after tree to four experiments the MCPs must be exchanged.

The choice of the Diamond – solution has been triggered by considerations connected to the high risk of radiation damages for the focal plane detector. Diamond have proved to be extremely radiation resistive in tests performed width high energy, high intensity beams [26], [27].
However, there is an important aspect which needs more investigation: how does the diamond perform under the irradiation with slow, highly charged ions? Most of the information we have today have been won with minimum ionizing particles (mip) or high energy HCI (few hundred MeV/u) which deposit a small amount of energy into the material. Heavy ions with energy below 50 MeV/u deposit up to the whole kinetic energy they are carrying in a material layer thinner then 400 μm. Taking into account the energy needed to create an electron–ion pair in diamond- 13 eV- the energy loss by the HCI will produce a huge space charge which locally will polarize the diamond. It is not yet clear in which extent this phenomenon could affect the signal formation and finally the detector properties.
Using the proposed prototype, tests will be performed with beams from the existing GSI facility: most of the tests could be performed at UNILAC, but also SIS-ESR beams will be required.

Design
The final focal plane detector design will be decided after the tests with the proposed prototype will resume (Milestone). These include detector intrinsic properties and tests of the associated read-out electronics. For the design of the preamplifier a close collaboration with the NoRHDia[2] research collaboration, created around the GSI diamond detector expert group, is pursued.

Construction
The construction of the magnetic spectrometer will be realised at GSI, after purchasing the magnets. Depending on the final parameter list, the needed magnets could be constructed by our Chinese collaborators from the Institute of Modern Physics in Lanzhou.
The reduced dimensions of the focal plane detector for HCI will permit to entirely construct it at GSI using the GSI detector lab infrastructure. Only the segmentation of the Diamond foil must be done in a specialized lab, outside GSI. Due to the fact that more groups are interested in developing diamond detectors for the new generation of experiments at FAIR, we hope to find a way to optimize the costs. The collaboration with the NoRHDia will be extremely helpful in the realisation of the proposed detector.

Request for test beams

Test	Beam	Year
Delay–line readout test for the diamond detector	UNILAC	2005
2-D diamond detector prototype	UNILAC and SIS/ESR highly charge ion Beams E <11 MeV/u and E= 50 MeV/u	2007-2008
Test of the Beam Monitor detector	HCI beam from ESR, E<20 MeV/u	2009
Test and commissioning of the focal plane detector	LSR/NESR beams of highly charged ions	2011

[2] NoRDHia -Novel Radiation Hard CVD Diamond Detectors for Hadron Physics: Joint Research Activity in the frame of the EU supported Integrated Infrastructure Initiative on Hardon Physics (I3HP) (2004 to 2007)

1.6 Precision spectroscopy of antiprotonic atoms and antihydrogen for tests of fundamental interactions and symmetries (especially CPT)

1.6.1 Two-photon Laser Spectroscopy of the 1S–2S Transition in Antihydrogen

The goal is to observe the Doppler-free two-photon transition from the 1S ground state to the 2S metastable excited state in antihydrogen and to compare its transition frequency to ordinary hydrogen. The corresponding transition frequency in ordinary hydrogen at 2 466 THz (which corresponds to two photons at 243nm wavelength) has already been measured with an accuracy of better than two parts in 10^{14}. The comparison of antihydrogen and hydrogen 1 S – 2 S transition frequencies thus has the potential for a test of the fundamental CPT symmetry at an unprecedented level of experimental precision.

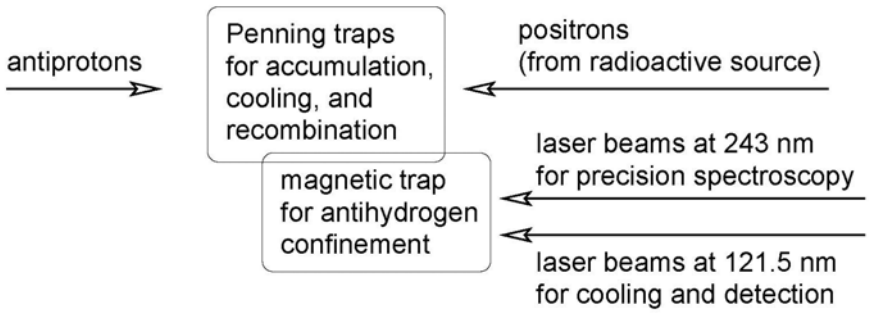

Fig. 54: Essential components for antihydrogen 1 S– 2 S spectroscopy.

Fig. 54 shows a schematic of such an experiment. Antiprotons and positrons are trapped, cooled, and recombined in Penning traps. The emerging antihydrogen atoms are electrically neutral and would leave the Penning trap. They do have a magnetic moment, however, and can thus be confined by magnetic gradient fields from a superimposed magnetic Ioffe trap. Once confined, the antihydrogen atoms can be cooled to the bottom of the magnetic trap using laser radiation at 121.5nm wavelength (Lyman-alpha). Laser beams at 243nm wavelength can eventually be employed to excite antihydrogen atoms on the narrow 1 S– 2 S transition.

Long-term perspective of physics program

Testing the fundamental CPT symmetry by using high-resolution spectroscopy of antihydrogen is a long-standing goal. The experiment involves several techniques which are each at the limits of what is technically feasible. Two international collaborations (with about 60 active physicists) pursue the goal of antihydrogen spectroscopy in ongoing experiments at CERN's Antiproton Decelerator (AD). The current state-of-the-art is: cold antihydrogen atoms have been produced for the first time in fall 2002. Both the production mechanism and antihydrogen properties (velocity and state distribution) have been investigated since. Magnetic trapping of antihydrogen atoms has not even been attempted yet. This is actually a very challenging step as magnetic traps are extremely shallow compared to Penning traps. In addition, the radially inhomogeneous magnetic field of a Ioffe trap can make the motion of charged particles in a Penning trap unstable. Extrapolating from the rate at which progress has been made in the past, it seems safe to predict that it still will take several years before high-resolution laser-spectroscopy with trapped antihydrogen atoms can be performed. Thus, the ongoing experiments at the AD will pioneer the techniques needed. The goal of high-resolution antihydrogen spectroscopy will most likely be achieved in the FAIR era, after the low-energy antiproton community has moved to FLAIR. The goal of this sub-project is a measurement at very high precision. It will thus be essential to investigate systematic effects in great detail. Experience with other high-precision measurements shows that it easily can take several years between observing the

first antihydrogen 1 S–2 S spectrum and giving a final value for the corresponding test of CPT symmetry.
The planning foresees two zones for antihydrogen experiments at FLAIR. This is similar to the present situation at the AD, but it does not imply that the present AD collaborations should form again at FLAIR. We vision the two antihydrogen experimental zones at FLAIR as a space-holder for collaborations which may form in the coming years. It is very important to have two experimental antihydrogen zones: The experience from the AD shows that competition is very healthy for such challenging experiments and speeds up the rate at which progress is being made. In addition, once an experimental limit for CPT-violation or CPT-conservation is available from one of the collaborations, the other collaboration has to deliver a very valuable independent check. It is important, that this possibility is foreseen at FLAIR as these antihydrogen experiments cannot be performed at any other planned or existing accelerator facility in the world (except at the AD, which will then no longer be operational). The community is strong enough to easily equip two antihydrogen experiments at FLAIR.

Necessary R & D

Dedicated R&D for this sub-project is necessary on the atomic physics side. Topics which are being investigated include: (1) demonstrate/investigate compatibility of magnetic Ioffe trap and Penning trap. (2) develop stable, robust and day-to-day reliable laser source at 243nm wavelength for high-resolution spectroscopy. (3) develop more powerful laser-sources at Lyman-alpha for faster cooling times. (4) demonstrate/investigate laser-cooling and nondestructive laser-spectroscopy with trapped ordinary hydrogen.

Beam requirements

Short pulses (~ 100 ns) of antiprotons (as many as possible) at energies in the 10–100 keV range.

Total beam time per year

1000 hours of beam time per year for each experiment.

Infrastructure

Each of the two antihydrogen spectroscopy experiments will require an experimental zone of about 150m^2 plus counting/control room plus laser cabin (about 100m^2) plus preparation labs plus office space. Liquid Helium and Nitrogen is required. Other requirements depend very much on the development of laser technology: With present-day technology (using large frame ion lasers as pump lasers) three-phase electrical current is required at a power level of about 200kW per experiment. The power will eventually be dissipated in cooling water (5m^3/h at >4 Bar and about 20°C). It is hoped that solid-state laser technology advances sufficiently fast in the next few years. Then less than 10% of the above power and cooling power would be needed.

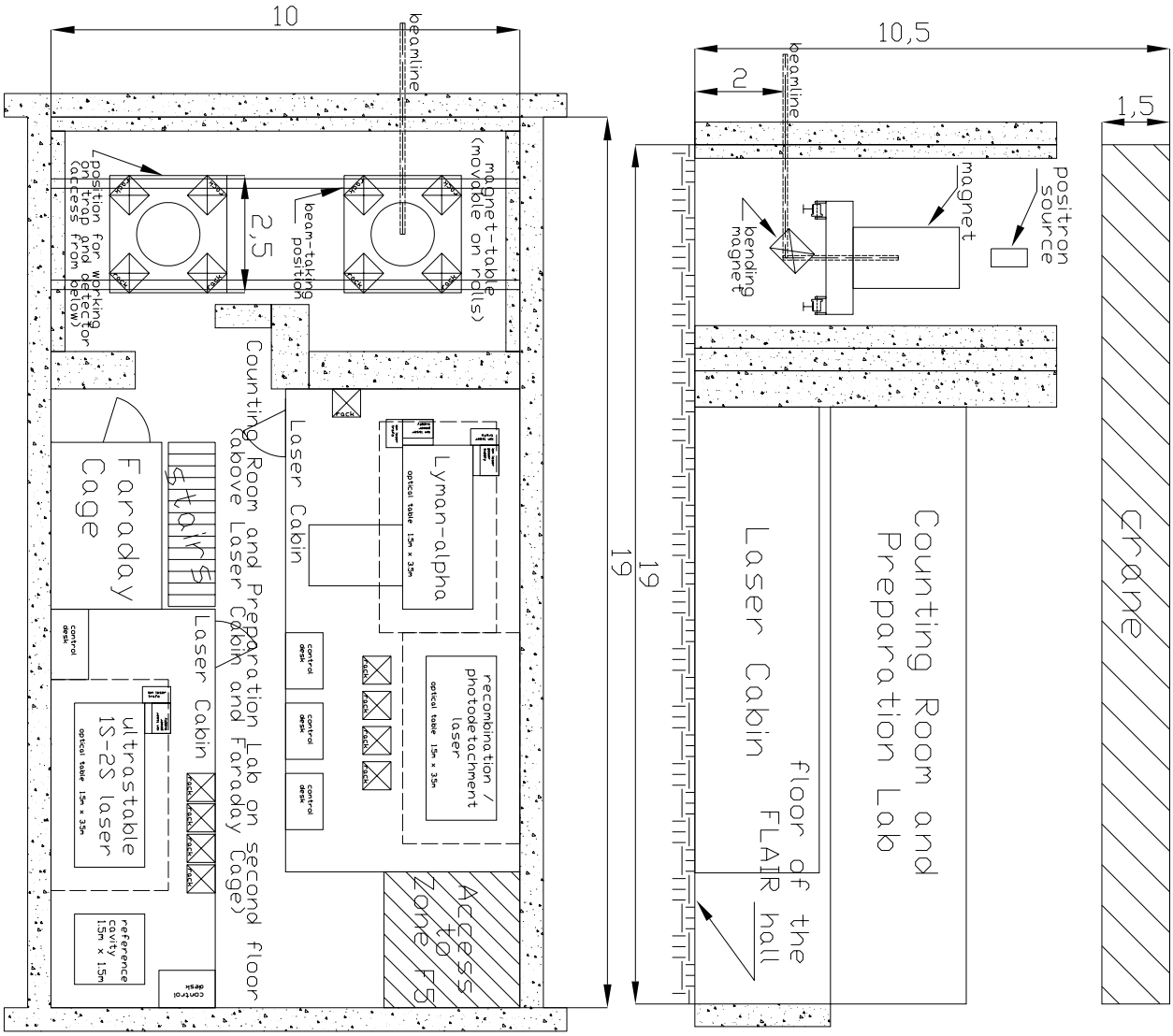

Fig. 55: Overview of the proposed setup.

Prospects of Funding

The community is strong enough and has succeeded in getting sufficient funding for the ongoing antihydrogen experiments at CERN's AD. A large part of this equipment can be moved to FAIR so that the investment is not lost.
Details of current fund-raising activities: J.Walz has an offer to become professor at Mainz University. He is planning to develop a new generation of laser sources for antihydrogen spectroscopy and cooling at Mainz. An application for funding from the German DFG is being written in the frame of a "TransRegio"-Proposal of the Universities München-Heidelberg-Mainz. Funding for antihydrogen activities at Mainz is expected at a level of 400 k€ and 2 positions for graduate students for four years, starting 2006.

Requests for Test Beams

A proton test beam would be very useful to test the part of the setup which deals with the initial trapping of antiprotons. This proton test beam can probably be generated within the proposed FLAIR facility. There are thus no implications for FAIR. The implication for FLAIR, however, is that the polarity of magnets in the beam-lines have to be reversible. But this is foreseen anyway.

1.6.2 Measurement of the Ground-state Hyperfine Structure of Antihydrogen

Introduction

The hyperfine splitting frequency ν_{HF} of the ground state of hydrogen is one of the best measured quantities in physics with a relative accuracy of 10^{-12}. Measuring ν_{HF} for antihydrogen therefore promises a very precise test of CPT. It is complementary to the measurement of the 1S–2S transition frequency ν_{1S-2S} because it addresses different topics: while ν_{1S-2S} is mainly determined by the positron mass, ν_{HF} is to leading order directly proportional to the antiproton magnetic moment, which is currently known only to an accuracy of 0.3 %. Below the level of several ppm accuracy, ν_{HF} also depends on the electric and magnetic form factors of the antiproton. The corrections due to the finite size of the proton are known as the Zemach corrections and are of similar origin as the BohrWeisskopf effect commonly studied in nuclei. The measurements of ν_{HF} of antihydrogen to a relative accuracy of better than 10^{-6} will therefore yield an improvement of the value of the antiproton magnetic moment by three orders of magnitude, and give some insight into the structure of the antiproton.

Experimental setup

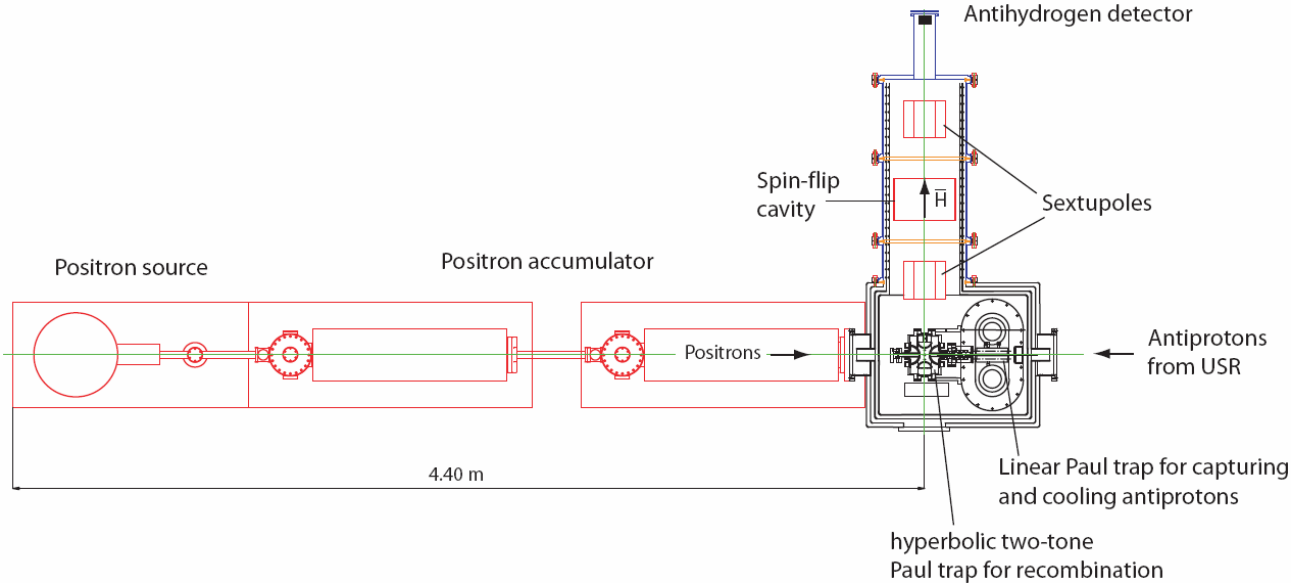

Fig. 56: Drawing of the experimental setup

For the measurement of ν_{HF} it is planned to use antihydrogen atoms “evaporating" from a formation region, and analyzing them in a typical atomic beam apparatus such as was used in the early days of hydrogen HFS spectroscopy. For the formation the same ingredients as for other antihydrogen experiments are needed: a positron accumulator, an antiproton capture trap, and a recombination trap. The above layout assumes the usage of radio-frequency Paul traps for the antiproton capture and recombination, which is currently being developed by the ASACUSA collaboration at the AD. For the measurement of ν_{HF}, an atomic beamline consisting of a sextupole magnet for spin state selection, a microwave cavity for spin flip, and another sextupole magnet for spin state analysis together with a detector for antihydrogen atoms will be used. Numerical simulations showed that such an experiment is feasible if 200 antihydrogen atoms per second in the ground state can be produced with temperatures up to 100 K. Relative accuracies of better than 10^{-6} can be reached within measurement times of a few days.

Beam time requirements

A pulsed beam containing >$3x10^7$ antiprotons of energy 100 keV to 20 keV, pulse length 100 ns, and emittance 10 π mm mrad at a repetition rate of 1 pulse per 1-3 minutes. A total beam time of 3 months per year is required.

Infrastructure

- An experimental area measuring 10 m x 6 m.
- A laser room measuring 100 m^2 located outside the radiation area.
- 80 kW 2-phase and 3-phase electrical power.
- 500 liters of liquid helium per 2 days.
- Helium recuperation lines.
- Compressed air and helium and nitrogen gas.
- Cooling water lines, standard 5 bars.
- Computer network connection.
- Office space for 3–4 people permanently, 6-8 during run periods.

1.6.3 Production of a Spin-polarized Antihydrogen Beam in the 1S State with a Cusp-trap for High Resolution Spectroscopy

Introduction

The key issue in making antihydrogen experiments like laser and/or microwave spectroscopy of antihydrogen atoms is first of all to prepare a high quality ensemble of a large number of antihydrogen atoms in the 1S ground state at low temperature and to confine these in a neutral atom trap. For efficient syntheses of antihydrogen atoms, the primary mechanism is the three body recombination process in a high density, low temperature plasma of antiproton and positron. Because antiprotons and positrons have opposite charge, they tend to separate when they are stored in a Penning type trap in a uniform magnetic field. In order to avoid the separation, antiprotons are usually kicked into a positron plasma, which however makes the temperature of the resultant antihydrogen atoms quite high [28], much higher than trappable with a known magnetic trap. Further, in the case of three body recombination, antihydrogen atoms are formed in high-Rydberg states with their binding energy of the order of the positron temperature. Some macroscopic time is necessary for these highly excited antihydrogen atoms to cascade down to their ground state.
Here a cusp trap scheme is employed, which could mix antiprotons and positrons in the same place even if their temperatures are zero [29]. In this case, cold antihydrogen atoms are automatically synthesized, and at the same time the synthesized antihydrogen atoms in the low-field seeking states are trapped for a time long enough to allow most of them to cascade down to the ground state for subsequent use in a variety of experiments. A fully-spin-polarized antihydrogen beam in 1S state is extracted from the cusp trap and used for high precision measurements of 1S state hyperfine splitting.

Experimental Setup

Fig. 57 shows a schematic layout of the cusp trap experiment in F9 Hall. Pulsed antiproton beams either from HITRAP or from USR are first stored in the catching trap, electron-cooled if necessary, re-shaped, and then transported to the cusp trap. The cusp trap consists of a pair of superconducting solenoids (Fig. 58) which provides a magnetic quadrupole field, and an electrostatic octupole (Fig. 67). An electron cooled positron source [30] is installed on-axis with the cusp trap, which is a full UHV-compatible system. Positrons from the source are transported to the cusp trap by a "traveling potential well" with a help of pulsed solenoid along the beam line.

Antihydrogen atoms in their low-field seeking 1S states are extracted, spin-flipped in the RF cavity, re-focused by the sextupole magnet spin selector, and finally detected by the antihydrogen detector.

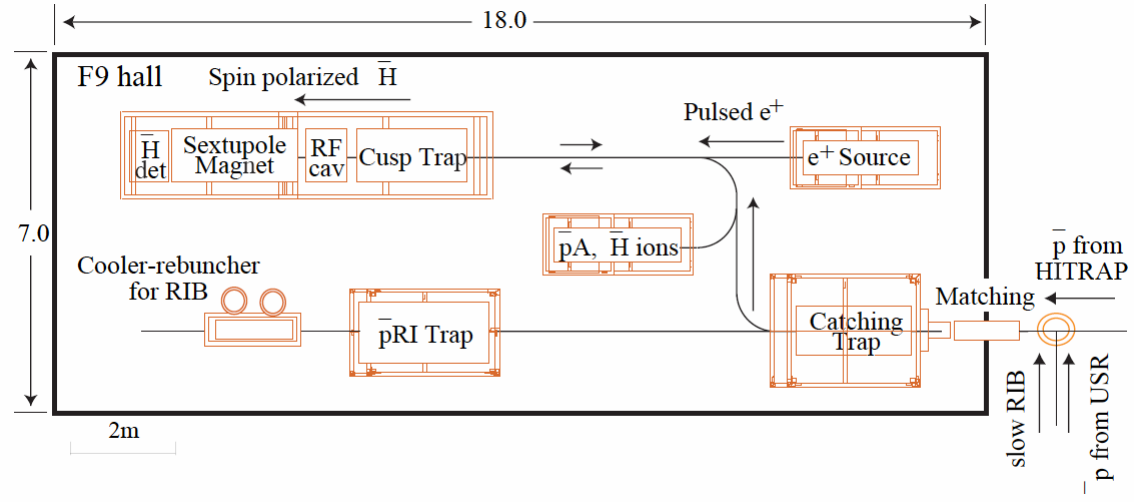

Fig. 57: A schematic layout of F9 hall for spin-polarized antihydrogen experiment.

Fig. 58: A photo of the superconducting quadrupole magnet.

Fig. 59: A photo of the electrostatic octupole.

As is described in the introduction, one of the unique features of the cusp trap is the ability to store charged particles with opposite charge and neutral particles in low field seeking states simultaneously in the same place for a macroscopic time. In other words, antihydrogen atoms collide with positrons and/or antiprotons for a macroscopic time, where the next three body reaction processes like

$$\overline{H} + e^+ + e^+ \rightarrow \overline{H}^+ + e^+$$

$$\overline{H} + \overline{p} + \overline{p} \rightarrow \overline{H}_2^- + \overline{p}$$

can take place. These charged particles should be stably accumulated in the cusp trap like antiprotons and positrons, which are later transported and stored in other traps for further investigation (first of all to confirm the syntheses of these exotic complexes), and manipulation like sympathetic cooling with laser cooled alkali earth ions.

Beam time requirements

A pulse of 10^7 antiprotons every 3 minutes is expected.

Infrastructure

Total height of experimental set-up (without crane): 2.5 m
Electric power consumption: 100 kW
Cooling water: 0.5 m^3/h (pressure range less than 7atm)
The setup will be installed permanently on the beam line.
Crane: 2tons at the maximum
A moderately clean room for handling UHV instruments
Data acquisition control room: 4x5m

1.6.4 g-Factor of the Antiproton

It is intended to develop and operate a cryogenic Penning trap setup for high-precision measurements of the proton and antiproton magnetic moments (g-factors) with an aimed experimental uncertainty of a few parts in 10^{-9}. This Penning trap will take beam from the HITRAP facility and will be located in the experimental area F10 on the second floor above HITRAP.
Similar high-precision measurements of g-factors in hydrogen-like ions have been performed before by use of related experimental methods. Recently, measurements on $^{12}C^{5+}$ [31], [32] and $^{16}O^{7+}$ [33] have been used to perform bound-state QED tests well below the 1%-level of sensitivity and to determine the electron mass four times more precise than before [34], [35]. The present kind of g-factor measurement is based on the "continuous Stern-Gerlach effect" [36] and relies on high-precision measurements of trapping frequencies of single particles stored in a Penning trap [37].
The measurement of the magnetic moment (or g-factor) of the proton and of the antiproton is a sensitive test of CPT invariance. Under the justified assumption that the motional frequencies of the stored particles can be determined with an uncertainty on the ppb-level, the resulting figure of merit [38] for a CPT-test is

$$\frac{h(\omega_c^+ - \omega_C^-)}{2mc^2} \leq 10^{-26}$$

To that end, a single proton/antiproton is confined in a cylindrical Penning trap at a magnetic field strength around 1.5 T which will ensure radial confinement of the ion, while the axial trapping is performed in a electric potential minimum of several eV. The trap and the vacuum enclosure of the apparatus are kept at liquid-helium temperature, thus the background pressure is below 10^{-16} hPa and the storage time before antiproton annihilation is longer than several months. The proton/antiproton is resistively cooled close to the ambience temperature of 4 K by keeping its oscillation frequencies at the resonance frequencies of high-Q resonance circuits attached to the trap electrodes. The trapped particle is monitored via the currents which are induced in the trap electrodes by its oscillations. The particle motion under this condition is a superposition of three individual trapping frequencies which can be measured independently in a non-destructive way and with high precision by resonant detection in electronic resonance circuits with high quality factors. The magnetic field at the particles' position is determined through the cyclotron frequency. The determination of the g-factor of the proton/antiproton results from a measurement of the spin precession frequency (Larmor frequency). The g-factor can be calculated from the two experimentally determined frequencies. Experimentally, the g-factor is obtained from the relation

$$g = 2\frac{\omega_L}{\omega_C}$$

where ω_L is the Larmor precession frequency of the particle spin around the magnetic field, ω_C is its cyclotron frequency. The frequency ratio ω_L/ω_C is determined by RF irradiation at a frequency ω_{RF} and a scan of the spin flip probability as a function of ω_{RF}/ω_C. The ratio with the maximum spin flip probability, ω_L/ω_C, yields the g-factor. Spin-flip detection is performed by transport of the proton/antiproton to one of the traps in which the magnetic field inhomogeneity is influenced by use of ferromagnetic elements. In such an inhomogeneous field, the trapping frequencies depend on the spin orientation. By use of the continuous Stern-Gerlach effect the spin direction can be determined. The ion is then transported back and the next RF frequency is applied, thus scanning the Larmor resonance.
The application of the continuous Stern-Gerlach effect in combination with the double Penning trap method and novel experimental techniques [39], [40], [41] for highly sensitive particle motion measurements offers exciting possibilities for a high-precision measurement of the magnetic moment of the proton/antiproton on the ppb-level or better. Such a measurement can be prepared

off-line with a single trapped proton, which in itself is a measurement of fundamental interest. The measurement on the antiproton would represent an improvement in accuracy by more than six orders of magnitude [42].

The measurement of the magnetic moment of the proton, which is an important fundamental constant, will be performed at the University of Mainz. Between the proton and the antiproton measurement, the setup has to be modified from in-trap production of the proton to the use of externally produced antiprotons. The measurement on the antiproton can be performed at the low-energy antiproton facility FLAIR at the future GSI-accelerator complex FAIR which is presently being planned.

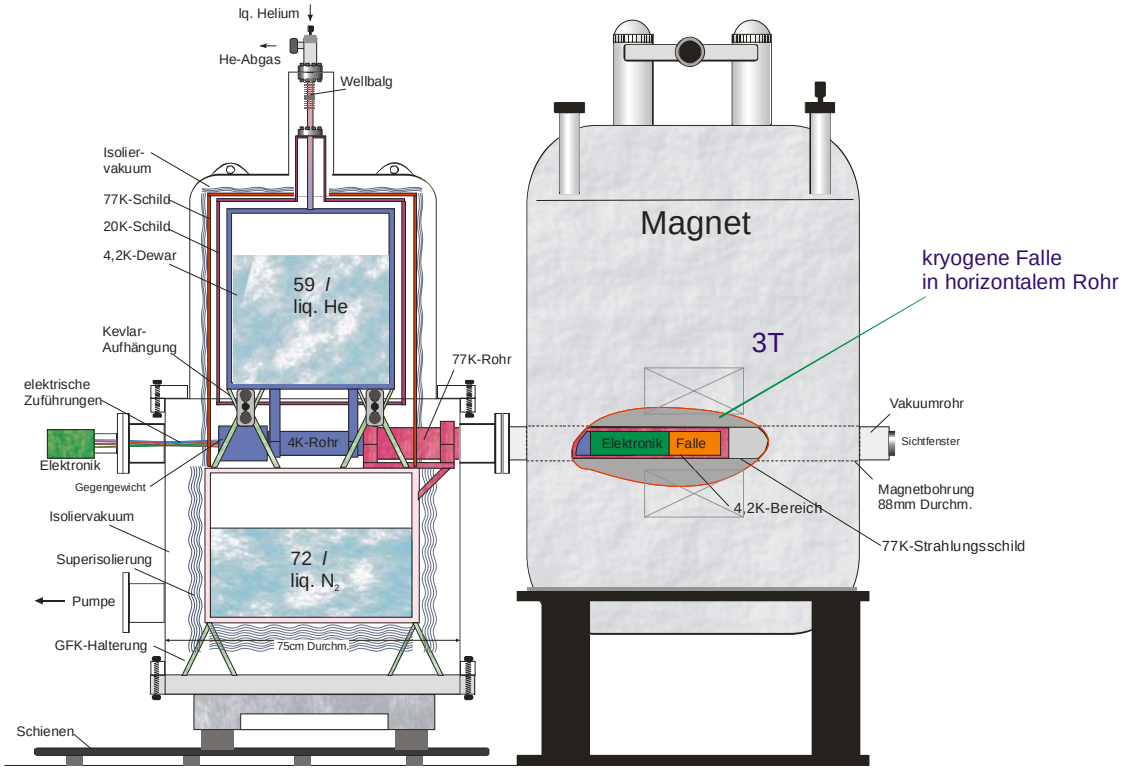

Fig. 60: Schematic drawing of the experimental setup.

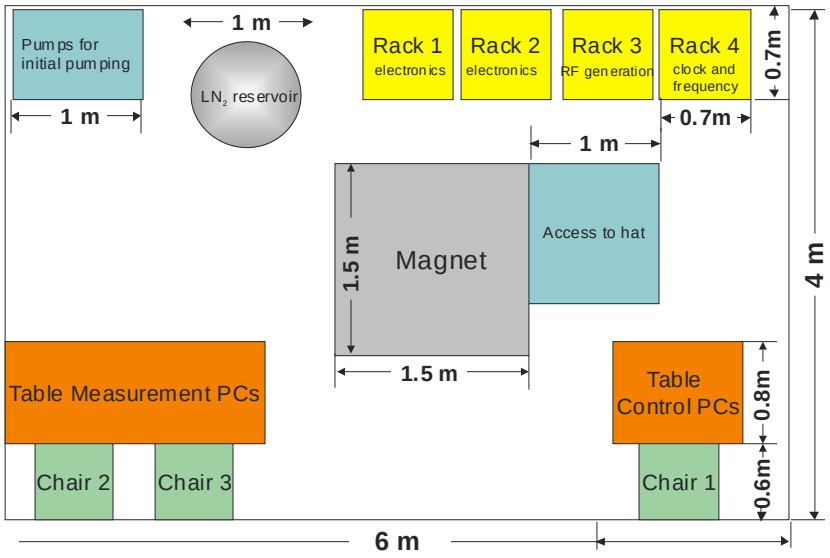

Fig. 61: Floor plan for the high-precision g-factor measurement setup which will be located in the experimental area F10 on the second floor above HITRAP.

The dimensions and the floor plan are given in the schematic drawing of Fig. 2. A minimum area of 24 m^2 is required. For the installation of the superconducting magnet (SuMa) as well as the cryogenic trap setup a roof crane (0.5-1 tons) is needed. The beam will be injected from below to the SuMa (see Fig. 1). The required overall height is minimum 3m. In proximity of the SuMa where the crane is used to insert the setup to the magnet the required height is 4.5 m. Room temperature stabilization to one degree or better would be preferable. It is of importance to minimize mechanical vibrations of the setup to the micrometer level in order to obtain a high precision of the experimental results.

b. Electronic Racks

Four electronic racks (two for electronic components, one for RF generation and one for timing) are needed.

c. Cooling of Detectors (heat produced = heat removed!)

Additional cooling of detectors is not needed

d. Ventilation

No special ventilation is needed.

e. Electrical Power Supplies

One high-current (32A) plug and 3*4 standard 16 A plugs are needed, permanent power consumption less than 2kW.

f. Gas Systems

No gas system (expect pressurized air) is needed.

g. Cryo Systems

The superconducting magnet needs LN_2 and LHe cooling. Thus, a permanent helium recovery line and a liquid nitrogen line should be installed.

Detector –Machine Interface

h. Vacuum

Inside the cryogenic trap system, a vacuum of better than 10^{-14} mbar is provided by the cryopumping effect. This is needed to avoid electron capture and therefore loss of the highly charged ions.

i. Beam Pipe

To obtain the required excellent vacuum heating of the beam pipe should be foreseen, an operation under cryogenic conditions is preferable during the transport of the antiprotons/ions.

j. Target, in-beam monitors, in-beam detectors

No targets foreseen, inexpensive charge collectors (Faraday Cups) for use as in-beam monitors

k. Timing

Timing systems as presently already in use will be installed and therefore can be re-used.

l. Radiation Environment

A radiation environment should be avoided to minimize background on the detection and to allow permanent access by the users.

m. Radiation Shielding

Experiments are performed with only one or very few single ions. No radiation shielding is needed therefore.

Assembly and installation

The Penning trap setup will be assembled and tested at the Institute of Physics at the University of Mainz. The final installation in the FLAIR building will be done after all parts are tested and specified. Permanent access to the setup is needed.

n. Size and weight of detector parts, space requirements

The superconducting magnet is the heaviest individual piece and weighs about 600 kg. The cryogenic trap system and the external cryostat/cooler with mounting has a weight of about 200 kg. For the final installation in the cave, access by a roof crane is needed.

o. Services and their connections

The superconducting magnet needs regular service, including twice a week filling of LN_2 (liquid Nitrogen) and about once a month filling of LHe (liquid Helium). A permanent LN_2 line and a LHe recovery line will be requested, also a lifting ramp for lifting up the liquid Helium vessels regulary up to the magnet, if located above zero-level. For the valves a permanent pressurized air line is needed.

p. Installation procedure

As described above, the whole device will be first installed and tested at the University of Mainz. The final installation at the HITRAP facility can be done within two years.

Structure of experiment management

Project leader 1: PD Dr. Wolfgang Quint/GSI
Project leader 2: Dr. Manuel Vogel/Institut für Physik, Univ. Mainz

1.6.5 Penning trap system for high-precision mass measurements on highly-charged ions and antiprotons

Introduction:

The mass and its inherent connection with the nuclear and atomic binding energies is a fundamental property of an atom, a unique ”fingerprint”. Precise mass measurements and mass comparisons have a wide variety of applications in physics and metrology, including new determinations of the fine structure constant [43], [44], [45], [46] and for a new definition of the kilogram [47], [48]; providing input data for the determination of the electron neutrino rest mass [49], [50] to search for neutrinoless double beta-decays [51], [52] and for reliable calculations in astrophysical heavy-element formation [53]; as test of the fundamental charge, parity, and time reversal symmetry [54] and Einstein’s mass-energy relationship $E = mc^2$ [55]. Furthermore, a relative mass precision of better than 10^{-11} (*i.e.* $\delta m \approx 2$ eV for ^{238}U) would allow one to measure the binding energy of highly-charged uranium, with one or a few electrons, as good as or even better then presently achieved by x-ray spectroscopy.

For a mass measurement program HITRAP at FAIR offers unique possibilities by providing light particles/antiparticles as well as highly-charged heavy ions. A relative mass uncertainty of 10^{-11} and better can be reached with a setup as shown in Fig. 62 by employing highly-charged ions and a non-destructive Fourier-Transform-Ion-Cyclotron-Resonance (FT-ICR) detection technique on single stored ions. The use of the FT-ICR technique provides true single ion sensitivity. This is essential to access particles/antiparticles that are produced or delivered with minimum rates.

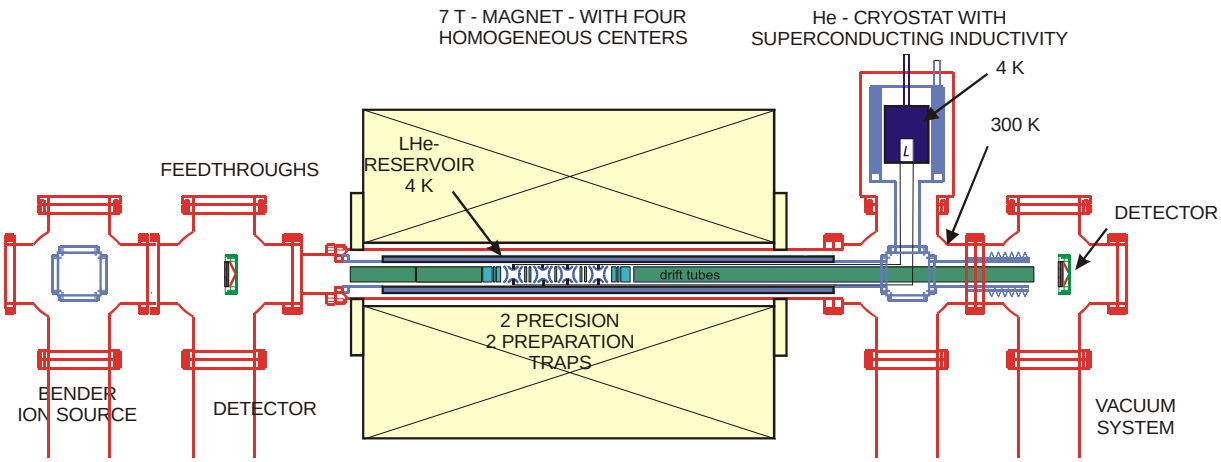

Fig. 62: Proposed high-precision mass spectrometer setup at the HITRAP facility. The trap system is installed in a 7 T superconducting magnet. Depending on the stored particle (light particle or highly charged heavy ions) either a destructive time-of-flight cyclotron resonance or a non-destructive Fourier transform ion cyclotron resonance detection will be used.

Penning trap system for high-precision mass measurements on highly-charged ions and the antiproton

The aim of this work is to build and operate a cryogenic Penning trap mass spectrometer for mass ratio measurements on light fundamental particles, as e.g. electron/positron, proton/antiproton, and highly charged ions with a relative uncertainty of $1 \cdot 10^{-12}$. This precision would allow to perform a stringent test of CPT symmetry by mass ratio measurements of particles/antiparticles and test of QED in highly-charged ions. Furthermore a precision of $1 \cdot 10^{-12}$ would allow one to measure the

binding energy of highly charged uranium, with one or a few electrons, better than presently achieved by X-ray spectroscopy.
In order to avoid uncertainties due to fluctuation of the electromagnetic fields, ion-ion interactions, and large field inhomogeneities, we plan to build a four-trap system, with two preparation and two high-precision Penning traps. All four miniaturized hyperbolical traps have to be installed in the same superconducting magnet with highest field stability and homogeneity and with a field strength of at least 7 T. Non-destructive phase-sensitive Fourier-Transform-Ion-Cyclotron-Resonance (FT-ICR) frequency measurements will be performed simultaneously by storing the two resistively cooled ions in different traps but within the same homogeneous region of the magnet. After such a measurement, the position of the ions will be exchanged by using the two preparation traps (or a new reloading of the traps from the preparation traps) and the measurement of the cyclotron frequency will be repeated. In this way ion-ion interactions are avoided and one can expect that magnetic-field changes as well as systematic errors will cancel to a large extent in the measured frequency ratios. At a later stage the ion of interest and the reference ion or both ions of interest will be cooled to below mK temperatures by exchange of energy with an ion (preferably $^{24}Mg^{+}$) which has been laser cooled to the zero-point state. The laser cooling of $^{24}Mg^{+}$ will take place in the preparation traps since no extreme field homogeneity is needed.

Simulations
Simulations are especially necessary to study the excitation of the ion motion inside the hyperbolic high-precision Penning traps. Detailed simulation studies of the ion motion have already been performed at ISOLTRAP, a Penning trap mass spectrometer for short-lived radionuclides at ISOLDE/CERN.

Simulation of the detectors
Destructive (time-of-flight ion cyclotron resonance, TOF-ICR [56]) as well as non-destructive detection techniques (Fourier-transform ion cyclotron resonance, FT-ICR [57], [58]) will be used to measure the cyclotron frequency of the stored ions. Both techniques are well known and novel detectors are presently under construction at the Institute of Physics at the University of Mainz and Greifswald. These detection techniques allow performing experiments with light charged particles as well as heavy ions. Detailed simulations are not needed.

Simulation of the beam
Beam simulation is mandatory to reach the envisaged accuracy. Mainly single particle trajectory tracking codes will be used, as e.g. SIMION. This program calculates magnetic and electrostatic fields from a given electrode geometry by solving the Laplace / Poisson equation via a finite differential method. Ion trajectories within a given field geometry are calculated by using a Runge-Kutta (4^{th} order) iteration technique. The injection, ejection, and storage in a Penning trap is well understood, however, there will be extensive calculations on these subjects to optimize the electrode shapes and setup. In addition self-written programs will be used to calculate ion trajectories within the traps. To calculate field inhomogeneities induced *e.g.* by the trap material itself a code (SUSZI) by Stefan Schwarz (MSU) is available.

Radiation Hardness (of detectors, of electronics, of electrical components nearby)
Since the high-precision mass measurements are performed preferably with a single trapped ion, radiation hardness is not an issue.

Design
The design will be made in close collaboration with the MSU, GSI, and Mainz groups. They have extensive experience in designing trap and detector setups. It is expected, that the design including calculations of the field inhomogeneities will take about two man-years.

Construction
The construction ideas are described above within this section. It is a very complex setup and a four-trap system has never been build before. Detailed calculations of the magnetic field distribution are therefore required. Cryogenic traps are already under operation at several places (CERN, MSU, and Mainz). The Mainz workshop is one of the leading places for the construction of hyperbolical precision Penning traps and their expertise will be used.

Acceptance Tests
A standard acceptance test will be required of the magnet manufacturer. After installation of the trap system, off line tests will assure that the required performance is reached. Since the traps are being built within the FLAIR/HITRAP collaboration, no formal acceptance tests as such are specified.

Calibration
The only calibration needed for the trap setup is in order to know the magnetic field strength of the trap magnet. This will be done first using a standard NMR probe by the manufacturer. Later the calibration will be performed by the determination of the cyclotron frequency of stable ions with well-known masses. To this end, an off-line reference ion source will be installed which provides preferably also highly-charged ions. Here, carbon or carbon cluster ions provide the reference mass of choice [59] since the unified atomic mass unit is defined as 1/12 of the mass of ^{12}C. Mass measurements on well-known masses allow studying the accuracy limit of the proposed setup [60].

Requests for test beams
In order to get the precision mass spectrometer operational, there is no external test beam needed. Stable (highly-charged) ions provided by the test ion source will be used to make the necessary tests.

Trigger, DACQ, Controls, On-line/Off-line Computing

To capture efficiently the light particle or highly-charged ion bunches delivered by the HITRAP Cooler Trap, a time resolution for trigger signals of about 50 ns is required.
The data acquisition and controls will be very similar to systems used in presently operated trap systems and detector setups. The data rates are low and the main technical challenge is in the real-time handling of a large number of different parameters. With today's technology the control and data acquisition requirements for this setup can be satisfied with 2 standard PCs and standard interfaces like GPIB, ProfiBus and cards connected to the PCI slots of one of the PCs.
Recently a new LabVIEW-based control system [61] has been implemented at the ISOLTRAP (ISOLDE/CERN, Switzerland), SHIPTRAP (GSI Darmstadt, Germany), and LEBIT (NSCL-MSU, USA) facilities by using the Control System (CS) framework which has been developed by DVEE/GSI during the last two years [62]. CS is an object-oriented, multi-threaded, event-driven framework with Supervisory Control and Data Acquisition (SCADA) functionality. It allows one to implement distributed systems by adding experiment specific add-ons. Thus, this CS is ideally suited for the experiment proposed here and can be adapted and extended to our requirements.

Physics Performance

Special performances are required for the superconducting magnet of the Penning trap in respect to the magnetic field magnitude ($B \geq 7$ T), homogeneity ($\leq \pm 0.01$ ppm measured over a 10 mm diameter spherical volume), and stability ($\delta B/\delta t \times 1/B \leq 10^{-10}$ / h). Limitations in the precision of mass determinations are temperature and pressure fluctuations in the helium and nitrogen reservoir of the superconducting magnet. They cause changes in the magnetic susceptibility of the materials surrounding the precision Penning traps and thus in the magnetic field homogeneity. The effect of temperature and pressure fluctuations should be minimized by the implementation of a temperature

($\Delta T < 0.1$ K) and pressure ($\Delta p < 0.2$ mbar) stabilization system. The transport, capture, and ejection efficiency of a trap are about 100%.
The resolving power achieved in a Penning trap is approximately equal to the product of the cyclotron frequency and the excitation duration T_{ex} and the accuracy scales with the resolving power. With the technique proposed here a resolving power of 10^9 can be reached.
The Channeltron detectors used for mass spectrometry experiments have overall efficiencies of 100%, MCP detectors in the order of 30-40%, depending on the kinetic energy of the ion.

Cave and Annex Facilities, Civil Engineering, Cranes, Elevators, Air Conditioning

a. Floor plan

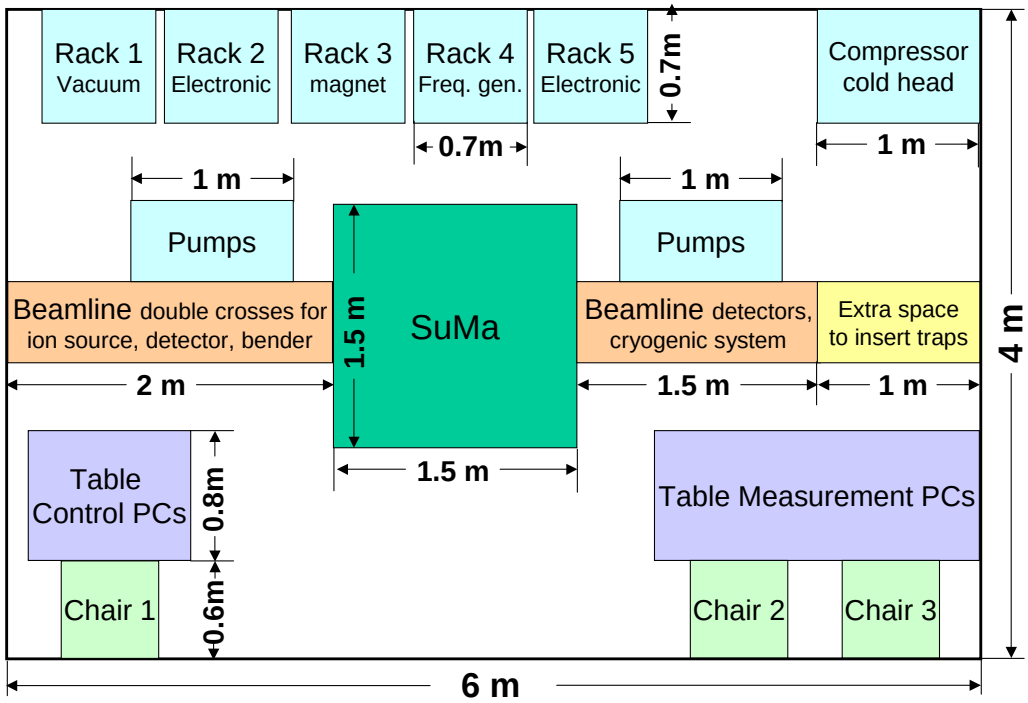

Fig. 63: Floor plan for the high-precision mass spectrometer setup.

The dimensions and the floor plan is given in the schematic drawing of Fig. 63. A minimum area of 24 m^2 is required. For the installation of the superconducting magnet as well as the cryogenic trap setup (see Fig. 62) a roof crane (0.5-1 T) is needed. The beam height will be about 1.25m, the required overall height is minimum 3m. Room temperature stabilization to one degree would be preferable. The option of an air conditioned container serving as counting house should be considered. Alignment possibility for the beamline, the installation of the superconducting magnets and of the detector onto the trap ejection axis has to be provided.

b. Electronic racks
Fife electronic racks (one for vacuum controllers, one for frequency generators, one for magnet supplies, and two for electronics) are needed.

c. Cooling of detectors (heat produced = heat removed!)
10 kW of 16°C cooling water for cryocoolers needed, 5 kW for turbopumps

d. Ventilation
No special ventilation is needed.

e. Electrical power supplies
10 kW for cryocoolers, 10 kW for remaining components including detectors.

f. Gas systems
No gas system is needed. Pressurized air is needed for the MCP detectors and vacuum valves along the beam line.

g. Cryo systems
The superconducting magnet needs LN2 and LHe cooling. Thus, a permanent liquid nitrogen line and a helium recovery line should be installed. The cryogenic trap systems will be installed in a cryogenic free cold head cryostat.

Detector –Machine Interface

h. Vacuum
Since the experiment will be performed with highly-charged ions special care on the vacuum is required. In the cryogenic trap system a vacuum of better than 10^{-12} mbar is needed.

i. Beam Pipe
A 100 mm diameter beam pipe is typically used for the beam transport, although much smaller diameters can be sufficient. To obtain the required excellent vacuum, backing of the beam pipe is planned.

j. Target, in-beam monitors, in-beam detectors
Multi-Channel-Plate detectors will be used to optimize and control beam transport between the HITRAP cooler trap and the precision mass spectrometer.

k. Timing
Standard timing systems as presently already in use will be installed.

l. Radiation environment
A radiation environment should be avoided to minimize background on the detector.

m. Radiation shielding
No radiation shielding needed. Experiments are performed with one or few ions.

Assembly and installation

The Penning trap mass spectrometer will be assembled and tested at the institute of physics at the University of Mainz. The final installation in the cave will be done after all parts are tested and specified. The space needed for handling is indicated in the schematic drawing of Fig. 62. Permanent access is needed.

n. Size and weight of detector parts, space requirements
The superconducting magnet is the heaviest part with about 500-800 kg. The cryogenic trap system including FT-ICR detector has a weight of about 300 kg. For the final installation in the cave access by a roof crane is needed.

o. Services and their connections
The superconducting magnet needs regular services, including twice a week filling of LN_2 and about once a month filling of LHe for the magnets. A permanent LN2 line and a LHe recovery line will be requested. For the beam line valves and MCP detectors a permanent pressurized air line is needed.

p. Installation procedure
As described above, the whole device will be first installed and tested at the University of Mainz. The final installation in the cave can be done within two years. Sufficient space (about 2m × 3m) will be needed for eventual repair works, maintenance, and temporary storage

Commissioning

a) magnetic field measurements

Magnetic field measurements of the superconducting magnet will be first done offline. For the final installation at FAIR a mapping of the magnetic fields in the near and far environment of the setup has to be performed to check the eventual influence of the strong (but shielded) magnetic field to the beamline and to other experiments. For the mapping a NMR probe will be used.
Note: External magnetic field sources and magnetic field fluctuations in the environment have to be avoided. The stray field of the Penning trap magnet will be minimized by shielding.

.

b) alignment

The alignment of the setup is very crucial since the injection of the highly-charged ions into the strong magnetic field is extremely critical. Help by an expert is needed for the alignment of the setup at its final position in the cave.

c) test runs

Since all tests can be performed with our off line ion source (for light particles an electron/proton source can be used) or with highly-charged ions from the cooler trap (see off-line ion source of HITRAP) only a very limited amount of shifts for test runs will be requested.

Operation

a) of each of the sub-projects

After optimisation, the setup will be operated at fixed conditions for periods of several hours up to several days. Experimental concerns are limited to preparation, cooling, and transport of the highly-charged ions. This aspect is decoupled from the operation of the production facility and will be performed by members of the HITRAP collaboration.

For the stability of the system (vacuum, voltage, magnetic fields, etc.) it is required to have all individual components of the Penning trap most of the time under full operation, even without a running on-line experiment. The superconducting magnets will be cooled down without any interruption and need therefore permanent maintenance, *i.e.* filling of LN_2 and LHe.

b) Auxiliaries

During the on-line operation of the setup stable conditions in respect to room temperature, magnetic stray fields etc. are mandatory to perform high-precision experiments. In addition crane movements and ramping of magnets in the near environment have to be avoided during operation since they cause magnetic field fluctuations in the trapping region and thus frequency shifts and systematic errors.

c) power, gas, cryo, etc

Power: 10 kW for cryocoolers, 10 kW for remaining components including detectors.
Gas: N/A

Cryo: The superconducting magnet needs LN2 (200 liters per week) and LHe (60 liters per month) cooling. Thus, a permanent liquid nitrogen line and a helium recovery line should be installed. The cryogenic trap systems will be installed in a cryogenic free cold head cryostat.

General comment: Pressurized air is needed for the MCP detectors and vacuum valves along the beam line.

Safety

a. General safety considerations
The electrical safety of the setup will be assured at both sites by the responsible teams.

b. Radiation Environment
The experimental setup is freely accessible since the experiments will be performed with one or a few stored ions per second.

c. Safety systems
The high magnetic field of the Penning trap will be indicated with signs at the laboratory entrances. The high voltages will be indicated as well. Only authorized people are allowed to enter the experimental area.

Stucture of experiment management

Project leader 1: Dr. Klaus Blaum, Institut f. Physik, Johannes Gutenberg-Universität Mainz
Project leader 2: Dr. Frank Herfurth, GSI Darmstadt

Responsibilities and Obligations

The institute of physics of the University of Mainz intents to apply for money to pay for the high-precision Penning trap mass spectrometer (~650 kEUR) and to apply for two PhD positions. Other institutes (e.g. University of Greifswald) may also apply for PhD positions.

WBS- work package break down structure

- Definition of the specification of the superconducting magnet, especially with respect to the required homogeneity of the magnetic field and the dimension of the magnet bore
- Simulations and design of the Penning traps with respect to, e.g., the dimensions and materials (influence on homogeneity) and especially the FT-ICR detection system
- Design of an off-line ion source for later tests of the Penning trap systems
- Design of the cryogenic system for the Penning traps, especially with respect to the ion detection with the narrow band FT-ICR detection system
- Simulations of the beam transport from the external ion source and from the cooler trap to the precision trap, and finally to the MCP/Channeltron detector
- Design of the injection/ejection into/from the Penning trap in close collaboration to the simulations of the beam transport
- Construction of the Penning trap
- Ordering and delivery of the superconducting magnet including the installation
- Development and commissioning of the control system
- Machining and installation of the beam line into/from the superconducting magnet
- Installation of the FT-ICR and TOF-ICR detectors and first off-line tests
- Installation of the Penning traps and first off-line tests

Relation to other projects

In the Technical Proposal of "MATS" (within NUSTAR) it is proposed to measure masses of short-lived highly-charged ions aiming for a mass precision of 10^{-9}. However, the measurements performed within MATS are complementary since they are aiming for short-lived nuclei with half-lives well below 1 s, which are not accessible at HITRAP. The measurements within this proposal are limited due to the used cooling and production techniques to nuclei with half-lives above 10 s.

1.6.6 Antiprotonic Atom Spectroscopy using cw Laser Beams (Antiprotonic Helium, Antiprotonic Helium Ions, Protonium)

Introduction

A pulsed beam containing more than $3 \cdot 10^7$ antiprotons, ejected at an energy of 100 keV will be captured by an ion trap and decelerated to an energy of a few electron-volts and compressed to a diameter d < 1 mm. An atomic target gas (hydrogen or helium) or vapour (lithium) is then injected into the trap. These react with the trapped antiprotons and produce antiprotonic hydrogen, helium, or lithium atoms, or their ionic forms. The atoms and ions are irradiated with a high-precision continuous-wave laser or a pulsed XUV laser, the wavelengths of which are precisely tuned to the atoms' Doppler-free two-photon transition energies, Fig. 64.

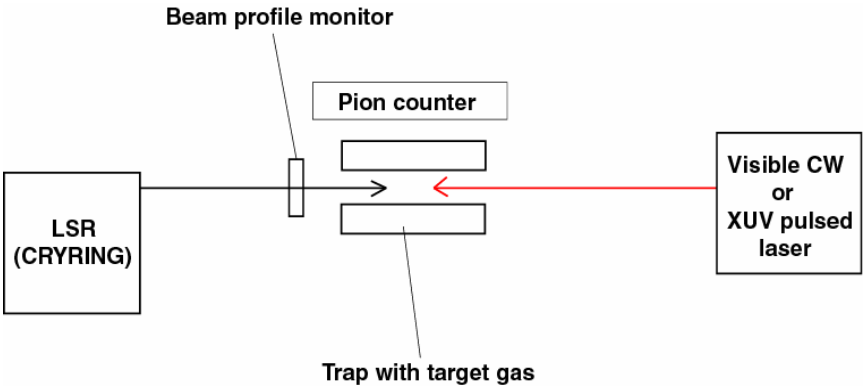

Fig. 64: A low energy antiproton beam is captured in a trap where antiprotonic atoms are created by a target gas jet. These atoms are then irradiated by a CW or XUV pulsed laser.

The resulting antiproton transitions are detected by observing one of the following, i): charged pions emerging from the ensuing antiproton annihilation using electromagnetic shower counters, ii): the electron emitted by the ensuing internal Auger process using micro-channel plate detectors, iii): the atomic fluorescence using an optical spectrometer. The antiproton transition frequencies can be measured to a precision of 10^{-10} in the best case. These results will yield i): antiproton mass to a precision of 10^{-10}, which is higher than the known proton value, ii): important feedback to high-precision 3- and 4-body QED calculations.
The laser system consists of continuous-wave titanium-sapphire and dye lasers, the frequencies of which are stabilized to an acoustically-isolated and temperature-stabilized etalon. The etalon is referenced to an optical frequency comb generator. XUV generation will be carried out using a pulse amplifier.

Beam requirements
A pulsed beam containing 3×10^7 antiprotons of energy 300 keV (but more ideally 100 keV) with a pulse length of 100 ns and an emittance of 10 π mm mrad is required for the injection into the experimental apparatus at a repetition rate of 1 pulse per 1-3 minutes. The experiment can run parasitically to other (main) users.
The total beam time per year will be 2 months.

Infrastructure
An experimental area in the beamline measuring 5 m x 6 m.
A laser room measuring 60 m^2 located outside the radiation area.
40 kW 2-phase and 3-phase electrical power.
500 liters of liquid helium per 2 days.
Helium recuperation lines.

Compressed air and helium and nitrogen gas.
Cooling water lines, standard 5 bars.
Computer network connection.
Safety exhaust line for toxic fumes and explosive gases (hydrogen).

Long-term perspective of physics program
We plan to systematically measure the atomic transition frequencies of all the fundamental antiprotonic atoms, i.e. antiprotonic hydrogen, three-body antiprotonic helium atoms, two-body antiprotonic helium ions, and antiprotonic lithium to the highest possible experimental precision, limited by their natural lifetimes.

1.7 Gravitation of Antimatter

Introduction

It is proposed to measure the gravitational acceleration of antimatter for the first time. Antihydrogen is a unique system for the investigation of antimatter gravity, because it is the only system available, which is both electrically neutral and stable. Neutral antihydrogen atoms are insensitive to stray electric fields which have plagued experiments in gravitational physics with charged particles for decades.
According to the Equivalence Principle, the inertial mass and gravitational mass are equal. The inertial mass of antimatter has already been measured to high precision in experiments at CERN which involved both Penning-trap mass-spectrometry and laser spectroscopy of antiprotonic helium atoms. The gravitational mass of antimatter, in contrast, has never been measured directly. The proposed measurement of the gravitational mass of antimatter could thus be interpreted as a first test of the Equivalence Principle in the antimatter domain.

Long-term perspective
The proposed measurement of the gravitational acceleration of antimatter using ultracold antihydrogen atoms is beyond the horizon of established experimental techniques. The main challenge is to produce antihydrogen atoms at ultracold temperatures in the sub-milli-Kelvin range. Novel techniques have to be identified and developed.
The test of the Equivalence Principle in the domain of antimatter is of very fundamental importance, which justifies the extraordinary effort.

Necessary R & D
The experimental challenge is that a practical measurement of the gravitational acceleration of antihydrogen requires very low temperatures. Laser-cooling of antihydrogen is limited by the photon recoil and by the natural linewidth of the Lyman-alpha transition to temperatures of several milli-Kelvin. This laser-cooling will be very important to suppress line-broadening and line-shifts of the narrow 1S-2S transition for high-resolution laser-spectroscopy of magnetically trapped antihydrogen atoms. For experiments in antimatter gravity, however, even lower temperatures are desirable. Atoms at temperatures of a few milli-Kelvin spread over several meters in the gravitational field of the Earth. It is therefore important to investigate new techniques which can cool antihydrogen atoms down to ultracold temperatures in the 10-100 micro-Kelvin range.

One scheme has been proposed which is based on the production of positive antihydrogen atoms, the antimatter partner to the familiar negative hydrogen ion. Once produced, these ions can be stored in a trap together with ordinary ions. Coulomb repulsion keeps the ions sufficiently far apart so that annihilation is not a problem. Ordinary ions (like In^+, or Mg^+) can have laser-cooling limits in the ten-micro-Kelvin-range. Sympathetic cooling then provides a mechanism to obtain positive antihydrogen ions at similar ultracold temperatures. Photodetachment with a pulsed laser can then be used to remove one of the positrons. The remaining ultracold antihydrogen atoms begin to fall and their gravitational acceleration can be determined from the time-of-flight between the photodetachment laser-pulse and the annihilation event in some detector. The main challenge for this scheme, at present, is to identify an efficient way of producing positive antihydrogen ions.

Another scheme (not published yet) is based on sympathetic cooling of antiprotons to ultracold temperatures. As "coolant" this requires negative ions. Osmium is the only known element whose negative ion has a bound electric-dipole transition. Thus, laser-cooling of negative osmium ions should be feasible. These ions can then be employed for sympathetic cooling of antiprotons. Again, annihilation is not a problem since the Coulomb repulsion keeps the negative osmium ions and antiprotons sufficiently far apart. This scheme is unique, as no other technique is known which can

yield antiprotons in the sub-millikelvin range. These antiprotons can be used to form ultracold antihydrogen atoms by charge-exchange with Rydberg-Positronium. This step has recently been demonstrated by the ATRAP collaboration at CERN. The resulting ultracold antihydrogen atoms can eventually be utilized to measure the gravitational acceleration of antimatter.

In addition to developing novel cooling schemes, the potential of atom-interferometric techniques for experiments in antimatter gravity should also be explored.

Infrastructure and beam requirements
The infrastructure and beam requirements of the proposed experiments to measure the gravitational acceleration of antimatter are identical with the requirements outlined above for the 1S-2S spectroscopy of antihydrogen in section 1.6.1. Large parts of the apparatus are also identical, for example antiproton and positron catching and cooling. The antimatter gravity experiment thus could use the same experimental area.

1.8 Interaction of Antimatter with Matter: Exploring Subfemtosecond Correlated Dynamics

1.8.1 USR Internal Target - Reaction Microscope

Introduction

Recoil-ion and electron momentum spectroscopy is a rapidly developing technique that allows one to measure simultaneously the vector momenta of several ions and electrons resulting from atomic or molecular fragmentation. In a unique combination, large solid angles close to 4π and superior momentum resolutions around a few percent of an atomic unit (a.u.) are typically reached in state-of-the art machines, so-called Reaction Microscopes. Evolving from recoil ion and COLd Target Recoil-Ion Momentum Spectroscopy" (COLTRIMS), Reaction Microscopes – the "bubble chambers of atomic physics" – mark the decisive step forward to investigate many-particle quantum-dynamics occurring when atomic and molecular systems or even surfaces and solids are exposed to time-dependent external electromagnetic fields.

Description of experimental goal and method

The USR shall provide antiprotons in the energy range from 300 keV down to 20 keV and might even approach the eV regime. At these energies, the interaction time between an antiproton passing atoms or molecules is on the order of 70 attoseconds (as) up to 1 femtosecond (fs) and, thus, comparable to the revolution time of outer-shell electrons in atoms or molecules. Moreover, the antiprotons' electric field is so strong that any perturbative theoretical approach must fail. Therefore, slow antiprotons provide an unsurpassed, precise and the only tool to study many-electron dynamics in the strongly correlated, non-linear, sub-femtosecond time regime, the most interesting and, at the same time, most challenging domain for theory.

The increased luminosity of the beam in these storage rings as compared to single pass experiments in combination with state-of-the-art in-ring reaction microscopes to record the vector momenta of several emitted electrons and ions simultaneously, will be the key technology to reach unrivalled event rates and resolution.

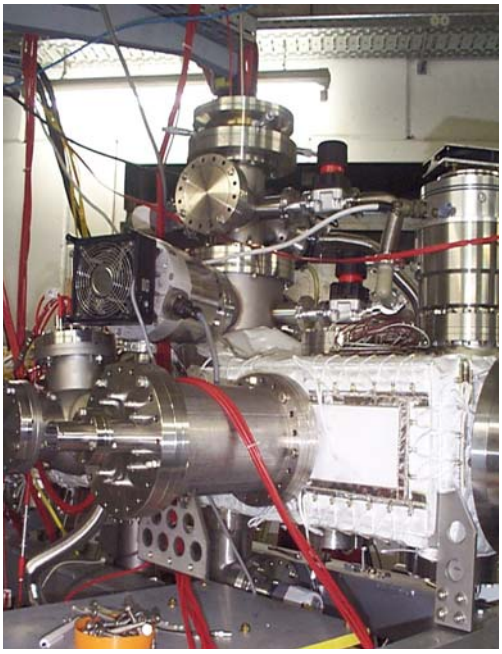

Fig. 65: Reaction microscope as it will be installed in the ESR.

Such a spectrometer has up to now only been tested at CRYRING, but never been integrated in an electrostatic machine or operated at ultra-low energies of the circulating projectile beam. An in-ring reaction microscope as it is shown in Fig. 65 has been successfully tested and will be integrated into the ESR at GSI in 2005. Even though the basic concepts can be used for a future spectrometer in the USR, a lot of R&D is necessary to achieve the required separation of the different fragments at the lowest energies without at the same time heavily disturbing the stored ions.

Beam requirements

For collision experiments inside the rings, a total number of 10^5 antiprotons per bunch will be sufficient, which is well below the space charge limit even at the lowest energies.
However, the time structure of the bunch needs to be around a few nanoseconds, which is an extremely demanding requirement, especially if one thinks about the coupling between transverse and longitudinal phase space in electrostatic deflectors.

Therefore, measurements at the cryogenic storage ring (CSR) that is presently built up at MPI-K, Heidelberg are required in order to demonstrate the technical feasibility.

1.8.2 Reaction Microscope after Penning Trap

Behind the HITRAP facility a wide spectrum of highly charged ions as well as of slow antiprotons with energies ranging from some eV up to some keV will become available. In combination with a reaction microscope, this opens up the possibility of kinematically complete experiments not feasible anywhere else.

Slow antiprotons will be captured into bound states of various rare gas target atoms with large cross sections into well-defined quantum states (n, l) which sensitively depend on the velocity of the antiprotons [63]. During the capture reactions as well as afterwards, when the antiproton cascades to lower and lower n-states, electrons are emitted. Measuring the complete momentum vectors of these electrons in a reaction microscope will provide unique information on the (n, l) distribution as well as on the dynamics of the cascade process. Moreover, pushing the momentum resolution to the limits, we expect, as has been demonstrated before for electron capture into slow highly charged ions [64], [65] to obtain precise spectroscopic information on the populated exotic $\bar{p}$, n e^- states in various rare gases.

At somewhat higher energies, pure ionization of the target atoms by antiproton impact dominates. Here, puzzling results on total cross sections have been obtained within the PS 194 collaboration at CERN for single ionization of various rare gases, especially for helium, being in troubling discrepancy with nearly all available theoretical predictions [66], [67], [68]. A reaction microscope behind the trap could provide, for the first time, fully differential cross sections on single and multiple ionization by antiproton impact at very low velocities, possibly not reachable in the USR. This velocity regime, where the antiprotons move about as fast as the bound-state electrons is extremely interesting and challenging for theoretical treatment, but on the same time, represents a prototype system for exploring correlated dynamics on the sub-femto to attosecond time scale not accessible by any other means.

Using highly charged ions extracted from the trap, we can explore, again in kinematically complete experiments, single and multiple electron capture reactions at ultra-low collision velocities, where only few investigations have been reported so far in the literature [69], [70] with strong deviations from theoretical predictions. As for the antiprotons (n, l) distributions for the captured electrons will be accessible and the energy levels of populated states will be determined with a precision that challenges many-particle atomic structure codes. Moreover, until now, no multi-electron transitions and rearrangement processes occurring after the capture of many electrons were investigated at these very low velocities.

In the reaction microscope, a supersonic He beam is crossed with the projectile beam from the trap. The electrons and recoil ions are momentum-analyzed simultaneously by the same spectrometer system. It consists of two parallel resistive plates which are oriented along the projectile beam axis. An electric field between these electrodes is generated by applying a voltage of some 10 V across the plates so that the electrons are extracted parallel and the recoil ions anti-parallel to the projectile beam direction. After traversing a field free drift tube following the extraction region, the recoil ions and electrons are detected by two two-dimensional position-sensitive channel plate detectors.

Typically, the extraction field is not strong enough to guide a sufficiently large fraction of the electrons onto the detector and, thus, a modest uniform magnetic field of typically some 10 G pointing in the same direction is generated by two Helmholtz coils and overlaid with the electric extraction field.

As a result, the electrons are forced into cyclotron motion with a radius proportional to the transverse momentum component of the electrons. In order to simultaneously record the time of flight and position information of both electrons emitted in the same collision with a single detector, a delay line anode in conjunction with a multi-hit time to digital converter (TDC) is used.

In direct comparison to in-ring spectrometers, the demands in terms of the final vacuum pressure are far more relaxed, the detectors need not to be movable and the costs for the device are considerably less. Furthermore, the required momentum acceptance for the beam of the spectrometer in this single pass setup is below the acceptance of in-ring reaction microscopes and thus reduces the costs even further.

A schematic drawing of the setup is shown in Fig. 66.

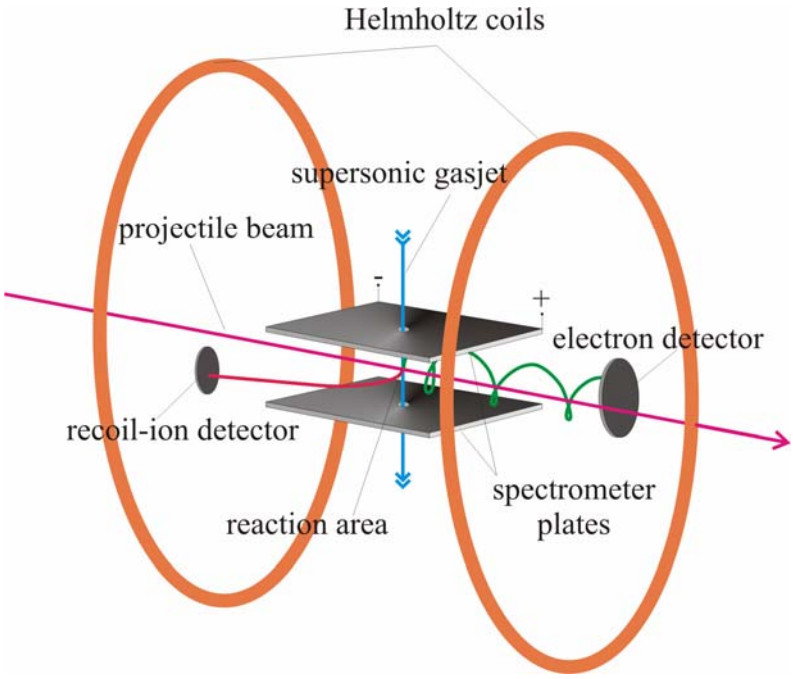

Fig. 66: Schematic drawing of the reaction microscope

Beam requirements

For collision experiments with highly charged ions a total number of 10^6 ions or antiprotons per deceleration cycle, continuously extracted from the trap in a DC mode, will be sufficient to explore capture of antiprotons in rare gas atoms, ionization of the rare gas atoms by antiproton impact as well as single and multiple electron capture into highly charge (exotic) heavy ions.

1.8.3 Energy loss and Ionization of Slow Antiprotons

A detailed knowledge of the interaction between slow antiprotons and matter is important for the design of scientific apparatus, antiproton radiation therapy, detectors, and not the least for the advancement of atomic collision theory.

Our group has performed a thorough investigation of the energy loss of antiprotons in matter and of the cross section for ionization of atoms and molecules by antiprotons in the energy range from several MeV to a few keV.

There are, however, a number of outstanding problems still to be solved. Among them is the energy loss of slow antiprotons in insulators and gases, where very little firm data exist. Furthermore, the cross total section for single and multiple ionization by slow antiprotons of atoms and molecules is a field which is only recently opened up to experimental investigation.

The experimental method for measuring energy loss is simple, as we will use two electrostatic analyzers, separated by a (solid or gaseous) target. In the first analyzer, the energy of the antiprotons is determined, while in the second, the energy loss is measured.

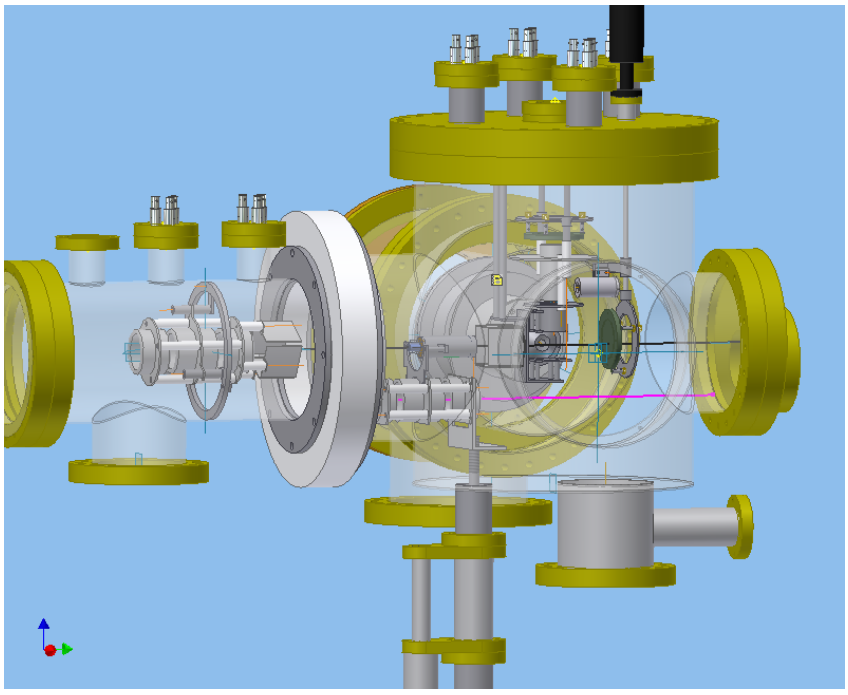

Fig. 67: Schematic of the interaction region of the ionization apparatus.

For ionization cross section measurements, we will use a setup like that shown in Fig. 67: The antiprotons are post accelerated to the desired energy and pass through a gas-jet, after which each is detected by a channel plate. The ions created in the collision region are extracted to another channel plate, whereby their flight time can be measured. This identifies the species of ion, and therefore the cross section can be obtained, via a normalization of the target density using an electron beam and the well known cross sections for ionization by keV electrons.

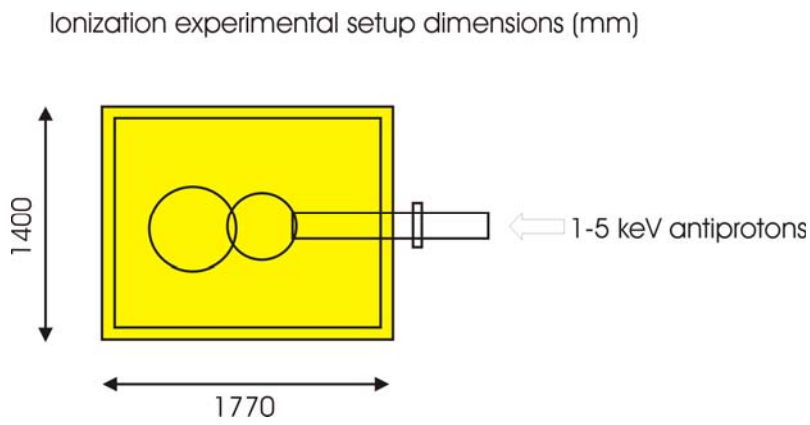

Fig. 68: Dimensions of the ionization apparatus.

Beam requirements

DC beams of 1 – 100 keV are required, with intensities larger than 10^4 . Emmittances should be better than 1 mm mrad @ 1 keV. Thus, the beam could come either from direct extraction from the USR or from a Penning trap to obtain even smaller $\bar{p}$ energies.

Beam time requirements per year
4 weeks.

1.8.4 Antihydrogen Collision Experiments

Introduction

Based on the production of antihydrogen at rates higher than a few 10^2 per second, it will be of great interest to investigate the inelastic interaction of these anti-atoms with atoms and molecules will be studied at well-defined relative velocities below ~1 atomic unit (a.u.). The experiments will explore the dynamics between initially neutral, composite matter and antimatter systems. They probe new types of quantum dynamics [71], [72], [73] in systems containing both leptonic and hadronic pairs of particles and antiparticles, involving also important influences of other fundamental interactions. This is illustrated [73], [74] by the role of annihilation and by the significant effect of the strong interaction on the scattering length, as predicted by recent calculations.
Antihydrogen interaction studies with hydrogen and with heavier atoms and molecules give experimental access to the signatures of annihilation between neutral antimatter and matter in astrophysical environments [75]. Moreover, matter-antimatter interactions are of considerable practical importance; thus, cooling and excitation transfer in hydrogen-antihydrogen collisions are intensely discussed with regard to scenarios for cooling and de-exciting cold antihydrogen atoms in hydrogen-antihydrogen mixtures [72]. Scenarios of this type are considered since antihydrogen is formed mainly in highly excited states in nested traps, which strongly hinders cooling and precision spectroscopy aiming at CPT tests.
Some aspects of the unique, otherwise unaccessible quantum dynamics are: (i) the competition between annihilation in flight on the one hand and the re-arrangement into positronium and antiprotonic atoms on the other hand; (ii) the interaction potential between antihydrogen and matter atoms or molecules and the possible existence of scattering resonances; (iii) excitation exchange in $\overline{H}^*$ – H interaction; (iv) in case of interaction with a positronium target, charge exchange processes leading to the formation of the antimatter counterpart $\overline{H}^+$ of the negative hydrogen ion (H^-), which in turn would open up a window to antimolecule formation by associative detachment.

Description of experimental goal and method

The development of these experiments is inseparable from the realization of efficient antihydrogen production at the FLAIR facility. The basic requirement is a directed flux of antihydrogen out of a production zone into a separate interaction zone, where the neutral antihydrogen beam is crossed with a neutral (atomic or molecular beam) target.

The following scenarios can be envisaged:

<u>Antihydrogen from merged positron and antiproton beams in the USR</u>

Arrangement and requirements

The basic arrangement is shown in Fig. 69 (a); fast antihydrogen atoms from the USR merged positron beam interaction zone interact with a thin gas target conntected to a straight section of the USR via a vacuum coupling and differential pumping section. For an antihydrogen velocity below 1 a.u., the energy of the stored antiproton beam must be below 25 keV. Hence, the formation of a suitable antihydrogen beam is related to two experimental frontiers. (i) Storage of an antiproton beam at the lowest USR energy of 20 keV, using electron cooling with an electron beam of ~11 eV, at high intensity (e.g., 10^7 antiprotons) with a beam diameter <2 mm. (ii) Production of an intense merged, 2 mm diameter positron beam at low internal temperature (e.g., 1 meV) at a density of, e.g., 2×10^7 cm^{-3}. This appears feasible only with a storage scheme, such as the one proposed by Meshkov et al. The positron storage ring must use again low-energy electron cooling, with a very cold electron beam. To reach reasonable positron beam lifetimes (~100 s) at the low energies given,

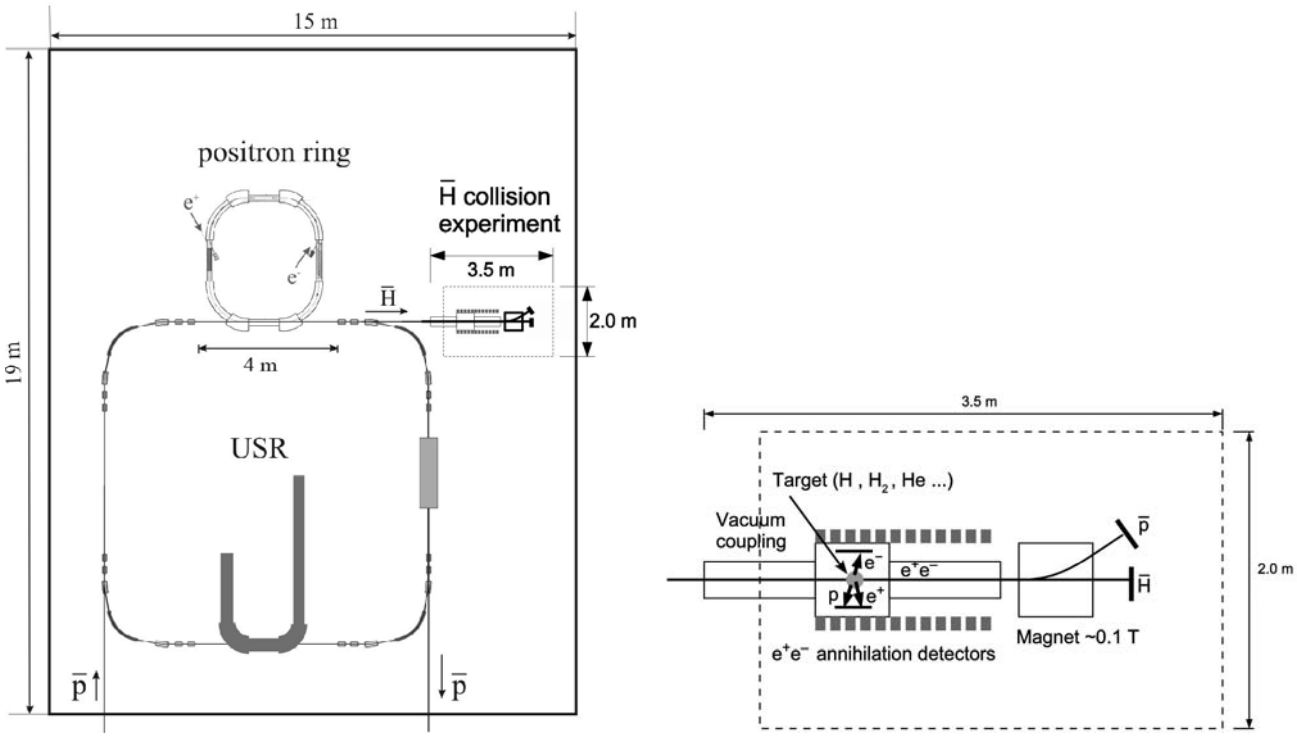

(a) (b)

Fig. 69: Layout of an antihydrogen collision experiment at the USR. (a) Placement in the USR hall (F4). (b) Detailed layout. The target ion fragment p stands symbolically for other target ions

the positron storage ring must have a cryogenic vacuum system with a residual gas density lower than standard UHV conditions (10^{-11} mbar) by a factor of >100. This would also call for construction of the USR with the cryogenic option. – With 5% relative overlap length of the merged positron beam, assuming a radiative recombination rate coefficient of 2 x 10^{-11} $cm^{-3}s^{-1}$ for a positron temperature of 1 meV, an antihydrogen rate of 200 per second is estimated.

Detector arrangement and experimental goals

While the collision velocity can be below 1 a.u., this scenario will always employ high collision energies, of order 10^2 a.u. even if the merged beams are operated with antiprotons of few keV only. The dominant processes will hence be electron or positron loss or possibly positronium formation. This motivates detection of electron, positron and target-ion fragments by an electrostatic extraction field, as shown in Figure Fig. 69 (b), of the antiproton projectile fragment and of the antihydrogen projectile. In addition, positronium formation can be detected by a gamma detector array localizing the annihilation vertex. For orthopositronium a drift length of 1 m is foreseen, corresponding to three times the decay length of ~30 cm at a velocity of 1 a.u. With an atomic target of 10^{14} cm^{-2}, the event rate would be 10^{-2} per antihydrogen atom for a cross section of 10^{-16} cm^2. Cross sections of 0.1 up to a few × 10^{-16} cm^2, as observed for electron loss in keV hydrogen-hydrogen collisions [76], can be expected. Fragments can be detected with high efficiency; coincidence measurements may have efficiencies of ~10%. This yields typical event rates of 0.01-1 per sec.
The principal processes studied will be electron and positron loss and positronium formation. Measurements of absolute cross sections appear possible with suitable target thickness calibration. A more elaborate detector setup, similar to a reaction microscope, may be considered to study the fragmentation momenta; such an arrangement should still fit into the indicated space.

Antihydrogen from an antihydrogen production trap

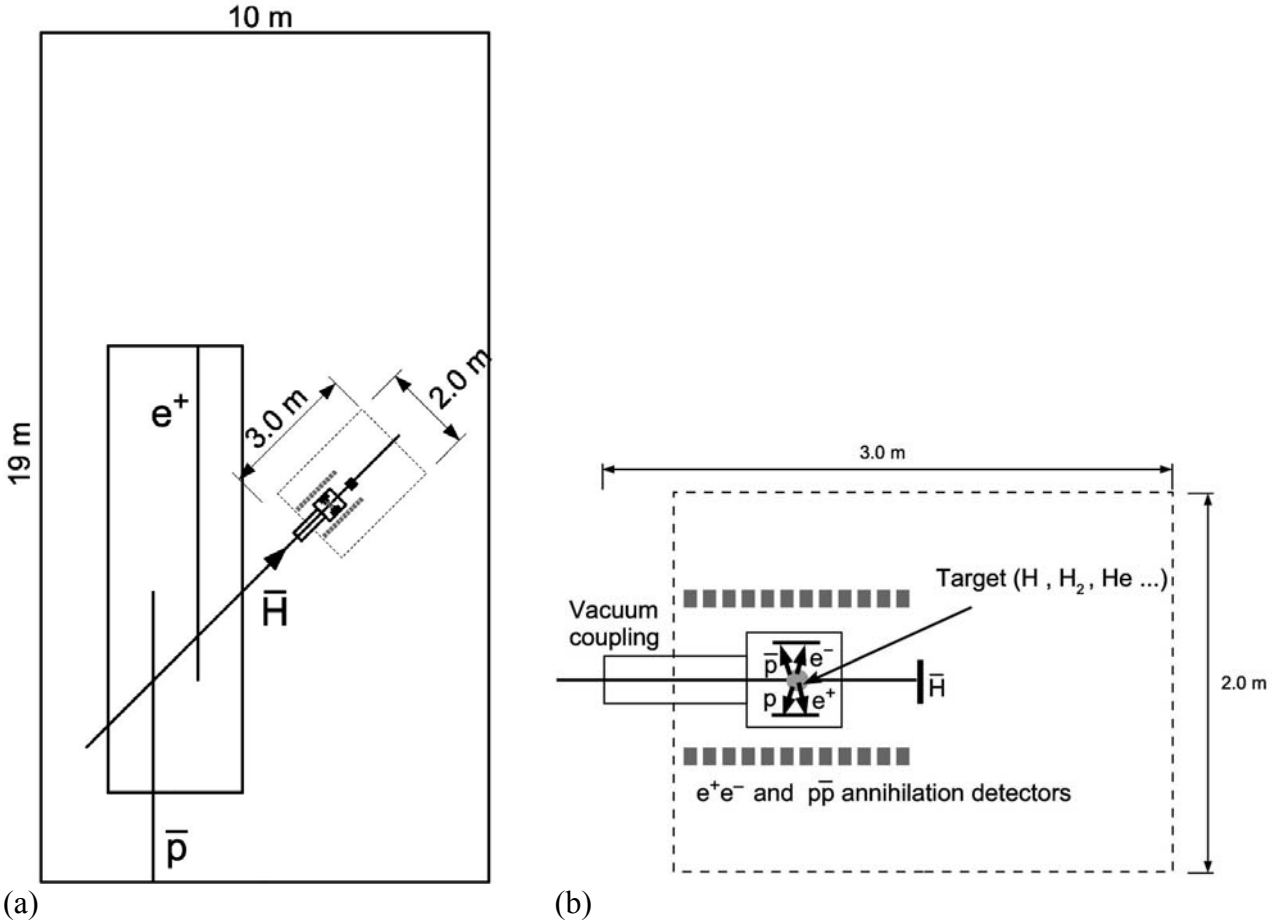

(a) (b)

Fig. 70: Layout of an antihydrogen collision experiment at an antihydrogen production trap. (a) General arrangement, shown for a nested trap similar to the hyperfine structure measurement of Sec. 1.6.2 (the space requirement would be similar at the cusp trap of Sec. 1.6.3). (b) Detailed layout. The target ion fragment p stands symbolically for other target ions.

Arrangement and requirements

Several arrangements are foreseen for producing thermal antihydrogen ions in an "effusing" beam, such as the setup for ground-state hyperfine structure measurements (Sec. 1.6.2) or the cusp trap (Sec. 1.6.3). To produce antihydrogen atoms for collision experiments, control of the collision velocity is desired. In a nested trap setup, this can be achieved by propagating antiprotons through a stationary positron cloud, where the antiproton velocity will define that of the antihydrogen atoms and the recombination rate will not be reduced significantly for antiproton velocities up to the thermal positron velocity. For 4 K positrons, this would yield an "effusing" antihydrogen beam with energies up to ~0.3 eV, with a corresponding center of mass energy in $\overline{H} - H$ collisions of <0.005 a.u. Threshold processes for rearrangement collisions to various $p\overline{p}$ and e^+e^- final states occur at somewhat higher center of mass energies, in the range of ~0.02 up to 1 a.u. (antihydrogen energy ~1 to 50 eV). To reach this energy range, it would be desirable to apply controlled offset energies in the milli-eV range to trapped positron clouds in a modified nested trap scheme. The positron and antiproton densities have to be sufficient to yield an antihydrogen production rate of ~100 s. In addition, the antihydrogen atoms should be in the ground state (or possibly the 2s metastable state).

Detector arrangement and experimental goals

In this scenario it can be expected that $p\bar{p}$ and e^+e^- bound systems will be the main products of inelastic reactions. By recent calculations [72], [73] the inelastic reaction cross section is predicted to decrease fast with the center of mass collision energy, reaching $\sim 10^{-18}$ cm^2 at 0.1 a.u. For the smallest collision energies, reached with standard nested or cusp traps, it will amount to several 10^{-16} cm^2. Suitable detectors for $p\bar{p}$ and e^+e^- formation and possibly for their quantum states seem to be of main importance; in addition, an extraction field for detection of charged fragments should be foreseen. For higher energies (region of the rearrangement thresholds) the use of a dense, possibly extended target of up to 10^{16} cm^{-2} may be considered. A very tentative experimental layout is shown in Fig. 70 (b). The focusing and guiding of the slow antihydrogen beam needs to be considered. Altogether, it can be expected that the space requirement will be moderate, as indicated, and can fit, together with a production trap, into one of the trap areas of the FLAIR hall.
The measurements will be mainly directed to the detection of various annihilation channels, partly via intermediate bound systems. In case of "in flight" annihilations, the momenta of remaining ionized fragments can be studied in addition. Also in this case, the use of imaging detectors in an arrangement similar to a reaction microscope may be considered.

Beam requirements

Operation of USR; operation of antihydrogen production trap. Lowest beam energies in USR (20-50 keV antiprotons). Merged positron beam in USR (energy down to 10 eV). Probably requires cryogenic options both for the positron storage ring and for the USR.

Beam time requirements per year

With typical event rates of 0.1-1 per second, the experiments may require 1-2 months per year of beam time

Needed infrastructure

Moderate electrical power and cooling requirements (~20 kW, rough estimate); gas handling for atomic beam target.

1.8.5 Antiprotonic Atom Formation

Antiprotonic atoms (ions) are formed when antiprotons of several tens eV or lower collide with atoms/molecules. With mono-energetic ultra slow antiprotons, the antiprotonic atom (ion) formation processes are fully studied for atomic as well as for molecular targets, see Fig. 71.

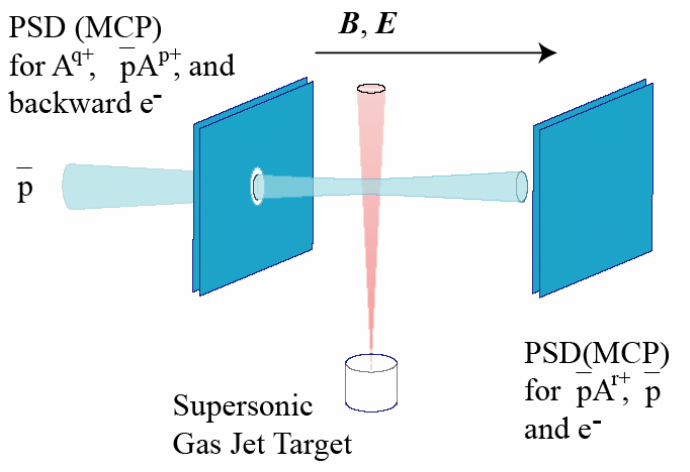

Fig. 71: The experimental setup

For this purpose, differential cross sections with respect to the final charge state of antiprotonic atoms (ions), the emitted electron momenta are determined as a function of antiproton energy as low as a few eV. Collisions with even lower energy will be studied with a nested-trap scheme in conjunction with the "antiprotonic radioactive nuclides in traps" project (Wada, et al.). Threshold behavior and ionization features (angular and energy distributions of antiprotons and electrons) just above the threshold energy are also studied with the same setup.

Beam requirements

DC beams of 1-100eV, 104 pbars/sec with emittances ~50mm mrad extracted from a multi-ring trap

Beam time requirements per year

Weeks

1.9 Nuclear and Particle Physics with Antiprotons

1.9.1 Measurement of Protonium and X-ray Spectra of other light nuclei

Introduction

The measurement of the characteristic X-radiation emitted from antiprotonic atoms constitutes an antinucleon-nucleus scattering experiment at relative energy zero [77]. The strong interaction manifest itself in an energy shift and broadening of the low-lying atomic states. Shift and broadening are directly related to the complex antiproton-nucleus scattering lengths and test the medium- and long range part of the $\overline{\mathbf{N}}\mathbf{N}$ interaction. In particular, the hydrogen isotopes give access to the elementary systems antiproton-proton and –neutron. Light nuclei serve as a testing ground to build the antinucleon-nucleus interaction. In antiprotonic hydrogen the resolution of hyperfine states, which is equivalent to a double polarisation experiment at threshold, became already possible during the LEAR. The low precision, however, hinders a sensitive test of the various theoretical approaches [78, 79]. The experimental information on the antiproton-deuteron s-wave interaction [80] urgently needs confirmation from a new measurement and the accuracy of the measurements of the helium isotopes is modest [81].

In order to achieve sufficiently high X-ray yields antiprotonic hydrogen and helium must be formed in dilute gases to reduce non-radiative de-excitation processes owing to collisions. Therefore, gas targets in the mbar range having both thin entrance and exit windows must be used. An antiproton beam of about 100 keV of correspondingly adjusted parameters is well suited. The possibility to combine an antiproton plasma inside a trap with a gas jet might be considered in context with the improving performance of such devices (e. g., ASACUSA experiment at AD, CERN) [82, 83].

Energies of the low-lying X-ray transitions in the hydrogen and helium isotopes are in the 2-12 keV range. For hydrogen, the hadronic effects are of the order of 1 keV and 10-500 meV for the s-wave and p-wave interaction, respectively. Their measurement, hence, requires two different approaches: a direct measurement with semiconductor detectors, e. g., fast CCDs [84] and with ultimate resolution by using a Bragg crystal spectrometer [79, 85].

Whereas fast CCD allow an efficient reduction of the annihilation induced background by the analysis of the hit pattern, a Bragg spectrometer is self collimating due to the small angular acceptance. Even fast CCDs, processing about 500 frames per second, are limited to a continuous beam of about 10^5 $\overline{\mathbf{p}}$/s to avoid over illumination, whereas the crystal spectrometer is not yet rate limited at the design parameters of FLAIR:

On site requirements

inside area installations
typically 1 crate and 1 PC per device (max. 6 devices)
outside area control installations
typically 1-2 electronics racks, 3-4 PCs/notebooks and 2desks
Beam
– ca. 100 keV antiproton kinetic energy
– suitable phase space to achieve in dilute gases a stop volume of a few cm3
Area
– about 2m x 2 m for fast CCD set-up
– about 2 m x 3 (6) m for single (double) arm crystal spectrometer

Experiment description - summary

Type	stop experiment in low-density gases detection of few keV X-radiation		
beam & target	100 keV & gas cell with thin windows		
Measurements	I)	direct measurements	fast CCDs slow extraction $10^4 – 10^5$ /s
	II)	ultimate resolution	crystal spectrometer slow or fast extraction $\geq 10^6$ /s in average
Measuring periods	Typically once per year - 1 - 2 weeks in the start-up phase or if new set-up - 2 - 4 weeks in the production phase		

1.9.2 Antiprotonic X-rays of Heavy Isotopes and Nuclear Structure

Introduction

It is proposed to measure X-rays from antiprotonic heavy atoms (20<Z<90). The measurements will be an extension of the research program realized at CERN (LEAR) [86]. FLAIR will offer a unique beam of antiprotons (low energy, continuous) well suitable for this measurements. In particular the low energy of the beam will be a big advantage in measurements of rare isotopes: one will be able to use thin targets. (However in this case the experimental set-up presented in the figure below should be modified: instead of trigger from $\bar{p}$ counter one will have to use a trigger from pion counter placed behind the target).

Characteristics of antiprotonic X-rays (level widths and shifts) can give information on:

- Matter and neutron density at nuclear peripheries;
- Antiproton-nucleus potential.

New measurements will allow to:

- Get more extended data on densities;
- Elaborate phenomenological antiproton-nucleus potential;
- Verify and explain several puzzling observations of the previous experiments (e.g. LS-splitting, even-odd isotope effect, effect of loosely bound protons, abnormal upper level shifts).

Description of experimental method

Antiprotons impinge onto a target and are slowed down to an energy of some tens of eV and are captured by a target atom into an orbit with a high principal quantum number. The antiproton then cascades down the orbits emitting Auger electrons and X-rays. When the antiproton reaches a state with a low principal quantum number, the strong interaction reveals its presence and probability of annihilation increases.

As a result, low lying levels are broadened and shifted. The emitted X-rays have energy ranging from several tens up to several hundreds keV and can be registered by HPGe detectors with a good resolution (less than 1 keV for energies lower than 300 keV). The schematic drawing of the experimental set-up is presented in Fig. 72. The antiprotonic beam passes the telescope counter (scintillator) and impinges onto a target. Several germanium detectors measure the antiprotonic X-rays.
In addition, a “control room” (with a place for 3-4 racks and 1-2 computers) is needed. An air condition in order to stabilise the temperature is required. Office space for about 3 persons during the run will be also needed.

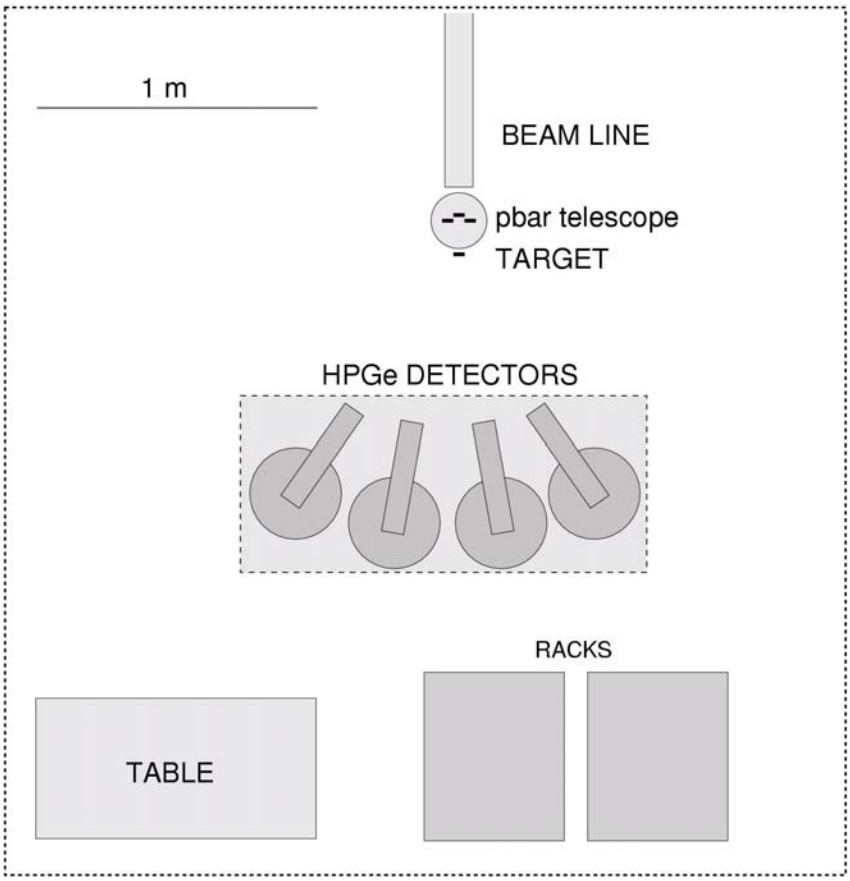

Fig. 72: Illustration of the measurement

The experimental set-up will be installed in a cave temporally (only for run). The detectors and the $\bar{p}$ telescope will be tested at our home laboratory. The installation will take about 1 week (assemble mechanical parts, cables etc.).

Beam requirements

The experiments require a continuous antiprotonic beam at an energy of about 5- 10 MeV and at a rate of ~$5 \cdot 10^4$ $\bar{p}$ /s. For thin targets, beam energies of 300 keV or lower are preferable. Each year, a beam time of 2-4 weeks is required.

1.9.3 Production of Strangeness −2 Baryonic States

Introduction

Studies of the baryon-baryon interaction are a basic tool for investigations of the strong interaction. While for the NN-system an extended data base exists the hyperon sector is much less explored and studies of strangeness S=-2 systems are practically limited to searches for the H-particle, a system of B=2, S=-2 first proposed by Jaffe [87] which up to now could not get a definite proof of the existence of the H.
The cascade hyperons Ξ are normally used as entrance into the B=2 systems with S=-2. Slow Ξ particles can go into interacting ΞN systems which can couple to YY or the H particle.

The proposed experiment [88] for the observation of strangeness -2 baryonic states is based on the production of Ξ-baryons in the special condition of recoil-free kinematics where in a fixed target experiment: a+b → c+d one of the reaction products has zero momentum in the laboratory system.
In the conventional Ξ-production studies via K- induced reactions recoil-free kinematics is not feasible because the mass of K^- is too low. With a 2 GeV K^- beam as example the produced Ξ have momenta above 500 MeV/c. This Ξ "beam" has to scatter on a secondary target to undergo a hadronic interaction with the target nucleons. A direct production of Ξ with zero momentum in a nuclear environment would be much more effective.
To perform such recoil-free kinematics for the Ξ production a K^* "beam" would be particularly suitable whereby the K^* momentum should be at about 160 MeV/c for mK*= 982 MeV/c. The K^* momenta resulting from the antiproton annihilation via: $\bar{p}$ p → $\bar{K}$*K* amounts to about 290 MeV/c at the nominal K^* mass.
Taking into account the K^* width of about 50 MeV/c2 the produced K* momenta very well match the required condition for recoil free kinematics.

Experimental programme

The first stage in these studies will be the pure Ξ production. The most suitable reaction channel is: $\bar{p}$ d → Ξ- K_s^0 K^{*+} which results in 8 charged particle tracks in the exit channel. A sketch of this reaction channel is shown in Fig. 73.

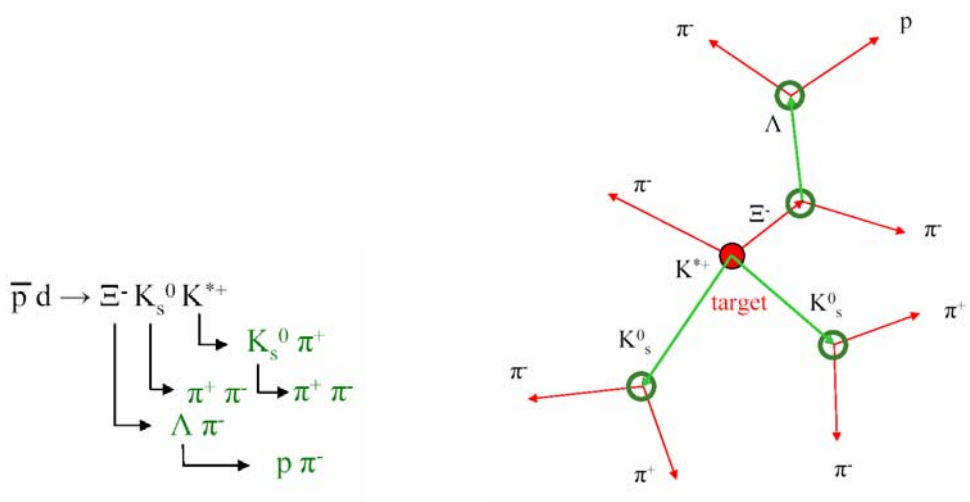

.

Fig. 73: Simulation Sketch of a suitable reaction channel to study the production of Ξ. The primary produced K^{*+} decays within a few fermi into a K_s^0 and a π^+ resulting in 3 delayed decays.

The event identification runs via the geometry of the particle tracks. Such techniques have been applied successfully at the PS185 experiment at CERN and are in use at the COSY TOF experiment. From the charged pions the decay vertices of the Ks0 are reconstructed and with the known target vertex their tracks are determined. The Λ track is given from the vertices reconstructed from the (p, π^-) and (Ξ^-,π^-) tracks. With this information all momentum directions of all particles are known and applying a mass hypothesis for the detected particles the events are completely reconstructed.
A clean trigger for this type of reaction channels is the high multiplicity of charged particle in the final state and the multiplicity increase. By measuring the number of charged particles close to the target which is only 2 in comparison to the multiplicity at a reasonable distance a very efficient trigger signal can be generated due to the delayed decays in this multistrangeness production.
The branching ratio for annihilations into charged particles with a multiplicity of 8 or more is already rather low. By adding a multiplicity increase the expected event rate is sufficiently low that it can be handled without any problems using only a standard data acquisition system like those operated at the present COSY experiments.
The next step in the experimental programme will be the study of the Ξ^-N, $\Lambda^-\Lambda$ or H system. Here ^{3}He has to be used as target gas. The particle configuration in the exit channel is similarly, only an additional proton appears in the exit channel. Therefore the arguments given above for the pure Ξ production are the same.
A further extension of the programme could be the production of double hypernuclei. With the technique of recoil-free kinematics the Ξ can also be produced and deposited in more extended nuclei. A high efficient production of double hypernuclei is expected with this method

Detection system

The detector system is foreseen to be installed in the experimental area F7 where the extracted beam from the LSR is available. In Fig. 74 a floorplan of the area is given and the detection system is sketched in Fig. 75. The required area is about 6 m x 6 m and an additional area of about 2.5 m x 5 m outside but close to the experimental zone is needed for the electronics (5 racks).

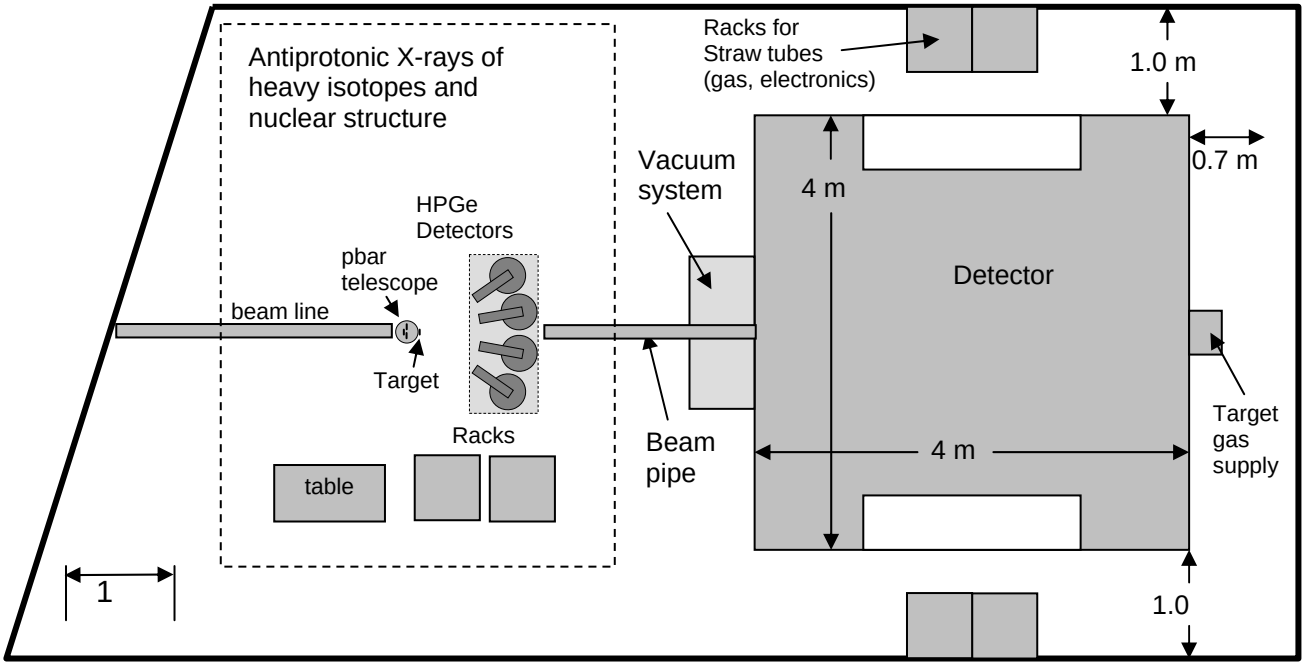

Fig. 74: Floorplan of the experimental area F7. On the right side the experiment for the S=-2 production is located and on the left side the setup of the antiprotonic X-ray experiment is shown which will be moved up when the beam is used for the S=-2 experiment.

As target a small volume of deuterium or ^{3}He within a thin-walled container (for double hypernuclei a target foil) will be used. The total target volume will be a few mm^3 and with the gas pressure the optimum thickness will be adjusted. By choosing the appropriate beam energy and target density a high efficient stopping of the beam in the target gas can be achieved.
The target is surrounded by a segmented scintillation detector. Here plastic scintillators readout by mirror foils or a cylinder out of scintillating fibres could be used. Experience in both techniques is available in the collaboration. Small segmented plastic scintillators with air lightguides are used at TOF and at the ATRAP experiment scintillating fibres with PM readout are widely used.
For charged tracks with a short decay length like the Ξ^- in the reaction channel sketched in Fig. 73, a vertex detector very close to the target is necessary. Two layers of Si-microstrip detectors are foreseen. The charged particle tracking will be done by straw tubes. Several layers of straw tubes in different orientations will allow a 3 dimensional track reconstruction. These technique is applied e.g. at the WASA detector at TSL/Uppsala and is foreseen for the PANDA detector. For the COSY TOF detector presently a straw detector is produced using pressurized straw tubes which do not need a massive frame or thick tubes to hold the wire tension. Extremely light weight constructions can be built with this technique. The sketched configuration should be considered as a first guess. To work out the final configuration some more detailed Monte Carlo studies are needed.
The closure of the detection volume is done by plastic scintillator hodoscopes, a barrel type combined with two endcaps. Similar detector components are used at COSY. They deliver information on the position and the timing of the charged reaction products.

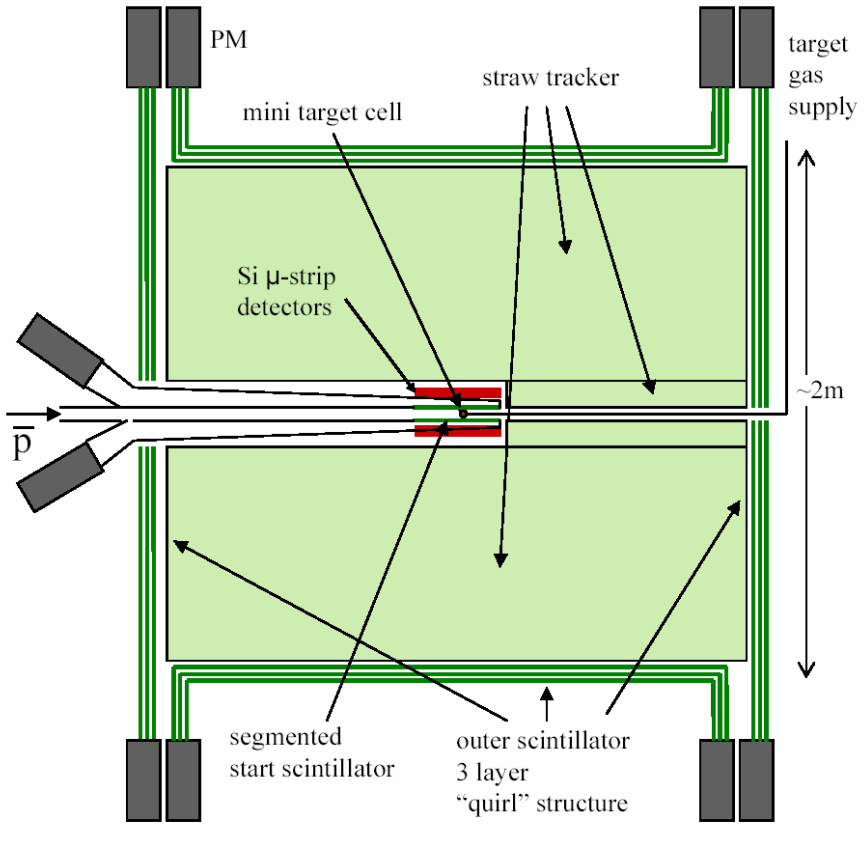

Fig. 75: Sketch of the detection setup

To perform these experiments a well defined target vertex is required. Therefore a cooled beam with small emittance is necessary (Detailed numbers will be deduced from MC). A slow stochastic extraction with a high duty factor is requested.
A veto scintillator in front of the target can be used to reject events from beam halo outside the defined target vertex size.

The assumed beam current is in the order of $5 \cdot 10^5$ antiprotons/s which can be handled by the detector components without any problems. A Ξ production rate of about 4700 per day is estimated based on the following assumptions:
$3 \cdot 10^5$ antiprotons are stopped in the target, BR into $\overline{K}^*$ $K^* = 6 \cdot 10^{-3}$, 0.3 of the $\overline{K}^*$ hit the remaining two nucleon system, 0.5 of $\overline{K}^*$ survive until interaction, $\sigma(\overline{K}^* N \rightarrow K \Xi) / \sigma(\overline{K}^* N \rightarrow \text{anything}) > 10^{-3}$, trigger efficiency ~ 20 %.
If a special reaction channel is concerned like : $\overline{p}$ $d \rightarrow \Xi^- K_s^0 K^{*+}$, the expected event rate is in the order of 100/day taking into account the BR to this special channel and the detection efficiency of the Ξ^- with the Si-μ-strip detectors positioned in a reasonable distance to the target.
It is too early to estimate the total beam time per year. It will start may be in the first year with two blocks of a few weeks data taking followed by a period of data analysis. This will include pure Ξ-production at a deuterium target as well as the study of S=-2 baryonic systems with a ^{3}He target. For the following years a similar relation of may be 6-10 weeks data taking per year seems to be reasonable. This will of course depend on the outcome.

The proposed experimental setup includes detector components which are widely used in the experiments presently operated at COSY. In view of the moderate expected beam current new developments concerning the detectors as well as electronics and data acquisition system are not necessary.

A large part of the hardware components especially electronics could be available from COSY experiments which most likely have stopped their operation before the FLAIR facility will be ready for the installation. This will drastically reduce the total costs of the project. In view of the time scale and the relatively low costs it is realistic that the collaboration can get the funding of the project.

Simulation studies

First simulation studies to check the performance of the proposed detector system have been started. In the following some results of a GEANT 3 MC are shown where the reaction: $\overline{p}$ $d \rightarrow \Xi^- K_s^0 K^{*+}$ was generated. In the MC geometry a scintillator tube around the target (plastic scintillator, 5 mm diameter,10 cm length, thickness 1mm), a Si detector tube (2 cm diameter, 10 cm length, 0.6 mm thickness) and the outer scintillator hodoscopes (barrel: diameter 2 m, length 2 m, endcaps: diameter 2m, 2cm holes for the beam and the target) are included. Instead of straw tubes the whole volume is filled with chamber gas (Ar 90%, CO_2 10%) and to account for the straggling in the straw tube walls 10 mylar sheres (each 0.1 mm thick) around the target starting at a diameter of 25 cm separated by 8 cm are positioned.

In Fig. 76 the multiplicity of charged particles in the outer scintillator and the multiplicity increase between inner and outer scintillator are given. A multiplicity of 8 or more, due to the production of secondary particles, is detected in 20 % of the events and the multiplicity increase is 2 or more in 90% of the events.

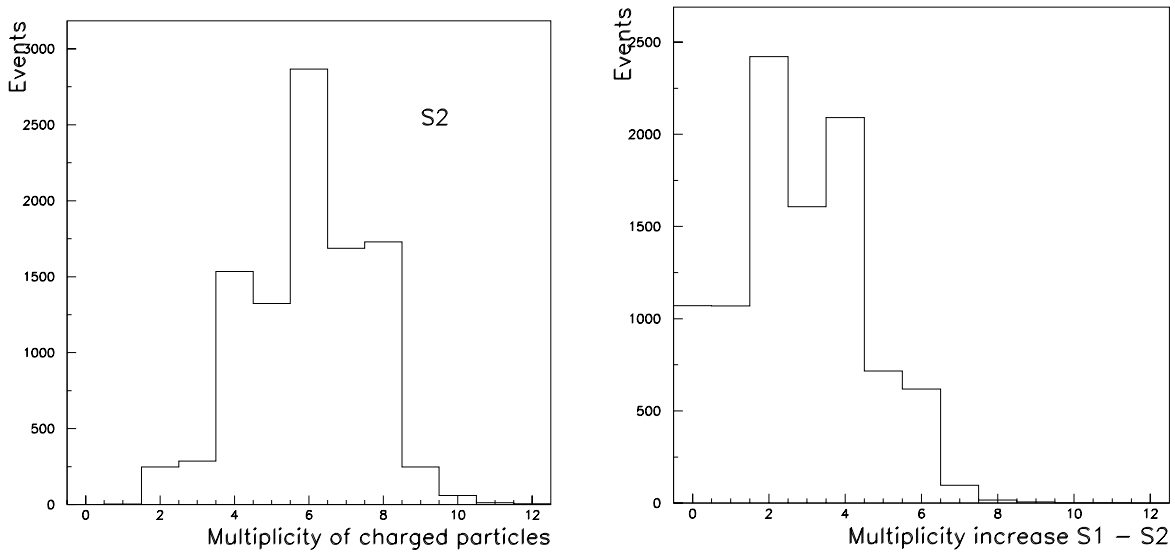

Fig. 76: Multiplicity of charged particles detected in the outer scintillator hodoscopes (left) and multiplicity increase between inner and outer scintillator.

The detection of tracks from particles with a short decay length like the Ξ is problematic. The straw tubes are not well suited because they need too much pathlength. Here the tracks have to be determined by measuring a vertex in the Si detector combined with the target vertex. In Fig. 77 the probability is plotted that the Ξ- survive within a tube around the target as a function of the tube radius. Within a radius of 1 cm which is a reasonable distance for the Si μ-strip detector the survival probability is about 35%. The correct detection efficiency has be checked when the detection setup is finally designed but it can not deviate too much from this rough estimate which gives a rather high detection efficiency. An improvement of the track determination would be possible by adding more Si layers to get a second measured vertex. These possibilities will be studied via simulations in the near future to get an optimum design.

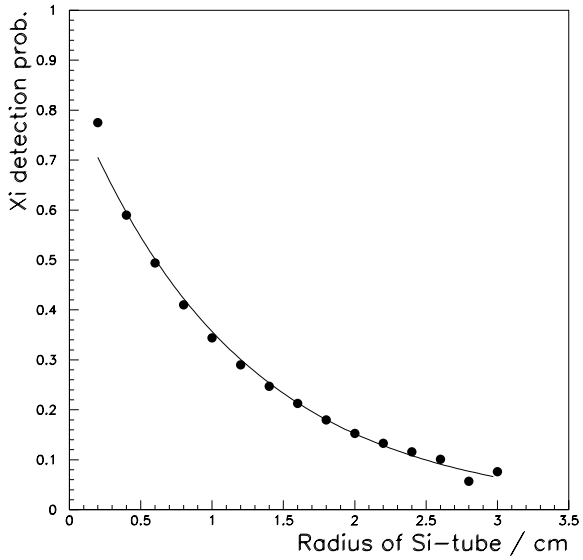

Fig. 77: Probability for the detection of a Ξ- resulting from the reaction $\bar{p}$ d → Ξ^- K_s^0 K^{*+} within a tube around the as a function of the tube radius.

Fig. 78 shows the momentum distribution of the primary produced π^+, the Λ decay proton, and the π^- and π^+ from a K_s^0 decay and in Fig. 79 the straggling angles for these particles are given.

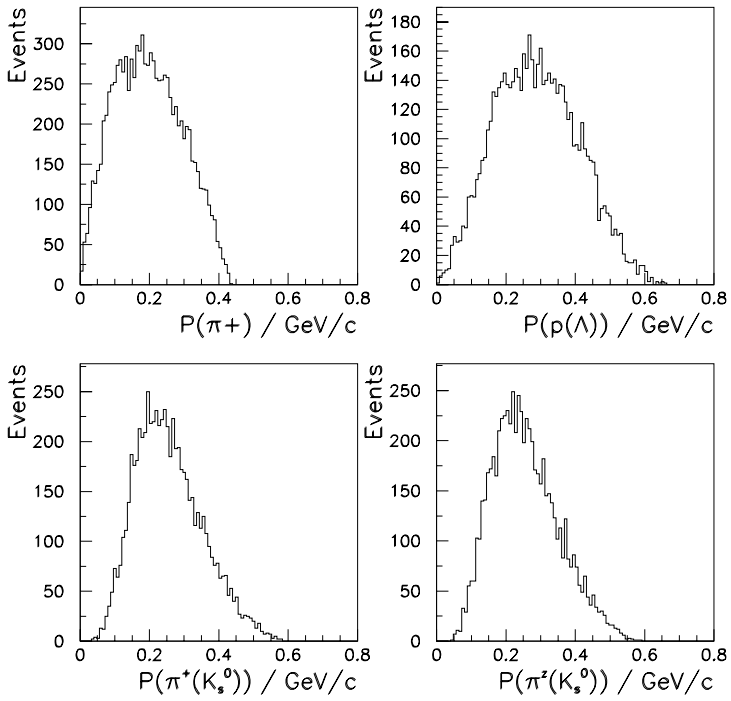

Fig. 78: Momentum distribution of some ejectiles resulting from: $\bar{p}$ d → Ξ^- K_s^0 K^{*+}, namely the primary produced π^+ (top left), the Λ decay proton (top right), the π^+ from one K_s^0 decay (bottom left) and the π^- from the K_s^0 decay.

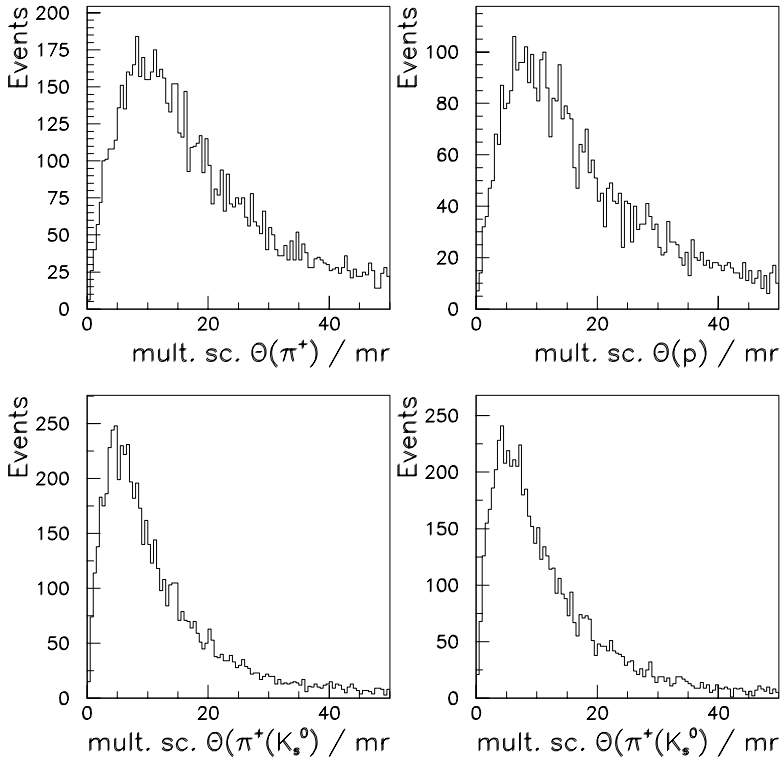

Fig. 79: Distribution of the straggling angle due to multiple scattering in the detector material for the primary produced π^+ (top left), the Λ decay proton (top right), the π^+ from one K_s^0 decay (bottom left) and the π^- from the K_s^0 decay.

The momenta of the reaction particles are sufficiently high to allow a reasonable track determination as is shown by the distribution of angle deviation due to multiple scattering when traversing the detector material.
To generate the track and event reconstruction efficiency the final detector geometry has to be included in the simulation programme and the reconstruction software needs to be written which will be the next step. These first steps of detector simulation demonstrate the feasibility of the proposed reaction study.
Simulations concerning the effect of beam parameters (size and divergence) still have to be done.

Other topics

Radiation Hardness
Radiation hard components are not required for the experimental setup. The expected beam current is low enough that the used detector components will work over the whole experimental programme foreseen.

Design
A rough design is given in the figure of the setup. The final design needs some more MC studies and will be available within the next year.

Construction
The construction of the experimental setup will be done within the collaboration. It will be done as a removable facility which will be installed at the target station for the beam times and could be moved to free the space for other experimental installations if necessary.

Acceptance Tests
No special acceptance tests are necessary. The acceptance will be determined from MC studies and will be checked with experimental data.

Calibration
The adjustment of the detection system will need a few days of data taking.

Requests for test beams
The adjustment of the detection system will need a few days of data taking.
First tests of the detection system could be done with higher energy beam particles. The measurement of the S=-2 channel needs a low energy antiproton beam in the MeV range adjusted to an optimum stopping within the target material. But for tests of the detector performance higher energy antiprotons or protons could be used.

1.10 **Options** (Not approved by PAC or technically uncertain)

1.10.1 Antihydrogen Formation in Merged Antiproton-Positron Beams (Positron Cooler Ring)

Precise spectroscopy of antihydrogen atom can be performed using atomic interferometer technique on flux of the antihydrogen atoms at energy of 20 – 100 keV. The antihydrogen in flight generation can be realized at USR together with a small positron storage ring, as shown in Fig. 80. The machine is described in more detail in section 1.3.6.

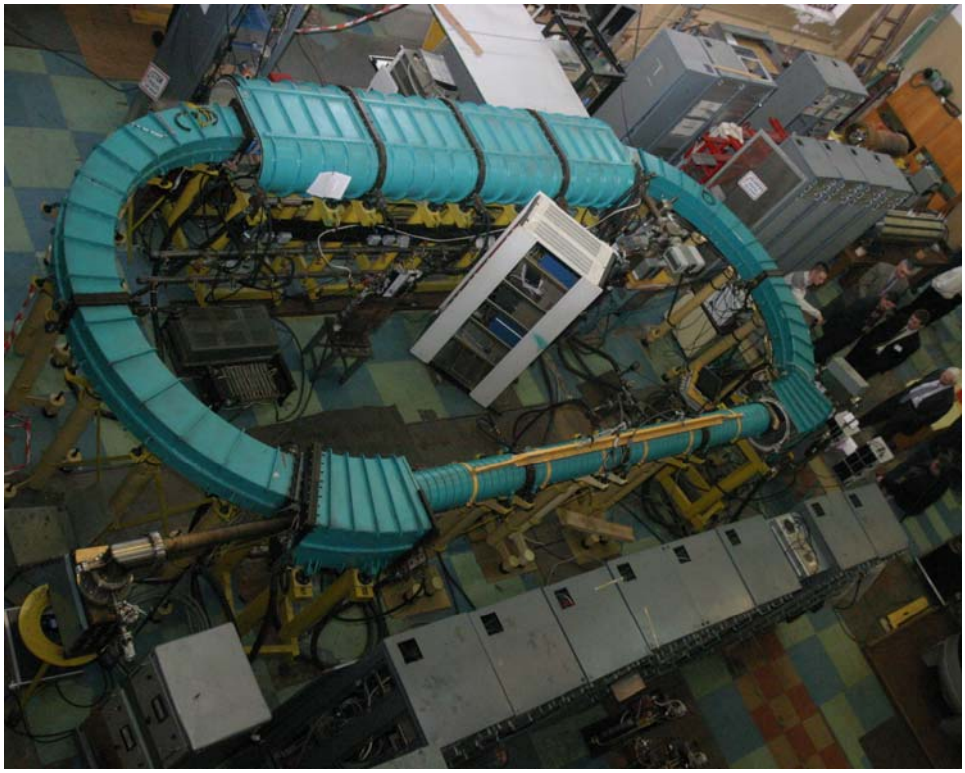

Fig. 80: Low Energy Positron Toroidal Accumulator (LEPTA).

A ring with solenoidal focusing system is preferable for the positron storage due to small positron energy. The positron ring circumference can be about 10 m, longitudinal magnetic field value of 50 G, positron energy of 2 – 3 keV. To provide equal positron and antiproton velocities in the recombination section the positrons are decelerated by application of corresponding potential to the electrostatic screen located in this section.
At such parameters of the ring and at $1 \cdot 10^{8} - 1 \cdot 10^{9}$ circulating positrons the expected antihydrogen generation rate is $1 \cdot 10^{-7} - 1 \cdot 10^{-6}$ s^{-1} per one circulating antiproton (intensity of the positron beam is chosen typical for positron trap of the ATHENA experiment.)

To have a data for the positron ring technical design one needs to solve the following problems:

- to tune injection system in order to minimize distortion of positron beam,
- to provide stability of the circulating beam motion,
- to provide circulating positron beam life-time of about 100 sec,
- to test a scheme of positron and electron beam superposition and separation,
- to realize and investigate electron cooling of positrons.

Particle dynamics in the ring with longitudinal magnetic field, life-time of a circulating beam, electron cooling of positrons will be investigated in experiments at LEPTA ring which is in

operation in JINR. Now the LEPTA ring is operated with circulating electron beam (see http://lepta.jinr.ru). The ring can be tuned for the beam energy and longitudinal field value required for antihydrogen generation. Feasibility of injection system was preliminary proved during the ring commissioning. Experimental studies of the beam dynamics are in progress. Positron injection and investigation of electron cooling of positrons are scheduled for year 2005.

Time line, milestones

	2004	**2005**	**2006**
Investigations at LEPTA			
Investigations of the circulating beam dynamics, life-time of the beam			
Accurate tuning of the injection system using optical measurements of the beam temperature			
Positron injection, beam superposition and separation			
Investigation of electron cooling of positrons			

If the tests with LEPTA are successful, the technical design of the positron ring for antihydrogen generation will be fulfilled in 2007.

The next stage is construction of the positron ring, design and construction of the positron injector, assembly the facility at USR. After demonstration the antihydrogen formation in merged antiproton-positron beams and measurements of the antihydrogen flux intensity, angular and velocity spread one can start spectroscopy. The detector system is the same as for hydrogen atoms.

1.10.2 Antiprotonic Radioactive Nuclides in Traps (Exo+pbar)

Introduction

Exotic atoms play important roles in nuclear structure studies. Muonic X-ray measurements, for instance, provided reliable root-mean-square charge-radii of nuclei. However, so far, those experiments are limited to stable nuclei. Antiproton is also an exotic particle but the lifetime is understood to be infinite, so that antiprotonic radioactive nuclear atoms could be the only possible exotic-exotic nuclear atoms. Antiprotonic atoms would be new probes for nuclear structure studies, especially for the different peripheral distribution of protons and neutrons in a nucleus, which is in particular interesting for nuclei far from stability.
The present proposal of producing antiprotonic radioactive atoms is submitted to NUSTAR and APPA PAC's since the experiment requires both antiprotons and low-energy radioactive nuclei simultaneously. A long beam transport line (LBTL) for low-energy radioactive ion beams from the Low-Energy Branch of NUSTAR facility to FLAIR or a BTL for antiprotons from FLAIR to NUSTAR is needed. It is described in detail in section C1.4.

Physics case

Different abundance of protons and neutrons at the surface of the nuclei is an important concern for nuclear structure studies. Exotic properties of nuclei, such as halo and skin, have been investigated in nuclei far from the stability line [89]. Antiprotonic atoms would be excellent probes for such different nucleon abundance at the surface, since annihilation of an antiproton dominantly occurs with a nucleon at the surface of a nucleus and the vanished nucleon can be identified by the total charge of the emitted pions or the residual nucleus. FAIR will provide both, slow antiprotons and simultaneously slow radioactive nuclei at the Low-Energy Branch of NUSTAR. Using a beamline, which connects the Low-Energy Branch and the FLAIR area, this is a unique opportunity to create antiprotonic radioactive atoms of a wide variety of nuclides of all elements.

Table 16: Experimental methods for antiprotonic atom and obtainable physical quantities

Physical quantity	**Observable**	**Method**	**for RIB**	**Previous works for stable nuclei**
Nuclear size	X-ray		?	A. Trzcinska et al, PRL 87(2001)82501
p,n abundance at nuclear surface	pion's net charge	calorimetric	possible	Bugg et al, bubble cham exp for C, Ti, Ta, Pb PRL 31(1973) 475
		statistical		
		γ-ray		
	Cold residue	PI by Recoil momentum	possible	J.Jastrzebski et al. Nucl. Phys A558 (1993) 405c
Surface nucleon's momentum	Cold residue	Recoil momentum	possible	

Antiprotonic atoms have been studied exclusively for stable nuclei with various experimental methods as shown in Table 16. Antiprotonic atoms were produced by irradiating an antiproton beam on a fixed target material. When an antiproton is captured in an electronic orbital of an atom, it decays to lower levels by radiating auger electrons and X-rays. The lowest X-ray transition level indicates the matter radius of the nucleus [90]. At a certain level where a sizeable overlapping of the wavefunctions of the antiproton and the nucleons, an annihilation between the antiproton and a nucleon of the nucleus occurs. The highlight of these studies should be that the annihilation dominantly occurs with a nucleon at the surface of the nucleus and that one can distinguish whether the vanished nucleon is a proton or a neutron by the following phenomena. One is that $\bar{p}$-n and $\bar{p}$-p annihilations produce charged pions with a net charge of -1 and 0, respectively. Bugg et al. used a bubble chamber to detect charged pions and identified the annihilated nucleons [91]. The other is the fact that the "cold" residual nucleus ${}^{A}_{N}Z$ becomes ${}^{A-1}_{N-1}Z$ and ${}^{A-1}_{N}(Z-1)$, as consequences of $\bar{p}$-n and $\bar{p}$-p annihilations, respectively. Warsaw group detected γ-rays to identify the cold residues [92].

All the previous experiments used a fixed target and a fast antiproton beam. However, such methods are impossible to be applied to radioactive nuclei, since the amount of radioactive nuclei is always much smaller compared to that of stable nuclei and they decay within finite lifetimes. The detection methods should also be high for such limited amount of radioactive species. In this proposal, therefore, we will use a cloud of antiprotons trapped in a Penning trap as target and singly ionized slow radioactive nuclear ions as projectiles [93].

Fig. 81 shows a schematic of the experimental setup. Here negatively charged antiprotons are confined in a positive well at the center of a nested trap while positively charged slow ions are bunch injected into the negative outer well of the trap.

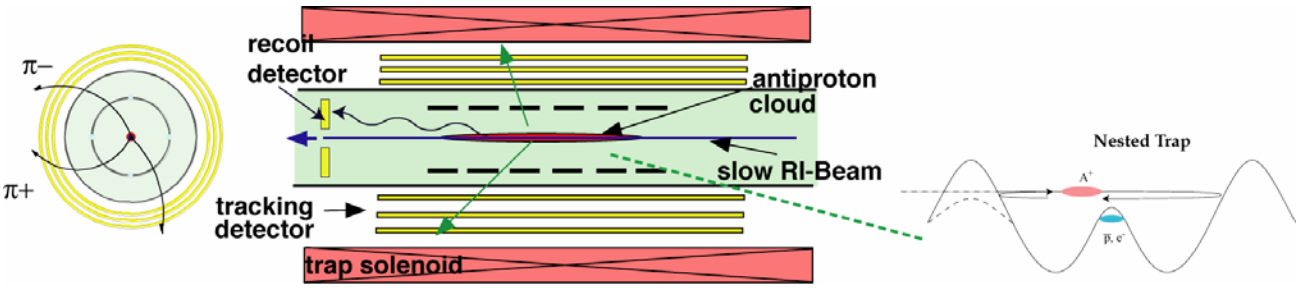

Fig. 81 Proposed experimental setup for antiprotonic radioactive nuclear atoms.

Among several detection schemes, the statistical analysis of the ratio of the detected π^+ to π^- is the most feasible and universal method for antiprotonic radioactive atoms. The detection efficiency for γ-rays is much lower than that for charged pions and the radiochemical method is not effective for nuclei close to the drip line. The detection of X-rays enables us to investigate the matter radii of nuclei, however, the detection efficiency is also limited if possible geometries are concerned. Furthermore, the matter radii can be measured much easily, for instance, by the measurements of the total interaction cross sections in intermediate energy reactions. The particle identification of recoiling residual nuclei is also a possible method for antiprotonic radioactive atoms. Details of the detection scheme will be discussed in the later section. In this proposal, we focus on the detection of charged pions, so far.

Experimental Case

Production rate

The antiproton capture cross sections of slow singly charged ions are theoretically estimated by Cohen [94] and are as large as that of neutral atoms (Fig. 82). A typical value is $4*10^{-16}$ cm^2 for $^{11}Li^+$ ions when the relative energy is 0.1 atomic units which corresponds to a $^{11}Li^+$-beam energy of 33 eV in the antiproton rest frame. Assuming the number of trapped antiprotons is $5*10^6$ [95] and that they are confined to 1 mm^2, the target density is $N(\bar{p}) = 5*10^8$ cm^{-2}. Slow RI ions are bunch-injected in a nested trap and pass through the antiproton cloud for $5*10^5$ s^{-1} if the ions are 33 eV $^{11}Li^+$ and the trap length is 4 cm.

Since we are mainly interested in very short-lived nuclei, we assume a short measurement cycle of 10 ms, in which only 10 RI-ions are involved when the RI-beam intensity is 10^3 s^{-1}. The production rate per cycle is then $Y= 4*10^{-16} * 5*10^8 * 10 * 5*10^3 = 1 * 10^{-2}$. Thus, in total 1 antiprotonic-$^{11}Li^{2+}$ ion can be produced per second. It is quite feasible number.

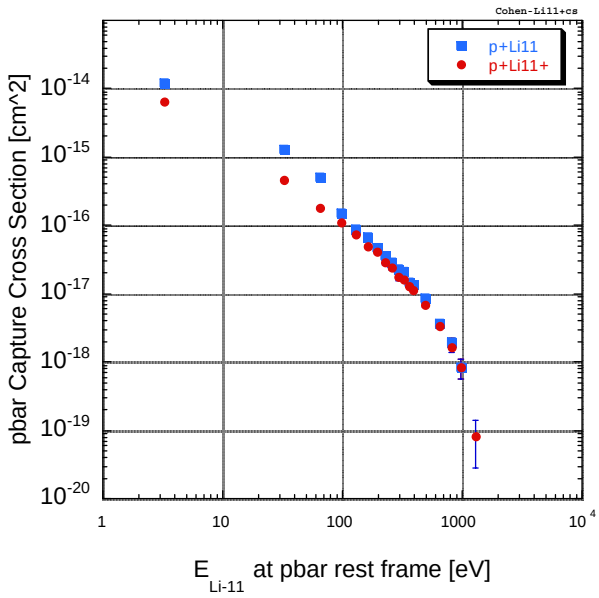

Fig. 82: Capture cross section of antiproton in Li^+ ion and neutral atom. [95]

Detector setup

The purpose of the detectors is to identify the polarity of the charged pions from annihilation events. A stack of position sensitive detectors cylindrically covers the nested trap in order to truck the path of the charged pions. The polarity can be deduced from the deflection direction in high magnetic field (~5 T) and noise events from the annihilations caused not in the center of the trap can be discriminated. For the charged pions of 100 MeV to 400 MeV, the curvatures of the paths under 5 T are ~100 mm to ~200 mm. If three layers of detectors are located with 10 mm distances, the position at the central layer is shifted for more than 0.5 mm from the other two layers. Relatively simple position sensitive detector (PSD) can be used for this purpose. The actual material of the detector is still under consideration.

Discrimination of the background events is an important concern for the detector setup. Major background events would be: 1) energetic protons directly emitted from the annihilated nucleus, 2) γ-rays due to uncharged pions and X-rays from cascade, and 3) pions due to the annihilation events with background gas. Protons and γ-rays can be discriminated by the response of the detectors and also by the curvature of the paths in the trucking detectors. Note that the multiplicity of direct proton event is as small as one [96]. Pions originate to the background gas would be the biggest effect, since 10^7 antiprotons in a trap with a long storage lifetime of one day already annihilate with a rate of 100 Hz, much higher than the expected true event rate. However, the residual gas at cryogenic temperature is almost purely H_2, i.e., such an annihilation does not produce any recoil nuclei. If we detect a recoil nucleus coincident with pions, we could clearly identify a true event. Fig. 83 shows the detection efficiencies of recoil ions by a detector of 40 mm diameter located at a 400 mm distance from the center of the trap under a magnetic field of 5 T. Even if the solid angle is as small as 0.06%, high efficiencies, especially for heavier ions, are expected due to the presence of the strong magnetic field.

The detector of recoil ions could be used not only to eliminate background events but also to identify the recoil particles, if the position in the recoil ion detector and the position of the annihilation point are accurately measured.

The relation of the longitudinal distance between the two positions L and the radial distance between the two positions d are described as

$$d = 2\frac{m}{qB}\sqrt{\frac{2E}{m} - \left(\frac{L}{tof}\right)^2}\left|\sin\left(\frac{qB}{2m}tof\right)\right|$$

where E is the kinetic energy of ion, m the mass, q the charge, B the magnetic field and tof the time-of-flight. Here we see that even the kinetic energy of recoil ion can be determined from the measured quantities. It should be noted, however, that accurate measurement of the annihilation position to determine the kinetic energy is difficult for the present technique. Further development would be needed for this particular purpose.

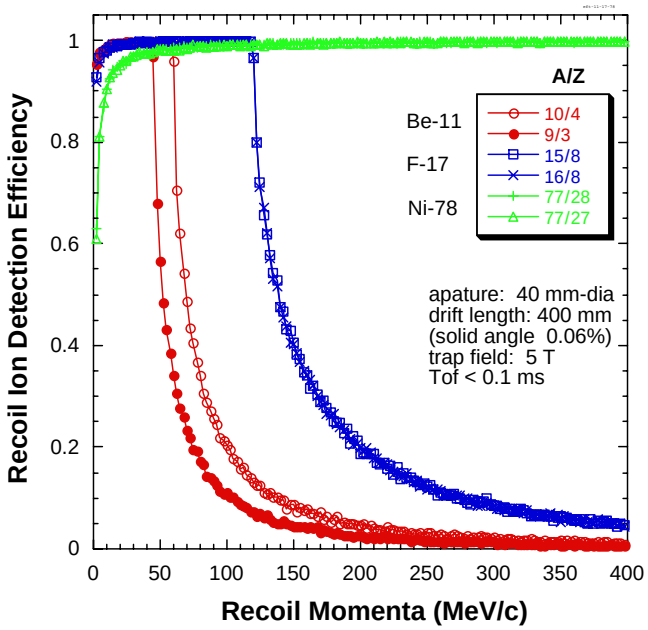

Fig. 83: Detection efficiencies of recoil ions from annihilation events.

Physical quantity

A statistical analysis of the number of detected charged pions provides the nucleon density ratio ρ(n)/ρ(p) at the surface of a nucleus. Note that if we can detect all the charged pions, a single event can determine the net charge of an annihilation event so that it already distinguishes $\bar{p}$-n or $\bar{p}$-p annihilation events. However, the detection efficiency cannot be unity in usual cases. Even if the detection efficiency is low, one can compare the total numbers of detected π^+ and π^- throughout a measurement. A simple simulation (Fig. 5) showed that the nucleon density ratio ρ(n)/ρ(p) at the surface can be obtained with a 5% accuracy from 50 k antiprotonic atoms.

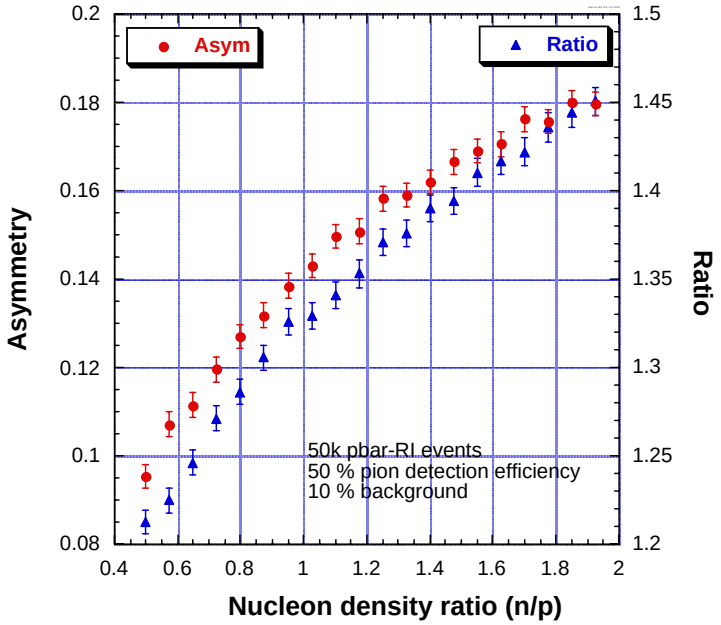

Fig. 84: Simulation of a statistical analysis for nucleon density ratio ρ(n)/ρ(p).

Uniqueness

FAIR will be the only one facility that provides both trapped-antiprotons and wide variety of low-energy radioactive nuclei. It must be a unique opportunity to investigate the surface of nuclei far from stability where extremely different abundance of protons and neutrons are expected.
There are two proposals aiming at investigation of nuclear structure using antiprotons. One is the present one, Exo+pbar, and the other is the intermediate energy collision in a collider ring, AIC. These two experiments are complementing each other. The major physical quantities which can be measured are the abundant ratios of protons and neutrons at the surface for the former but at the root-mean-square radius for the latter.
Advantages of the present proposal compared with the other are listed in Table 17. Note that the first candidates to be studied are ^{8}He, ^{11}Li, ^{11}Be, ^{8}B, ^{17}F, which are so called skin or halo nuclei, and ^{2}H for calibration; none of them can be investigated by the cold residue measurement method. Also note that the matter distributions, without distinguish p or n, can be measured by other simpler methods such as proton scattering where a solid hydrogen (proton) target can be used.

Table 17: Comparison of Exo+pbar (pbar-RI) and pbar-A proposals.

	Exo+pbar (pbar-RI) in TRAP	**AIC in Collider RING**
Observable	Ratio of π^+ and π^-	Distribution of residual nuclei Interaction cross section
Measurable Quantity	ρ(n)/ρ(p) at surface	ρ(n)/ρ(p) at rms radius matter rms radii
Drip-line Nuclides	Possible (pion detection is universal)	Impossible (cold residue = unbound)
Short-lived Nuclides	Possible 10 ms (intensity > 1 kcps)	Difficult Beam-cooling takes time (>1s)
Recoil Momentum measurement	Difficult (Requires accurate position measurements)	Possible (Inverse kinematics)

Beam requirements

A bunched Antiproton beam of low energy (< 1keV) with high intensity is needed as well as a low energy (~30 keV) singly charged radioactive ion beam from the NUSTAR-LEB.

Antiprotons should be injected into the trap for a few times in a day and slow radioactive ion beams continuously transported from NUSTAR-LEB to the rebuncher trap.

Relation to other Projects

The comparison between the present proposal and AIC proposal is discussed in the "Uniqueness" section.
An antiprotonic radioactive nuclear atom experiment is also proposed to RIKEN RIBF as one of possible experiment at the slow RI-beam facility (SLOWRI). The development will be carried out mainly at RIKEN as its own project so far. However, the feasibility of the RIKEN project depends on the development of a portable trap for antiprotons to transport antiprotons from CERN to RIKEN. The priority will be decided due to the developmental status and the FAIR schedule.

1.10.3 Biological Effectiveness of Antiproton Annihilation

Introduction and Overview

The use of ions to deliver radiation to a body for therapeutic purposes is advantageous because the profile of deposited energy peaks at the end of range of the charged particle rather than near the surface as is the case with photon based therapy. This is particularly important for deep-seated tumors or tumors located near radiation sensitive regions that must be spared. Furthermore, the biological effectiveness of charged particle radiation varies widely with the density of ionization or LET (linear energy transfer) of the particle as it moves through the body, which depends on the charge and momentum of the ion. These facts have supported the development of proton and heavy ion therapy centers. Alternatively, antiprotons can also be used to deliver radiation to the body in a controlled way and are expected to have additional advantages over other types of radiation currently used in radiation therapy. The slowing down of antiprotons is similar to that of protons except at the very end of range beyond the Bragg peak. When the antiprotons stop they annihilate producing a variety of low and high-energy particles. The relatively low energy heavier particles deposit biologically effective high LET radiation in the immediate vicinity of the annihilation point. The high-energy pions, muons, and gammas leave the body and have the potential to be used for imaging.

Gray and Kalogeropoulos [97] estimated the additional energy deposited by heavy nuclear fragments within a few millimeters of the annihilation vertex to be approximately 30 MeV. While this is small compared to the total annihilation energy of 1.88 GeV, for biological purposes it can be very significant. An additional enhanced biological effectiveness results from the fact that this additional energy is delivered in the form of heavy recoils and fragments from the annihilation event. These have a short range and deposit all their energy in a localized region around the annihilation vertex.

In 1985, Sullivan [98] measured the relative magnitude of the enhanced energy deposition at the Low Energy Antiproton Ring (LEAR) at CERN, but did not measure the biological effect. We therefore have initiated an experiment at CERN (AD-4/ACE) [99], [100], [101] which is the first to measure directly the biological effects of antiproton annihilation. At this time the experiment can only be done at CERN where the AD (Antiproton Decelerator) has a low energy, mono-energetic beam of antiprotons able to deliver a biologically meaningful dose at an appropriate dose rate. Initial experiments have addressed the three most crucial issues: (a) what is the enhancement of the biological effect in the Bragg peak compared to the entrance channel for antiprotons and how does this compare to protons (and heavy ions); (b) is there a significant biological effect outside the direct beam and/or beyond the Bragg Peak due to the mid range annihilation products, and (c) can we demonstrate the real-time imaging capabilities of antiproton annihilation in a target volume. Preliminary results from these very limited measurements are promising and R&D in this field will We propose to continue this experiment at the GSI facility where we expect to have beams available with higher intensity and a time structure better suited for medical applications.

Experimental Methods and Current Status

Currently the experiment at the AD uses a beam of 300 MeV/c (46.8 MeV) antiprotons from the AD extracted into a biological sample of live cells of known radiation sensitivity (Chinese hamster, V-79 WNRE) placed within a phantom situated in air at the end of the DEM beam line. Different samples are irradiated with varying (calculated) doses and then analyzed by taking sample slices of 0.5 to 1 mm thickness along the beam channel in the plateau, the (spread-out) Bragg peak (SOBP) and in the distal region. These samples are dissolved in growth medium and plated in Petri dishes and are then placed in an incubator. The quantitative cell survival studies involve counting the

number of colonies that grow during a certain incubation period after irradiation. The analysis of cell survival at serial 1 mm depths along the beam central axis enables us to determine the lethality of antiprotons as a function of depth along the path of antiprotons. Cell survival is a direct measurement of the net effect of all the different ionization species along the antiproton path. The response relative to both protons and ^{60}Co gamma radiation has been used to standardize the biological effectiveness of antiprotons. The possible peripheral biological effects of the non-localized mixed radiation fields away from the point of annihilation is measured in cell samples located at appropriate distances from the region of annihilation.
Comparing biological effectiveness of antiproton annihilation in the peak versus plateau regions of the stopping ionization distribution gives us a measurement of potential differentials in "biological" dose in the tumor and surrounding normal tissues for a therapeutic beam of antiprotons. In other words, the questions we are addressing with our current experiment are the following:

"If we compare two particle beams, i.e. protons or carbon ions and antiprotons, having the same physical characteristics (energy, momentum distribution, beam geometry) and delivering identical dose to the entrance channel, by how much will the biological effectiveness of the antiproton stopping peak be enhanced by the densely ionizing annihilation products? Will this enhancement be significant enough to make antiproton beams potentially useful for tumor treatment?"

This experiment must be considered an enabling measurement, establishing if this field warrants further research. If our initial indications hold up, we envision an active research program not only in the medical/biological area, but also in understanding the detailed dynamics of the annihilation events. While data analysis is not finished yet, at this time we can say that (a) the enhancement of biological effects for antiprotons in the peak region compared to the entrance channel (plateau) is significant, and (b) the effect on cells peripheral to the target volume is small. In addition we have performed initial demonstration experiments on the real-time imaging, testing two different types of detectors.

Future Work and Beam Requirements

To cover the depth of tumors found in realistic treatment situations higher energy beams are required. Ideally the energy of the beam should be variable between 50 and 300 MeV, covering a penetration depth between a few millimeters and about 30 cm..
According to initial estimates an effective biological dose of 1 Gy delivered to 1 cm^3 requires approximately 1 x 10^9 antiprotons and should be delivered in a short time period ($\approx$ 1 minute).
To study important issues on non-linear effects of standard dosimeters for the mixed, high-LET radiation from the antiproton annihilation, and to develop a high precision dosimetry protocol for actual dose planning, as well as for R&D on the real time imaging systems to monitor the location of the beam in a target at sub-therapeutic dose it is also necessary to extract the beam at a rate slow enough to use ultra-thin ionization chambers or thin silicon-diodes and standard detector read-out electronics modules. A spill duration of 1 – 5 seconds would be adequate for these applications.

It is our understanding that these requirements can be met by direct beam extraction from the NESR into the foreseen high energy cave F8.

In addition to the above mentioned R&D, which will continue between now and the start-up date of the FAIR facility, we expect to have advanced to the state of knowledge to perform treatment tests in animals and eventually to start experimental treatments of patients. While animal testing can easily be accommodated in the high energy cave, to perform experimental treatments on patients it would be necessary to add a dedicated building outside the FLAIR hall and/or along the injection channel from the NESR to FLAIR. This would have to be foreseen as a later addition to the FAIR/FLAIR lay-out and will be presented as a new letter of intend at a later stage.

Additional Experimental Work

Antiproton annihilation in biological material and the complexity of biological response to this mixed, high LET radiation do not lend themselves to calculation from first principles. From a potential therapeutic perspective the short-range, low-energy recoils and fragments are the most significant because they deposit high LET radiation that is known to produce an enhanced biological effect. To enhance our understanding of the relevant processes and to allow developing predictive models it is necessary to further the detailed knowledge of the annihilation dynamics in human tissue. If a complete data set would be available on the mass and energy distribution of the recoils and fragments generated in the annihilation event one could envision to use a derivative of the local effect model (LEM) developed at GSI for the field of heavy ion therapy. For these measurements it will be necessary to stop individual antiprotons in very dilute targets, necessitating to lower the energy to the sub keV range. For this purpose we propose to field a second line of experiments using ultra-low energy beams from the USR and/or from a final Penning trap, where the particle energy is reduced to a few eV before they are extracted into a target. This work presents a broad challenge to the ultra-low energy community and we anticipate to develop collaborations with several groups participating in this overall proposal.

The set-up will consist of a standard beam line for lateral scanning and beam monitoring (two dipoles, one quadrupole and beam monitoring equipment – total length of beam line of approximately 5 meters). For these tests we requite a semi-slow (1 – 5 seconds) antiproton beam with intensities of 1 x 10^6 to 1 x 10^7 antiprotons per spill at energies between 50 and 250 MeV). We anticipate a total beam time requirement/year of between 200 and 300 hours.

Design
The experiment requires a well focussed (r ≈1 mm) beam at variable energy (30 MeV to 250 MeV) delivered to the entrance of a beamline equipped by the ACE collaboration for beam monitoring and lateral position scanning. The beam will exit the vacuum system at the end of this line and enter the biological targets.

The target stations with auxiliary equipment for real-time imaging and beam diagnostics will occupy a floor space of approximately 5 meter in the direction of the beam with a width of 2 – 3 meters. All equipment is easily removeable if necessary to accommodate other experiments in the same cave.

Beam Requirements:

A ‘semi-slow’ extracted beam of antiprotons 30 < E < 300 MeV with high intensity extracted over the time interval of a few minutes. Extraction rate/second should be < 5 x 10^6 particles/second. Beam focus should be < 5 mm (1 sigma) diameter. Antiprotons are required typically for short time periods (1 – 8 hours) every 2 – 3 weeks, strongly depending on the detailed research programme.

Relation to other projects

A strong overlap in scientific questions with sub-project “B1.8.3 Energy loss and Ionization of Slow Antiprotons” exists in our group. We will attempt to set up collaborations with teams studying the kinematics of antiproton collisions with atoms in order to develop a better understanding of the details of the interaction. These data can be used in theoretical models for future treatment plans.

1.11 New idea after submission to PAC

1.11.1 Double Antikaon Production in Nuclei by slow Antiproton Annihilation

In view of the strongly attractive K^-N interaction below threshold it is suggested by Akaishi and Yamazaki [102] to look for an even stronger attraction in nuclear clusters with more than one K^-, such as K^-K^-NN. Double antikaonic nuclear clusters are predicted to have densities exceeding ~5-6 times the average nuclear density $\rho(0)= 0.17$ fm^{-3}, thus reaching in the phase diagram of hadronic matter conditions were phase transitions to kaon-condensation [103] or colour superconductivity at low temperature [104] may be reached. Thus the question comes up about possible processes by which several antikaons may be produced and transferred under kinematical conditions which keep the momentum transfer to the nuclei small. Several processes have been discussed such as double strangeness transfer in (K^-,K^+) reactions [105] or search for such clusters in residues of high energy heavy ion collisions [106]. Here we propose [107] to produce simultaneously 2 K^- at close distance in a nuclear target and explore the expected "strong attraction" mediated by 2 antikaons in the nuclear environment, leading to cold and dense fermionic matter which may undergo a phase transition similar to the ones recently observed in cold gases of fermions [108]. The elementary reaction considered is

$$\bar{p} + p \rightarrow K^+ + K^+ + K^- + K^- - 0.098 \ \text{GeV}$$

with a negative Q- value of 98 MeV, so it is forbidden for stopped antiprotons. But let us consider now a reaction induced by stopped antiprotons in a ^{4}He target

$$\bar{p} + {}^4He \rightarrow K^+ + K^+ + pnnK^-K^- + Q$$

This process occurs if the binding energy of the *2 K*$^-$ in a $pnnK^-K^-$ cluster B_{KK} exceeds 125 MeV plus the Coulomb repulsion of the 2 kaons, a condition which is fulfilled for deeply bound double kaonic states [109, 110, 111]. Of particular interest would be the production of double strangeness cluster states, such as ppK^-K^-, $ppnK^-K^-$ and $pnnK^-K^-$ using various targets.

In the following we consider some kinematics aspects of the antiproton annihilation in a ^{4}He target at rest producing a $pnnK^-$ cluster and 2 K^+, which are detected. For this case B_{KK} is expected to be larger than 200 MeV, most likely around 400 MeV, i.e. double the experimental value of $pnnK^-$. In the following we assume that B_{KK} takes an arbitrary value. The kinematics of the three body final states are shown in Fig. 85: (Upper) correlation of $E1=E_{K+}$ and $E3=E_{K+}$ for $B_{KK}=0.4$ *GeV* in the ^{4}He (stopped-$\bar{p}$, K^+K^+) reaction. (Lower) The decay density distribution of K^+ versus energy $E1=E_{K+}$. in which the correlation of the energy of the 2 K^+ (E_3-E_1) is plotted for a binding energy B_{KK} = 400 MeV. Since $m_1=m_3=m_K$ is much smaller than m_X, the mass of the formed double strange cluster, the 2 K^+ carry away most of released energy. Fig 1 shows also the statistically distributed decay density distribution Γ as function of the kaon energy E_1. In Fig. 86: The maximum energy ($E^{\max}_{K^+}$) and momentum ($cP^{\max}_{K^+}$) of K^+'s versus B_{KK} in the ^{4}He (stopped-$\bar{p}$, K^+K^+) reaction. the maximum energy and momentum of the K^+ is plotted as function of the binding energy B_{KK}. In addition the recoil momentum $p_X = -p_1 - p_3 = p_{max}$ which is transferred when the double strange cluster is formed amounts to about 500 MeV/c which is in the range of the internal momentum of the bound K^-.

From the momenta of the 2 K^+, which have to be measured, the mass of the cluster *X,* M_X is determined as follows:

$$\vec{P}_2 = -\vec{P}_1 - \vec{P}_3$$

$$E_2 = M - E_1 - E_3 = M - \sqrt{m_K^2 + P_1^2} - \sqrt{m_K^2 + P_{31}^2}$$

$$M_X = \sqrt{E_2^2 - P_2^2}$$

Note that the appearance of a discrete mass M_X in the spectrum of 2 K^+ is a unique signature of the formation of a double strange nuclear cluster. In addition one can study the decay of the double kaonic cluster into the open Λ, Σ and nucleon channel for an exclusive experiment.

If one aims at exclusive experiments which measure in addition to the missing mass from the 2 K^+ also the decay products, a detector with 4π covering, detection of at least all charged particles, preferable also neutrons, particle identification, and momentum measurement up to 500MeV/c is asked for. Detailed simulations of relevant particle spectra are anticipated as basis to define the detection system, for which place should be reserved.

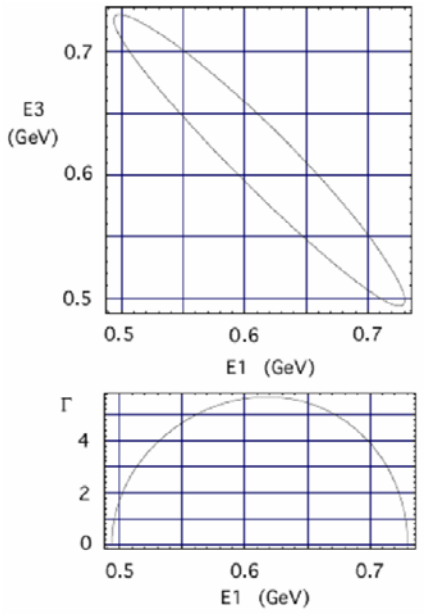

Fig. 85: (Upper) correlation of $E1=E_{K+}$ and $E3=E_{K+}$ for $B_{KK}=0.4\ GeV$ in the ^{4}He (stopped-$\bar{p}$, K^+K^+) reaction. (Lower) The decay density distribution of K^+ versus energy $E1=E_{K+}$.

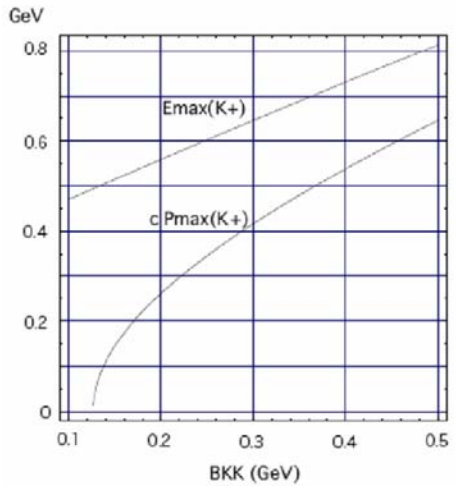

Fig. 86: The maximum energy ($E_{K^+}^{\max}$) and momentum ($cP_{K^+}^{\max}$) of K^+'s versus B_{KK} in the ^{4}He (stopped-$\bar{p}$, K^+K^+) reaction.

2 Trigger, DACQ, Controls, On-line/Off-line Computing

2.1 CRYRING

CRYRING at present has its own pc-based control system which was taken into operation in 2003. The software of the control system was developed at Aarhus University, originally for use at the ASTRID storage ring, and is fully modern. The hardware is based on older standards such as G64 and CAMAC, with some more recent additions based on newer standards. While it will be perfectly possible to continue running LSR/CRYRING with this system, there ought to be a substantial advantage in integrating not only the LSR/CRYRING controls and diagnostics, but also the control of all beamlines in the FLAIR hall into the general FAIR control system. No reliable cost estimate is available at the moment for the integration of LSR/CRYRING into the FAIR control system.

2.2 The Low Energy Experimental Area for HCI / HITRAP

The control of the experiments performed at the Low-energy HCI Cave and HITRAP will be done locally, in the data acquisition rooms of the experimental areas. A correlation with the accelerator is needed: a machine signal is desired for coincident measurements. The beam transport to the experiment must be included into the accelerator control. Beam diagnosis elements, slits, vacuum systems situated inside the caves must be under the control of the experimenters but also connected to the general FAIR (NESR) control. The HITRAP facility needs trigger signals from the extraction kickers of the storage rings NESR and LSR for exact timing of the HITRAP decelerator and the cooler trap.
It is desired that also the control over the whole beam line inside the FLAIR building will be accessible for the experimenters and also for the accelerator operators. Especially for experiments using ions from the LSR injectors, the control over the beam must be accessible also from the FLAIR building.
Multiparameter data acquisition software is needed: the GSI support for a general platform is welcomed and considered necessary especially for small experiments.

2.3 Antiproton Experiments

Most antiproton experiments will use their own software for data acquisition and control and standard hardware. Some of the experiments using pulsed beam will use standard GPIB based hardware controlled by Labview for DAQ and control, others probably standard CAMAC or other nuclear electronics. A local support at FAIR for both standard hard- and software as mentioned above would be of essential importance for the small groups.

Further detailed descriptions are given in the individual chapters of the experiments.

3 Beam requirements

3.1 Beam requirements from NESR for injection into CRYRING

We at present assume that a cooled beam in NESR with an emittance of 1 π mm mrad or better is transferred to LSR/CRYRING in a single bunch every 10–20 seconds, and that the rigidity of the transferred beam is that of 30 MeV antiprotons. As an alternative, in order to reduce the incoherent tune shift in LSR/CRYRING, the NESR beam could be bunched at a higher harmonic, and the smaller bunches could be transferred and decelerated in successive machine cycles of LSR/CRYRING. The space-charge limit is discussed further in section B4. Details of the transfer must be coordinated with the NESR team.

3.2 Beam requirements from The Low Energy Experimental Area for HCI / HITRAP

Beam specifications Low-Energy HCI Cave:

- Highly charged (few electrons) ion beams, up to uranium
- Decelerated and cooled in NESR, slowly extracted to the experimental area into the FLAIR building
- Emittance: 1 x 1 π mm mrad
- Energies of 130 MeV/u and lower
- For few-electron heavy ions, E_{ion}> 4 MeV/u. For beams from the ion injector of the LSR (N, Ar, Kr with intermediate charge state) energies E_{ion} ~ 1 MeV/u
- For channeling experiments: halo free, almost parallel beams; especially for experiments with low energy beams; an angular divergence much smaller than the critical channeling angles (typically 0.3 mrad) rms values in x and y
- A beam stability in position at the level of 1 mm: this implies a stability of the magnet power supplies at the level of 10^{-4}
- The maximum beam intensity is given by the NESR parameters and is expected to be up to 10^7 ion / spill for decelerated bare uranium. The intensity of the extracted beams depends on the extraction energy, ion species and extraction time.
- Beam spot on target: better 2 x 2 mm^2
- Long pulses: 50 to 200 s

Beam specifications HITRAP:

- Highly charged heavy-ion beams, up to uranium U^{92+}, at 4 MeV/u, from NESR
- Antiprotons at 4 MeV from LSR/CRYRING
- Decelerated and cooled in NESR or LSR, fast extraction to the HITRAP area in the FLAIR building, bunch length ≤ 1 microsecond
- Emittance: 1 π mm mrad
- Commissioning with beam from the ion injectors of the LSR at 4 MeV/u, ion species: protons, H^- ions, light highly charged ions, e.g. Ar^{16+}
- Beam stability in position at the level of 1 mm, this implies a stability of the magnet power supplies at the level of 10^{-4}
- The maximum ion beam intensity delivered to HITRAP is given by the parameters of NESR or LSR (see corresponding sections) and is expected to be up to 10^7 U^{92+} ions every 20 s at 4 MeV/u
- The maximum antiproton beam intensity delivered to HITRAP is given by the antiproton production yield at the production target and is expected to be up to 5×10^8 antiprotons every 50 s at 4 MeV/u
- Beam spot on target: 2 x 2 mm^2

3.3 Beam requirements for high-energy antiprotons

Slow extracted beam in the energy range of 30 – 300 MeV from NESR up to a rate of 10^7 $\bar{p}$/s. Typical emmitances are 1 π mm mrad.

3.4 Running scenario incl. exemplary beam time planning in a year

FLAIR expects to run with antiprotons in parallel to the HESR during antiproton production periods. The running mode with highly charged ions is described in the SPARC technical proposal. The beam time allocation for these periods has to be done by appropriate committees of FAIR and/or FLAIR.

3.4.1 Antiproton experiments with LSR

The LSR expects to receive about 10^8 antiprotons in a short bunch. The repetition rate is limited by the deceleration time in the NESR, which is estimated to be about 20 seconds. The resulting average rate of $5x10^6$ $\bar{p}$/s up is about an order of magnitude smaller than the production rate at FAIR.

3.4.2 Experiments with direct antiproton beam from NESR

Slow extracted beam in the energy range of 30 – 300 MeV from NESR up to a rate of 10^7 $\bar{p}$/s.

3.4.3 The Low Energy Experimental Area for HCI / HITRAP

For one experiment: Pulse by pulse, at a time interval given by the cooling and deceleration time in NESR. Blocks of 15 to 25 shifts beam on target. Additional 10 to 12 shifts should be foreseen for the settings of the extraction and transport beam line. At the beginning of the operation it is advisable to plan one or two beamtimes, after the commissioning of the beam line of the Low-energy HCI cave and HITRAP, only with the purpose of exercising the beam transport to the caves. The present experience gained at the ESR in GSI showed that at the beginning the transport setting takes longer and on the long run such a scenario will shorten the time needed for this operation during the physics experiments.

Experiment schedule: Due to the availability of an ion source at LSR, most of the testing and commissioning can be done without NESR beam (see the LSR and Ion Source for LSR sections). Commissioning beam time is needed for the different beam lines, the magnetic spectrometer together with the focal plane detector at the low-energy HCI cave, and the HITRAP decelerator and cooler trap. A final commissioning with NESR ion beam is also required. Also commissioning and tests of different set-ups must be foreseen. Most of these steps can be performed using only ion beams delivered from the LSR.

From the technical point of view, two different experiments for each beam time block can be performed in each of these two areas. For all experiments to be performed in the low-energy HCI cave, only the target region will be exchanged. With a modular concept of the setups a fast exchange of experiments is possible. Depending on the number of applications for the beam time, at least six different experiments of 15 to 25 shifts can be easily performed in the low-energy HCI cave. The following table present a tentative beam request for the years 2011/2012.

Table 18: Heavy ions beam time request at the low energy HCI cave / HITRAP

Year	Experiment	Nr. of requested shifts	Beam
2011	Commissioning beam line from LSR to Low-energy HCI cave and to HITRAP (including the cave beam line up to the target point)	15	Ar/ Kr ions from the ECRIS accelerated in LSR energy: few MeV/u
	Commissioning magnetic spectrometer and focal plane detector at Low-energy HCI cave	12	Ar/ Kr ions from the ECRIS accelerated in LSR E < 10 MeV/u
	Commissioning HITRAP decelerator and cooler trap	27	Ar/ Kr ions from the ECRIS accelerated in LSR E = 4 MeV/u
	Commissioning beam line from NESR to Low-energy HCI cave and to HITRAP	30	Hydrogen-like heavy ion species (Xe, Pb, U) 20 MeV/u < E < 130 MeV/u
	In-beam test of the HCI-cluster interaction experimental setup	10	Ion beam from LSR
2012	Fragmentation and charge exchange processes in HCI-cluster interaction experiment	36	H-like U from NESR, E < 10 MeV/u and E = 100 MeV/u
	Precision spectroscopy of slow HCI with Reaction Microscope	30	bare U from NESR, E = 4 MeV/u
	Ion-surface interaction studies	30	bare U from NESR, E = 4 MeV/u
	g-Factor measurements, mass measurements (can run in parasitic mode, 10%)	36	H-like Pb or U from NESR, E = 4 MeV/u

4 Physics Performance

4.1 FLAIR

The physics of FLAIR covers a wide range in atomic, nuclear and particle physics and has potential medical applications. Precision spectroscopy of antiprotonic atoms and antihydrogen (Sec. B1.6) is the current topic of the Antiproton Decelerator (AD) at CERN. The main goal here is to study fundamental symmetries and interactions by providing high-precision data of particle and antiparticle properties for tests of CPT symmetry and QED calculations. Until 2010 initial results on spectroscopy are expected from the AD, but the ultimate goal of reaching accuracies similar to hydrogen requires the trapping and laser-cooling of antihydrogen atoms which will take a long time to achieve. Once trapped and laser-cooled antihydrogen is available, other challenging experiments can be performed. The gravitation of antimatter (Sec. B1.7) is a long standing question that has never been answered experimentally, because in the case of charged particles, gravitational effects are covered by the many orders of magnitude stronger electromagnetic interaction. Collisions between antihydrogen and matter atoms as well as the creation of larger antimatter systems like $\overline{H}^+$ (one antiproton and two positrons, equivalent to the well known H^- ion) are of big interest for atomic collision theory (Sec. B1.8).

Atomic collision physics (Sec. B1.8) will greatly benefit from the availability of ultra-slow, cooled antiproton beams in storage rings. This will enable for the first time ever the detailed study of ionization processes with antiprotons in kinematically complete experiments. The energy loss can be investigated at ultra-low energies to answer open questions about the velocity dependence in this regime. Antiprotons are best suited for such studies, because unlike protons their charge is not screened by electrons which make the theoretical treatment very difficult. The very short interaction time of less than femtoseconds for antiproton energies above 1 keV makes antiprotons a perfect and unique tool to study many-electron dynamics in the strongly correlated, non-linear, sub-femtosecond time regime, the most interesting and, at the same time, most challenging domain for theory.

In nuclear physics, the antiproton is used as a hadronic probe to study the nuclear structure. X-ray spectroscopy of the low-lying states of $\overline{p}p$ or other light atoms (Sec.B1.9.1) gives important information on the nucleon-antinucleon interaction in the low-energy limit, where scattering experiments cannot provide precise values. These data are vital for the improvement of QCD calculations in the low-energy (hence non-perturbative) region. X-ray spectroscopy of heavy antiprotonic atoms (Sec. B1.9.2) can be used to obtain information about the density ratio of neutron and protons at the nuclear periphery, i.e. to investigate neutron halo or skin effects. The PS209 experiment at LEAR has in this way provided benchmark data for nuclear structure calculations over a wide range of nuclei. This technique is much more sensitive than others like total absorption cross section measurements, and further systematic measurements with stable isotope targets will provide a more complete and systematic picture of the nuclear surface. Since halo effects are expected to be more pronounced in nuclei with a large neutron excess which are unstable, the application of this technique to unstable radioactive ions (Sec. B1.10.2) available at FLAIR via the SuperFRS will generate important contributions to the study of the structure of nuclei far from stability.

The study of baryon-baryon interactions as a basic tool for investigations of the strong interaction can be extended to the hyperon sector, where much less data exist than in the nucleon sector (Sec. B1.9.3). Especially few data exist on strangeness S= -2 systems. Stopped antiprotons are very efficient for the production of S=-2 systems via the double strangeness and charge exchange reaction ($\overline{K}^*$, K). With a sizeable branching ratio the annihilation of antiprotons results in the production of a $\overline{K}^*$ "beam" which interacts with another nucleon via $\overline{K}^* \, N \rightarrow K \, \Xi$. The momenta of

the $\overline{K}^*$ are well matched for the production of slow Ξ particles which undergo efficient Ξ N interactions. The proposed studies will result in detailed information of S=-2 baryonic and possible dibaryonic states.

Recently, interest has been shown in the medical application of antiprotons for tumour therapy (Sec. B1.10.3). This comes from the fact the antiprotons, in addition to depositing energy via their energy loss like other charged particles, annihilate when stopped in material. The annihilation produces residual nuclear fragments of high charge and low energy, which deposit a large biological dose in the immediate surrounding of the $\overline{p}$ stopping distribution. Since the cooled low-emittance antiproton beams can be stopped in a well-defined region, the presumably large energy deposited locally makes them a suitable tool for tumour therapy. A test experiment is under way at the AD of CERN and, if this effect is confirmed, the method can be extended at FLAIR where the high-energy antiproton beams (50 - 300 MeV) needed to penetrate deep enough into human tissue are available directly from the NESR.

4.2 The Low Energy Experimental Area for HCI

In the past the energy range of few MeV/u for few electrons highly charged ions could not be explored at the present ESR. Up to now, no decelerated and cooled highly charged ion beam with energies below 12 MeV/u was extracted from the ESR. One reason for this is the fact that for decelerating further down, below this energy, the beam must be rebunched due to the limited range of the radio frequency cavities of the ring. It is proposed and under study, that the NESR will be designed in such a way that the deceleration of the ions from the highest accepted energy to 4 MeV/u will be performed in a continuous way, with a single RFQ covering the whole frequency range. This will improve the ring operation and make it easier to decelerate to the range of few MeV/u. Also slowly extracted bare heavy ions have not yet been delivered from the ESR for off-ring experiments. This will be possible in the future, for a large energy range (from 130 MeV/u down to few tens of keV/u) in the experimental area F1. With these beams the high perturbation regime in ion- atom (also molecules, clusters surfaces) can be investigated. These phenomena can not be explained anymore using simple perturbation theory.

4.3 Antiproton Rates at FLAIR

In CRYRING, the space-charge limit for a coasting beam of protons at 300 keV is $N = 5\times10^8$, assuming $\Delta Q = -0.1$ and $\varepsilon = 1\ \pi$ mm mrad. The electron cooling at 300 keV is probably not strong enough to reach down to 1 π mm mrad with 5×10^8 particles, but in a recent quick test it was shown that 1×10^8 protons could be stored at 300 keV with an emittance of approximately 1 π mm mrad. This is thus, at a minimum, what LSR/CRYRING should be able to deliver once every NESR cycle of 20 s, losses during extraction not counted. Since the space-charge limit is proportional to energy (non-relativistically) while equilibrium emittances in our case shrink with energy, one can expect that the number of antiprotons per unit time and emittance increases at least linearly with energy.

Some improvement could be obtained if the NESR beam is bunched at the 4th harmonic before extraction, and the four bunches are transfered to LSR/CRYRING and decelerated in four consecutive machine cycles. Each cycle taking about 5 s, LSR/CRYRING could thus be able to deliver four batches of 1×10^8 antiprotons, minus extraction losses, within approximately 1 π mm mrad emittance every 40 s.

For highly charged ions, the space-charge limit scales with A/Z^2. The rates for intrabeam scattering and electron cooling also change, such that one can expect that the equilibrium emittance, at the space-charge limit, does not depend strongly on the ion species for a given particle velocity. Again,

the emittance shrinks with increasing energy. From this scaling, we can find, for example, that 1×10^8 antiprotons at 300 keV corresponds to 4×10^7 U^{92+} at 4 MeV/u.

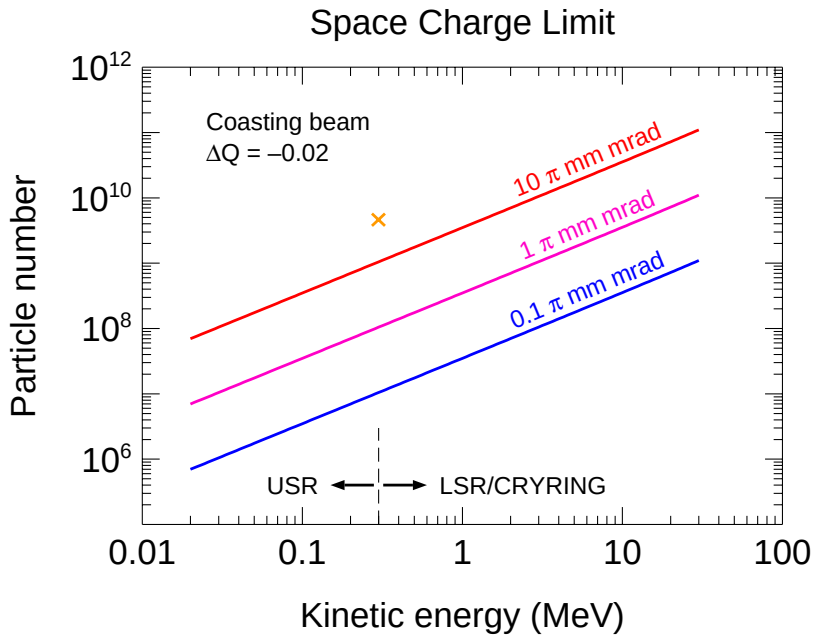

Fig. 87: Antiproton space-charge limit in LSR/CRYRING with a Laslett tune shift of -0.02. During deceleration the particle number must be multiplied by a bunching factor of approximately 0.3. The cross shows the highest number of protons that has been stored in CRYRING at 300 keV.

The resulting antiproton rates per unit time, averaged over the duration of a deceleration cycle starting from injection into NESR, are listed in Fig. 87.

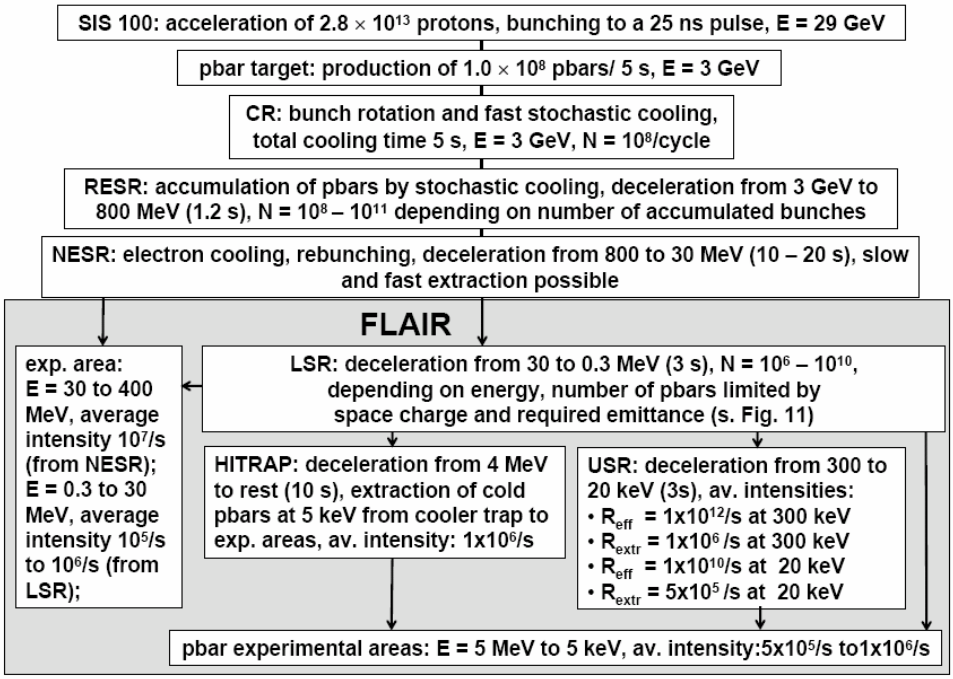

Fig. 88: Estimated antiproton intensities available at FLAIR. Reff: effective antiproton rates in the ring, Rextr: average rates of extracted antiprotons, assuming 90% losses.

C Implementation and Installation

1 Cave and annex facilities

1.1 The FLAIR building

The floor plan and a description of the building are presented in the section B1. This plan presents only the ground floor of the building. In principle, additional place on the top of the concrete roofs of some caves will also used for experiments, acquisition rooms, laser labs and for power supply storage.

The building should be designed to accommodate approximately 10 different experimental areas with different requirements, different labs, electronic and control rooms, spaces for power supplies, storage areas for setups which will share the same beam line and access ways between all these locations. It is very important that all these ways are roofed, so that the transport of different parts between the laboratories and the experimental area can be done in secure conditions . The building should be accessible through two large access door for heavy transports. To give the possibility to move heavy parts, like large magnets or concrete parts, one crane of 5 tons covering an area of about 20 x 60 m are required in the region of the LSR and the low-energy antiproton experiments (F4 to F6) where parts of 2 to 5 tons should be often moved or lifted at the second floor level. Taking into account that the maximal height of the different concrete shielded caves will be 6 m, the hook height must be in approximately 9.5 m height. Additional, smaller, up to 2 tons cranes will be mounted in fix positions at the different experimental areas. The beam line height should be all over the hall 1.5 m. Due to the fact that some concrete shielding will be movable and during the operation time the requests for the size of the experimental areas can change, it is practical to keep the floor height at the same level all over the building. To make the access between the mounting areas, laser labs, acquisition rooms and experiments easier, an access way approximately 2 m wide, along the building, at least on two sides is strongly requested (included into the layout presented here). The floor loading depends from experiment to experiment. More details are presented in the description of the proposed experiments.

The ion and antiproton beams extracted from the NESR will be delivered towards the Flair building via a beam line which, behind the NESR, will split into two parts: one going to the LSR and the second branch going direct to HITRAP (F2), Low –energy HCI area (F1) and F8, area dedicated to the biological studies with medium energy antiproton beams. The beams decelerated/accelerated in the LSR will be distributed further to the experimental places (F1, F2, and F4-F10) through additional beam lines. In the present building design, the total length of the beam lines is estimated at about 160 m.
A scheme of the beam distribution inside the FLAIR building is presented in Fig. 89.

The broad energy range available at FLAIR requests beam lines with different rigidities: the maximum of 4 Tm is available for highly charged ions and antiprotons and will be a magnetic transport line. For the low-energy range (300 keV and below) the transport lines for both, antiprotons and ions, will be based on electrostatic elements .Vacuum conditions, stability and polarity of the power supplies for the magnets and optical elements must be taken into account.. Some segments of the beam lines should transport antiprotons and ions. For a cost-benefit optimization, a detailed simulation of the beam lines is mandatory.

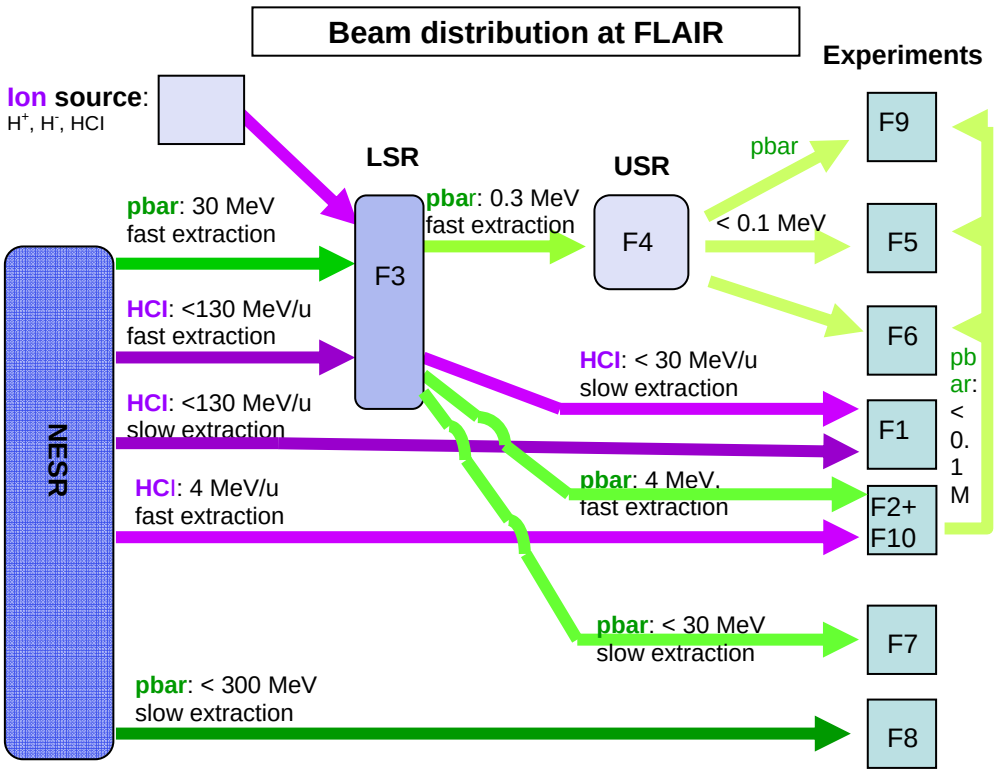

Fig. 89: Beam distribution inside the FLAIR building

Special care must be taken for the parameters of the transported beams. For example, channeling experiments proposed to be performed in the F1 area, parallel beams with a divergence below 0.3 mrad on directions, well focused (better then 2 x 2 mm) and halo free are strongly requested. To achieve these parameters in the beam quality two sets of slits must be inserted into the beam line as close as possible to the NESR. Each set of slits should consist of two pairs of slits –one horizontal and one vertical- remote controlled by the users. The final beam optics calculations and simulations still to be performed by the collaboration should take into account these devices. The transfer of the beam between the facilities (LSR, USR and HITRAP) and the experiments requires a good matching of beam parameters between the different installations and experiments. .

Beam monitoring, able to determine the beam profile in real time with high accuracy, must be considered for this beam lines. Again, the difference in the energy and the particle type requires specially designed beam monitors. The beam lines transporting HCI and Antiprotons must include detectors for both types of beam, since there is no universal profiler to do the job. These monitors should be x and y position sensitive, and sensitive to the beam intensity. Part of the today GSI standard beam diagnosis can be overtaken. The fluorescent screen with digital read-out, scintillators and the gas profiler are used as in-beam viewer. The present GSI standard is not suited for energies below 10 MeM/u and for antiprotons. More R&D is required in this direction. Also beam intensity monitors for low intensities highly charged heavy ion beams are not jet available at GSI. We hope that the development works for the focal plane detector in F1 and the on going development for HITRAP at the present ESR will offer a spin-off for beam monitoring. A two dimensional position sensitive detector with 100 % efficiency at high count rate capability (up to few hundred kHz) is needeed. In this sense diamond based detectors are very promising for the beam diagnosis.

Between the LSR and the low-energy antiproton experimental setups an electrostatic beam line of approximately 40 m is proposed. This option is possible due to the extremely low antiproton energy, E < 300 keV, and has the advantage to be lower in cost then a magnetic one. Lifetime limits of the low energy antiprotons impose UVH conditions al over this beam line.

The building must have standard infrastructure: water, electrical power, ventilation, compressed air.

1.2 LSR / CRYRING

The hall for LSR/CRYRING should preferably be big enough to have 3 m free space between the ring (which has a diameter of 16.5 m) and the walls. Additional space is needed for the injectors. The power supplies, except main magnet power supplies, need a floor space of approximately 40 m^2 plus some space inside the ring. Also the 40 m^2 area could be inside the ring, although this would make access more difficult. Another alternative would be on a second floor above the ring. At MSL, the main magnet power supplies at present occupy a hall of dimensions 10×18 m^2, which could perhaps be reduced to 9×15 m^2 with the entrance at an optimal location. The height of this hall is 4 m (with a computer floor at 0.9 m and 3.1 m above that). In addition, switchgear occupy 3.6×11 m^2 and transformers 4×7 m^2, although these need not be located in the FLAIR building if one accepts the cost for longer cables.

The heaviest parts of CRYRING are the dipole magnets with a weight of 4.5 tons each and a footprint of approximately 1 m^2. Total weight is estimated at 100 tons.

Beam height of CRYRING is at present 1.5 m, but it is suggested that this be increased to 2.0 m at FLAIR.

Required crane hook height is approximately 5.5 m and required ceiling height is approximately 6.0 m with 2.0 m beam height.

All relevant magnets are equipped with alignment fiducials, allowing the alignment to be checked at any time provided that the fiducials are properly surveyed after initial magnet alignment (c.f. section D). Alignment issues will put restrictions on the positioning of columns for roof support inside the ring.

b See (e).

c. The total active power consumption of CRYRING is approximately 1 MW at maximum magnetic field. A corresponding water-cooling capacity is required at 7 bar and 4 bar overpressure. Also, a cooling system with 3.5 bar and 10°C is used at present.

d. According to a rough estimate, 25 kW is released into the air.

e. Power supplies consume, at maximum load, 1 MW active power and 3.5 MVA reactive power. Input voltages are 10 kV, 400 V and 230 V at 50 Hz. Total floor space required by power supplies is 200-250 m^2 (c.f. section C1 a)

f. Compressed air in the vicinity of LSR/CRYRING is required.

g. The superconducting electron-cooler magnet consumes approximately 50 l of liquid helium per week.

1.3 The Low Energy Experimental Area for HCI

a. This hall will have an area of 20 x 15 m^2 where the magnetic spectrometer, the target chamber for the experiments using the NESR / LSR beams, the target chamber and detection systems for the beam extracted from HITRAP and different beam diagnosis elements will be mounted. The proposed positioning of the low energy HCI experimental area inside the FLAIR building permits to access beams coming directly from the NESR, from the LSR and extract highly charged ions at very low energy from HITRAP installation. The cave height to the ceiling will be 4.5 m. This

height will permit the installation of two fix cranes (1000 and 2000 kg) in the region of the target chamber and close to the spectrometer. For the ion beams of higher energy delivered from the NESR the cave mus have a beam dump to stop the primary beam after the interaction with the target region.
The floor will have a maximum loading in the region of the magnet separator (maximum 2 t/m^2). The access into the cave will by permitted through a labyrinth

Alignment fiducials for the spectrometer, beam lines and target chambers, are required. The whole setup including the transport beam line from the NESR must be aligned relative to the FAIR facility. For regular alignments which must be performed for different parts of the setups when the experiments are exchanged and for the beam diagnosis. two telescopes placed at the end and on one side of the cave, having a permanent, reproducible alignment are requested.

b. The cave must accommodate six to ten electronic racks for detectors read-out electronic, vacuum controlling, remote control of the diagnosis elements, etc. For this an area of 10 m^2 is needed. The estimated electrical power needed in cave for electronics is about 12 kV. Additional 10 kV are needed for all other equipment.

c. For the detectors cooling liquid nitrogen must be available. The needed amount will depend on the number of detectors used for the experiment (usually three to four x-ray detectors). To assure a permanent cooling of the detectors during test and experiment an automatic filling system , placed in the cave is planned. Depending on the storage place of the solid state x-ray detectors, a permanent source of Liquid nitrogen in the neighbourhood is compulsory. Water cooling for the magnets and electronic is also needed.

d. The cave must have constant temperature between 19°C to 26°C and a constant humidity of about 65%.

e. Outside the cave a storage room for the magnet power supplies, of about 10 m^2 must be foreseen. In principle, this room can be shared with other groups working in the FAIR building.

f. Filtered, compressed air and a gas (Ar/CO_2) system for the automatic filling of the multi wire beam profilers are also needed at this experimental area.

g. If finally the charge spectrometer will be based on a superconducting magnet, a cryo system will be necessary. The decision about such a system must be discussed with the antiproton community which uses also liquid helium for theirs setups, including the LSR.

An electronic and data acquisition room of 50 m^2 with an electrical power of 20 kV is also needed. To shorten the cabling between the cave and this room, it must be placed close to the cave. This room must have a constant temperature of 19°C to 22°C and constant humidity of about 65%.

A small workshop (~ 30 m^2) and a clean room of the same size can be shared with all other groups working in the FLAIR building. Also a social room for 10 to 15 persons is needed inside the FLAIR building.

1.4 The Long Beam Transport Line

Since the Exo+pbar experiment (cf. sec. B1.10.2) would require trapped antiprotons and low-energy radioactive nuclear ions simultaneously, a beam transport line between NUSTAR –LEB and FLAIR facilities would be needed. The long beam line (LBTL) described here can transport low-energy (~30 keV) singly-charged radioactive nuclear ion beams (RIB) from the Low-Energy Branch of NUSTAR to the FLAIR building where the experimental setup will be placed. The LBTL can also transport highly-charged medium energy radioactive nuclear ion beams in the opposite direction, from CRYRING in the FLAIR building to the AGATA detector setup in the NUSTAR building. In this section, a possible design of the LBTL is described. Due to the changed internal structure of the FLAIR building, the design of the LBTL is greatly facilityted. The extraction line from CRYRING to the F7/F8 cave (see Fig. 1) can now directly be used as it points towards the position of the SFRS building and the previously described 154 degree bend is not any more necessary. The exact layout, i.e. whether the LBTL will just go straight through the areas F7/F8 or whether it needs to cross on top of the cave can be decided at a later stage.

Low-energy (~30 keV) radioactive nuclear ion beams from NUSTAR-LEB are transported to the Exo+pbar experimental setup in F9 of the FLAIR building through the LBTL and the common low-energy beam line of the FLAIR facility. Medium energy (~6 MeV/u) radioactive nuclear ion beams from CRYRING in F3 of FLAIR are also transported by the LBTL to the AGATA detector setup in the NUSTAR building. The straight section of the LBTL can be as long as ~50m and is made of a periodic array of electrostatic quadrupoles, a so called FODO lattice structure. This straight section is shared by two different types of beams in opposite directions.

FODO lattice structure

The most effective mode of the beam transport line for a long distance is a so called FODO lattice structure which is made of a periodic array of quadrupole elements. In this mode, the beam envelope has maximum size for horizontal and minimum size for vertical direction at the center of 'even' quadrupoles, while it has maximum size for vertical and minimum size for horizontal direction at the 'odd' quadrupoles. The actual sizes at matching condition are $R_i \approx 0.88\sqrt{\varepsilon d}$ and $R_{i+1} \approx 1.82\sqrt{\varepsilon d}$ where ε is the emittance of the beam and d the distance of the quadrupole elements. The acceptance of the beam transport line is proportional to the square of the aperture of the quadrupole elements and inversely proportional to the distance of the quadrupole elements. The aperture size and the period of the quadrupole elements should be defined from the required acceptance of the beam transport line.

The characteristics of the two types of beams to be transported are quite different as shown in Table 19. The usage of magnetic elements is suited for such a wide variation of the characteristics of the beams, since the variation of magnetic rigidities are much smaller than that of electrostatic rigidities. However, the use of electrostatic elements is advantageous in particular for low-energy ion beams of weak intensities, since the electrostatic rigidity is independent to the mass of ions in non-relativistic regime. One can use any intense stable nuclear ion beam of the same energy-to-charge ratio as the desired radioactive nuclear ion beam when tuning the ion optical elements. A high reproducibility of the optics parameter is also guarantied due to the absence of hysteresis in electrostatic optical elements. In the present design, fully electrostatic optical elements are used for the low energy RIB while a few magnetic deflectors in addition to the common electrostatic quadrupole elements are used for the medium-energy RIB.

Table 19: Characteristics of the beams to be transported

	Energy	Emittance	Magnetic Rigidity	Electrostatic Rigidity
Low energy RIB M^{1+}	30 keV	~50 π mm mrad	~0.2 Tm	60 kV
Medium energy RIB $^{200}Au^{79+}$	~6A MeV	< 5 π mm mrad	~0.9 Tm	~30 MV

The ion optics designs of the straight section of the LBTL are shown in Fig. 90 and Fig. 91. For the low-energy RIB, electrostatic quadrupole elements of 24 mm aperture diameter and 100 mm length are periodically used with a half periodic distance of 400 mm. Typical voltages on the electrodes are +-150 V for 30 keV singly charged ions. For the medium-energy fully stripped RIB, the same quadrupole array can be used but only one out of four are activated with typical voltages of +/– 17 kV.

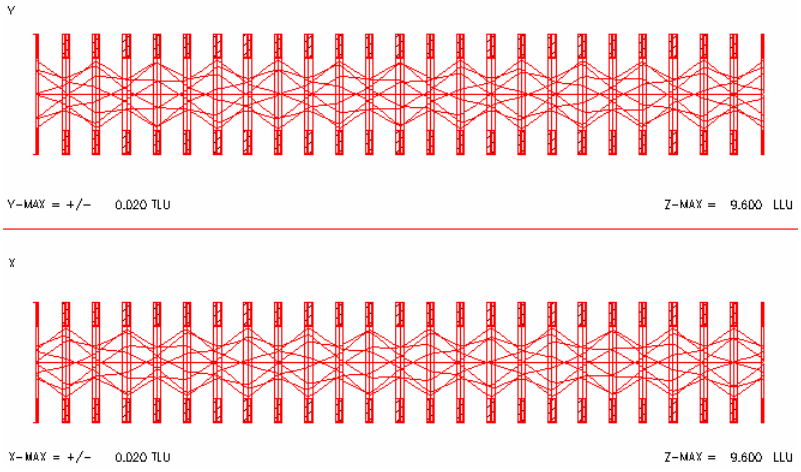

Fig. 90: Part of the beam optics design for low-energy RIB (30 keV, A^+, 60 π mm mrad). Electrostatic quadrupoles with an aperture diameter of 24 mm and a length of 100 mm are placed with a period of 400 mm.

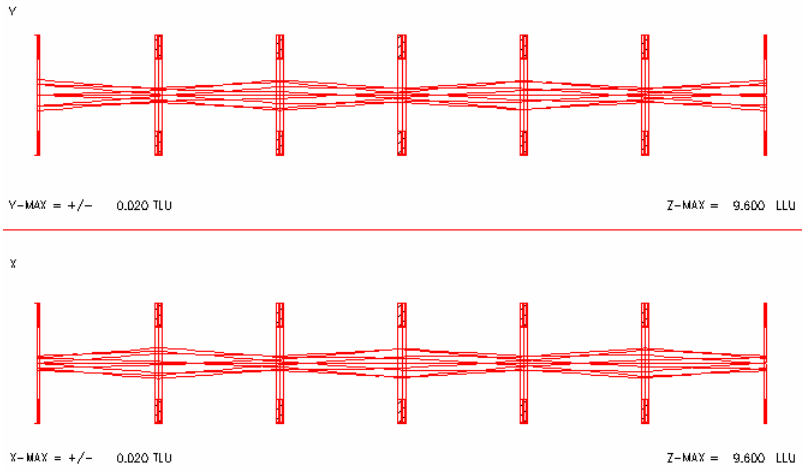

Fig. 91: Part of the beam optics design for medium-energy RIB (6 MeV/u, A=200, Z=79, Electrostatic Regidity = 30 MV, 5 π mm mrad) from CRYRING. The same periodic structure of electrostatic quadrupoles for low-energy RIB is used, but only one out of 4 elements is activated with a typical voltage of +-17 kV while three elements in between are turned off.

Merging and splitting of AGATA beam

The medium-energy RIB for the AGATA experiment is provided from CRYRING, while the low-energy RIB is further transported to the F9 area of FLAIR through the common BTL of FLAIR. The two beam lines should be merged at a certain point of the periodic array of the electrostatic quadrupole elements. The phase-space of the beams from CRYRING should be matched with that of the FODO lattice at the merging point. The ion optics design of this merging and matching section is shown in Fig. 92. An eight degree magnetic deflector is placed at the periodic array while one electrostatic quadrupole element with the same voltage with the one in the periodic array and four magnetic quadrupoles are used for this purpose. One quadrupole element for the low-energy RIB is located in the deflector magnet. This particular element can be made by a set of multiple plate electrodes placed at the surface of the vacuum chamber on which appropriate voltages are applied so as to form a quadrupole electric field. The same structure can be used for splitting the beam in the NUSTAR building.

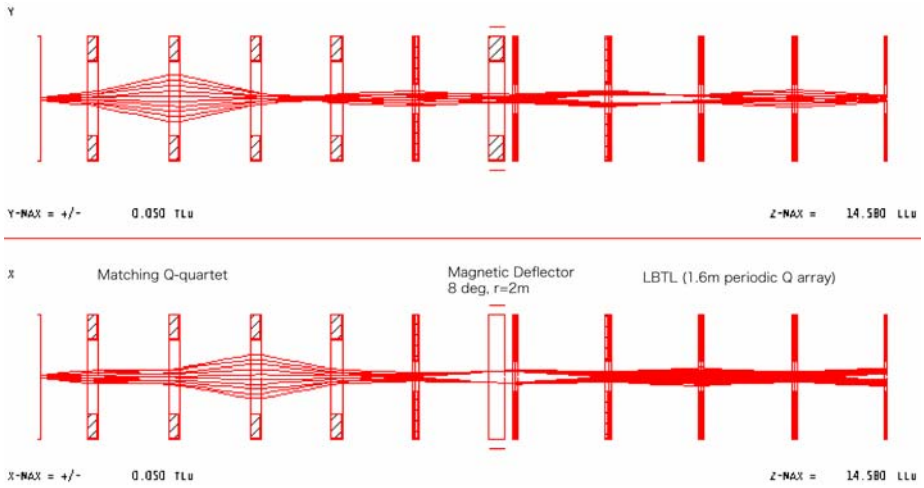

Fig. 92: Merging beams from CRYRING to LBTL. Four magnetic quadrupoles are used for phase matching to the periodic structure and an 8° magnetic deflector merges the beam into straight line.

Vacuum

The vacuum of the beam transport line should be order of 10^{-8} mbar, which can be maintained by turbo-molecular pumps of 300 l/s placed every 4 meters. Baking capability, especially at installation phase, is indispensable, since a large amount of materials are contained in the chamber. A unit cell of 800 mm length contains two quadrupole elements and five units are grouped to be a macro cell. Use of Helico-Flex type flanges is recommended to preserve accurate alignment between each unit cell of the beam line. An in-line valve of 1.5 inch o.d. and bellows with an expandable mounting using a linear guide should be used for each macro cell.

Beam diagnostics

A unit of the beam monitor device consists of two motor controlled bellows. They move in the direction normal to the beam axis and are inclined by 45 degrees relative to the horizontal plane. One axis contains a vertical and a horizontal slit and the other contains two wire detectors, a Faraday cup and a secondary-electron detector. The monitor units are installed at 1) behind each deflector, 2) at a few points in the long straight beam-line and 3) behind the matching units. The last one should have two independent slit axes for a measurement of the emittance phase-space. An effective way to monitor the bi-directional beams in the present case is being investigated.

1.5 The LSR – USR transfer line

The transfer line between LSR and USR is shown on Fig. 95. Two dipole magnets with deflection angles of 720 and 900 are used to transfer the antiproton beam from the LSR storage ring to the electrostatic storage ring USR. For focusing the beam two quadrupole duplets are used. At the end of the beam transport line there is on triplet to match the anti-proton beam.

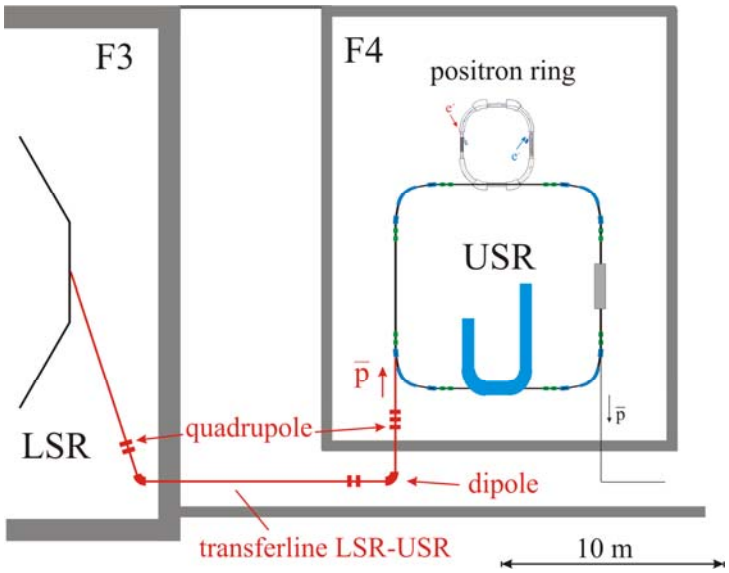

Fig. 93: Transfer-line between LSR and USR

To calculate the beam envelope in the transport line a horizontal and a vertical emittance of 10 π·mm·mrad was used. The ß function at the beginning of the transverse channel was assumed to be equal as the values at the centre of one straight section of LSR (CRYRING). In the Low dispersion mode of CRYRING $ß_x$=8.7 $ß_y$=4.3 m [112].

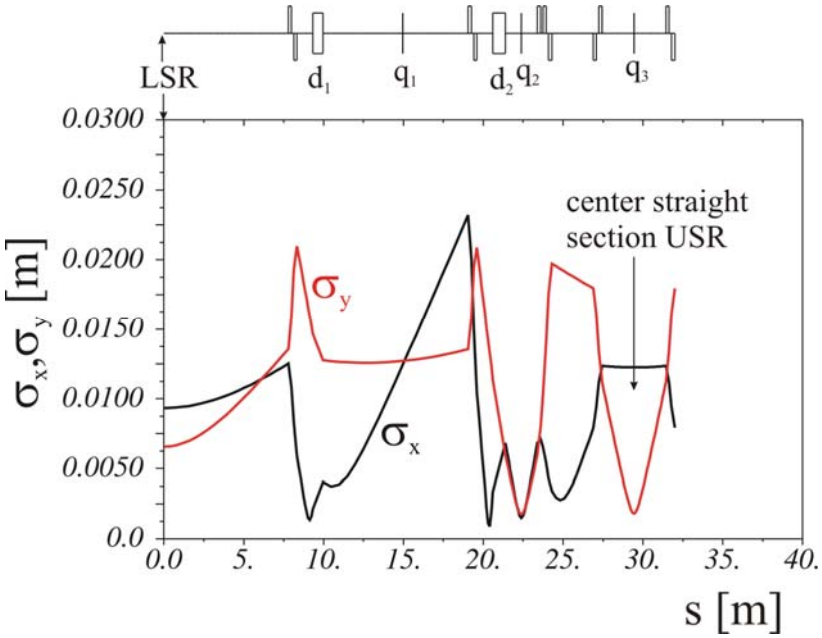

Fig. 94: Horizontal and vertical beam envelopes for $\varepsilon_x,\varepsilon_y$=10π mm·mrad

The first quadrupol duplet is used to create a horizontal waist of the beam at the detection position q_1 [compare Fig. 94], the vertical size of the envelope is there the same as the horizontal one. With the second qudrupole duplet a horizontal and a vertical waist is produced at q_2. A quadrupole triplett in front of the USR is used to mach the TWISS parameters of the transfer line to the values required by the USR.

1.6 Laboratory Space, Offices, etc.

The following space for laboratories for off-line monitoring and testing, offices, etc. is needed inside the FLAIR hall, 600m^2 shall be foreseen on the two levels of the FLAIR building.

Since some of the spaces can be shared by different groups, we currently plan a total area of 700m^2 distributed over two floors.

In addition, laser labs can be placed on top of the experimental areas F5, F6, or F9 to minimize the laser light path.

Table 20: Overview of the required floor space of each experimental area.

Exp. area	Contact person	Control room	Prep. lab	Laser lab	Office for # of persons	Clean room
F1	A. Bräuning-Demian *GSI*	50 m^2	65 m^2	no	4 p + 6 temp	*30 m^2
F2	W. Quint *GSI*	50 m^2	60 m^2	no	3 p + 2 temp	*20 m^2
F3	H. Danared *MSL*	50 m^2	15 m^2	no		no
F4	C.P. Welsch, M. Grieser *MPI-K*	*50 m^2 + *20 m^2	50 m^2+ *20 m^2	*30 m^2	6 p	*20 m^2 + *15 m^2
F5	J. Walz *MPQ Garching*	70 m^2	30 m^2	100 m^2	3 p + 2 temp	no
F6	E. Widmann, *SMI Vienna*	50 m^2 + 50 m^2	*50 m^2 + *50 m^2	*100 m^2 + *100 m^2	5 p + 6 temp	*30 m^2 + *30 m^2
F7	D. Grzonka, *FZ Jülich*	20 m^2	25 m^2	no	5 temp	no
F8	M. Holzscheiter *Pbar Labs, USA*	combined with F7	yes, for biological probes	no	2 temp	no
F9	Y. Yamazaki *Tokyo University*	10 m^2+ 10 m^2+ *10 m^2	10 m^2+ 10m^2+ *10 m^2	no	2 p + 2 p + 1 temp + 1 temp + 1 temp	10 m^2
F10	W. Quint *GSI*	combined with F2	60 m^2	24 m^2	3 p + 4 temp	*20 m^2

* requested area can be shared with other groups.

2 Detector – machine interface

2.1 FLAIR building

a. The FLAIR facility, as a whole, interferes with the NESR and SFRS through the transfer beam lines (~160 m). Almost half of this length (LSR-F4 towards F9 and LSR-F7 and the HITRAP surroundings) requires Ultra High Vacuum (UHV). Around the beam injection point into the LSR the high vacuum quality of the ring (10^{-11} mbar) must be guaranteed. Due to the fact that the NESR and LSR have both UHV requirements and between the NESR extraction point and the LSR injection point are around 20 m away one should consider to make also this segment UHv compatible. A special care should be paid to the cross point of the high energy transport line (NESR to F1) and the beam lines exiting the LSR

The distance between the extraction point from the LSR and the crossing point with the beam line coming from the NESR is relatively short – below 20 m- and is necessary to adjust the vacuum quality in this region (10^{-8} mbar) to the LSR requirements.

As a solution for this problem two scenarios are currently discussed:

1. the beam line connecting the LSR with HITRAP and low-energy cave will be a UHV region beyond the point where the LSR beam enters the NESR beam line, toward the F1/F2.

2. a system of differential pumping, implying short segments with a smaller beam pipe diameter a additional pumping power

Both solutions have advantages and disadvantages. The final decision will be taken after a careful cost benefit analysis.

An additional beam line, 60 m long, connecting the Super Fragment Separator low-energy branch (SFRS) with the FLAIR building was proposed by the Exo-Pbar collaboration (for details see section B1.10.2 in the FLAIR Technical Report). This beam line should be able to transport low-energy radioactive beams from SFRS to FLAIR and ions with intermediate energies from LSR toward SFRS and is proposed to be mounted in between LSR and Ultra-low energy Storage Ring (USR) locations (F3 and F4 in Figure 1).

b. beam pipe. No final beam optics simulations for the whole hall are presently available. Details about the requested beam parameters are given in the description of the experiments. For cost saving reasons it is possible to have different diameters of the beam lines, depending on the needed acceptance for the beams and beam parameters.

2.2 Low-energy storage Ring LSR

Please refer to 2.1.

2.3 The Low Energy Experimental Area for HCI

This area will need two different beam pipes: one for the experiments with NESR beams and the second one for beams extracted from the HITRAP. Due to the different life times for highly charged ions at 100 Mev/U and few hundreds keV/u the two beam lines will have different requirements.

a. The vacuum all over the cave must be at least as good as the vacuum in the transport beam line before the cave.: 10^{-8} mbar in thy high energy part and lower for the low-energy part. For ion-

surface interaction studies the vacuum inside the reaction chamber should reach the $1 \cdot 10^{-10}$ mbar region. This requires adequate differential pumping, and UHV-compatible target chamber setup.

b. The beam pipes will be made out of stainless steel in CF100 or even CF150 standard. In some places, where diagnosis and slits will be mounted it can be wider then this. Preliminary simulations show that the magnet vacuum chamber will be around 160 mm x 80 mm.
To separate the different sections of the beam lines a number of 5 vacuum valves must be installed in the high energy line and at least three for the low-energy part.

At the present time we have no final layout of the beam line into the cave. This is strongly connected to the transport beam line, the final design of the spectrometer and the experiments wich will be placed here.
c. The experiments proposed to be performed here foresee usually thin solid state targets (~ 1 μm, only for channeling thicknesses of few tens of micrometer are planed), effusive clusters and vapour target (e.g. Hg). The density of the gaseous targets will barely exceed 10^{13} particle/cm^3.

At least six beam monitors are needed in the cave. For the high energy segment:
- 2 upstream the target, separated by around 2 m, the second one being as close as possible to the target.
- a third one at the end of the beam line at zero degree exit of the dipole magnet, and the fourth one at the end of the deviated beam line.
None of the monitor will be transmission detectors and consequently they will destroys the beams, especially the those of lower energies.

For the low-energy branch the concept for the beam monitors is not yet clear, but at least two detectors will be needed.

d. In this cave slow extracted NESR/LSR and HITRAP heavy ion beams will be used. The experiments will take every spill and a correlation of the data acquisition with the beginning and the end of the spill will improve the accuracy of the measurements.

e. Although the radiation level during the experiments will be higher then the accepted safety limit, no tremendous levels are expected here, due to the limited beam intensity and energy range. For more details refer to section F, Safety.

f. The aspects connected to the radiation hardness of focal plane detector have been mentioned in the section B1.5. No additional shielding for the particle or x-ray detectors which will be installed at the different experiments is foreseen. If in some special cases additional shielding of the detectors is needed, mobile Lead walls will be locally installed

3 Assembly and Installation

3.1 LSR

It is foreseen that CRYRING is moved to GSI as soon as the FLAIR hall is ready, see section G e. During the installation, resources such as mechanical and electronics workshops will be needed.

3.2 The Low Energy Experimental Area for HCI

The heaviest part of the whole setup will be the dipole magnet (maximum 9 t). The spectrometer can be mounted directly in the cave.

It is proposed to mount the experiments outside the cave, as smaller units on wheels which can easily be transported through the labyrinth and fixed at the target position

To install large parts into the cave, which can not be introduced through the labyrinth, it is proposed to build the end part of the cave from movable concrete beams. They can be occasionally removed and the large, heavy parts can be installed using a rails system or some other equivalent equipment, available at GSI. To install the beam line, vacuum systems, beam diagnosis detectors and the setups for the target region, the two fix cranes will be available. For all experiments proposed to be performed in this cave the parts which need to be often exchanged or mounted are weighting less then 2000 kg and for the moment no logistical problems are foreseen.

During the mounting activities performed in the cave, no interference with the rest of experiments situated at FLAIR will take place. Mechanical, electrical and vacuum technical assistance from the GSI infrastructure will be needed be each experiment change.

D Commissioning

1 FLAIR building

The commissioning of setups installed in the FLAIR building will be done by each responsible group. The commissioning of the common parts- LSR and beam lines- must be, finally, discussed and done in collaboration. In principle almost all commissioning can be done using ions delivered by the LSR and his ion sources. For the high energy beam line, connecting the NESR with the caves F1, F2, F7 and F8 NESR beam is requested.

2 CRYRING/LSR

The CRYRING/LSR installation will include a dedicated low-energy injector for commissioning of the FLAIR facility and its experiments. Ion sources for protons and negative hydrogen ions will be mounted on a high-voltage platform at 10 kV. For injection into CRYRING/LSR the particles will then be accelerated by the present CRYRING RFQ from 10 keV to 300 keV.
FLAIR will take and provide beams of both antiprotons and ions. Thus, the polarity of many of the bending magnets has to be changeable. Having ions with both sign of charge available from the CRYRING/LSR ion sources is essential, as this allows commissioning with both polarities of the beam-lines.
It is important to have proton beams available from CRYRING/LSR at similar energies as the antiprotons later. In this way, experiments using degrader foils can adjust a large part of the apparatus at an early stage.
The present CRYRING facility also has an ECR (electron cyclotron resonance) ion source which injects through the RFQ. This opens up the possibility to commission beamlines, injection timings and so on for those FLAIR experiments which use highly charged ions.
It should be stressed that the possibility to use ion-sources for commissioning of the whole FLAIR facility is a very considerable advantage. In this way beamlines and timings can be checked and adjusted even before the first beam from NESR arrives. This possibility can speed up the start of the physics program at FLAIR by many months or perhaps even years.

3 The Low Energy Experimental Area for HCI

If the present target hall at the SIS18-ESR accelerator will be not decommissioned before 2009, the new magnet spectrometer can be tested in the present cave for atomic physics experiments with heavy ion beams from SIS. Final alignment of the spectrometer, beam line and reaction chamber will be performed in the new cave, after installation. A preliminary timing of the commissioning is presented in the Table 18 in section B3.4.3. It is expected that for the many small experiments planed to be performed in this area test beams will be required before going to production runs. Additional commissioning is expected for the experiments using very low energy beam extracted from the HITRAP facility. For this, beams from the ion injector coupled to the LSR are sufficient.

For the alignment of the full setup, the help of professionals is demanded.

4 HITRAP

Magnetic field measurements
Magnetic field measurements with a NMR or Hall probe are required for the HITRAP cooler trap and the Penning trap experiments utilizing superconducting magnets. For all the other experiments such measurements are not required.

Alignment:
For the HITRAP cooler trap and the Penning trap experiments the alignment of the magnetic-field axis is very important since the injection of the antiprotons and highly-charged ions into the strong magnetic field is extremely critical. The HITRAP decelerator requires careful mechanical alignment during the production process. Alignment of the particle beams will be done by steerer magnets at the HITRAP facility.
The alignment of the reaction microscope setup on the axis of the antiproton and ion beams is crucial. For the ion-surface interaction experiments alignment is of great importance to have good beam control. For the X-ray spectroscopy the alignment of the setup is crucial since the injection of the antiprotons and highly-charged ions into the gas target area is extremely critical. In general standard alignment marks are expected to be available. However, help by an expert is requested for the alignment of the setup at its final position in the cave.

Test runs
The HITRAP decelerator and the cooler trap will be commissioned with beam from the ion injectors of the LSR at 4 MeV/u, ion species: protons, H^- ions, and light highly charged ions, e.g. Ar^{16+}. Final commissioning will be done with highly charged heavy-ion beams up to uranium U^{92+} at 4 MeV/u from NESR and with antiprotons at 4 MeV from LSR/CRYRING.

E Operation

1 FLAIR building

It is strongly requested that this infrastructure will be integrated in the whole FAIR infrastructure (power, cranes, gas, ventilation, water, cryo system, vacuum controlling, networking, etc.).

2 The Low Energy Experimental Area for HCI / HITRAP

a) After the construction phase the oversight over these experimental places should lie in the responsibility of the SPARC collaboration represented by a cave responsible, permanently located at GSI. For the preparation, testing and performing of the different experiments, the responsibility over the experimental set-ups will be on the group itself. It is requested that these groups get technical support, either from the SPARC collaboration itself, or from the GSI/FAIR technical infrastructure, if needed. The present experience at GSI shows that the external groups must be assisted, with hardware and with technical manpower, during the experiments.
The cave infrastructure must be integrated into the general FAIR infrastructure (power, magnet, cranes, gas, ventilation, water, cryo system, vacuum controlling, and networking).
The experiments will be controlled by the experimenters from the local electronics room. For beam adjustments on the target at CaveA and to the HITRAP decelerator, the support of the operating team from the facility is expected.
It was already mentioned that LSR gives better possibilities for testing and commissioning independent from the NESR, and the SPARC collaboration is determined to use them. For the moment no final decision over the operation mode of the caves with ion beams delivered by the LSR was taken. The SPARC and FLAIR collaborations will discuss about this aspect also with the accelerator group at GSI, before taking the final decision.

b) auxiliaries: no special requirements
c) power, gas, cryo, etc. (low-energy ion experiments)

Collision dynamics:

- Power: One high-current (32A) plug and 3*4 standard 16 A plugs
- Gas: Ar/Co2 for the beam profilers
- Cryo: no
- Cooling water:50 litres per min
- Others: A pressurized air line for valves and an exhaust line for the pre-pumping system are needed.

Reaction microscope:

- Power: One high-current (32A) plug and 3*4 standard 16 A plugs.
- Gas: at least one line (gases foreseen: He, Ne, Ar, N_2) with adjustable pressure up to 20 bar.
- Cryo: not needed.
- Cooling water: 2*10 liters / minute (at about 16 °C)
- Others: A pressurized air line for valves is needed.

Ion-Surface Interaction Experiments:

- Power: 2 * 4 standard 16A plugs (400V)
- Gas: no requirements
- Cryo: 250 litres of LN2.per week
- Cooling water: 40 litres per min
- Others: A pressurized air line for valves and an exhaust line for the pre-pumping system are needed.

X-Ray measurements:

- Power: One high-current (32A) plug and 4*4 standard 16 A plugs
- Gas: gas handling system for the gas target
- Cryo: 100 liters of LN2 per week (running experiment)
- Cooling water: 4*15 liters / minute
- Others: A pressurized air line for valves and an exhaust line for the pre-pumping system are needed.

g-Factor measurements:

- Power: One high-current (32A) plug and 3*4 standard 16 A plugs are needed, permanent power consumption less than 2kW .
- Gas: not needed
- Cryo: The superconducting magnet needs LN2 and LHe cooling. Thus, a permanent helium recovery line and a liquid nitrogen line should be installed.
- Cooling water for turbo pump
- Others: A pressurized air line for valves and an exhaust line for the pre-pumping system are needed.

Mass measurements:

- Power: One high-current (32A) plug and 3*4 standard 16 A plugs
- Gas: not needed
- Cryo: 200 liters of LN2 per week and 60 liters of LHe per month
- Cooling water: 3*15 liters / minute
- Others: A pressurized air line for valves and an exhaust line for the pre-pumping system are needed.

Laser spectroscopy:

- Power: 70 kW
- Gas: not needed
- Cryo: possibly 200 liters of LN2 per week and 60 liters of LHe per month
- Cooling water: 50 litres per min

3 CRYRING/LSR

It is advised that operation and control of LSR/CRYRING is coordinated with the control for other accelerators at FAIR, see section B2. For power, gas, cryo, etc., see section C1.

F Safety

1 General safety considerations

Generally speaking, the hazards possible in the caves refer to the

- Handling of High Voltages needed to power the detectors: up to 10 kV Voltages will be used by different experiments
- Thin Be-windows mounted on the solid stale detectors or as x-ray windows integrated in the experimental setups (usually mounted on the target chamber)
- Thin metal windows of the beam gas-profilers
- Magnetic field of the spectrometer
- Radioactive sources used for calibration purpose
- Moving heavy parts, handling the cranes.

The access to the magnet power supplies must be regulated. Also the handling of the beam line when under vacuum must be strictly supervised.

2 Radiation Environment

During the beam times, the access to the caves must be regulated according to the German safety rules. The responsibility to implement and control this should lay with the GSI security and radiation protection group.

All caves in the FLAIR hall will be built in a way that work is possible in an area when beam is on in an adjacent area. This requires adequate shielding of all areas as well as controlled access through labyrinths. An estimation of the shielding has been performed by the GSI radiation group and incorporated into the drawing of the layout in Fig. 1. A detailed calculation of radiation dose and necessary shielding is ongoing and is done in parallel to the construction optimization.

3 Safety systems

Systems for measuring the radiation level in the cave must be mounted. To avoid vacuum accidents, the vacuum control system must be equipped with a feed-back option which is able to automatically close the valves to avoid the fluting of the beam lines and, in the worse case of the whole facility, with gas.
Depending on the extension of the water cooling system, flow controllers and/or thermometer for water and an alarm system are desirable.

G Organisation and Responsibilities, Planning, WBS- work package break down structure

1 Structure of experiment management

Spokesperson:	E. Widmann	SMI Vienna
Co- Spokesperson	W. Quint	GSI
Co- Spokesperson	J. Walz	MPQ Munich

Decisions within FLAIR are taken by the steering committee. Members are

E. Widmann	SMI Vienna, Austria
J. Walz	MPQ Munich, Germany
W. Quint	GSI, Germany
M. Charlton	Swansea, UK
H. Danared	Stockholm, Sweden
D. Grzonka	Jülich, Germany
M. Holzscheiter	Pbar Labs, LLC, Santa Fe, USA
M. Hori	CERN, Switzerland
H. Knudsen	Aarhus, Denmark
M. Steck	GSI, Germany
Th. Stöhlker	GSI, Germany
G. Testera	INFN Genova, Italy
A. Trzcinska	Warsaw, Poland
J. Ullrich	Heidelberg, Germany
Y. Yamazaki	Tokyo, Japan

The leaders of subprojects are listed in the following table.

2 Responsibilities and Obligations

Table 21: Overview of the responsibilities within FLAIR

WP	Subprojects / Working Packages	Project leader(s)	Collaborating institutes	Area
1	FLAIR hall	A. Bräuning-Demian W. Quint	GSI, FLAIR collaboration	
2	LSR	H. Danared	MSL, SMI Vienna	F3
3	USR	C.P. Welsch, M. Grieser	MPI-K	F4
4	HITRAP	W. Quint	HITRAP collaboration (SPARC)	F2
5	New low-energy HCI cave	A. Bräuning-Demian	GSI, NIPNE Bucharest, INP Lyon, Uni. Giessen, Uni. Zarqa, JINR Dubna, IMP Lanzhou	F1
6	Antihydrogen experiments	J. Walz, E. Widmann	MPQ, Harvard, York, Jülich, Amsterdam, SMI, U Tokyo, RIKEN, Budapest, Atomki, Debrezen U, ISA, Aarhus U, Brescia	F5/F6
7	Cusp trap for production of spin-polarized antihydrogen	Y. Yamazaki	RIKEN, Tokyo U	F9
8	g-factor of $\bar{p}$	W. Quint, M. Vogel	GSI, Mainz (SPARC)	F10
9	Mass measurement of $\bar{p}$ and HCI	K. Blaum	Mainz, GSI (SPARC)	F10
10	Antiprotonic atom spectroscopy	M. Hori	Tokyo U, SMI, Budapest, Atomki, Debrezen U, Brescia	F6/F10
11	USR internal target	C.P. Welsch, J. Ulrich	MPI-K	F4
12	Reaction microscope after Penning trap	R. Moshammer	MPI-K, IKF Frankfurt	F10
13	Energy loss and ionization	U.I.Uggerhøj	Aarhus U, MPI-K, Belfast QU, Swansea	F9
14	Antihydrogen collision experiments	A.Wolf	MPI-K, ISA Aarhus, HU Berlin, GSI	F4/ F5,F6, or F9
15	Antiproton atom formation	N. Kuroda	RIKEN, Tokyo U, Brescia	F9
16	X-rays of light $\bar{p}$ atoms	D. Gotta	Jülich	F7
17	X-rays of heavy $\bar{p}$ atoms	A. Trzcinska	HIL Warsaw, Soltan Inst. Warsaw	F7
18	Strangeness –2 baryons	D. Grzonka	Jülich, Albuquerque	F7
19	Positron cooler ring	I. Meshov	Dubna	F4
21	Exo+pbar	M. Wada	RIKEN, GSI, Warsaw, JYFL Jyvaskulä	F9
22	Biological effectiveness of $\bar{p}$ annihilation	M. Holzscheiter	Aarhus U, Aarhus U Hospital, VINCA Institute, Belgrade, HUG Geneva, David Geffen Medical School Los Angeles, Maastricht U, Montenegro U, Pbar Labs Santa Fe, Britisch Columbia Cancer Agency Vacouver	F8
23	LSR – USR transfer line	M. Grieser	MPI-K, MSL	

The working packages listed in Table 21 are essentially all “facilities” and experiments as listed in chapter B.

The required funding for all experiments is described in their respective sections. Most of the groups have been doing similar experiments at the AD or before at LEAR and have a record of obtaining sufficient funding. This is especially true for the AD community, which has not only succeeded to obtain significant funding (several MEuro for each collaboration), but also external funding for the construction of the AD at a level of > 5 MCHF.

Funding for the USR is supposed to come from the Max Planck Institute for Nuclear Physics in Heidelberg, which has presently obtained funding for a cryogenic ring CSR. The CSR can be regarded as a prototype for the USR and will serve as a proof-of-principle machine.

The rebuilding of CRYRING for its function as LSR is technically manageable by the staff of the Manne Siegbahn Laboratory in Stockholm. Due to the time horizon of FAIR, it will require an extension of its operation at MSL and investment for the modifications. These funds are currently under discussion as a part of the Swedish contribution to FAIR as a whole. Further stronger contributions by other members of the collaboration are currently being investigated.

HITRAP and the low-energy HCI cave are primarily undertaken by the SPARC collaboration and are described in their technical proposal.

The FLAIR collaboration will seek further funding via appropriate sources of the European community.

Although the Low-energy antiproton physics was initially not included into the Conceptual Design Report (CDR) and the FLAIR collaboration was formed during the year 2003, after the CDR submission, the research program proposed by this collaboration was strongly recommended by the APPA-PAC after the evaluation of the FLAIR Letter of Intent in spring 2004. Originally, only the locations for the low-energy experimental area for highly charged ions extracted from NESR and HITRAP were included in the CDR. By the time of CDR preparation is was assumed that all cost for the needed civil construction will be supported by the German part (GSI). From the Project management side there is presently a statement that this building will be treated in the same manner as all other buildings.

In the following a few working packages are described in more details.

(WP1) FLAIR Building

Due to the large number of the proposed experiments and the diversity of different devices the FLAIR building implies a high degree of complexity.
The responsibility for the FLAIR building is shared by both collaboration SPARC and FLAIR.For the actual phase (internal structure planning) the responsibility over the FLAIR building is shared by A. Braeuning-Demian and W. Quint from GSI.

Tasks	**Contributing Groups**
Data Collection for Planning	GSI, FLAIR Collaboration
Building Planning	GSI, FLAIR Collaboration, MPI-K Heidelberg
Civil Construction and Infrastructure Installation	GSI, Civil Construction Contractor
Final Construction Acceptance	GSI, Collaboration Groups
Mounting of the Common Parts (Beam Lines)	SPARC and FLAIR Collaborations

Although the Low-energy antiproton physics was initially not included into the Conceptual Design Report (CDR) and the FLAIR collaboration was formed during the year 2003, the research program proposed by this collaboration was strongly recommended by the APPA-PAC after the evaluation of the FLAIR Letter of Intent. Originally, only the locations for the low-energy experimental area for highly charged ions extracted from NESR and HITRAP were included in the CDR.

(WP 2) Low Energy Storage Ring (LSR)

Most of the tasks generate by the need to transform the CRYRING into a dedicated antiproton and highly charged ions decelerator for FLAIR (LSR) will be performed at MSL in Stockholm by the Swedish operating team.

Tasks	**Contributing Groups**
Design of CRYRING modifications	CRYRING Team at MSL
Ordering Components	
Installation and Commissioning of the Modifications	
Disassembly of CRYRING at MSL	
Transfer to FLAIR	
Reassembly and Alignment at FLAIR	tbd.
Commissioning with p, H^- and HCI	

3 Organisation

The following working groups have been created to proceed with the working packages defined above:

(WG 1) FLAIR Building

A. Braeuning-Demian	*GSI Darmstadt*
W.Quint	*GSI Darmstadt*
E. Widmann	*SMI Wien*
C.P. Welsch	*MPI-K Heidelberg*
M. Grieser	*MPI-K Heidelberg*
H. Danared	*MSL Stockholm*
Y. Yamazaki	*Tokyo University*
J. Walz,	*MPQ Garching*
D. Grzonka	*FZ Jülich*
M. Holzscheiter	*Pbar Labs, LLC Santa Fe*
M. Wada	*RIKEN, Japan*

(WG 2) LSR

H. Danared	*MSL Stockholm*
G. Andler	*MSL Stockholm*
L. Bagge	*MSL Stockholm*
M. Engström	*MSL Stockholm*
A. Källberg	*MSL Stockholm*
L. Liljeby	*MSL Stockholm*
P. Löfgren	*MSL Stockholm*
A. Paál	*MSL Stockholm*
K.-G. Rensfelt	*MSL Stockholm*
A. Simonsson	*MSL Stockholm*

(WG 3) USR

C.P. Welsch	*MPI-K Heidelberg*
M. Grieser	*MPI-K Heidelberg*
J. Ullrich	*MPI-K Heidelberg*
R. von Hahn	*MPI-K Heidelberg*
A. Wolf	*MPI-K Heidelberg*

(WG 4) HITRAP

K. Blaum	*Univ. Mainz/GSI*
M. Block	*GSI*
J. Burgdörfer	*Techn. Univ. Vienna*
C. Dimopoulou	*MPI-K Heidelberg*
S. Djekic	*Univ. Mainz/GSI*
F. Herfurth	*GSI*
H.-J. Kluge	*GSI*
C. Kozhuharov	*GSI*
R. Morgenstern	*KVI Groningen*
W. Quint	*GSI*
U. Ratzinger	*Univ. Frankfurt*
A. Robin	*KVI Groningen*
R. Schuch	*Stockholm University*
S. Stahl	*Univ. Mainz*
A. Schempp	*Univ. Frankfurt*
L. Schweikhard	*Univ. Greifswald*
R. Thompson	*Imperial Coll. London*
J. Ullrich	*MPI-K Heidelberg*
M.l Vogel	*Univ. Mainz*
A.j Warczak	*IP JU Krakow*
C. Weber	*GSI/Univ. Mainz*
D. Winters	*Imperial Coll. London*

(WG 5) New low-energy HCI cave

A. Braeuning-Demian	*GSI Darmstadt*
D. Dauvergne	*INP Lyon*
H. Braeuning	*Giessen University*
X. Ma	*IMP Lanzhou*
F. Afaneh	*University Zarqa*
S. Tiberiu	*NIPNE Bucharest*
C. Ciortea	*NIPNE Bucharest*
D. Dumitriu	*NIPNE Bucharest*
D. Fluerasu	*NIPNE Bucharest*
A. Enulescu	*NIPNE Bucharest*
L. C. Penescu	*NIPNE Bucharest*
A. T. Radu	*NIPNE Bucharest*
G. Shirkov	*JINR Dubna*

(WG 6) Antihydrogen exepriments

J. Walz	*MPQ Munich*
G. Gabrielse	*Harvard University, USA*
E.A. Hessels	*York University, Canada*
W. Oelert	*FZ Jülich, Germany*
K.S.E. Eikema	*Laser Centre Vrije Universiteit, Amsterdam*
W. Hogervorst	*Laser Centre Vrije Universiteit, Amsterdam*
W. Ubachs	*Laser Centre Vrije Universiteit, Amsterdam*
E. Widmann	*SMI Vienna, Austria*
M. Cargnelli	*SMI Vienna, Austria*
H. Fuhrmann	*SMI Vienna, Austria*
J. Marton	*SMI Vienna, Austria*
J. Zmeskal	*SMI Vienna, Austria*
R.S. Hayano	*Tokyo University*
M. Hori	*Tokyo University*
A. Dax	*Tokyo University*
D. Horváth	*KFKI Budapest, Hungary*
M. Barna	*KFKI Budapest, Hungary*
B. Juhász	*ATOMKI Debrecen, Hungary*
H. Knudsen	*Aarhus University, Denmark*
U. I. Uggerhøj	*Aarhus University, Denmark*
A. Kellerbauer	*GSI*
M. Corradini	*Brescia University and INFN Brescia*
M. Leali	*Brescia University and INFN Brescia*
E. Lodi Rizzino	*Brescia University and INFN Brescia*
L. Venturelli	*Brescia University and INFN Brescia*
N. Zurlo	*Brescia University and INFN Brescia*
H. A. Schuessler	*Texas A&M University, College Station, Texas*
A. Ray	*Variable Energy Cyclotron Center, Kolkata*

(WG 7) Cusp trap for production of antihydrogen

Y. Yamazaki	*RIKEN, Univ. Tokyo*
A. Mohri	*RIKEN*
N. Kuroda	*RIKEN*
M. Shibata	*RIKEN*
Y. Kanai	*RIKEN*
M. Wada	*RIKEN*
H. Torii	*Tokyo University*
Y. Nagata	*RIKEN*
K. Komaki	*Tokyo University*

(WG 8) g-factor of the antiproton

K. Blaum	*Univ. Mainz/GSI*
S. Djekic	*Univ. Mainz/GSI*
H.-J. Kluge	*GSI*
S. Kreim	*Univ. Mainz*
W. Quint	*GSI*
S. Stahl	*Univ. Mainz*
J. Verdú	*Univ. Mainz*
M. Vogel	*Univ. Mainz*
G. Werth	*Univ. Mainz*
J. Walz	*MPQ Garching*
A. Ray	*Variable Energy Cyclotron Center, Kolkata*

(WG 9) Mass measurement of antiprotons and highly charged ions

K. Blaum	*Mainz*
F. Herfurth	*GSI*
W. Quint	*GSI*
H.-J. Kluge	*GSI*
C. Weber	*Mainz*
S. Stahl	*Mainz*
S. George	*Mainz*
A. Kellerbauer	*GSI*
A. Ray	*Variable Energy Cyclotron Center, Kolkata*

(WG 10) Antiprotonic atom spectroscopy

M. Hori	*Tokyo University*
R.S. Hayano	*Tokyo University*
A. Dax	*Tokyo University*
D. Horvath	*KFKI Budapest, Hungary*
B. Juhasz	*ATOMKI Dpbrecen, Hungary*
K. Tőkési	*ATOMKI Debrecen, Hu*
E. Widmann	*SMI Vienna, Austria*
M. Corradini	*Brescia University and INFN Brescia*
M. Leali	*Brescia University and INFN Brescia*
E. Lodi Rizzino	*Brescia University and INFN Brescia*
L. Venturelli	*Brescia University and INFN Brescia*
N.Zurlo	*Brescia University and INFN Brescia*

(WG 11) USR internal target

C.P. Welsch	*MPI-K, Heidelberg, Germany*
J. Ullrich	*MPI-K, Heidelberg, Germany*

(WG 12) Reaction microscope after Penning trap

R. Moshammer	*MPI-K Heidelberg, Germany*
C.P. Welsch	*MPI-K, Heidelberg, Germany*
J. Ullrich	*MPI-K, Heidelberg, Germany*
R. Dörner	*Universität Frankfurt*

(WG 13) Energy loss and Ionization

U. I. Uggerhøj	*Aarhus University, Denmark*
S. P. Møller	*ISA Aarhus*
H. Knudsen	*Aarhus University, Denmark*
T. Ichioka	*MPI-K Heidelberg, Germany*
R. McCullough	*Queens University, Belfast*
M. Charlton	*University of Swansea*
J. Burgdörfer	*TU Wien*

(WG 14) Antihydrogen collision experiments

A. Wolf	*MPI-K Heidelberg*
J. Ullrich	*MPI-K Heidelberg*
H. Knudsen	*University, Denmark*
A. Saenz	*HU Berlin*
W. Quint	*GSI Darmstadt*

(WG 15) Antiprotonic atom formation

N. Kuroda	*RIKEN*
M. Shibata	*RIKEN*
H. Saito	*RIKEN*
Y. Kanai	*RIKEN*
Y. Yamazaki	*RIKEN*
H. A. Torii	*University of Tokyo, Komaba*
K.-i. Komaki	*University of Tokyo, Komaba*
M. Corradini	*Brescia University and INFN Brescia*
M. Leali	*Brescia University and INFN Brescia*
E. Lodi Rizzino	*Brescia University and INFN Brescia*
L. Venturelli	*Brescia University and INFN Brescia*
N. Zurlo	*Brescia University and INFN Brescia*

(WG 16) X-rays of light antiprotonic atoms

D. Gotta	*FZ Jülich*

(WG 17) X-rays of heavy antiprotonic atoms

A. Trzcińska	*Heavy Ion Laboratory, Warsaw University, Poland*
J. Jastrzębski	*Heavy Ion Laboratory, Warsaw University, Poland*
S. Wycech	*Sołtan Institute for Nuclear Studies, Warsaw, Poland*

(WG 18) Strangeness -2 baryons

D. Grzonka	*FZ Jülich*
W. Oelert	*FZ Jülich*
K. Kilian	*FZ Jülich*
T. Sefzik	*FZ Jülich*
A. Gillitzer	*FZ Jülich*
J. Ritman	*FZ Jülich*
P. Winter	*FZ Jülich*
B. Bassalleck	*University of New Mexico, USA*
P. Kingsberry	*University of New Mexico, USA*

(WG 19) Positron cooler ring

I. Meshkov	*JINR, Dubna, Russia*
I. Seleznev	*JINR, Dubna, Russia*
A. Smirnov	*JINR, Dubna, Russia*
A. Sidorin	*JINR, Dubna, Russia*
E. Syresin	*JINR, Dubna, Russia*
G. Trubnikov	*JINR, Dubna, Russia*
S. Yakovenko	*JINR, Dubna, Russia*
Yu. Korotaev	*JINR, Dubna, Russia*
A. Kobets	*JINR, Dubna, Russia*

(WG 20) Exo+pbar

J. Äystö	*JYFL, Jyvaskyla Univeristy*
A. Jokinen	*JYFL, Jyvaskyla Univeristy*
S. Kopecky	*JYFL, Jyvaskyla Univeristy*
I. Moore	*JYFL, Jyvaskyla Univeristy*
A. Nieminen	*JYFL, Jyvaskyla Univeristy*
H. Geissel	*GSI, Darmstadt*
C. Scheidenberger	*GSI, Darmstadt*
M. Winkler	*GSI, Darmstadt*
W. Quint	*GSI, Darmstadt*
M. Wada	*Atomic Physics Laboratory, RIKEN, Wako*
Y. Yamazaki	*Atomic Physics Laboratory, RIKEN, Wako*
Y. Ishida	*Atomic Physics Laboratory, RIKEN, Wako*
T. Nakamura	*Atomic Physics Laboratory, RIKEN, Wako*
A. Takamine	*Atomic Physics Laboratory, RIKEN, Wako*
N. Oshima	*Atomic Physics Laboratory, RIKEN, Wako*
Y. Nakai	*Atomic Physics Laboratory, RIKEN, Wako*
K. Okada	*Sophia University, Tokyo*
W. Kurcewicz	*Stefan Pienkowski Institute, Warsaw University, Warsaw*
A. Trzcińska	*Heavy Ion Laboratory, Warsaw University, Poland*
J. Jastrzębski	*Heavy Ion Laboratory, Warsaw University, Poland*

(WG 21) Biological effectiveness of antiproton annihilation

N. Bassler	*University of Aarhus, Denmark*
S. Pape Møller	*ISA Aarhus, Denmark*
J. Peterson	*University Hospital, Aarhus, Denmark*
S. Vranjes	*VINCA Institute, Belgrade, Serbia & Montenegro*
M. Doser	*CERN, Geneva, Switzerland*
R. Landua	*CERN, Geneva, Switzerland*
G. Beyer	*University Hospital Geneva, Switzerland*
R. Withers	*David Geffen Medical School, UC Los Angeles, USA*
K. Iwamoto	*David Geffen Medical School, UC Los Angeles, USA*
B. Wouters	*University of Maastricht, Netherlands*
D. Hajdukovic	*University of Montenegro, Montenegro*
M. H. Holzscheiter	*PBAR Labs, LLC, Santa Fe, NM, USA*

(WG 22) LBTL

M. Wada	*RIKEN, Japan*
C. Scheidenberger	*GSI Darmstadt*
M. Winkler	*GSI Darmstadt*
J. Gerl	*GSI Darmstadt*
W. Quint	*GSI Darmstadt*
H. Danared	*MSL Stockholm*
C.P. Welsch	*MPI-K Heidelberg*
M. Grieser	*MPI-K Heidelberg*

(WG 23) LSR – USR transfer line

M. Grieser	*MPI-K Heidelberg*
C.P. Welsch	*MPI-K Heidelberg*
H. Danared	*MSL*

H Relation to other Projects

The common location of the low-energy HCI experimental area, HITRAP and all low-energy antiproton experiments imply a strong correlation between the Low-energy HCI cave Working Group and the FLAIR collaboration. Although, for the moment no common experiments are foreseen, close collaboration at the technical level is needed. This extends over planning and designing of common parts, testing and commissioning, sharing of common infrastructure and beam time

At experimental level there is an interaction with the other SPARC member groups working at NESR: planning common experiments, exchanging hardware and know-how. One example is the position sensitive solid state detector for x-ray, which is mainly developed for the NESR experiments. This device can be successfully use in some experiments with cooled, decelerated heavy ions.

For R&D phase the collaboration with CBM and the NoRHDia collaborations in the field of diamond detector developing very valuable.

The availability of short-lived nuclei produced at the SFRS and low-energy antiprotons offers a unique possibility to make use of $\bar{p}$ as hadronic probes for nuclear structure studies. This would require a beam line to transport HCI from SFRS to FLAIR for the Exo+pbar experiment, which could also provide HCI beams from FLAIR to SFRS for the AGATA experiment. This beam line, as described in sec. C1.4, is technically in principle feasible, but the possibility of its realisation strongly depends on the relative location of the FLAIR and SFRS buildings. A close proximity of both buildings would therefore be desirable to enable these experiments combining the FLAIR and NUSTAR physics programs.

I Other issues

The FLAIR building

Apart of the, originally in CDR proposed, atomic physics experiments with decelerated, cooled highly charged ions (HCI) extracted from the NESR, a large number of experiments, promoting physics topics connected to the low-energy antiprotons ($\bar{p}$) interactions with atoms and radioactive nuclei have been later proposed. A presentation of the physics case of these experiments is done in the Letter of Intent (LoI) submitted by the FLAIR collaboration for the FAIR Project in January 2004.

All these experiments will use beams extracted from NESR. Therefore, it was naturally to try to group all these experiments in a single area, close to the NESR. Like this, emerged the need of a larger building which will accommodate ten different experimental areas, where more then 20, already proposed, experiments will be performed.

Fig. 1 presents the layout of this building, as it is today designed. Most of the new $\bar{p}$ experiments need very low energy antiprotons, in the range of keV. This limit is far below the design parameters of the NESR and to reach it without high losses in beam intensity, a further deceleration must be performed. As already mentioned in section B of this report, this task can be successfully performed by the CRYRING, a facility at Manne Siegbahn Laboratory at Stockholm University.

Although the proposed HCI experiments are not strongly dependent on the existence of an additional decelerator, they can tremendously benefit from using beams from this ring. First of all, the HITRAP facility, originally proposed only for HCI physics, can start a new physics program at the FAIR facility, if beams of 4 MeV antiprotons can be transferred from the CRYRING. If provided with his own ion injectors, as it is today in Stockholm, the ring can also accelerate and provide ion beams for tests and commissioning of all experiments, independent on the NESR. On long term this will increase the efficiency of using the main beams delivered by the FAIR accelerator complex.

J References and Acknowledgements

[1] FLAIR LOI, available from http://www.flair.eu.tt
[2] Conceptual Design Report
[3] SPARC LOI
[4] S.P. Møller, "ELISA – an Electrostatic Storage Ring for Atomic Physics", Proc. European Particle Accelerator Conference, Stockholm, Schweden, 1998
[5] T. Tanabe et al, "An Electrostatic Storage Ring for Atomic and Molecular Science", Nucl. Instr. and Meth. A 482 (2002) 595
[6] C. P. Welsch et al, "Design Studies of an Electrostatic Storage Ring", Proc. Particle Accelerator Conference, Portland, USA, 2003
[7] R. von Hahn et al, "CSR – a cryogenic storage ring at MPI-K", Proc. European Accelerator Conference, Lucerne, Switzerland, 2004
[8] C.P. Welsch et al, "Electrostatic Ring as the Central Machine of the Frankfurt Ion stoRage Experiments", PRST-AB 7, 080101 (2004)
[9] C.P. Welsch et al, "FIRE – the Frankfurt Ion stoRage Experiments", NiM A 527/3 (2004) 284-288
[10] M. Berz, K. Makino, "COSY infinity V 8.1 User's Guide and Reference Manual", Technical Report MSUHEP-20704 (2002)
[11] C.P. Welsch et al, "An Electrostatic Quadrupole Doublet with an Integrated Steerer", Proc. European Accelerator Conference, Lucerne, Switzerland, 2004
[12] N. Madsen et al, "Equilibrium Beam in the Antiproton Decelerator (AD)", Nim A 441 (2000) 54-59
[13] H. Danared, "Cryring at FLAIR", Talk FLAIR user meeting, 15.3.2004
[14] S. Pastuszka et al., J. Appl. Phys. 88, 6788 (2000)
[15] D. Orlov et al., Appl. Phys. Lett. 78, 2721 (2001)
[16] G. Trubnikov et al., "The Low Energy Positron Storage Ring for Positronium Generation: Status and Developments", Proc. European Accelerator Conference, Paris, France, 2002
[17] I.Meshkov, A.Sidorin, I.Seleznev, E.Syresin, "Antihydrogen Generation Scheme based on LEPTA-type ring", Joint Institute for Nuclear Research, 25.11.2003
[18] I.N.Meshkov, A.N.Skrinsky, "Antihydrogen beam generation using storage rings », NiM A 379, 1996, p. 41-49
[19] I.N.Meshkov et al., "The particle dynamics in the low energy storage ring with longitudinal magnetic field", Proc. European Accelerator Conference, 1998, 1067
[20] D. Zajfman, "Physics with Colder Molecular Ions: The Cryogenic Storage Ring CeSaR", D. Zajfman, talk at the DR conference, Mosbach, Germany, 2004
[21] Impact parameter dependent electron capture by decelerated U91+ ions at 20 MeV/u using crystal channeling conditions, NIM B, Vol. 205,773(2003)
[22] E.Berdermann, K. Blasche, P.Moritz, H. Stelzer, F. Zeytouni, Diamond detectors for Heavy Ion measurements, GSI-Preprint-98-23
[23] E.Berdermann, K. Blasche, P.Moritz, H. Stelzer, B.Voss, The use of CVD-Diamond for heavy-ion detection, Diamat. 10(2001) 1770-1777
[24] S. Toleikis, Lebensdauermessungen metastabiler atomarer zustände in heliumähnlichen schweren Ionen, Ph.D Thesis, GSI preprint Diss.2002-11
[25] A.Braeuning-Demian, E. Berderman, M. Ciobanu, P.Verma, S.Toleikis, Position sensitive diamond detector for highly charged ions at intermediate energies, to be published in 2005.
[26] W.Adam et. al. (RD42 Collaboration), Radiation Tolerance of CVD Diamond Detectors for Pions and Protons, Proc. Int. Conf. Rad. Eff. on Semicon. and Mat., Florence 2000.
[27] E. Berdermann, private communication
[28] G. Gabrielse et al., Phys. Rev. Lett. 93, 073401 (2004)
[29] A.Mohri and Y.Yamazaki, "A possible new scheme to synthesize antihydrogen and to prepare polarized antihydrogen beam", Europhys. Lett. 63 (2003) 207-213

[30] N.Ohshima, T.M.Kojima, M.Niigaki, A.Mohri, K.Komaki, and Y.Yamazaki, "A new positron accumulation scheme in ultra high vacuum", Phys.Rev.Lett. 93 (2004) 195001-4.
[31] N. Hermanspahn et al., Phys. Rev. Lett. 84 (2000) 427
[32] H. Häffner et al., Phys. Rev. Lett. 85 (2000) 5308
[33] J. Verdu et al., Phys. Rev. Lett. 92 (2004) 093002
[34] T. Beier et al., Phys. Rev. Lett 88 (2002) 011603
[35] V.A. Yerokhin et al. Phys. Rev. Lett. 89 (2002) 143001
[36] G. Werth et al., Adv. At. Mol. Opt. Phys. 48 (2002) 191
[37] L.S. Brown and G. Gabrielse, Rev. Mod. Phys. 58 (1986) 233
[38] R. Bluhm, V.A. Kostelecky and N. Russell , Phys. Rev. D 57 (1998) 3932.
[39] M. Vogel et al., submitted to Nucl. Inst. Meth. B
[40] J. Verdu et al, Physica Scripta T112 (2004) 68
[41] S. Stahl et al., submitted to Eur. Phys. J. D
[42] K. Hagiwara et al., Phys. Rev. D 66 (2002) 010001
[43] E. Kruger, W. Nistler, and W. Weirauch, Metrologia 35 (1998) 203.
[44] M.P. Bradley et al., Phys. Rev. Lett. 83 (1999) 4510
[45] C. Carlberg, T. Fritioff, and I. Bergström, Phys. Rev. Lett. 83 (1999) 4506
[46] A. Wicht, J.M. Hensley, E. Sarajlic, and S. Chu, Phys. Scr. T102 (2002) 82
[47] F. DiFilippo et al., Phys. Rev. Lett. 73 (1994) 1481
[48] I. Bergström et al., Phys. Scr. 66 (2002) 201
[49] V.M. Lobashev, Nucl. Phys. A719 (2003) 153c
[50] A. Osipowicz et al., Letter of Intent, KATRIN: A next generation tritium beta decay experiment with sub-eV sensitivity for the electron neutrino mass (2003)
[51] G. Douysset et al., Phys. Rev. Lett. 86 (2001) 4259
[52] H.V. Klapdor-Kleingrothaus et al., Phys. Lett. B586 (2004) 198
[53] B. Fogelberg et al., Phy. Rev. Lett. 82 (1999) 1823
[54] G. Gabrielse et al., Phys. Rev. Lett. 82 (1999) 3198
[55] G.L. Greene et al., Phys. Rev. D44 (1991) R2216
[56] M. König et al., Int. J. Mass Spec. Ion Processes 142 (1995) 95
[57] A.G. Marshall et al., Mass Spectrom. Rev. 17 (1998) 1
[58] C. Weber, Doctoral thesis, Ruprecht-Karls-University Heidelberg, 2004
[59] K. Blaum et al., Eur. Phys. J. A 15 (2002) 245
[60] A. Kellerbauer et al., Eur. Phys. J. D 22 (2003) 53
[61] D. Beck et al., Nucl. Instrum. Methods A 527 (2004) 567
[62] D. Beck and H. Brandt, GSI Scientific Rep. 2002 (2003) 210
[63] P. Hvelplund, H. Knudsen, U. Mikkelsen, E. Morenzoni, S.P. Møller, E. Uggerhøj, T. Worm, J. Phys. B 27 (1994) 925
[64] A. Cassimi et al., Phys. Rev. Lett. 76 (1996) 3679
[65] D. Fischer et al., J. Phys. B: At. Mol. Opt. Phys. 35 (2002) 1369
[66] L. H. Andersen, P. Hvelplund, H. Knudsen, S. P. Møller, J. O. P. Pedersen, S. Tang-Petersen, E. Uggerhøj, K. Elsener and E. Morenzoni, Phys. Rev. A 41 (1990) 6536
[67] H. Knudsen, U. Mikkelsen, K. Paludan, K. Kirsebom, S. P. Møller, E. Uggerhøj, J. Slevin, M. Charlton and E. Morenzoni, Phys. Rev. Lett. 74 (1995) 4627
[68] K. Khayyat, T.Weber, R. Dörner, M. Achler, V. Mergel, L. Spielberger, O. Jagutzki, U. Meyer, J. Ullrich, R. Moshammer, W. Schmitt, H. Knudsen, U. Mikkelsen, P. Aggerholm, E. Uggerhøj, S. P. Møller, V. Rodriguez, S. F. C. O'Rourke, R. E. Olson, P. D. Fainstein, J. H. McGuire and H. Schmidt-Böcking, J. Phys. B 32 (1999) L73
[69] Lubinski et al PRL 86 (2001) 616
[70] Bodewits et al APJ Lett. 606 (2004) 81
[71] Zygelman at al., Phys. Rev. A 63, 052722 (2001)
[72] S. Jonsell et al., Phys. Rev. A 64, 052712 (2001)

[73] S. Jonsell et al., J. Phys. B 37, 1195 (2004)
[74] Yu. Voronin and J Carbonell, Nucl. Phys. A 689, 529c (2001)
[75] L. Morgan, Jr. and V. W. Hughes, Phys. Rev. D 2, 1389 (1970)
[76] M. W. Gealy and B. Van Zyl, Phys. Rev. A 36, 3100 (1987)
[77] D. Gotta, "Precision spectroscopy of light exotic atoms", Prog. Part. Nucl. Phys. 52 (2004) 133-195
[78] M. Augsburger et al., "Measurement of the strong interaction parameters in antiprotonic hydrogen and probable evidence for an interference with inner bremssstrahlung", Nucl. Phys. A 658 (1999) 149
[79] D. Gotta et al., "Balmer α transitions in antiprotonic hydrogen and deuterium", Nucl. Phys. A 660 (1999) 283
[80] M. Augsburger et al., "Measurement of the strong interaction parameters in antiprotonic deuterium", Phys. Lett B 461 (1999)
[81] M. Schneider et al., "X-rays from antiprotonic ^{3}He and ^{4}He", Z. Phys. A 338 (1991) 217
[82] D. Gotta, "X-ray measurements of light antiprotonic atoms", FLAIR meeting, Sept.2004, http://www.flair.eu.tt
[83] H. Gorke et al., "Light antiprotonic atoms", AIP conf. proc., vol. 793 (2005) 169
[84] H. Gorke et al., "A compact setup of fast pnCCDs for exotic atom measurements", AIP conf. proc., vol. 793 (2005) 341
[85] N. Nelms et al., "A large area CCD X-ray detector for exotic atom spectroscopy", Nucl. Instr. Meth. A 484 (2002) 419
[86] A. Trzcińska et al., Nucl. Phys. A 692 (2001) 176c
[87] R.L. Jaffe, Phys. Rev. Lett. 38 (1977) 195
[88] K. Kilian, Proc. 4th LEAR Workshop, Villars-sur-Ollon 1987, C. Amsler et al., ed., Harwood Academic Publishers, Chur, 1988 p. 529; K. Kilian et al., Memorandum PSCC CERN 1990
[89] I.Tanihata,et al., Phys.Rev.Lett. 55 (1985) 2676
[90] A. Trzcinska et al., Phys. Rev. Lett. 87 (2001) 82501
[91] Bugg et al., Phys. Rev. Lett. 31 (1973) 475
[92] J. Jastrzebski et al., Nucl. Phys. A588 (1993) 405c
[93] M. Wada and Y. Yamazaki, Nucl. Instr. Meth. B214 (2004) 196
[94] J.S. Cohen, Phys.Rev.A 69 (2004) 022501
[95] N. Kuroda, H. A. Torii, K. Yoshiki Franzen, Z. Wang, S. Yoneda, M. Inoue, M. Hori, B. Juhász, D. Horváth, H. Higaki, A. Mohri, J. Eades, K. Komaki, and Y. Yamazaki, Phys. Rev. Lett. 94**,** 023401 (2005)
[96] Phys. Rev. C51 (1995) 1167
[97] L. Gray and T. E. Kalogeropoulos, "Possible biomedical applications of antiproton beams: Focused radiation transfer"; Radiation Research 97, 246-252 (1984)
[98] A. H. Sullivan, "A measurement of the local energy deposition by antiprotons coming to rest in tissue-like material"; Phys. Med. Biol. 30(12), 1297-1303 (1985)
[99] "Relative Biological Effectiveness and Peripheral Damage of Antiproton Annihilation", CERN-SPSC-2002-030; SPSC-P-324. Geneva: CERN, 08 Oct 2002
[100] C. Maggiore, et al., "Biological effectiveness of antiproton annihilation"; NIM B 214 (2004) 181- 185
[101] M. Holzscheiter et al., "Biological effectiveness of antiproton annihilation", NIM B 221 (2004) 210 - 214
[102] Y. Akaishi and T. Yamazaki, Phys. Rev. C 65 (2002) 044005
[103] G.E. Brown, C.H. Lee, M. Rho and V. Thorson, Nucl. Phys. A 567 (1994) 937
[104] D.B. Kaplan and A.E. Nelson, Phys. Lett. B 175 (1986) 57
[105] see LOI M. Cargnelli et al to JPARC 2003
[106] Y. Akaishi, A. Doté and T. Yamazaki, Phys. Lett. B 613 (2005) 140

[107] A. Akaishi, P. Kienle, W. Weise, Y. Yamazaki to be published
[108] see R. Grimm, Nature, 435 (2005) 1035
[109] T. Yamayaki and Y. Akaishi, Phys. Lett. B 535 (2002) 70
[110] T. Yamazaki, A. Doté and Y. Akaishi, Phys. Lett. B 587 (2004) 167
[111] A. Doté, H. Horiuchi, Y. Akaishi, and T. Yamazaki, Phys. Lett. B 590 (2004) 51; Phys. Rev. C 70 (2004) 044313
[112] Ansgar Simonsson, Dissertation, University Stockholm, 1991